APPLICATION OF GREEN IRON NANOPARTICLES SUPPORTED ON BIOCHAR FOR THE REMOVAL OF SELECTED ORGANOCHLORINE PESTICIDES FROM WATER

SAMAVIA BATOOL

FACULTY OF SCIENCE
UNIVERSITY OF MALAYA
KUALA LUMPUR

2019

APPLICATION OF GREEN IRON NANOPARTICLES SUPPORTED ON BIOCHAR FOR THE REMOVAL OF SELECTED ORGANOCHLORINE PESTICIDES FROM WATER

SAMAVIA BATOOL

THESIS SUBMITTED IN FULFILMENT OF THE REQUIREMENTS FOR THE DEGREE OF DOCTOR OF PHILOSOPHY

FACULTY OF SCIENCE
UNIVERSITY OF MALAYA
KUALA LUMPUR

2019

UNIVERSITY OF MALAYA

ORIGINAL LITERARY WORK DECLARATION

Name of Candidate: Samavia Batool

Matric No: SHC140038

Name of Degree: PhD

Title of Thesis ("Application of green iron nanoparticles supported on biochar for the removal of selected organochlorine pesticides from water"):

Field of Study: Geology (Environmental chemistry)

I do solemnly and sincerely declare that:

(1) I am the sole author/writer of this Work;
(2) This Work is original;
(3) Any use of any work in which copyright exists was done by way of fair dealing and for permitted purposes and any excerpt or extract from, or reference to or reproduction of any copyright work has been disclosed expressly and sufficiently and the title of the Work and its authorship have been acknowledged in this Work;
(4) I do not have any actual knowledge nor do I ought reasonably to know that the making of this work constitutes an infringement of any copyright work;
(5) I hereby assign all and every rights in the copyright to this Work to the University of Malaya ("UM"), who henceforth shall be owner of the copyright in this Work and that any reproduction or use in any form or by any means whatsoever is prohibited without the written consent of UM having been first had and obtained;
(6) I am fully aware that if in the course of making this Work I have infringed any copyright whether intentionally or otherwise, I may be subject to legal action or any other action as may be determined by UM.

Candidate's Signature Date:

Subscribed and solemnly declared before,

Witness's Signature Date:

Name:

Designation:

APPLICATION OF GREEN IRON NANOPARTICLES SUPPORTED ON BIOCHAR FOR THE REMOVAL OF SELECTED ORGANOCHLORINE PESTICIDES FROM WATER

ABSTRACT

In this work, novel green iron nanoparticles supported on biochar (INPs-B_g) were prepared for the efficient removal of organochlorine pesticides (OCPs) from water system. For this purpose, four biochars were prepared from four biomass wastes of Rambutan fruit peel (B_{RtP}), Oil palm leaf (B_{OpL}), Jackfruit peel (B_{JfP}) and Sugar cane leaf (B_{ScL}). Both green and conventional (chemical) methods were applied for the synthesis of biochar supported iron nanoparticles. Four types of green synthesized biochar supported iron nanoparticles (INPs-B_{RtP}, INPs-B_{OpL}, INPs-B_{JfP} and INPs -B_{ScL} collectively named as INPs-B_g) were developed using four extracts of the four biomass wastes named as Rambutan fruit peel (E_{RtP}), Oil palm leaf (E_{OpL}), Jackfruit peel (E_{JfP}) and Sugar cane leaf (E_{ScL}), respectively. These extracts act as a green reducing mediator to reduce ferrous oxide (Fe(II)) to zerovalent iron (Fe^0), while chemical synthesized biochar supported iron nanoparticles (INPs-B_{Che}) were developed using sodium borohydride as a reducing agent. All samples of nanocomposites (INPs-B_{Che} and INPs-B_g) were characterized by field emission scanning electron microscopy (FESEM), energy dispersive spectroscopy (EDS), Fourier transform infrared spectroscopy (FTIR), BET surface area and X-ray diffraction (XRD). All samples of nanocomposites were applied for the removal of highly toxic six selected organochlorine pesticides (OCPs) named as *p,p'*-dichloro-diphenyl-trichloroethane (*p,p'*-DDT), *o,p'*- dichloro-diphenyl trichloroethane (*o,p'*-DDT), endosulfan I, aldrin, heptachlore and hexachlorobenzene from aqueous solution and oil palm plantation drainage (OPPD) water samples. Variable parameters including pH, dosage of adsorbent, initial concentration of adsorbate and time were studied. The equilibrium data of isotherm adsorption for OCPs on all

nanocomposites were fitted well to Langmuir isotherm. The kinetic isotherms were fitted first to Pseudo-second order adsorption model and then to Pseudo-first order reduction rate model for all types of nanocomposites. The removal percentage, adsorption capacity (mg/g) and reaction rate constant (k_{obs}) values of all types of nanocomposites for OCPs were found in the following order: INPs-B_{RtP} > INPs-B_{OpL} > INPs-B_{Che} > INPs-B_{JfP} and > INPs-B_{ScL}. The INPs-B_{RtP} nanocomposite successfully removed OCPs in OPPD water system as well. Nevertheless, the reactivity of INPs-B_{Che} nanocomposites decreased almost 2 folds after being aged in air for one month, whilst all green INPs-B_g nanocomposites remained almost same. The detected metabolites of OCPs in the treated water showed that OCPs degraded by reductive dechlorination process. The application of these as-prepared INPs-B_g nanocomposites could represent a potential functional material for adsorption and subsequent reduction of OCPs in aquatic system.

Keywords: Organochlorine pesticides, green approach, biochars, water pollution, removal.

APLIKASI BESI NANOPARTIKEL HIJAU BIOCHAR UNTUK PENYINGKIRAN RACUN SERANGGA ORGANOKLORINE YANG TERPILIH DARI AIR

ABSTRAK

Dalam kajian ini, novel nanopartikel besi hijau yang disokong pada biochar (INPs-B_g) telah disediakan untuk penyingkiran racun makhluk perosak organoklorin (OCPs) dari sistem air. Untuk tujuan ini, empat biochar disediakan dari empat biomas dari kulit buha Rambutan (B_{RtP}), daun kelapa Sawit (B_{OpL}), kulit buah Nangka (B_{JfP}) dan daun Tebu (B_{ScL}). Kaedah hijau dan konvensional (kimia) digunakan untuk sintesis nanopartikel besi yang disokong biochar. Empat jenis nanopartikel besi disokong biochar hijau (INPs-B_{RtP}, INPs-B_{OpL}, INPs-B_{JfP} dan INPs-B_{ScL} dinamakan sebagai INPs-B_g) telah dibangunkan dengan menggunakan empat ekstrak bahan buangan biomas dinamakan sebagai buah kulit rambutan (E_{RtP}), daun minyak kelapa sawit (E_{OpL}), kulit buah nangka (E_{JfP}) dan daun tebu (E_{ScL}). Ekstrak ini bertindak sebagai mediator untuk menurunkan oksida besi (Fe(II)) kepada besi zerovalen (Fe^0), manakala bahan kimia nanopartikel besi (sintesis biochar disokong kimia) telah dibangunkan menggunakan natrium borohidrida sebagai agen pengurangan. Semua sampel nanokomposit (INPs-B_{Che} dan INPs-B_g) dicirikan oleh mikroskop elektron pengimbasan pelepasan (FESEM), spektroskopi penyebaran tenaga (EDS), Transformasi spektroskopi inframerah (FTIR), permukaan permukaan BET dan difraksi sinar X (XRD). Semua sampel nanokomposit digunakan untuk menyingkirkan enam racun organik terpilih yang sangat toksik (OCPs) yang dinamakan sebagai *p,p'*-dichloro-diphenyl-trichloroethane (*p,p'*-DDT), *o,p'*- dichloro-diphenyl trichloroethane (*o,p'*-DDT), endosulfan I, aldrin, heptachlore dan hexachlorobenzene daripada larutan air dan saliran perladangan kelapa sawit (OPPD). Parameter ubahsuaian termasuk pH, dos penyerap, kepekatan awal penyerap dan masa dan. Data keseimbangan penjerapan isotherm untuk OCP pada semua nanokomposit dipadankan dengan baik kepada isotherm

Langmuir. Isotherms kinetik dipadankan terlebih dahulu untuk model penjerapan urutan Pseudo-kedua dan kemudian kepada model kadar pengurangan tertib Pseudo-first untuk semua jenis nanokomposit. Peratusan penyingkiran, nilai kapasiti penjerapan (mg/g) dan kadar tindak balas kadar tindak balas (k_{obs}) bagi semua jenis nanokomposit untuk OCP didapati dalam susunan berikut: INPs-B_{Che} > INPs-B_{JfP} dan > INPs -B_{ScL}. Nanokomposit INPs-B_{RtP} berjaya menyingkirkan OCP dalam sistem air OPPD juga. Walau bagaimanapun, kereaktifan INPs-B_{Che} nanokomposit menurun 2 kali ganda selepas terdedeh di udara selama satu bulan, manakala semua INPs-B_g nanokomposit hijau kekal hampir sama. Metabolit OCP yang dikesan di dalam air yang dirawat menunjukkan bahawa OCPs direndahkan oleh proses dechlorination reduktif. Penggunaan nanokomposit INPs-B_g seperti ini boleh mewakili bahan yang berpotensi berfungsi untuk penjerapan dan penurunan pengurangan OCP dalam sistem akuatik.

Kata kunci: Racun perosak organoklorin, pendekatan hijau, biochar, pencemaran air, penyingkiran.

ACKNOWLEDGEMENTS

First of all, I would like to express my gratefulness to The Almighty God for all his blessings and wishes for accomplishing this work.

I wish to express my deep sense of gratitude and heartfelt thanks to my research supervisor **Dr. Ahmad Farid Bin Abu Bakar**, for his most valuable guidance, whole hearted support and encouragement in accomplishing the present investigation successfully for their valuable suggestions throughout my research work. I am also grateful for all the expertise, intellectual concern and encouragement he devoted in helping me over many obstacles to complete this dissertation.

I would like to express my sincere gratitude to my supervisor **Dr. Nor Kartini Binti Abu Bakar** for her uncompromising guidance, advice, moral support and persistent motivation throughout the period of my study. It is my honor to have such a great opportunity to work in his fascinating research group, which provided a critically scientific and familiar working environment. I am also grateful for all the expertise, intellectual concern and encouragement he devoted in helping me over many obstacles to complete this dissertation.

I wish to make special acknowledgement to **Prof Dato, Dr. Mohd Jamil Bin Maah** for his overall help and lab support. Thanks, him to allow me to have the full access to enter and use the equipment in their laboratories. I am also grateful for the technical support, valuable comments and fruitful discussions in my experiments for their valuable suggestions throughout my research work. It is my honor to have such a great opportunity to work in his fascinating research group, which provided a critically scientific and familiar working environment.

I am also grateful to all the **Faculty Members** of the Department of Geology and Department of Chemistry, University of Malaya, Malaysia for their prompt help and words of encouragement at various phases of the work.

A large debt of gratitude is owed to all my colleagues from my research group. These talented fellows created a friendly and wonderful study atmosphere, which are treasures to cherish in my life.

Last, but by no means least, the special gratitude is dedicated to my parents for being a supportive and loving family, bringing happiness into my life. Particularly, my deep gratitude goes to my mother, for her constant source of love, unequivocal support, persistence and unwavering encouragement to accomplish this challenging career and my pursuits in life. **Dr. Aisha Siddiqa** deserves special thanks for being such a great friend, surrounded me with her generous support and encouragement.

Finally, I would like to acknowledge my brother **Dr. Syed Athar Ali Shah** from the bottom of my heart, for helping, encouraging and inspiring me throughout my research work and thesis writing toward the completion of my degree. Without his dedication, none of this work would truly have been delivered.

TABLE OF CONTENTS

LIST OF FIGURES

LIST OF TABLES

LIST OF SYMBOLS AND ABBREVIATIONS

°A	:	Angstrom units
B	:	Biochar
θ	:	Theta
μm	:	micrometer
μL	:	Microliter
BET	:	Brunauer, Emmett, Teller
B_{RtP}	:	Rambutan fruit peel biochar
B_{OpL}	:	Oil palm leaf biochar
B_{JfP}	:	Jack fruit peel biochar
B_{ScL}	:	Sugar cane leaf biochar B_{ScL}
cm^{-1}	:	Per centimeter
E_{RtP}	:	Extract of Rambutan fruit peel
E_{OpL}	:	Extract of Oil palm leaf
E_{JfP}	:	Extract of Jack fruit peel
E_{ScL}	:	Extract of Sugar cane leaf
EDS	:	Energy dispersive spectroscopy
Fe^0	:	Zerovalent iron
Fe^{2+}	:	Ferous ion
Fe^{3+}	:	Ferric ion
$FeSO_4$	:	Ferrous sulfate
EL-INPs	:	Eucalyptus leaf synthesized iron nanoparticles
FESEM	:	Field emission scanning electron microscopy
FTIR	:	Fourier transform infrared spectroscopy
g/L	:	gram per liter

g/mg	:	gram per milligram
HCB	:	Hexachlorobenzene
ID	:	Inner diameter
INPs	:	Iron nanoparticles
INPs-B_{Che}	:	Chemical synthesized biochar supported iron nanoparticles
INPs-B_{RtP}	:	Iron nanoparticles supported on rambutan peel biochar using rambutan peel extract
INPs-B_{OpL}	:	Iron nanoparticles supported on oil palm leaf biochar using oil palm leaf extract
INPs-B_{JfP}	:	Iron nanoparticles supported on jackfruit peel biochar using jackfruit peel extract
INPs-B_{ScL}	:	Iron nanoparticles supported on sugar cane leaf biochar using sugar cane leaf extract
JfP	:	Jackfruit peel
J/mole	:	Joule per mole
K	:	Kelvin scale of temperature
Kg	:	Kilogram
Kv	:	Kilovolt
k_{obs}	:	Observed reaction rate constant
INPs	:	Iron nanoparticles
L	:	Liter
ma	:	Milli ampere
mg	:	milligram
mg/g	:	milligram per gram
mg/L	:	milligram per liter
MHz	:	Millihertz
mL min^{-1}	:	Milliliter per minute
mm	:	Millimeter
Mol/L	:	Moles per liter

N_2	:	Nitrogen
$NaBH_4$	:	Sodium borohydride
nm	:	nano metre
nZVI	:	Nano zero valent iron
OD	:	Outer diameter
OpL	:	Oil palm leaf
OPPD	:	Oil palm plantation drainage
o,p'-DDT	:	*o,p'*- dichloro-diphenyl trichloroethane
p	:	Actual vapour pressure
p^s	:	Saturated vapour
p/p^s	:	Relative vapour pressure
PCBs	:	Pentachlorobiphenyls
POPs	:	Persistent organic pollutants
qHg	:	Mercury density
r_p	:	Pore radius
rpm	:	rotations per minute
RtP	:	Rambutan peel
SEM	:	Scanning electron microscope
ScL	:	Sugar cane leaf
W	:	Watt
XRD	:	X-Ray Diffraction
V_{micro}	:	Micropore Volume
v/v	:	Volume by volume
V_{Pc}	:	Total pore volume
ZVI	:	Zerovalent iron

LIST OF APPENDICES

CHAPTER 1: INTRODUCTION

1.1 Water Pollution

The complexity and level of water pollution worldwide has reached unparalleled levels in such a way that the intricacy of the problem appears persistent. However, there is an inclusive range of different pollutant species, the US environmental protection agency divides most of the commonly found pollutants in surface water into six categories (USEPA, 2007). These pollutants have been described in Table 1.1.

Table 1.1: Pollutants categorized by US environmental protection agency (USEPA, 2007).

Types of Pollutants	Examples
Inorganic compounds	Oxoanions (chromates, arsenates), toxic heavy metal ions (e.g. mercury, chromium, lead, cadmium, copper) and nonmetal anions such as fluoride
Organic compounds	Dioxins, benzene, 1, 2 dichloroethene (1, 2-DCE), polyaromatic hydrocarbons, trichloroethylene (TCE), tetrachloroethene (PCE), polychlorinated biphenyls (PCBs) and organochlorine pesticides (OCPs) etc.
Disinfection byproducts	Haloacetic acids and trihalomethanes
Disinfectants	chloramines, chlorine (as *Cl*) and chlorine dioxide
Radionuclides	Atoms with unstable potentially radioactive nuclei, such as promethium-147, phosphorous-32 and americium-243.
Microorganisms	Fungi, bacteria and archaea, but not prions nor viruses.

Specifically, the worldwide existence of organochlorine compounds such as OCPs, retains a potential risk to terrestrial and aquatic life (Wang & Zhang, 1997). "Organochlorine pesticides (OCPs) are the chlorinated hydrocarbons with very strong bonds between their chlorine and carbon components". OCPs have consumed for long duration throughout the world to control pests in agriculture (Li, 2006). Owing to their persistence, hydrophobic in nature, bioaccumulation, biomagnification in food chain and existence of chlorine atoms mark OCPs potentially ecotoxic to human and animals (Behrooz et al., 2009). Exposure to these OCPs may damage the central nervous system, respiratory system disorders, DNA damage in blood cells and interference of production and breakdown of endogenous hormones (Remor et al., 2009). With regard to its

persistence and toxicity, production and usage of OCPs was restricted in many developing countries during nineteen seventies and records in the dirty dozen list of persistent organic pollutants (POPs) recognized by dint of the Stockholm Convention on POPs. Estimated half-life values of OCPs have been estimated ranging from 4 to 30 years (Aktar et al., 2009). Though, application of these OCPs comprising hexachlorocyclobenzene, aldrin, endosulfan, DDT (1,1,1-trichloro-2,2-bis(p chlorophenyl)ethane), and heptachlor were banned in most developing countries three decades ago, these are still being used in some countries in a limited way and their residues and metabolites have been identified in the terrestrial and water system (Guo et al. 2014). The pollution by theses OCPs in our water system is a main concern for the environment and human health.

1.2 Iron Nanotechnology

Nanotechnology seems to be the way out to the look for an effective, financial and environmentally friendly technique to resolve or decrease this issue. The application of nanotechnology is very broad. This technology uses nano dimension particles with approximately 1-100 nm size and has even now found applicable in several fields of daily life, e.g. in engineering, electronics, chemical industry, health as well as military industries, cosmetics optical, and automotive. Iron nanoparticles (INPs) can be applied as in situ applications (recirculation by injection/extraction wells, direct push injections, pneumatic fracturing) or on-site reactors for example, pump-and-treat systems (Grieger et al., 2012). The INPs have considerably higher accessible reactive surface areas, owing to their nano-sized dimensions, (for example, up to four times of degree) (Macé et al., 2006) in comparison iron particles having large dimensions, which consequently boosts the breakdown reactions of pollutant (Crane and Scott, 2012; Lin et al., 2008). The core-shell structure of iron nanoparticles comprises of zero-valent iron core (85 %) whereas the shell generally comprises of oxyhydroxides and iron oxides. Hence, INPs reveal

properties of both an adsorbent and a reducing agent (Cerník et al., 2010). The application of INPs is a very favorable way for eliminating organochlorinated pesticides.

In recent times, nanotechnology has presented a novel generation to combat the most challenging environmental cleanup problems. The INPs have been successfully tested intended for the eradication of organochlorine contaminants including OCPs (El-Temsah et al., 2016; Huang et al., 2014; Shih et al., 2011; Pillai and Kottekottil, 2016; Chen et al., 2016; Khan et al., 2015; Saif et al., 2016; Gao et al., 2015; Wang et al., 2015; Simkovik et al., 2015; Dien et al., 2013; Vodyanitskii et al., 2014; Su et al., 2012). In order to prevent their agglomeration in water, surface modified INPs have been stabilized by adsorption of hydrophilic or amphiphilic organic species on INPs surface, such as water-soluble starches (He and Zhao, 2005, Allabaksh et al., 2010), surfactants (Wei et al., 2012, Wang et al., 2017) and polymers (Chen et al., 2014).

Alternatively, INPs could be effectively immobilized onto a compact medium support, for instance hydrophilic carbon particles (Kumar et al., 2017; Li et al., 2017; Huang and Shi, 2008). Owing to their exceptionally large surface area, and large micro-porosity (Selvaraju and Bakar, 2017; Mackenzie et al., 2008; Laura et al., 2008), carbon-based prevent the agglomeration of INPs (Ambashta et al., 2010; Kroschwitz, 1993). Biochar is a carbonaceous, solid byproduct resulting after pyrolysis of biomass under N_2 and low temperature conditions (Agrafioti et al., 2014). Biochar has been studied for its potential as a support for environmental applications, as a result of its micro porous structure, large surface area, unique surface properties and relatively low cost (Femando et al., 2015; Devi et al., 2014). Therefore, much attention has been paid for the preparation of biochar supported INPs using Fe^{3+} salts along with sodium borohydride or potassium borohydride (Wang et al., 2014C). Nevertheless, sodium

borohydride and potassium borohydride have several limitations and drawbacks such as toxic, corrosive, flammable and highly expensive.

A variety of natural origins for instance plant surfactants (Liu et al., 2012), vitamins (Murgueitio et al., 2016), amino acids (Siskova et al., 2013), oleic acid (Kumar et al., 2014), flavonoids (Daniel et al., 2013) and polyphenols (Wang, 2013) have emerged in the last few years as an alternative to these well-established chemicals for green synthesis of INPs. Some studies used agrowastes as low-cost bioreducing agents. Till now most of the INPs have been synthesized using agrowaste extracts as low-cost bioreducing agents such as Nettle and thyme leaf (Leili et al., 2018), *Calotropis gigantea* (CG) flower (Sravanthi et al., 2018), banana peel (Sunardi et al., 2017), coffee (Pattanayak et al., 2013) green tea leaf (Wang et al., 2014B; Borja et al., 2015) and eucalyptus leaf (Wang et al., 2014B; Nang et al, 2014), pomegranate leaf (Rao et al., 2013), plantain peel (Venkateswarlu et al., 2013), orange peel (Lopez-Tellez et al., 2013), banana peel ash (Thakur and Narak, 2014). These green INPs have been applied for the remediation of nitrate, heavy metals, dyes, antibiotics and chlorinated hydrocarbon.

The synthesis of green INPs with polymeric support has been done by several researchers and has been applied for the remediation of heavy metals (Martínez-Cabanas, et al., 2016; Prasad et al., 2014; Tandaon et al., 2013) and chlorinated hydrocarbon (TCE) (Kuang et al., 2013; Smuleac et al., 2011; Shahwan et al., 2011; He and Zhao, 2005). However, a little work is known about green synthesis of INPs on carbonaceous support such as biochar and their application for the removal of highly complexed OCP compounds

Peels of rambutan and jackfruit and leaves of oil palm and sugar cane are abundant biomass wastes in Malaysia. They are disposed as wastes. To make these agricultural byproducts more useful, their use in preparation of biochar and biochar supported green

INPs using extract from these biomass wastes is suggested. To the best of our knowledge, there are still no reports on development of these novel engineered biochar supported green iron naoparticles using these plant extracts as a reducing agent and removal of highly complex OCP compounds from water samples using green INPs. Therefore, our latest efforts were focused towards the directly incorporate and disperse the green INPs in the pores and on surface of these biomass waste derived biochar involving a powerful, cost-effective and environmentally eco-friendly above-mentioned plant extracts as a reducing mediator consequently taking advantage of the richness of polyphenols of these biomass wastes.

1.3 Problem Statement

Organochlorine pesticides (OCPs), creating from a range of human actions (industrial and agronomic), are highly poisonous and complex chemicals that resist biological and chemical breakdown in the atmosphere. These are known as highly toxic contaminants for animal and human health because of their persistence, hydrophobic in nature, lipophilic in nature, bioaccumulation, biomagnification in food chain and existence of chlorine atoms causes these OCPs to be potentially ecotoxic to human and animals. Major health problems cauused by OCPs include the central nervous system disorder, DNA damage, cancer, respiratory system disorder, immunological disorder and disruption of endocrine system (Remor et al., 2009). Although, application of these OCPs including hexachlorocyclobenzene, aldrin, endosulfan, DDT (1,1,1-trichloro-2,2-bis(p chlorophenyl)ethane) and heptachlor was restricted in most developing countries, the remaining of these toxic compounds are still present in our aquatic environment (Guo et al., 2014). Due to their adverse health effects and related environmental threats even at low concentration, remediation of these OCPs in aquatic system is a major concern.

1.4 Aim of the Research

The aim of the research is:

- To assess the removal of selected OCPs from water using green synthesized nanocomposites.

1.5 Objectives of the Research

The objectives of the research are:

- To synthesize and characterize a chemical mediated nanocomposite (INPs-B_{Che}) and four green nanocomposites (INPs-B_{RtP}, INPs-B_{OpL}, INPs-B_{JfP}, INPs-B_{ScL}) prepared by unique green method using biomass wastes of rambutan peel, jackfruit peel, oil pal leaf and sugar cane leaf.
- To evaluate the best optimized conditions such as pH, adsorbent dose, adsorbate dose and time for maximum removal of OCPs from synthetic aqueous solution and OPPD samples using the synthesized nanocomposites.
- To investigate the removal efficiency, applicability of isotherm models and kinetic models of OCPs in several water matrices using the fresh and aged nanocomposites synthesized.

1.6 Hypothesis of the Research

Hypothesis of the research are:

- If extracts obtained from peel waste of rambutan and jackfruit and leaf waste of oil palm and sugar are used as a reducing agent in place of toxic chemical sodium borohydride then biochar supported iron nanoparticles can be successfully synthesized.

- If polyphenol content is higher in the extract then green nanocomposite can be synthesized with high wt% of iron which in turn will give the higher removal efficiency of OCPs in several water systems and vice versa .
- If chemical mediated nanocomposite (INPs-B_{Che}) and four green nanocomposites (INPs-B_{RtP}, INPs-B_{OpL}, INPs-B_{JfP}, INPs-B_{ScL}) are aged in air then reactivity of green nanocomposite with OCPs will not affected while that of INPs-B_{Che} nanocomposite will change.

1.7 Scope of this Research

Various removal methods for OCPs have been proposed from time to time (Brooks, 1980; Kusvuran & Erbatur, 2004). However, all these methods have some drawbacks and were not able for reduction of OCP compounds from water system (Barbusinski, 2009). During the last few decades, attention has been shifted towards the nanotechnology (Shih et al., 2009; Lowry & Johnson, 2004), which has emerged as one of the widely accepted methods for the simultaneous adsorption and reduction of OCPs. In order to improve the removal proficiency of OCPs, INPs have been supported on solid matrix such as biochar.

One of the major contests related to the synthesis of biochar supported INPs nanocomposites is its cost-effectiveness and environmentally friendly. Literature review reveals that a large number of chemical mediated biochar supported INPs have been synthesized using toxic and expensive chemicals as a reducing agent for the eradication of organochlorine compounds from water system (El-Temsah et al., 2016; Huang et al., 2014; Pillai and Kottekottil, 2016; Chen et al., 2016; Khan et al., 2015; Gao et al., 2015; Wang et al., 2015; Simkovik et al., 2015; Dien et al., 2013; Vodyanitskii et al., 2014). A detailed study of the synthesis of green mediated biochar supported INPs using fruit peel waste of rambutan and jackfruit and leaf waste of oil palm and sugar cane has, not to the best of our knowledge, been published. Hence, an attempt was made in this work to

synthesize a series of biochar supported green INPs from fruit peel waste of rambutan and jackfruit and leaf waste of oil palm and sugar cane with varying morphology, wt % of iron and surface area using various plant extracts. An evaluation of these as prepared novel green INPs-B_g nanocomposites used for the simultaneous adsorption and reduction six OCPs was done. Adsorption isotherm and kinetic isotherm parameters were also evaluated.

CHAPTER 2: LITERATURE REVIEW

2.1 Organochlorine Pesticides (OCPs)

Water contamination is a well-known concern all over the world owing to human activities such as industrials, agricultural and non-agricultural pollution. A wide range of toxic organic compounds have been contaminated thousands of sites worldwide. Specifically, organochlorine compounds, such as organochlorine pesticides (OCPs), are recognized as the significant contaminants in water system, because of their substantial human carcinogenicity (Cao et al., 2011). Organochlorine pesticides (OCPs) are chemically produced pesticides which include DDT, heptachlore, dieldrin, endosulfan, hexachlorobenzene, aldrin, mirex, dicofol and etc. Many types were widely used in agriculture and mosquito controll throughout the 1950's and 1960's until their use was banned in developing countries of Asia since 1970's (Aktar et al., 2009). These pollutants were discharged to the water system (surface water and groundwater) as unwanted substances from industrial manufacture or from materials known as fungicides, herbicides and insecticides which have been practiced in agricultural and forestry for several decades. The extent of potentially harmful substances inflowing the environment is increasing day by day. These pollutants are persistent in the ecosystem. They can be intake by animal, plants, and human being as well and bioaccumulate in their body. Animals and humans are exposed to them generally by way of their food, prenatally or occupationally. Above 90% exposure comes from animal foodstuffs because of biomagnification through the food chain and bioaccumulation in fat tissues (Ritter et al., 2007). Originally, they were used as pesticides in terrestrial ecosystem. However, they are flushed away from terrestrial ecosystems through rivers and end up in marine ecosystems. Pollution of aquatic system by organochlorine pesticides has been a worldwide environmental challenge and cost effective removal practices have been searching for several years.

2.2 Nanomaterial Remediation Technology

With the implication of developing nanotechnique, iron nanoparticle represents a novel development of removal technique to eradicate the persistent organochlorine pollutants, for instance PCE, TCE, PCBs and OCPs, in water and sediment. Compared to the conventional techniques implemented, nano zerovalent iron technology has a great potential in degradation and elimination of organochlorine contaminants more rapid and efficiently, thus making it economically feasible solution. There are several methods for the synthesis of iron-containing nanoparticles (Figure 2.1).

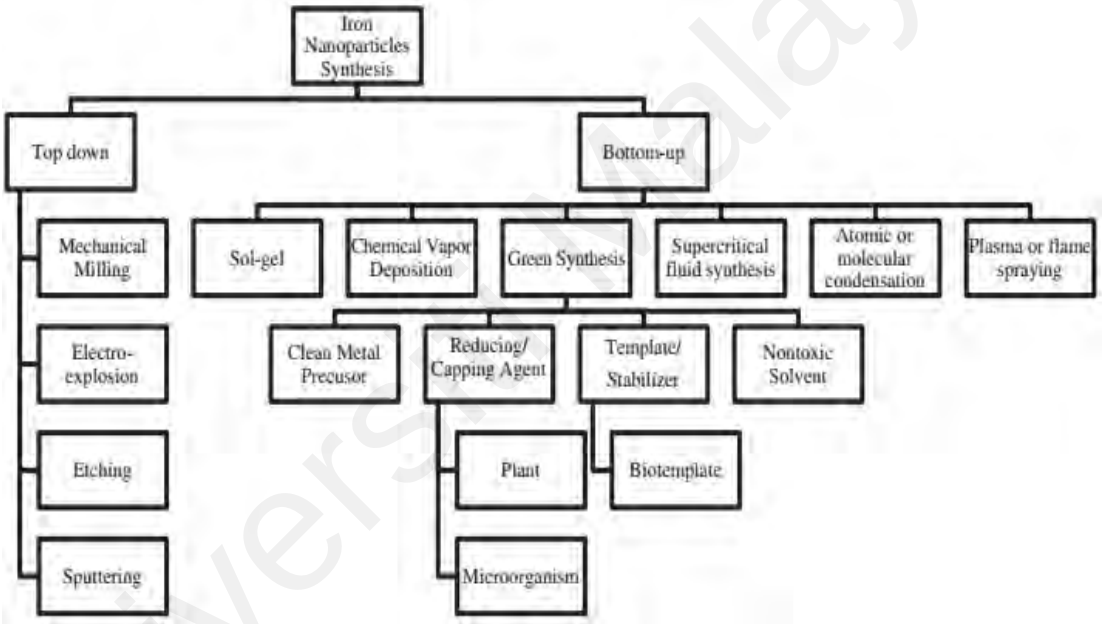

Figure 2.1: A number of methods for the synthesis of iron-containing nanoparticles.

2.2.1 Synthesis of Iron Nanoparticles (INPs)

2.2.1.1 Physical and Chemical Method

So far, various approaches have been settled for the formation of metallic nanoparticles to make different forms and dimensions. These synthetic approaches could be categorized into two main classes: either a physical synthesis method or a chemical fabrication technique. The physical synthesis techniques consist of: plastic deformation, inert gas condensation, ultrasound shot peening and high-energy ball milling (Luborsky, 1957; Lin

& Samia, 2006). Conversely, the chemical synthesis techniques involve controlled chemical co-precipitation, reverse micelle, pulse electro-deposition liquid flame spray, liquid-phase reduction and chemical vapor condensation (Laurent et al., 2008; Wu et al., 2011; ElBayoumi et al., 2010; Ling & Hyeon, 2013).

Predominently, there are two approaches to synthesize the nano zerovalent iron particles, divided into "top-down" and "bottom-up" methodologies (Iravani et al., 2011)."Top-down" discusses the synthesis of iron nanoparticles by mechanical and/or chemical phases comprising milling, machining or etching. It begins with an appropriate bulk substance of enormous dimension (e.g. granular or microscale), and then breaks them into small fragments. For the later method of "bottom-up", it involves the "grown" of nanostructures atom-by-atom or molecule-by-molecule by chemical method or biological method, self-assembling and positional assembling (Yabe & Oliveria, 2003). Conversely, for "top-down" technique, wide-ranging size, different form or geometry, and contaminations from the milling medium are the key elements of concern for the final products. Thus, a more useful method of "bottom-up", synthesis of nano zerovalent iron particles on a commercial scale has great potentials for the consumption in the establishment of technologically innovative and valuable substances.

Owing to its easiness and output, liquid-phase reduction method is most comprehensively examined and extensively applied in the environmental clean-up. The basic concept of liquid-phase reduction, denoting to borohydride reduction, is to introduce a strong reluctant into a metallic ion solution to reduce it into nano sized metal particles. For instance, the most common technique to synthesize the nano zerovalent iron particles is by reduction of ferric (Fe(III)) (Liu & Huang, 2003) or ferrous (Fe(II)) ions (Miyaka & Suzukit, 1993) salt in the solution with sodium borohydride ($NaBH_4$) at room temperature (Equation 2.1 and Equation 2.2):

$$4Fe^{3+} + 3BH_4^- + 9H_2O \rightarrow 4Fe^0 \downarrow + 3H_2BO_3^- + 12H^+ + 6H_2$$ **Equation 2.1**

$$2Fe^{2+} + BH_4^- + 3H_2O \rightarrow 2Fe^0 \downarrow + H_2BO_3^- + 4H^+ + 2H_2$$ **Equation 2.2**

A main benefit of this technique is its easiness that requires merely two most commonly used reagents without using any distinct apparatus or tools. The process starts with gradually adding newly prepared solution of ferric chloride ($FeCl_3$) or ferrous sulfate ($FeSO_4$) solution into a reaction flask having $NaBH_4$ solution (Council, 2010) or adding a solution $NaBH_4$ into a solution of ferrous sulfate or ferric chloride (Raichur & Panvekar, 2002). The procedure is generally performed under nitrogen atmosphere to evade oxidation of the metallic iron surface.

Application of stabilizer such as a soluble surfactant or polymer to stop aggregation of metallic nanoparticles is a common practice. This stabilizer can be added at any one of two stages, either before the formation of aggregates, or after agglomerations have been automatically shattered apart. Inter-particle electrostatic and steric repulsions have been created in order to compensate the magnetic attractive and inherent Van der Waals forces causing the nanoparticles to agglomerate (Nadagouda, 2009). Iron nano zerovaent particles typically display a core-shell structure with zero-valent iron enclosed by a mixed valent (Fe^{2+} and Fe^{3+}) oxide shell. A variety of stabilizers can be selected to successfully impede oxidation and of the iron cores and agglomeration of these nanoparticles. Certain organic specimens comprise polyacrylic acid, methoxyethoxyethoxyacetic acid (MEEA) and polyethylene glycol (PEG) (Kharisov et al., 2012).

2.2.1.2 Green Method

The chemical methods have several restrictions and drawbacks; the physical methods are usually costly, high energy cost and involve particular and expensive equipment while the chemical techniques have some drawbacks associated with safety problems because

of the harmfulness of sodium borohydride that generates the of igneous hydrogen gas throughout the process, environmental pollution (Li et al., 2006), and the potential to produce large sized agglomerates, very fast and at a high extent, and consequently have a less reactivity and breakdown efficiency. In particular, the reducing agents, capping agents, templates, and solvents used are considered hazardous, posing signifcant environmental and biological risks (Nadagouda, et al., 2010). These drawbaks originated inducements to integrate green chemistry principles, for instance the selection of 'greener' reducing agents or solvents and the consumption of suitable capping agents (Hoag et al., 2009). Hence, in the last few years, a greener approach for the development of INPs has been established. In this approach a variety of natural sources such as plant surfactants (Liu et al., 2012), vitamins (Murgueitio et al., 2016), aminoacids (Siskova et al., 2013), oleic acid (Kumar et al., 2014), flavonoids (Daniel et al., 2013) and polyphenols (Wang, 2014) have emerged in the last few years as an alternative to these well-established chemicals for the green synthesis of INPs. Some authors have used agrowastes as low-cost bioreducing agents. Till now most of the INPs have been synthesized using agrowastes as low-cost bioreducing agents such as coffee (Pattanayak et al., 2013) green tea leaf (Wang et al., 2014B; Borja et al., 2015) and eucalyptus leaf (Wang et al., 2014A; Nang et al, 2014), pomegranate leaf (Rao et al., 2013), orange peel (Lopez-Tellez et al., 2013), plantain peel (Venkateswarlu et al., 2013), banana peel ash (Thakur and Narak, 2014), and in most cases green tea leaves (Chrysochoou et al., 2012; Valle-Orta et al., 2008) with high antioxidant capacities are used. The compounds present in these extracts react with iron(III) in solution to form the INPs (Nadagouda et al., 2010). The main advantages of this method are: i) the lower toxicity of the used reducing agent compared with borohydride; ii) the capping ability that the polyphenol extract matrix induces on the INPs, prolonging their reactivity (Nadagouda et al., 2010); iii) the valorization of natural products that, in some cases, are considered wastes or do not have

any added value; and iv) the fact that the extracts have high water solubilities, low toxicities and can act as a nutrient source which can enhance complementary biodegradation (Hoag et al., 2009). Nadagouda et al. (2010) compared the INPs produced using the green and borohydride methods and observed that some of the green INPs were found to be nontoxic when compared with control samples prepared using the conventional borohydride reduction protocols.

Synthesis of green iron nanoparticles by a single-step method was first suggested by Hoag et al. (2009) and Nadagouda et al. (2009). They proposed that the polyphenols detected in green tea can be not only used as a reducing mediator for synthesis of INPs but also as a stabilizing agent by coating nanoparticles surface before their agglomeration. The most abundant of the polyphenols are catechins, other groups present are flavanols, flavanones, phenolic acids and glycosides (Pan et al., 2003). These polyphenols are soluble in various solvents such as water, ethanol, methanol and acetone. The formation of INPs using polyphenols occurs through the binding of a catecholate or gallate ligand to Fe^{3+} forming semiquinone which reduces Fe^{3+} to Fe^{2+} with the formation of quinone species (Hider et al., 2001). Though there is no definite explanation for the formation of zero valent Fe^0 (ZVI), there are speculations that this is due to the reduction potential of catechin which is sufficient to reduce Fe^{2+} to Fe^0 (Smuleac et al., 2011). Mystrioti et al, (2012) suggested the overall mechanism for the formation of Fe^0 using polyphenols as shown in Equation 2.3 where Ar represents the aromatic ring and n is the number of groups oxidised by Fe^{3+}.

$$nFe^{3+} + 3(Ar - OH)_n \rightarrow nFe^0 + 3n(Ar = O) + 3nH^+$$

Equation 2.3

2.2.2 Polyphenols Properties and Reaction with Fe^0

The structural properties of polyphenols have been studied deeply in biochemistry and food chemistry. Polyphenols are extremely important components of plants because of their antimicrobial, antiviral, and anti-inflammatory properties as well as their antioxidant activity (Ignat et al., 2011). This last property is essential in the INPs production process because the antioxidant compounds can reduce iron(III) ions producing zero-valent iron. According to Hoag et al. (2009), the reaction between iron(III) ions and extracts with high polyphenol contents produces INPs by the reduction process.

Tree leaves and fruit peels have high polyphenol contents as well as eminent antioxidant ability (Khan et al., 2015). It is essential to find the lowest quantity of leaves that give the polyphenol rich extract so as to optimize the whole process. Using a range of extraction temperature and contact time and various composition ratio of biomass to water (mass:solvent) were tested in order to detect best optimized ratio and condition for more rich extraction. For most of the peels and leaves, 20 min contact time and 80 °C were set up as most favorable states for the efficient polyphenol extraction. Nevertheless, a wide range was analyzed regarding the mass:volume composition ratio (Machado et al., 2013). A strong positive correlation was occured between the mass:volume ratio and the antioxidant capacity for several leaves (apple, oak, strawberry, raspberry, kiwi, lemon and vine). For plum tree leaves, eucalyptus and avocado, a slight deviance from linearity was observed as mass:volume ratio was reached more than 2.4. In the same way, orange, walnut, green tea, quince and olive tree leaves exhibited the reduction of antioxidant capacity by rising the mass:volume ratio higher than 0.9 (Machado et al., 2013). Most of the studies observed that water usually exhibits higher extraction proficiencies for flavolanic and phenolic compounds from vegetation compared to ethanol (Kong et al., 2012; Zhang et al., 2011).

2.3 Structure and Characterization of INPs

2.3.1 Structure of INPs

Usually, INPs displays a core-shell configuration. The inner core is comprised of metallic iron or zero-valent iron whereas the outer shell consists of mixed valence (e.g. Fe(II) or Fe(III) oxide shel whichl is developed by oxidation of the metallic ions, as shown in Figure 2.2 (Li & Daniel, 2006).

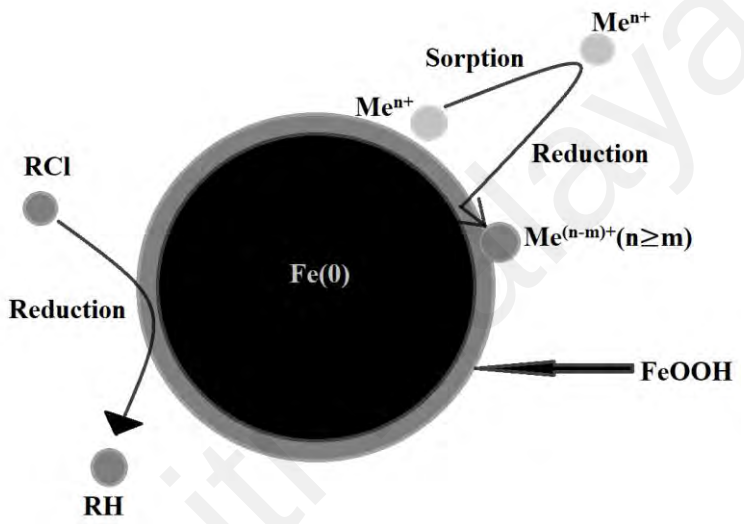

Figure 2.2: Core-shell model of INPs (Li et al., 2006).

Ambient environment is a most favorable condition for the reactivity of INPs with water and its functions as an exceptional electron donor that contributes to make it a useful remediation substance (Stumm et al., 1996). Environmental organic contaminants can be reduced by the zero-valent iron nanoparticles developing core. In the meantime, INPs are oxidized and generate outer shell consisting of iron oxides/hydroxides which make available sites for the generation of chemical complex and shelters INPs from further oxidation.

Characteristics of INPs count on their production and synthesis procedure and can be categorized by a number of techniques and devices such as scanning electron microscope (SEM), TEM, Fourier emission scanning electron microscope (FESEM), EDX, Brunauer-Emmett-Teller isotherm (BET) measurement, powder X-ray diffraction (XRD) and FTIR

for green INPs. These appliances assist to measure the characteristics of particles such as their morphology/shape, specific surface area and particle size, element composition and functional groups. Wang et al, (2014) used FESEM in order to investigate the morphology of INPs synthesized by green method using green tea (GT) and eucalyptus leaf (EL) extracts for the reduction of $FeSO_4$. FESEM images of fresh green tea, GT-INPs (Figure. 2.3a) and eucalyptus leaf, EL-INPs (Figure. 2.3c) revealed that they are both spherical shaped nanoparticles with a diameter ranging from 20 to 80 nm.

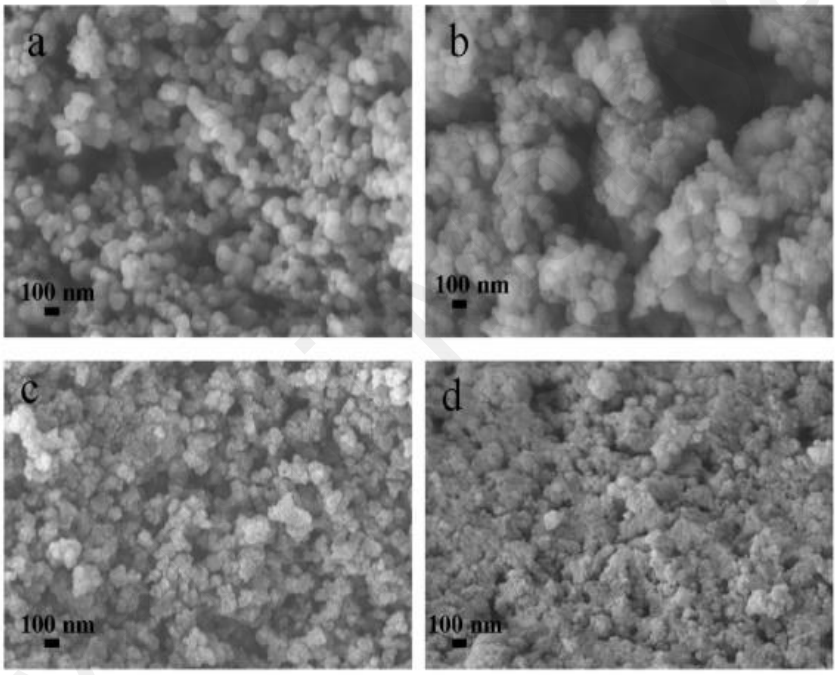

Figure 2.3: FESEM images of the green synthesized materials (a) GT-INPs, (b) GT-INPs after reaction, (c) EL-INPs, (d) EL-INPs after reaction (Wang et al., 2014B)

2.4 Reactivity of INPs with Organochlorine Compounds

Nano iron particle has been documented as an exceptional electron donor, irrespective of their particles dimension it is highly reacted equally to dissolved oxygen and oxygenated water (Zhang et al., 2011). Fe^0 reveals a strong affinity to gradually oxidize to ferrous irons ($Fe^{2+)}$ and electrons are released in the surroundings consistent with the subsequent oxidation half reaction, as shown in Equation 2.4:

$$Fe^0_{(s)} \rightarrow Fe^{2+}_{(aq)} + 2e^-_{(aq)} \qquad \textbf{Equation 2.4}$$

In the subsurface environment, water is the major electron acceptors and to some level remaining dissolved oxygen (DO) (Liu et al., 2005).

$$Fe^0_{(s)} + 2H_2O_{(aq)} \rightarrow Fe^{2+}_{(aq)} + H_{2(g)} + 2OH^-_{(aq)} \quad \textbf{Equation 2.5}$$

$$Fe^0_{(s)} + O_2 + 2H_2O_{(aq)} \rightarrow Fe^{2+}_{(aq)} + 4OH^-_{(aq)} \quad \textbf{Equation 2.6}$$

Fe^0 particles readily react with water and dissolved oxygen to generate Fe^{2+} and produce electrons in both anaerobic and aerobic conditions (Equation 2.5 and 2.6). These electrons thus can possibly conduct a range of reactions that result in the conversion of target chlorine containing complexes. Generally, three possible conversion mechanisms are suggested throughout the reactivity INPs (Cheng & Wu, 2000):

- Direct reduction at the metal surface: direct transfer of electrons from the iron metal to chlorinated organic molecules adsorbed on the metal surface, leading to the generation of chloride ions and production of hydrocarbons;
- Reduction by ferrous ions: reduction by the Fe^{2+}, which outcomes from oxidization of the metal;
- Catalyze hydrogenolysis by H_2 that is produced by reduction of H_2O all through anaerobic oxidization: hydrogenation of the chlorinated organic compounds with adsorbed hydrogen formed all through metal oxidization by water, wherein the metal works as a catalyst (Lin et al., 2004) Most researchers support the dechlorination procedure by means of electron transfer mechanism, where the electrons transfer from the metal to the chlorinated compounds (Cheng & Wu, 2000). It is proposed that noxious polychlorinated organic pollutants (for instance, OCPs) would be reductively dechlorinated to principally less toxic complex with fewer chlorine substitutions. The chemical reduction of polychlorinated biphenyls (PCB) has also been demonstrated (Wang and Zhang, 1997). In an experiment,

performed by Shih et al, (2009) it was observed that hexachlorobenzene (HCB) reductively reduced to pentachlorobenzene (PCB) by INPs subsequently losing single atom of chloride (Cheng & Wu, 2000). A comprehensive organochlorine compound, symbolized as R-Cl, as a specimen, would be reduced in line with the subsequent reaction mechanism (Dorathi and Kandasamy, 2012; Deng et al., 1999).

$$Fe^0 + RCl + H^+ \rightarrow Fe^{2+} + RH + Cl^- \quad \textbf{Equation 2.7}$$

$$2Fe^0 + O_2 + 2H_2O \rightarrow 4OH^- + 2Fe^{2+} \quad \textbf{Equation 2.8}$$

$$Fe^0 + 2H_2O \rightarrow H_2 + 2OH^- + Fe^{2+} \quad \textbf{Equation 2.9}$$

$$2Fe^{2+} + RCl + H^+ \rightarrow 2Fe^{3+} + RH + H^+ + Cl^- \quad \textbf{Equation 2.10}$$

$$H_2 + RCl + \rightarrow RH + H^+ + Cl^- \quad \textbf{Equation 2.11}$$

$$Fe^{3+} + 3OH^- \rightarrow Fe(OH)_3 \quad \textbf{Equation 2.12}$$

The chlorine group of organochlorine complex is electron withdrawing and extremely electronegative group (Dorathi and Kandasamy, 2012). Owing to the negative potential of INPs, it tends to lose electrons to become ferrous ion (Fe^{2+}) (Equation 2.7). Therefore, it is exceedingly attracted to the chlorine group of organochlorine compounds, leading to the dechlorination of chlorinated organic compounds (Equation 2.10). The released electron from INPs is first shifted to the chlorine group subsequently it discharges as chloride ion. This phenomenon might be caused by proliferation of electron deficit in the vicinity of chlorine group. Henceforth, dechlorinated byproducts have produced in the process of dechlorination of organochlorine compounds. It has been shown in Equations (2.7) and (2.10) that the hydrogen ions are used up in dechlorination of OCPs (Pouretedal & Saedi, 2014). The significance of electron donors in the reduction of organochlorine complexes has got substantial responsiveness in the research and environmental remediation groups.

The reductive dechlorination of organochlorine complexes by zero-valent irons is directly attached to the oxidative suspension of the zero-valent metal as the prevailing mechanism (Matheson and Tratnyek, 1994). On the whole, several phases are included for these surface reactions: (1) molecular mass transfer of organochlorine complexes from the bulk liquid medium to the iron surface; (2) adsorption of chlorinated organic complexes on the iron surface; (3) reductive dechlorination on the iron surface; (4) desorption of oxidized and reduced products; (5) molecular mass transfer of products into the bulk solution (Stone and Morgan, 1990; Matheson and Tratnyek, 1994).

Elliott et al, (2009) found that tetrachlocyclohexene (TeCCH) is the principal degradation intermediate produced by the iron-mediated degradation of lindane. TeCCH is generated by the dihaloelimination of vicinal chlorides from carbons 1 and 2 of lindane as shown in Equation 2.13:

$$C_6H_6Cl_6 + Fe^0 \rightarrow C_6H_6Cl_4 + Fe^{2+} + 2Cl^- \qquad \textbf{Equation 2.13}$$

The reduction sequence is depicted in Figure 2.4. Aqueous or from ethanol-water solution lindane must first sorb onto the iron surface before any reaction can occur. Once sorbed, the highly electronegative chlorine substituents act as the electron acceptors while Fe^0 serves as the electron donor. The reduction product, TeCCH can then undergo further sequential reductions ultimately yielding benzene, or it can desorb into bulk aqueous solutionIn the first step, an electron from Fe^0 is donated to the surface-associated lindane forming a neutral radical as one chloride ion is simultaneously ejected. Another electron is then lost from the transient Fe^+ species to the reacting carbon center of the radical, which then undergoes double bond formation and simultaneous loss of chloride from the beta carbon. In this manner, Fe^{2+} and TeCCH are produced along with the evolution of two Cl^- ions. A similar sequence of single electron transfers is expected to occur during the generation of the subsequent degradation products.

2.5 Supporting of INPs on Carbonaceous Material

As discussed above, iron nano technique has been extensively studied for removal of organochlorine compounds, such as OCPs, due to their enormously small particle dimension, high specific surface area and insitu reactivity. Nevertheless, INPs lacking a stabilizer are in fact agglomerated into macroscale aggregates, subsequent a substantial reduction of reactivity. Hence several approaches have been established to adjust their surface characteristics and boost their reactivity. This has been counteracted through the use of such materials supporting INPs as silica, zeolites, or polymer membranes (Doong et al., 2015; Li et al., 2018; Kumar et al., 2017), which, apart from immobilizing INPs, can affect its physicochemical properties. The immobilization of INPs by the above carriers can be achieved through the fixing of INPs on their surface or trapping inside their pores. Kumar et al. conducted a study on the removal of trichloroethylene in ground water with the use of INPs deposited on PVP (Kumar et al., 2017). The size of the PVP (polyvinylpyrrolidone) stabilized INPs ((PVP-INPs), average diameter: ~20 nm) is smaller than that of bare INPs (50–80 nm) due to the prevention of agglomeration of the resultant iron particles by PVP. PVP- INPs showed a complete removal of TCE in 1 h with superior dechlorination kinetics (k_{obs} = 5.702 h^{-1}) while non-modified INPs showed 5 times slower dechlorination kinetics (1.218 h^{-1}). It was also found that INPs fixed on polyvinylpyrrolidone (PVP) reduces the aggregation of nanoparticles with simultaneous preservation of their high reactivity. Apart from polymer, other natural materials also proved to be good carriers of INPs, such as bentonite (Wang et al., 2016), kaolinite (Li et al., 2018; Magdy et al., 2017), or palygorskite (also known as attapulgite) (Rusmin et al., 2017). High effectiveness of complexes of those materials with INPs in the removal of heavy metals, bisphenol A and organochlorine compounds from waters was demonstrated (Tomasevic et al., 2014).

Carbon protective INPs are getting much attention, since they have a lot of compensations above polymers or silica, for instance much greater thermal and chemical stability in addition to biocompatibility. The carbonaceous support not only shields the INPs from quick oxidation by the surrounding environs, furthermore it inhibits the agglomeration initiated by *van der Waals* forces between particles (Kroschwitz, 1993). Qu et al, (2017) and Qian et al, (2017) demonstrated that INPs adsorbed on the surface of activated carbon permits effective removal of hexavalent Cr(VI) by reduction and co-precipitation and, is also effective in dichlorination of chlorinated compounds (Zhang et al., 2016).

Among the carbonaceous materials, apart from activated carbon, biochar has been recommended to be the most feasible candidates because of their exclusive physical and chemical characteristics. Biochar is a carbon rich, solid byproduct resulting from the pyrolysis of biomass under N2 and low temperature conditions (Agrafioti et al., 2014). Biochar is one of the most effective supporters of the carbon family, since it owns the special features of remarkably large surface area and a greater extent of micro-porosity and numerous surface functional groups (Devi and Saroha, 2014). It has been studied expansively and implemented in a varied series of industrial applications and remediation of organic toxins from water, on account of its exceptional adsorption potential, a consequence of large porosity and inner surface area.

Appreciations to large efforts in investigational and speculative research, much advancement has been made over the preceding few years in the field of biochar for environmental application. Coupling of the two groups of adsorbing and reducing materials i.e biochar and INPs has led to a fruitful incorporation of the characteristics of two constituents into a new group of hybrid substance, giving an essential advantage for applications in environmental remediation and catalysis. Further than the scope of treating

biochar as an adsorbent media and INPs as a reductant, biochar supported INPs particles are deliberated as a possible applicant by eventual consumption of instantaneous adsorption and dechlorination for organochlorine contaminants. Therefore, much attention has been paid for the preparation of biochar supported INPs using Fe(III) salts with sodium borohydride or potassium borohydride (Wang et al., 2014C). Nevertheless, sodium borohydride and potassium borohydride have several limitations and drawbacks such as toxic, corrosive, flammable and highly expensive.

2.5.1 Synthesis of Carbon-supported INPs

Methods used to develop a carbon coat on metallic nanoparticles have been divided into physical and chemical methods. The application of a series of various physical methods consists of microwave irradiation (Kappe et al., 2012), high-energy milling (Xu et al., 2010), pulsed laser ablation (Dadashi et al., 2015) and supercritical fluids (Zhang & Erkey, 2006). However, all of these physical techniques are costly and time wasting which bound their uses. Several cost-effective and easy-handling chemical methods have been lately familiarized to fabricate hybrid nano-materials. The conventional approaches are impregnation (He et al., 2018), co-precipitation (Gong et al., 2012) deposition-precipitation (Fan & Xin, 2012) and liquid phase method (Li et al, 2017; Wu et al., 2017; Su et al., 2016; Wang et al, 2016). A number of other unique methods involve precipitation from reverse micelle (e.g. water-in-oil) emulsions (Cushing et al., 2004), chemical vapor impregnation (Serp et al., 2002) and electrochemical reduction (Jung et al., 2016). Out of these methods, liquid phase method generally has been implemented to develop a range of carbon-based nanomaterials. It is usually stated as “wetness incipient impregnation” by involving the ‘‘wetting’’ of the carbonaceous support with a solution having the metal precursor. Usually, a salt (e.g. ferric chloride or ferrous sulfate) is used as a metal nanoparticle precursor, which is dissolved in the appropriate amount of solvent to give its thorough dissolution. The subsequent solution is then added to the porous

carbonaceous medium, until a dense paste is made. The product is filtered and the final solid is treated thermo-chemically to attain the final product (Kappe et al., 2012; Choi et al., 2008).

Choi et al, (2008) initially introduced this approach to prepare Fe^0 nanoparticle symbolized as ZVI nanoparticles (zero-valent iron nanoparticles) supported on granular activated carbon (GAC) (depicted in Figure 2.4) The author successfully embedded Fe_0 nanoparticle in 7–40 nm GAC using $Fe(NO_3)_3$ as the Fe^0 source (Figure 2.4 a), followed by calcination (at 300°C) of the material to produce GAC-INPs nanocomposite precursor (mainly as GAC-Fe_2O_3) (Figure 2.4 b). This was subsequently reduced with $NaBH_4$ to produce GAC-INPs nanocomposite (Figure 2.4 c). These materials showed good adsorption capacity and good activity for the dechlorination of 2-chlorobiphenyl.

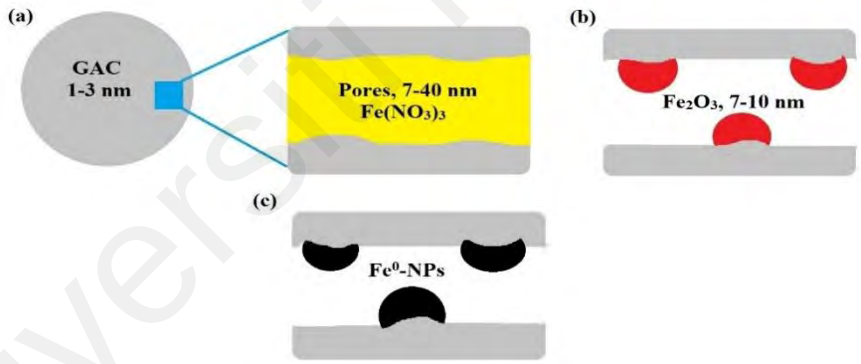

Figure 2.4: Incipient wetness impregnation approach for the preparation of Fe^0 metal nanoparticles supported on GAC

Devi & Sarah, (2014) and Quan et al, (2014) predominantly presented this method to synthesize Fe^0 nanoparticle supported on biochar. The researcher successfully synthesized Fe^0 nanoparticle on biochar surface using $FeSO_4$ as Fe^0 precursor, by subsequently drop wise addition of $NaBH_4$ as a reducing agent to the suspension and synthesized INPs-B nanocomposite and Fe^0 nanoparticles deposited into 7-40 nm sized pores in GAC. This adsorbent exhibited good adsorption capacity and good activity for

the dechlorination of pentachlorophenol.and acid orange 7, respectively from aqueous solution.

2.6 Environmental Applications of Carbon Supported INPs

The instantaneous adsorption and dechlorination that can possibly occur on the combined biochar and nanoparticle is a favorable method for insitu water and sediment removal of organochlorine toxins. Latest investigations have revealed that biochar media having INPs (INPs-B) can instantaneously eradicate certain organochlorine toxins. For example, Fe nanoparticles supported by biochar to stimulate the reduction of 1,1,1-trichloroethane (1,1,1-TCA) in groundwater remediation was investigated by Li et al, (2017). In order to enhance the reactivity of iron nanoparticles, surface modification of INPs was performed using biochar. The removal efficiency of 1,1,1-TCA increased from 42.3% to 99.3% as the biochar-to-Fe mass ratio increased from 0 to 1.0. However, a higher biochar-to-Fe ratio showed little difference in the 1,1,1-TCA degradation efficiency. The presence of Cl^{-}, CO_3^{2-}, HCO_3^{-} and SO_4^{2-} had negligible effects, but $NO_3^{-}$and HA (humic acid) showed a significant inhibitory effect on 1,1,1-TCA degradation. In conclusion, biochar supported Ni/Fe nanoparticles could be highly effective for 1,1,1-TCA degradation.

In another study conducted by Zhang et al, (2017), Fe nanoparticles supported by granular activated carbon, in order to enhance the reactivity of iron nanoparticles, and named as reactive activated carbon (RAC). These RAC adsorbents were applied for the removal of 2-chlorobiphenyl (2ClBP) and Trichloroethylene (TCE) in groundwater. The removal efficiency of 2ClBP, TCE was increased up to 50% with low iron content (1.32% Fe) on mesoporous granular activated carbon however reduction rate constant (k_{obs}) of 2ClBP was found higher than that of TCE because of the difference in the structures of these compounds. Yan et al, (2017) studied the coupling adsorption and degradation of

TCE through dechlorination using synthetic INPs-B nanocomposites. The degradation efficiency of TCE was 99.4% in the presence of INPs-B within 5 min, which was significantly higher than that (56.6%) in only INP system under the same conditions Their results indicated that TCE compounds, attracted by biochar adsorption, were firstly accumulated around INPs imbedded in pores on the surface of the biochar. They were then dechlorinated by INPs, which degraded both adsorbed and dissolved TCE compounds. The experiment confirmed that INPs-B nanocomposites combined the physical adsorption capacity of biochar with the dechlorination reactivity of INPs and could be used as a reactive biochar, which was not subject to the limitations of using biochar and INPs separately.

Devi and Saroha (2017) discovered that physical adsorption of pentachlorophenol to biochar and their electrochemical dechlorination by Fe deposited on the biochar possibly will be instantaneously attained on a biochar supported Fe^0 system. The outcomes exhibited that INPs showed merely 35 % adsorption while INPs-B revealed 100 % removal within 240 min and out of 100 % adsorbed pentachlorophenol, 85 % was dechlorinated by INPs-B. The concentration of chloride ions in the solution was found to increase with the contact time till 480 min after which no significant increase in the concentration of the chloride ions in the solution was observed. It was confirmed that INPs-B nanocomposite system could be applied for the fabrication of a proficient "reactive capping barrier" for the insitu treatment of water contaminated with hydrophobic organic compounds by means of reductive pathways.

Wheat straw biochar-supported INPs were synthesized by Li et al, (2017) using sodium borohydride as a reducing agent applied for the removal of TCE from ground water. Wheat straw biochar, as a carrier, significantly enhanced the removal of trichloroethylene (TCE) by INPs. The pseudo-first-order rate constant of TCE removal

by INPs-B (1.079 h^{-1}) within 260 min was 1.4 times higher and 539.5 times higher than that of biochar and INPs, respectively. TCE was 79% dechlorinated by INPs-B within 15 h, but only 11% dechlorinated by unsupported INPs, and no TCE dechlorination occurred with unmodified biochar. Weakly acidic solution (pH 5.7–6.8) significantly enhanced the dechlorination of TCE. Chloride enhanced the removal of TCE, while SO_4^{2-}, HCO_3^- and NO_3^- all inhibited it. Study suggested that INPs-B was promising for remediation of TCE contaminated groundwater.

In a more recent study conducted by He et al, (2018), Fe nanoparticles were supported on corn-straw biochar (BC) and Batch sorption experimental results showed that the nanocomposite, with larger surface area, more functional groups, and greaterstability exhibited excellent As(V) adsorption efficiency of 6.80 mg/g compared to 0.017 mg/g for unmodified BC (a 400-fold increase). In another study Zhu et al, (2018) synthesized bichar supported iron nanoparticles and applied for the removal of hexavalent chromium (Cr^{6+}) from ground water, electroplating wastewater and tannery wastewater. The prepared INPs-B owned better colloid stabilization and positive surface charge. XRD, XPS, FTIR, and TEM results explained that Cr^{6+} removal *i.e.* was occurred by electrostatic force, complexes, metal reduction, and precipitates on the edges. Presence of anions (SO_4^{2-}, PO_4^{3-}, and NO_3^-) showed some inhibitory effects on removal pocess.

Zhu et al, (2018) used modified corn-straw biochar (hydrochloric acid washing (HBC) for the deposition of Fe nanoparticles (INPs- HBC) and after aging they were applied for the removal of chriomium (Cr^{6+}) from ground water. Removal mechanism involves the reduction of Cr^{6+} to Cr^{3+} and more than 98% removal was achieved within. High Cr^{6+} removal rates under the acidic conditions within a wide pH range (< 7.0), indicating their good adaptability to pH change because of aging.

2.7 Summary

Organochlorine pesticides (OCPs) are chemically produced pesticides which include DDT, heptachlore, dieldrin, endosulfan, hexachlorobenzene, aldrin, mirex, dicofol and etc. Contamination of aquatic environment by organochlorine pesticides has been a worldwide environmental contest and economically feasible remediation techniques have been searching for decades. With the implication of developing nanotechnique, iron nanoparticle represents a novel development of removal technique to eradicate the persistent organochlorinepollutants, for instance PCE, TCE, PCBs and OCPs, in water and sediment. So far, iron nanoparticles have been synthesized by two techniques i.e physical method and chemical method. Generally, liquid phase reduction method has been most commonly utilized for the synthesis of iron nanoparticles. However, both methods present several limitations and problems such as expensive, high energy cost, toxicity and the tendency to form large agglomerates. Therefore, and in the last couple of years, a greener approach for the production of INPs has been developed. In this approach a variety of natural sources such as plant surfactants, vitamins, amino acids, oleic acid, and polyphenols have emerged in the last few years as an alternative to these well-established chemicals for the green synthesis of INPs.

Till now most of the INPs have been synthesized using agrowastes as low-cost bioreducing agents such as coffee, green tea leaf and eucalyptus leaf, pomegranate leaf, orange peel, plantain peel, banana peel ash, and in most cases green tea leaves with high antioxidant capacities are used. The compounds present in these extracts react with iron(III) in solution to form the INPs (Nadagouda et al., 2010). The main advantages of this method are: i) the lower toxicity of the used reducing agent compared with borohydride; ii) the capping ability that the polyphenol extract matrix induces on the INPs, prolonging their reactivity.

Usually, INPs displays a core-shell configuration. The inner core is comprised of metallic iron or zero-valent iron whereas the outer shell consists of mixed valence (e.g. Fe(II) or Fe(III) oxide shell is developed by oxidation of the metallic ions. Characteristics of INPs count on their production and synthesis procedure and can be categorized by a number of techniques and devices such as scanning electron microscope (SEM), TEM, Fourier emission scanning electron microscope (FESEM), EDX, Brunauer-Emmett-Teller isotherm (BET) measurement, powder X-ray diffraction (XRD) and FTIR for green INPs.

Nano iron particle has been documented as an exceptional electron donor. Fe^0 reveals a strong affinity to gradually oxidize to ferrous irons (Fe^{2+}) and electrons are released in the surroundings consistent with the subsequent oxidation half reaction. These electrons thus can possibly conduct a range of reactions that result in the conversion of target chlorine containing complexes. It is proposed that noxious polychlorinated organic pollutants (for instance, OCPs) would be reductively dechlorinated to principally less toxic complex with fewer chlorine substitutions. The chlorine group of organochlorine complex is electron withdrawing and extremely electronegative group. Owing to the negative potential of INPs, it tends to lose electrons to become ferrous ion (Fe^{2+}). Therefore, it is exceedingly attracted to the chlorine group of organochlorine compounds, leading to the dechlorination of chlorinated organic compounds. The reactivity of INPs with organochlorine compounds depends on the several factors including synthesis method, concentration of adsorbent, Size and surface area of nanoparticle and Stability of INPs.

Nevertheless, INPs lacking a stabilizer are in fact agglomerated into macroscale aggregates, subsequent a substantial reduction of reactivity. This has been counteracted through the use of such materials supporting INPs as silica, zeolites, or polymer

membranes, which, apart from immobilizing INPs, can affect its physicochemical properties. Carbon protective INPs are getting much attention, since they have a lot of compensations above polymers or silica, for instance much greater thermal and chemical stability in addition to biocompatibility. Among the carbonaceous materials, apart from activated carbon, biochar has been recommended to be the most feasible candidates because of their exclusive physical and chemical characteristics. Biochar is a carbon rich, solid byproduct resulting from the pyrolysis of biomass under N_2 gas and low temperature conditions. Further than the scope of treating biochar as an adsorbent media and INPs as a reductant, biochar supported INPs are deliberated as a possible applicant by eventual consumption of instantaneous adsorption and dechlorination for organochlorine contaminants. Therefore, much attention has been paid for the preparation of biochar supported INPs using Fe (III) salts with sodium borohydride or potassium borohydride. Nevertheless, sodium borohydride and potassium borohydride have several limitations and drawbacks such as toxic, corrosive, flammable and highly expensive. Carbon based nanomaterial can work as a high dimensions and discriminatory adsorbents for the complex organochlorine pollutants. However, a little work is known about the removal of highly complex OCPs using green iron nanoparticles supported on biochar and there is a dire need of research in this field.

2.8 Knowledge Gap

Organochlorine pesticides (OCPs) are fat-soluble pesticides that persist and bioaccumulate in the environment, even though their use has been banned or restricted in the past several decades. These toxic compounds enter the aquatic system from terrestrial ecosystem and move long distances in surface runoff or groundwater. Due to their low solubility in water and high adsorption to particles and lipids this takes years to decades. These are highly carcenogenic for the terrestrial and aquatic life. Removal of these toxic OCPs from the environment is a major concern.

Adsorption on carbonaceous matrix is an effective and reliable technique for the elimination of hydrophobic organic compounds from water (Sotelo et al., 2004; Shih and Gschwend, 2009). Over the past decade, vast studies have revealed that chemically synthesized INPs are effective for the decontamination and dechlorination of a varied range of organochlorine compounds in water system, comprising TCE, PCE, PCB, HCB, DDT, DDD, DDDE and HCH (Song and Carraway, 2005; Jovanovic et al., 2005; Lowery and Johnson, 2004). Amended INPs, for instance supported and catalyzed nanoparticles have been developed to further increase the rate and proficiency of remediation, and decrease the probability of aggregation and agglomeration. Moreover, carbon-based nanomaterial can work as a high dimensions and discriminatory adsorbents for the complex organochlorine pollutants. However, a little work is known about the removal of highly complex OCPs using green iron nanoparticles supported on biochar and there is a dire need of research in this field.

CHAPTER 3: METHODOLOGY

3.1 Flowchart of Methodology

Figure 3.1 represents the overall methodology of this research work. It demonstrates about method validation for OCP analysis using GC-ECD and GC-MS, synthesis of novel green synthesized nanocomposites and chemically synthesized nanocomposites, characterization of all nanocomposites and their application for the simultaneous adsorption and degradation of OCPs in various water matrices.

3.2 Collection of Biomass Waste Materials Used in the Study

3.2.1 Raw Materials

The oil palm leaves (OpL) were collected from oil palm fields, Kajang, Malaysia. Sugar cane leaves (ScL) were collected from sugar cane fields, Kajang, Malaysia. Rambutan peels (RtP) and Jackfruit peels (JfP) were collected from night market, Kuala Lumpur, Malaysia (Figure 3.1). The samples were collected in plastic bags and preserved in a cool room at 4 °C. The botanical name of the selected biomass waste materials from which low-cost nanoadsorbents were prepared and used in this study for OCPs removal are given below (Table 3.1):

Table 3.1: Common names and botanical names of biomass waste materials

Common names	Botanical names
Rambutan	*Nephelium lappaceum*
Oil Palm	*Elaeis guineensis*
Jackfruit	*Artocarpus heterophyllus*
Sugar cane	*Saccharum officinarum*

3.3 Plant Extraction

3.3.1 Preparation of Aqueous Extract

Biomass waste materials (rambutan peel, oil palm leaf, jackfruit peel and sugar cane leaf) were thoroughly washed with distilled water, then oven dried and ground into powder using a blender followed by extraction with distilled water. Blended powders were

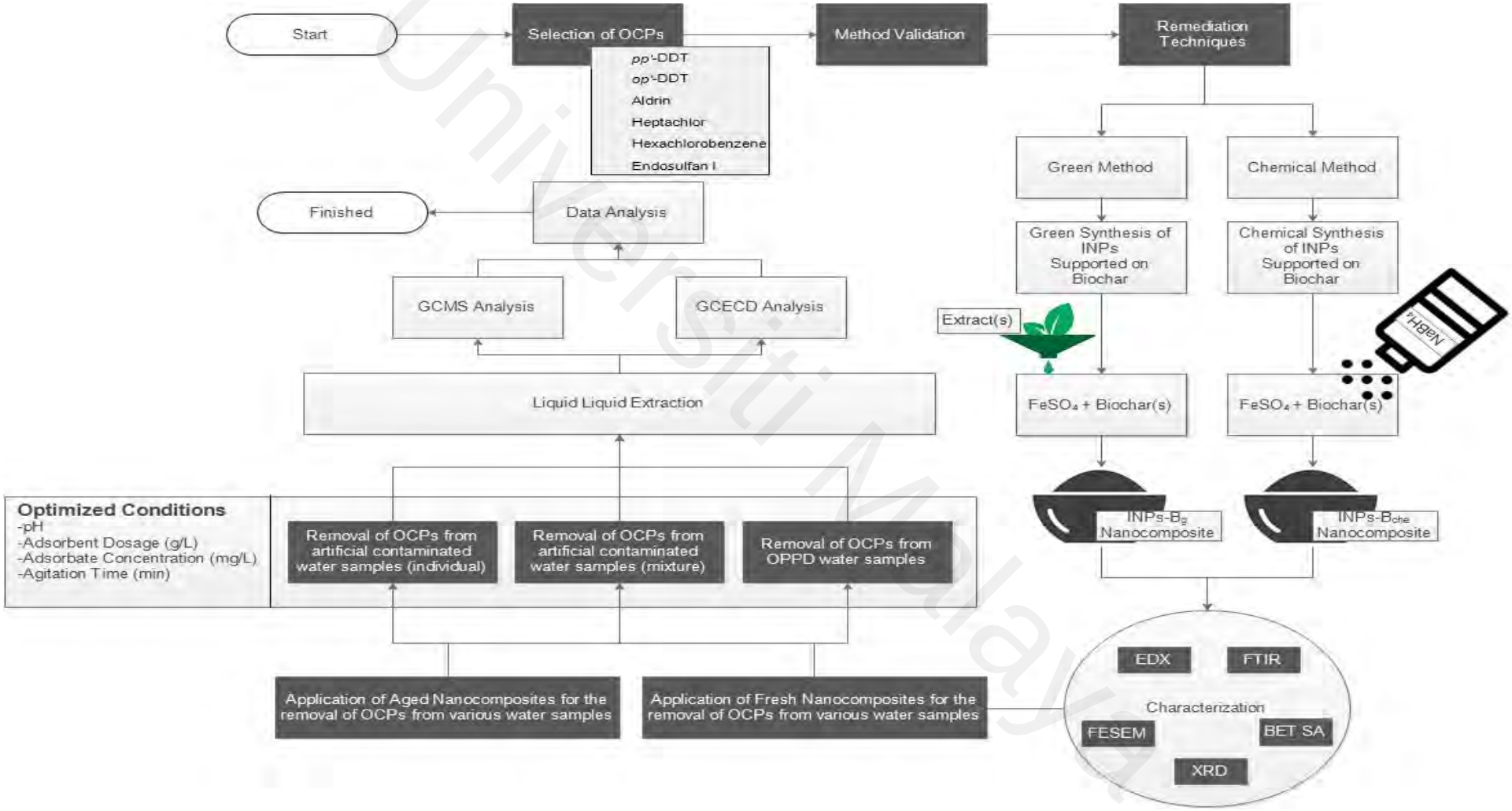

Figure 3.1: Flowchart of Methodology.

weighed and placed into a 1 L flask. The biomass (5, 10, 15 and 20 g) was added in 1000 mL of distilled water. The extraction was performed at four temperatures (60, 70, 80 and 90 °C) for 20, 40, 60 and 80 min stirring on a hotplate. The extracts were cooled and filtered through Whatman no. 40 filter paper (Whatman International Ltd., Kent, UK) using a Büchner funnel. Subsequently extracts were stored in refrigerator until analyses. The extracts of various biomass materials (rambutan peel, oil palm leaves, jackfruit peel and sugar cane leaves) were labeled as E_{RtP}, E_{OpL}, E_{JfP}, E_{ScL}, respectively (Figure 3.3).

3.3.2 Determination of Polyphenol Content

Total polyphenol content of all green solution at various times and temperatures were measured using a modified Folin-Ciocalteu assay as described in International Organization for Standardization (ISO) 14502-1 (ISO, 2005). A 1000 µg/mL gallic acid stock solution was prepared fresh daily by dissolving 110 mg of gallic acid monohydrate in 100 mL DI water. Green solutions were centrifuged at 3500 rpm for 10 minutes and diluted 1:100 for sample testing. A 5 mL of Folin-Ciocalteu phenol reagent from Sigma-Aldrich (catalog number 47641) was reacted with 1 mL of green solution and 4 mL of 7.5% sodium carbonate solution for 1 hour. The absorbance was measured at 765 nm. The polyphenol concentration was calculated from calibration curve.

3.4 Preparation of Nanocomposites

3.4.1 Preparation of Biochar by Microwave Pyrolysis

The biomass waste samples were first thoroughly washed with distilled water to remove water soluble impurities and surface adhered particles and dried at 105 °C for 24 h until a constant weight of the material was obtained. The dry biomass was then crushed and sieved into a particle size of less than 150 µm. The pyrolysis of all four biomass wastes was carried out in a HAMiab-C1500 microwave muffle system oven at frequency of 2450 MHz. The biomass sample was placed in a quartz tube of 35 mm OD, 28 mm ID

Figure 3.2: Biomass waste material of (a) rambutan peel, (b) oil palm leaf, (c) jackfruit peel, and (d) sugar cane leaf.

Figure 3.3: Extracts obtaind from biomass waste material of (a) rambutan peel, (b) oil palm leaf, (c) jackfruit peel, and (d) sugar cane leaf.

and 500 mm length. Nitrogen flow (50 ml min^{-1}) was kept constant. The microwave power was set at 200, 250, 300 and 350 W and the samples were processed for 30 minutes

irradiation time. After the pyrolysis finished, the samples were allowed to cool at room temperature. Then, the samples were collected from quartz tube and weighted to determine the yield of the product. The biochar samples then washed with distilled water and dried. Finally, the samples were stored in tightly closed bottles for further analysis. The prepared samples of various types of biochar from rambutan peel, oil palm leaves, jackfruit peel and sugar cane leaves were labeled as B_{RtP}, B_{OpL}, B_{JfP}, B_{ScL}, respectively.

3.4.2 Synthesis of Nanocomposites

3.4.2.1 Chemical Synthesis of INPs-B_{Che} Nanocomposites

Biochar supported INPs nanocomposites were prepared through the following procedure. A 250 mL of 0.54 mol/L $FeSO_4.7H_2O$ solution was prepared. The contents of the flask were agitated at 250 rpm by a mechanical stirrer to maintain a uniform concentration in the flask. Biochar was first dissolved in 250 mL of 0.54 mol/L $FeSO_4.7H_2O$ at pH 5.0, in a 3-neck flask, and then N_2 was purged into the solution from one neck for 1 h to exclude dissolved O_2 during the preparation. With strong stirring,

INPs deposited on the surface of biochar by the drop wise addition of various volumes of the 1.08 mol/L $NaBH_4$ solution ($FeSO_4$:$NaBH_4$ ratio; 1:1-1:5, v/v) from another neck in order to set the optimized $FeSO_4$:$NaBH_4$ ratio, and the solution was stirred for another 30 min under room temperature. The nanocomposited particles formed were settled and separated from the liquid phase by vacuum filteration (whatmann filter 41). Then, the solid was washed with 200 mL ethanol for several times, and finally vacuum dried in hot air oven at 60 °C for 24 hr. The final product was labeled as INPs-B_{che}.

3.4.2.2 Green Synthesis of INPs-B_g Nanocomposites

Four green synthesized biochar supported INPs nanocomposite samples were prepared using four biochars (B_{RtP}, B_{OpL}, B_{JfP} and B_{ScL}) derived from the above mentioned four biomass wastes and their corresponding extracts (E_{RtP}, E_{OpL}, E_{JfP}, E_{ScL}, respectively) as

reducing agents in place of $NaBH_4$ were prepared through the following procedure (Figure 3.4). A 250 mL of 0.54 mol/L $FeSO_4.7H_2O$ solution was prepared. The contents of the flask were agitated at 250 rpm by a mechanical stirrer to maintain a uniform concentration in the flask. Biochar was firstly dissolved in 250 mL of 0.54 mol/L $FeSO_4.7H_2O$ solution in a 3-neck flask at pH 5.0. Then N_2 was purged into the solution from one neck for 1 hr to exclude dissolved O_2 during the preparation. With strong stirring, INPs deposited on the surface of biochar by drop-wise addition of corresponding extracts with different volume ratios of $FeSO_4.7H_2O$ solution with corresponding extracts (1:1-1:7 (v/v), as shown in Table 3.2) from another neck, and the solution was stirred for another 30 min under room temperature. The nanocomposited particles formed were settled and separated from the liquid phase by vacuum filter (whatmann filter 41). Then, the solid was washed with 200 mL of ethanol for several times, and finally dried in hot air oven at 60 °C for 24 hr. Similar experiments were repeated with the various quantities of biochar (0.5, 1, 3, 5 and 7 g). The final products were labeled as INPs-B_{RtP}, INPs-B_{OpL}, INPs-B_{JfP} and INPs-B_{ScL}.

Table 3.2: Preparation of biochar supported green iron particles (INPs-B_g) using various biomass waste extracts

Samples	Composition description
INPs-B_{RtP}	Used various ratios, $FeSO_4.7H_2O$ solution : Extract (1:1-1:7 mL) with various quantities of biochar (0.5, 1, 3, 5 and 7 g), 250 mL 0.54 mol/L $FeSO_4.7H_2O$ solution + Rambutan peel extract (E_{RtP}) + biochar (B_{RtP})
INPs-B_{OpL}	Used various ratios, $FeSO_4.7H_2O$ solution : Extract (1:1-1:7 mL) with various quantities of biochar (0.5, 1, 3, 5 and 7 g), 250 mL 0.54 mol/L $FeSO_4.7H_2O$ solution + Oil palm leaf extract (E_{OpL})+ biochar (B_{OpL})
INPs-B_{JfP}	Used various ratios, $FeSO_4.7H_2O$ solution : Extract (1:1-1:7 mL) with various quantities of biochar (0.5, 1, 3, 5 and 7 g), 250 mL 0.54 mol/L $FeSO_4.7H_2O$ solution + Jackfruit peel extract (E_{JfP}) + biochar (B_{JfP})
INPs-B_{ScL}	Used various ratios, $FeSO_4.7H_2O$ solution : Extract (1:1-1:7 mL) with various quantities of biochar (0.5, 1, 3, 5 and 7 g), 250 mL 0.54 mol/L $FeSO_4.7H_2O$ solution + Sugar cane leaf extract (E_{ScL})+ biochar (B_{ScL})

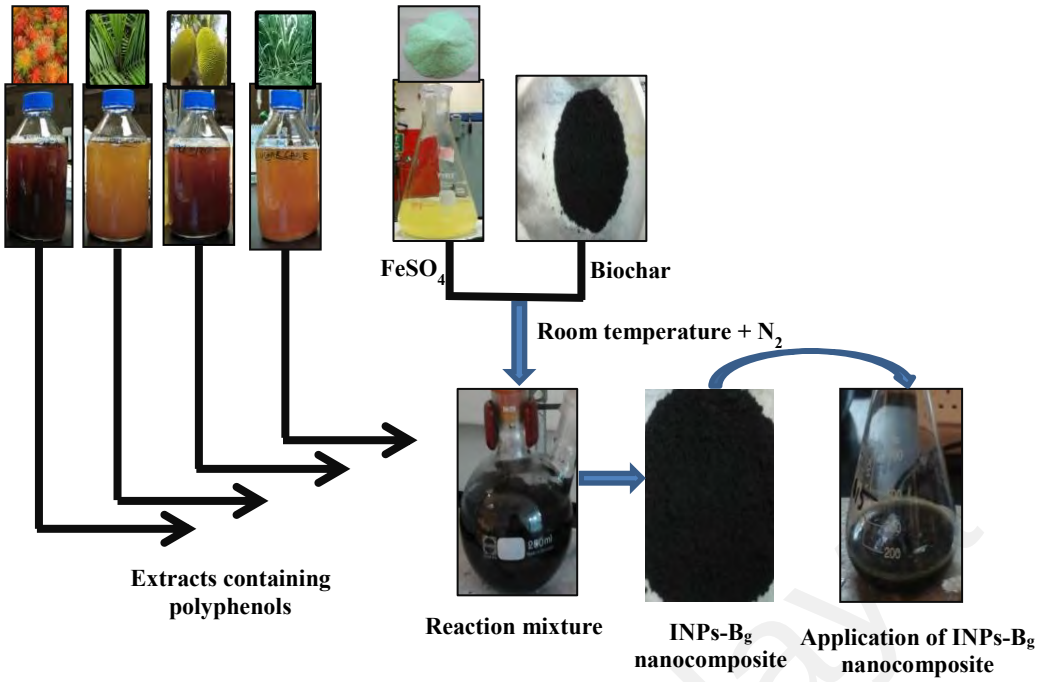

Figure 3.4: Schematic view of synthesis of green INPs-B_g nanocomposites.

3.5 Characterization of Nanocomposites

3.5.1 Field Emission Scanning Electron Microscopy (FESEM)

In this research, physical morphology of samples of pristine biochars and nanocomposite samples before and after reaction with OCPs were studied by using (Brand: Hitachi SU8220) field emission scanning electron microscope (FESEM). The FESEM determines the small structures (as small as 1 nanometer = one billion of a meter) of nanoparticles. The mechanism involves the emission of primary electrons from the electron source (field emission) and accelerated by a high electron field gradient. These electrons are focused by high vacuum column and deflected by electronic lenses to get a narrow scanning beam to bombard the sample. The angle between secondary electrons which are released from each spot on the surface of the sample and a detector and a velocity of these primary electrons relates to the structure\ector taps the secondary electrons and converts them to an electronic signal. This signal is transformed into a video scan-image or to a digital image after amplifying it and can be saved and processed further.

3.5.2 Energy Dispersive X-ray Microanalysis

Element composition analysis of above mentioned samples was carried out with 51P1000 Aztec Energy standard element diffraction spectrum (EDX). It is used for the chemical characterization or determines qualitatively the elemental composition of the sample (powder form).

The EDX principal is X-ray line separation based on the energy of their photon (Bertin, 1975) which is used to determine the element main composition in the sample. In general, the correction of absorption is the most important. It is dependent on the angle between the path of X-ray to the spectrometer and the surface of the sample. To excite the emission of characteristic X-rays from a sample, the beam of X-rays or electrons or protons is focused on the magnetic biochar samples being studied.

3.5.3 X-Ray Diffraction (XRD)

X-ray diffraction has been widely used for the study of the crystalline dimensions of carbon materials. X-rays with a wavelength on the order of the lattice spacing are elastically scattered (i.e., diffracted) from the atomic planes in a crystalline material, yielding diffraction peaks. The condition for diffraction from planes with spacing d, is given by the Bragg's Law: nl = 2d sinq, where q is the angle between the atomic planes and the incident X-ray beam. The resultant diffraction pattern can be used to identify crystalline phases and determine the preferred orientation. The X-ray diffraction (XRD) analyses of carbonaceous materials were first conducted by Warren in 1934. In this study, a representative amount of the powdered form of adsorbent was transferred to a quartz sample slide**.** XRD analyses of the samples were carried out using computer-controlled X-ray diffractometer. The X-ray tube was operated using Cu Ka radiation (λ=1.5418 Å) generated at 40 Kv and 40 mA with microprocessor. The existence of crystallites in carbon and iron structure has been proven by the appearance of the peaks. The data was

collected between 2θ values of 10° to 90° with a step size of 0.02° and an average counting time of 1 second per step.

3.5.4 BET Surface Area Measurement

The N_2 isotherms were determined in a Quantachrome surface area analyzer (model Autosorb-1). Biochar and nanocomposite samples before and after reaction with OCPs were out-gassed at 250 °C for 12 hr prior to adsorption measurements. The mercury density (qHg) was measured by obtaining the sample volume by exclusion of the mercury volume from the volume of a previously calibrated glass cell using a Quantachrome Poremaster mercury porosimeter.

The BET method was applied to evaluate the pore area and external area to determine the specific surface area in m^2/g of a powder which carried out with temperature. The specific surface areas (S_{BET}) were evaluated from the N_2 adsorption isotherms using Quantachrome surface area analyzer (Brand: Micromeritics ASAP2020, TRISTAR II 3020 Kr). It is performed by a gas (nitrogen) multilayer adsorption and based on the physical adsorption phenomenon between the molecules of the adsorbate gas and the surface area of the test adsorbent (powder) and describe it thermally, exothermic and reversibily.

BET is a widely used method for the surface area measurements. It is applicable in limited range of relative vapour pressure of p/p^s of 0.05-0.3 (or sometimes extended to 0.35), where p is the actual and p^s is the saturated vapour pressure of nitrogen. The volume of nitrogen adsorption (in the liquid form) at p/p^s as near to 1 as possible is considered as the total pore volume. The average pore size and diameter is calculated by the below Equations 3.1 and 3.2, respectively:

$$r_p = \frac{2V_P}{S_{BET}} \qquad \textbf{Equation 3.1}$$

$$D = \frac{4V_P}{S_{BET}} \qquad \textbf{Equation 3.2}$$

Where r_p is the pore radius and V_P is the total pore volume.

3.5.5 Fourier Transform Infrared Spectroscopy (FTIR)

FTIR spectroscope (Bruker Vector 22) was used to analyze the above-mentioned samples for determination of the surface functional groups. FTIR were recorded in the 4000–400 cm^{-1} region with a resolution of 4 cm^{-1}. When a highlight from the source of FTIR on chemical sample, it can absorb part of the light (frequencies) and transmit the rest to the detector to detect. Part of the light reflected back to the source.

3.6 Analytical Techniques

3.6.1 Analysis Conditions

For the detection of OCPs, GC-MS (Agilent 7890 GC System) coupled with an auto sampler (Shimadzu AOC-20 S) was employed. The target compounds were separated using a HP-5MS 19091S-433 capillary column (length, 30 m; id, 0.25 mm; film thickness, 0.25 μm). Identification was based on retention time and relative intensities of quantification and confirmation ions. Quantitative analysis was carried out in selected ion monitoring mode using internal standard calibration. For OCPs analysis, helium was used as the carrier gas at a constant flow rate of 2.25 mL/min. Ion source temperature was set at 250 °C, injector temperature at 270 °C and interface temperature at 300 °C. The oven temperature program was as follows; initial temperature 80 °C (held for 1 min), increased to 160 °C at a rate of 15 °C/min and thereafter increased to 200 °C at a rate of 2 °C/min. Finally, the temperature was increased to 300 °C at a rate of 15 °C/min and held for 5 min.

The OCPs were quantified using GC-ECD (Agilent Technologies 7890 GC System). The GC was operated at a programmed oven temperature from 100 °C (held for 1 min) to 250 °C at a rate of 10 °C/min, thereafter to 300 °C at a rate of 10 °C/min (held for 5 min). The injector temperature was set at 250 °C while interface temperature was maintained at 270 °C and ion source temperature was set at 230 °C while helium flow rate was maintained at 1 mL/min.

3.6.2 Extraction Method for OCPs

Twenty five milliliters of sample was transferred into a 50-mL glass-separating funnel and spiked with 80 ng of 13C *p,p′*-DDT (surrogate). The pH was then adjusted to 2–3 using hydrochloric acid (1:1) and 1.5 g of sodium chloride was added to produce a salt out effect. The sample was extracted twice with 8 mL n-hexane and shaken for 10 min each time. The combined organic phase was dried by passing it through anhydrous sodium sulphate and concentrated to 3–5 mL in a rotary evaporator and further dried under a gentle stream of nitrogen. The sample was reconstituted in 150 µL of hexane and 10 µL of 1 µg/mL internal standard (phenantrene-d10) was added. Two microliters of sample were injected into the GC-MS and GC-ECD.The glassware for OCPs analysis were initially rinsed with acetone, n-hexane and distilled water and baked at 70 °C for 24 hr.

3.6.3 Method Validation

The optimum GC-MS and GC-ECD conditions were used to determine the presence of any quantity target analytes as a way to verify the real world applicability of the method. The validation procedure was performed following the SANCO/10684/2009 European Guidelines. The analytical performance characteristics investigated included selectivity, calibration curve, ability to determine a linear calibration curve, the limit of detection (LOD) and quantification (LOQ), precision, stability and trueness (expressed as

a recovery rate. Precision was determined by measuring the relative standard deviation (RSD), and was evaluated as inter-and intra-day precision.

3.6.3.1 Selectivity

The selectivity of the proposed method was verified by comparing results from a control (pesticide-free) sample and a sample fortified with 6 pesticides. No interference peaks were observed at the retention times of individual compounds, providing that there was sufficient selectivity for the analysis of multiple pesticides at trace levels.

3.6.3.2 Calibration Curve and linearity

Calibration curves were constructed using standards working solutions at ten concentration levels obtained by diluting the standard stock solution with n-hexane (0.001, 0,005, 0.01, 0.05, 0.1, 0.2, 0.4, 0.6, 0.8 and 1 mg/L) for 6 OCPs. Calibration curve for each analyte was drawn by plotting the peak areas (Y) against standard concentrations (X) and $Y = AX - B$, was constructed to obtain the value of coefficient of determination (R). An internal calibration method based on the peak area of each analyte (A) and internal standard (IS) was used to quantify targets using following Equations 3.3:

$$Concentration_A = Peak\ Area_A \times \left(\frac{Concentration_{IS}}{Peak\ Area_{IS}}\right) \times \frac{1}{RRF_A} \qquad \textbf{Equation 3.3}$$

Relative response factor (RRF_A) was calculated using following Equation 3.4:

$$RRF_A = \frac{RF_A}{RF_{IS}} \qquad \textbf{Equation 3.4}$$

3.6.3.3 LOD and LOQ

LODs and LOQs were estimated using the minimum concentrations detected for all target analytes based on signal-to-noise (S/N) ratio of three and LOQs were set as ten times this ratio. LOD and LOQ were calculated using following Equations 3.5and 3.6:

$$LOD = \frac{SD}{average} \times 3$$ **Equation 3.5**

$$LOQ = \frac{SD}{average} \times 10$$ **Equation 3.6**

3.6.3.4 Precision and Stability

To get precision of the method, intra- and inter-day variations were estimated and expressed as RSD of the peak areas for each analyte following the analysis of 1 ppm standard working solution injected six times (0, 2, 4, 6, 8 and 10 hr) consecutively on the same day and injected six times over six consecutive days. All samples were extracted and analyzed in triplicates and then RSD % was calculated using the following Equation 3.7:

$$RSD\% = \frac{SD}{average} \times 100$$ **Equation 3.7**

3.6.3.5 Trueness

The trueness of the developed method was determined through recovery studies using water sample and three control wastewater samples. These samples were fortified at three (high, medium and low) spiking levels, which were 0.1, 1 and 10 mg/L for OCPs. All samples were extracted and analyzed in triplicates following the previously described procedure. The recovery percentages of water sample and wastewater samples were then calculated using the following Equations 3.8:

$$\text{Recovery (\%)} = \frac{\text{measured concentration for fortified sample}}{\text{spiked concentration}} \times 100$$ **Equation 3.8**

$$Recovery\ (\%) = \frac{\text{measured concentration for spiked sample} - \text{measured concentration for unspiked sample}}{\text{spiked concentration in sample}} \times 10$$ **Equation 3.9**

0

3.6.3.6 Quality Control

10SANCO/10684/2009 European Guidelines were used in the quality control process for the validation of the analytical methods. Calibration curves were constructed using standards working solutions at ten concentration levels obtained by diluting the standard stock solution with n-hexane (0.001-1 mg/L) OCPs of interest. The trueness of the developed method was determined through recovery studies using water sample and three control wastewater samples which were 0.1,1 and 10 mg/L for OCPs. Several quality control measures were also routinely used in this study and included running blanks with each sample set and analysing samples as triplicates. Gas chromatographic conditions were monitored daily by checking the range of response factors of the calibration standards and the recoveries of a test standard that was included in each run.

3.7 Batch Experiments to Optimize the Parameters for the Removal of OCPs in Water

3.7.1 Adsorbates

A stock standard solution of each pesticide was prepared in n-hexane with a concentration 1000 mg/L. Individual calibration solutions with concentration levels of 0.2, 0.4, 0.6, 0.8, 1 mg/L were freshly prepared in n-hexane. Similarly, calibration mixtures with cindividual concentration levels of 0.2, 0.4, 0.6, 0.8, 1 mg/L were freshly prepared in n-hexane. A stock solution of the (1000 mg/L) was prepared by dissolving 10 mg of each analyte from organochlorine pesticide (OCPs) group. Individual solutions of these OCPs (100 mg/L) were prepared in a 1:1 n-hexane: deionized water solution. A mixture of these analytes with individual pesticide concentrations (100 mg/L) was also prepared in a 1:1 n-hexane: deionized water solution. The other analyte concentrations were prepared by diluting the above solution with suitable volumes of deionized water. The above mixture solution containg 6 OCPs was also used to spike the wastewater samples. The removal of OCPs with four types of green INPs-B_g nanocomposites was

measured after a fixed period of time using standard method. The samples were filtered using 0.45 glass fiber filter (whattman GF/F), extracted and final concentrations of all OCPs were measured using GC-ECD. For comparison similar experiments were performed using chemical synthesized INPs-B_{Che} nanocompoiste as well. The removal percentage (R%) of each adsorbate on all types of nanocomposites was calculated using Equation. 3.10. Also, Eqution 3.11was used to calculate the mass of the individually adsorbed OCPs per gram of the sorbent (qe, mg/g).

$$R\% = \left[\left(\frac{C_0 - C_e}{C_0}\right)\right] \qquad \textbf{Equation 3.10}$$

$$q_e = \left[\left(\frac{C_0 - C_e}{m}\right)\right] \times V \qquad \textbf{Equation 3.11}$$

Where C_0 is the initial adsorbate concentration (mg/L), C_e is the equilibrium adsorbate concentration in solution (mg/L). *V* is the volume of the solution (mL), and *m* is the weight of the nanocomposites in milli grams (mg).

Performances were also evaluated for four green INPs-B_g nanocomposites (INPs-B_{RtP}, INPs-B_{OpL}, INPs-B_{JfP} and INPs-B_{ScL}) and chemically synthesized INPs-B_{Che} nanocomposite aged in air for one month. All experiments were performed in triplicate.

3.7.2 Effect of pH on the Removal Process

The study of the effect of pH solution of OCP compounds on the removal capacity of all types of nanocomposites is very important. The knowledge of chemical characteristics of both nanoadsorbent and adsorbate is very important to predict the effect of solution pH. In this study, 0.1 M hydrochloric acid (HCl) and 0.1 M sodium hydroxide (NaOH) were used for adjusting the initial pH of samples in order to study of pH effect on the removal efficiency. The pH measurements were made using a pH meter during all the experiments. The nanoadsorbent (0.01 g/L) was added to individual 300 mL adsorbate

solutions with 2 mg/L of OCP concentration in each 500 mL Erlenmeyer flasks covered with aluminium foil from top to bottom. Similar experiments were performed with 0.25 g/L of nanoadsorbent added to 300 mL solutions of mixed OCPs with 2 mg/L individual OCP concentration in 500 mL Erlenmeyer flasks. The pH values of the solutions were adjusted from pH 1–12 and then the flasks were stirred at room temperature in a digital incubator shaker at 150 rpm. The removal of OCPs was measured after a fixed period of time using standard method. The samples were filtered; extracted and final concentrations of all OCPs were measured using GC-ECD. At different pH solution the plots of removal % and adsorption capacity versus solution pH were obtained.

3.7.3 Effect of Adsorbent Dosage on the Removal Process

It is very important to study the effect of the adsorbent dosage on the removal process of OCP compounds by nanocomposites. In this study, 300 mL individual solutions of each OCPs containing 2 mg/L of each OCP compound was introduced into 500 mL Erlenmeyer flasks, similarly 300 mL solution mixture for 2 mg/L of each OCP compound was introduced into 500 mL Erlenmeyer flasks covered with aluminium foil from top to bottom. The Erlenmeyer flasks were placed into the shaker at 150 rpm. All the adsorption experiments of OCP compounds with four types of nanoadsorbents were performed by batch experiments where the room temperature, pH and revolution per minute were kept constant and the effect of all INPs-B_g nanocomposites dosage was investigated in the presence of 0.01, 0.05, 0.1, 0.15 and 2 g/L of nanoadsorbent for the individual removal of OCPs and 0.15, 0.25, 0.35, 0.45, 0.55 and 0.65 g/L for mixed OCPs. The final OCP compounds concentration readings were taken after a fixed period of time and they were determined by standard method. The samples were filtered; extracted and final concentrations of all OCPs were measured using GC-ECD. At different adsorbent dosage, the plots of removal % and adsorption capacity versus adsorbent dosage were obtained.

3.7.4 Effect of Initial Adsorbate Concentration on the Removal Process

Initial concentration of adsorbate is also one of the important factors that affect the removal of OCP compounds by nanocomposites. In this study, to determine the effect of initial concentration of the adsorbate in the individual solution of each OCP and solution of mixed OCPs as well, 300 mL of aqueous solutions with individual concentrations of OCPs 2, 4, 6, 8, 10 mg/L were introduced into the 500 mL Erlenmeyer flasks covered with aluminium foil from top to bottom and then placed inside the orbital shaker. All the adsorption experiments of OCP compounds treated with all types of nanocomposites were performed by batch experiments where the solution pH, adsorbent dosage and room temperature were kept constant. The final OCP compounds concentration readings were taken after a fixed period of time and they were determined by standard method. The samples were filtered; extracted and final concentrations of all OCPs were measured using GC-ECD. At different initial adsorbate concentration, the plots of removal % and adsorption capacity versus initial adsorbate concentration were obtained.

3.7.5 Effect of Agitation Time on the Removal Process

The contact time of adsorbent and adsorbate plays an important role in the removal process. In this study, individual 300 mL solutions for 2 mg/L of each adsorbate in the individual solutions of OCP compounds were introduced into 500 mL Erlenmeyer flasks. Similarly, 300 mL for 2 mg/L of each adsorbate in the mixture solution of OCP compounds was introduced into 500 mL Erlenmeyer flasks covered with aluminium foil from top to bottom and then placed inside the orbital shaker at 150 rpm. All the adsorption experiments of OCP compounds treated with all types of nanocomposites were performed by batch experiments where the solution pH, adsorbent dosage and revolution per minute and temperature were kept constant. Hence, the effect of contact time on the removal extent of OCPs by all types of nanocomposites was studied in batch experiments at an agitation time of 5, 10, 15, 20, 25, 30, 35, 40, 45, 50, 55 and 60 min for the individual

removal of OCPs and agitation time of 10, 20, 30, 60, 90, 120, 150 and 180 min for the removal of mixed OCPs. The plots of removal % and adsorption capacity versus initial adsorbate concentration were obtained. The experimental results were used for isothermal, thermodynamic and kinetic studies.

3.8 Removal of OCPs from Oil Palm Plantation Drainage (OPPD) Water Samples

3.8.1 Study Area

The study area is located in oil palm plantation of Shah Alam, Selangor, Malaysia. The area is characterized by land use predominantly comprises of oil palm plantation. Three main water drainage canals coming out from three main oil palm plantation areas, i.e. Persiaran Elmina (PE1), Persiaran Mokhtar Dahari 2 (PMD2) and Persiaran Mokhtar Dahari 3 (PMD3), Shah Alam, Selangor, Malaysia (as shown in Figures 3.5). A drainage water canal PE1 orginated from the Persiaran Elmina oil palm plantation enters another drainage canal PMD2 originated from the Persiaran Mokhtar Dahari 2. Another drainage water canal PMD3 receives the water from Persiaran Mokhtar Dahari 3.

3.8.2 OPPD Water Sample Collection

Three different OPPD water samples were collected at random from the water drained out from the dense old oil palm fields in Persiaran Elmina (PE1), Persiaran Mokhtar Dahari 2 (PMD2) and Persiaran Mokhtar Dahari 3 (PMD3), Shah Alam, Selangor, Malaysia (as shown in Figures 3.5 and 3.6). Four litres of grab water samples from a depth of 0.5 m were collected in solvent-cleaned amber glass bottles. The bottles were rinsed with sample water, filled to the brim and capped with an aluminium-foillined cap. In situ measurements of coordinates, pH, temperature, conductivity, DO, TDS, TSS, and were recorded. Samples were preserved from microbial activity by acidification with 50% nitric acid and transported to the laboratory in a cool box at 4°C. Samples were then stored in the dark at 4°C until analysis. Concentrations of anions and cations were determined

using Ion Chromatography System (DIONEX ICS-1100 RFIC) and Ion Exchange Chromatography instruments, respectively. The effect of agitation time, adsorbent dose and pH on OCPs removal from effluent by four types of green INPs-B_{RtP} nanocomposite and INPs-B_{Che} nanocomposite (for comparison) was studied.

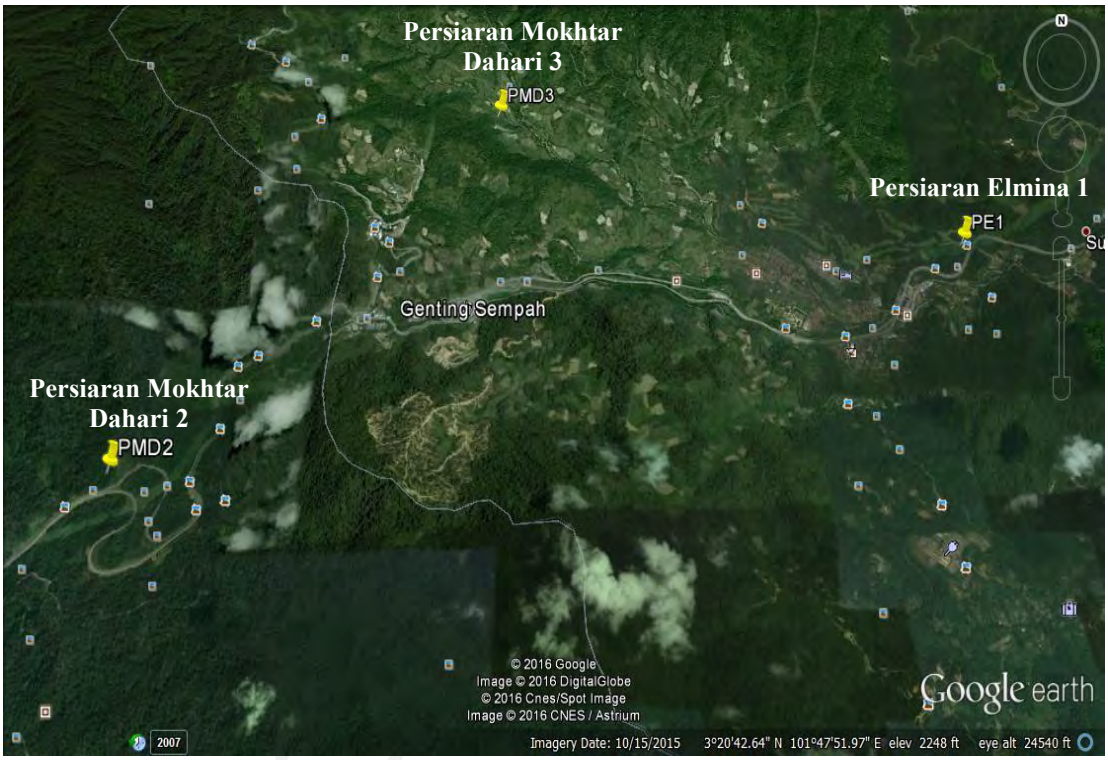

Figure 3.5: Location of sampling points

Figure 3.6: Sampling of OPPD water samples

3.8.3 Batch Adsorption Experiments for the Removal of OCPs from OPPD Water Samples

In order to test the removal efficiency of the best one found INPs-B_g nanocomposite i.e. INPs-B_{RtP} nanocomposite in real effluent, the drainage water samples samples were spiked with 6 OCPs at an individual concentration of 2 mg/L and treated with 1 g/L of nanoadsorbent. In order to investigate the effect of pH on removal of OCPs from OPPD water samples with INPs-B_{RtP} nanocomposite, pH was adjusted from 3-9 and OPPD water samples were collected after fixed time interval. To investigate the effect of adsorbent dosage on removal of OCPs from OPPD water samples, various nanoadsorbent dosage which is 1, 2, 4, 6, 8,10, 12 g/L of INPs-B_{RtP} nanocomposite were applied and OPPD water samples were collected after fixed time interval.and water sample were collected at various time intervals i.e. 0, 10, 20, 30, 60, 90, 120, 150 and 180 min. Final concentrations of OCPs in solution and amount of OCPs adsorbed on exhausted INPs-B_{RtP} were determined using Agilent technologies 7890A GC system. Same experiments were also performed with INPs-B_{Che} for comparison.

Performances were also evaluated for four green INPs-B_{RtP} nanocomposite and chemically synthesized INPs-B_{Che} nanocomposite aged in air for one month. All experiments were performed in triplicate.

3.9 Desorption Studies

After adsorption experiments, the adsorbate-loaded (exhausted) nanocomposites of all types were separated from the solution and centrifuged and the supernatant were drained out. The adsorbents were gently washed with distilled water to remove any unadsorbed adsorbate. Regeneration of OCPs from the OCP-loaded adsorbents was carried out using the various concentrations of n-hexane (6, 8, 10, 12, and 14 mL) as a desorbing agent with 0.01 g of each adsorbent.in order to find the optimum volume of solvent to desorb all OCPs simultaneously.

3.10 Equilibrium Studies

3.10.1 Freundlich Isotherm Model

At equilibrium conditions, the adsorbed amount, q_e can also be predicted by using the Freundlich equation (Freundlich, 1926; Hatt et al., 2013; Gupta et al., 2010) Equation 3.13, where,

$$\log q_e = \log K_\mathrm{f} + \left(\frac{1}{n}\right) \log \mathrm{C_e} \qquad \textbf{Equation 3.12}$$

$\mathrm{C_e}$ = equilibrium concentration of OCPs (mg/L)

q_e = amount of OCPs adsorbed at equilibrium (mg/g)

K_f = Freundlich constants related to the adsorption capacity

n = Freundlich constants related to the adsorption intensity

$\frac{1}{n}$ is the measurement of surface heterogeneity, ranging between 0 and 1, becoming more heterogenous as its value gets closer to zero. By plotting the $\log q_e$ vs. $\log \mathrm{C_e}$, a straight line with slope $\frac{1}{n}$ and intercept $\log K_\mathrm{f}$ is obtained. The intercept of the line, K_f shows the adsorption capacity, while the slope, indicates the adsorption effectiveness.

3.10.2 Langmuir Isotherm Model

The Langmuir model was developed based on the assumption of the formation of a monolayer of the adsorbate species onto the surface of the particle of the adsorbent. It has also been assumed that the surface sites are completely energetically homogeneous. But in the true sense, the adsorbent surface is energetically heterogeneous (Langmuir, 1918). The study of the Langmuir isotherms is essential in assessing the adsorption efficiency of the adsorbent. This study is also useful in optimizing the

operating conditions for effective adsorption. In this respect, the Langmuir isotherm is important, though the restrictions and the limitations of this model have been well recognized.

In this study, the most commonly used models i.e. Langmuir and Freundlich models were implemented to analyze the experimental data, and thus illustrate the adsorption characteristics between adsorbent and OCPs. The linear forms of Langmuir isotherms are displayed as Equation 3.12 (Hatt et al., 2013; Gupta et al., 2010)

$$\frac{\mathrm{C_e}}{q_e} = \frac{1}{(q_{max} \times b)} + \frac{\mathrm{C_e}}{q_{max}} \qquad \textbf{Equation 3.13}$$

The Langmuir and the rearranged Langmuir equations are given below.where,

$\mathrm{C_e}$ = equilibrium concentration of OCPs (mg/L)

q_e = amount of OCPs adsorbed at equilibrium (mg/g)

q_{max} = Languimir constants related to adsorption capacity (mg/g)

b = Languimir constants related to energy of the adsorption (mg/L)

q_{max} and b are Langmuir constants related to adsorption capacity (mg/g) and energy of the adsorption, respectively that can be calculated from the slope $\frac{1}{q_{max}}$ and intercept $\frac{1}{q_{max} \times b}$ of the line by plotting $\mathrm{C_e}$ vs $\frac{\mathrm{C_e}}{q_e}$.

The essential characteristics of Langmuir isotherm can be expressed in terms of a dimensionless parameter, R_L, which is defined by $R_L = \frac{1}{1} + bC_0$, where $\mathrm{C_0}$ is the initial dye concentration (mg/L) and b is the Langmuir constant (mg/L). The parameter indicates the shape of isotherm as follows: (Table 3.3)

Table 3.3: Use of separation factor ($\boldsymbol{R_L}$) to obtain information about the nature of adsorption (Ho et al., 2002, Nassar et al., 2004)

$\boldsymbol{R_L}$	**Type of isotherm**
$R_L > 1$	Unfavourable
$R_L = 1$	Linear
$0 < R_L < 1$	Favourable
$R_L = 0$	Irreversible

3.11 Kinetic Studies

The pseudo-first order reduction kinetic model has been applied for the reduction process involving iron-based nanoparticles for the organochlorine compounds (Rodríguez-Maroto et al., 2009). The expression is described below in Equation 3.16:

$$ln \times \frac{C_0}{C_e} = -k_{obs} \qquad \textbf{Equation 3.14}$$

where,

C_0 = OCPs concentrations at initial time

C_e= OCPs concentrations at t time

k_{obs} (min^{-1}) = the observed pseudo-first-order reaction rate constant

k_{obs} (min^{-1}) which is obtained from the slope of the regression line by plotting $ln \times \frac{C_0}{C_e}$ and reaction time. This pseudo-first order model describes apparent kinetics as a first-order process; however, this apparent order of the reaction might be influenced by the intrinsic reaction kinetics and diffusion. The experimental conditions result in a particularly controlled regime, in which diffusion through the pore structure might occur under the same time scale of the elementary reaction. If that is the case, the apparent kinetics will indicate first order processes since diffusion is a first-order process. Pseudo-second-order model is illustrated in Equation 3.17 as below:

$$\frac{t}{q_t} = \frac{t}{q_e} + \frac{1}{k_2 q_e^2}$$ **Equation 3.15**

3.12 Summary

Four types of biomass wastes (rambutan peel, oil palm leaves, jackfruit peel, sugar cane leaves) were used serving as both for the production of four biochars (B_{RtP}, B_{OpL}, B_{JfP}, B_{ScL}, respectively) and extracts (E_{RtP}, E_{OpL}, E_{JfP}, E_{ScL}, respectively) as a reducing agent for the synthesis of four types of green INPs-B_g nanocomposites (INPs-B_{RtP}, INPs-B_{OpL}, INPs-B_{JfP} and INPs-B_{ScL}, respectively). Chemically synthesized INPs-B_{Che} nanocomposites were also synthesized using sodium borohydride as a reducing agent. All nanocomposites were characterized by FESEM, EDX, FTIR, XRD and BET surface area analysis.

Batch adsorption experiments were performed for the removal of 6 OCPs in the synthetic individual solution and synthetic mixture solution as well using these as prepared nanocomposites. Conditions such as, pH, adsorbent dosage (g/L), adsorbate concentration (mg/L) and agitation time (min) and were optimized for the maximum removal of OCPs from water samples. In order to see the applicability of green INPs-B_g nanocomposites on real water samples, OPPD water samples were collected and spiked with OCPs of interest. The best one green INPs-B_{RtP} nanocomposite with maximum removal efficiency was applied on spiked OPPD water samples and conditions were optimized for the maximum removal of OCPs.

Both types of nanocomposites were aged to one month in air because the fresh synthesized nanoparticles are highly dynamic in nature and are expected to be changed rapidly with respect to their morphology and composition even under ambient environmental conditions which leads to changes in reactivity of nanoparticles. So as to see the removal efficiency of all one-month aged nanocomposites, batch adsorption

experiments were performed for the removal of OCPs in all water samples. Adsorption isotherm, adsorption kinetics studies were done. In order to confirm the potential of these green INPs-B_g nanocomposites for the reduction of these complex OCP compounds into less chlorinated compounds, desorption studies and GC-MS analysis were performed. GC-MS analysis was conducted to detect the dechlorinated byproducts of OCPs.

CHAPTER 4: RESULTS AND DISCUSSION

4.1 Synthesis and Characterization of Nanocomposites

4.1.1 Synthesis of Nanocomposites

In this study, two different methods i.e. green and conventional (chemical) methods were used for the synthesis of nanocomposites from the biomass wastes for the removal of OCPs in water system. In the green method, extracts of biomass wastes of rambutan peel, oil palm leaf, jackfruit peel and sugar cane leaf were used for the synthesis of green INPs supported on the biochar surface because these biomass wastes are abundantly available in Malysia. Batch experiments were performed in order to optimize the overall process that produces the polyphenol richest extracts. The detailed results are shown in Figures A.1-A.4 (Appendix A). Table A.1 (Appendix A) represents that four green polyphenol rich extracts obtained at the optimized conditions were found in the following order E_{RtP} (1510.36 mg GAE/L) > E_{OpL} (1249.50 mg GAE/L) > E_{JfP} (912.42 mg GAE/L) and > E_{ScL} (620.78 mg GAE/L). The surface area, mass yield% and element content of each biochar B_{RtP}, B_{JfP}, B_{OpL} and B_{ScL} obtained at four various pyrolysis temperatures 200, 250, 300 and 350 W for 30 min are shown in Table B.1 (Appendix B).

During the green synthesis of INPs-B_g nanocomposites, the biochar (owning to highest BET surface area m^2/g) was mixed in the $FeSO_4$ solution and Fe^{2+} was reduced to Fe^0 by the drop wise addition of various volumes of the green extracts in order to set the optimized $FeSO_4$:Extract ratio (v/v). The details on the effect of $FeSO_4$:Extract ratios for four types of green extracts during the synthesis of four types of green INPs-B_g nanocomposites on the OCPs removal efficiency using green INPs-B_g nanocomposites is presented in Figure C.1 (Appendix C) demonstrating the optimized $FeSO_4$:Extract ratios (v/v) for different types of green extracts during synthesis of four types of green INPs-B_g nanocomposites were found different for the maximum removal of OCPs.

Similarly, the INPs to biochar ratio is a key factor in the INPs-B_g synthesis as INPs and biochar complement each other by overcoming the mutual limitations. At higher INPs:biochar ratio, the excess amount of biochar compared to the optimum dosage may encase the INPs, thus hindering the direct contact of INPs with OCPs in the aqueous solution which resulted in the decreased OCPs removal efficiency (Dou et al., 2010). The results are shown in Figure C.2 (Appendix C) implying that in this study, 5 g of all biochars with 250 mL of 0.54 molar $FeSO_4$ solution were found to be optimum giving maximum OCPs removal and were selected for the synthesis of green INPs-B_g for use in further experiments.

During the chemical synthesis of INPs-B_{Che} nanocomposites, the biochar was mixed in the $FeSO_4$ solution and Fe^{2+} was reduced to Fe^0 by the drop wise addition of various volumes of the 1.08 mol/L $NaBH_4$ solution in order to set the optimized $FeSO_4$:$NaBH_4$ ratio (1:1-1:5, v/v). The details on the effect of $FeSO_4$:$NaBH_4$ ratios during the synthesis of INPs-B_{Che} nanocomposites on the OCPs removal efficiency using chemically synthesized INPs-B_{Che} nanocomposites is presented in Figure C.3 (Appendix C) demonstrating the optimized $FeSO_4$:$NaBH_4$ ratios (1:1) was found best for the maximum removal of OCPs. The INPs-B_{Che} nanocomposites removal capacity (R%) decreases from 60-75% to 15-11% with an increase in the $FeSO_4$:$NaBH_4$ ratio from 1:1 to 1:5. Further increase in the $FeSO_4$:$NaBH_4$ molar ratio from 1:1 to 1:5 resulted in the change in the INPs-B_{Che} colour from black to earthy brown and leading to a considerable decrease in the INPs-B_{Che} removal capacity. This may be due to the fact that the excess amount of $NaBH_4$ than needed for complete reduction of Fe^{2+} to Fe^0 causes the distorted surface morphology of INPs-B_{Che} nanocomposite due to the reduction of its surface leading to a decrease in its removal capacity at higher (>1:1) $FeSO_4$:$NaBH_4$ volume ratio (Devi & Saroha, 2014). Therefore, the $FeSO_4$:$NaBH_4$ volume ratio of 1:1 was found to

be optimum for the complete reduction of the Fe^{2+} to Fe^0 and was used in the synthesis of INPs-B_{Che} nanocomposite.

The above experimental results reveal that these biomass wastes having disposable problem can be converted into useful byproducts by replacing toxic and highly expensive $NaBH_4$ with cheaper, green and environmental friendly extracts with toxic and highly expensive $NaBH_4$ chemical during the synthesis of nanocomposites. These INPs-B_g nanocomposites synthesized by green method can be applied successfully as chemically synthesized INPs-B_{Che} nanocomposite for the cleaning of aquatic environment from OCPs. However, green synthesized INPs-B_g nanocomposites have some advantages over chemically synthesized INPs-B_{Che} nanocomposite.

4.1.2 Characterization of Nanocomposites

4.1.2.1 Fourier Emission Scanning Electron Microscopy

FESEM studies were performed on four types of biochar prepared from rambutan peel, oil palm leaf, jackfruit peel and sugar cane leaf and their respective four types of biochar supported green iron nanoparticles synthesized by using rambutan peel, oil palm leaf, jackfruit peel and sugar cane leaf bimass waste extracts as a reducing agent during reduction of Fe^{2+}. Figures 4.1 to 4.4 revealed the surface morphologies of bare biochar (B_{RtP}, B_{OpL}, B_{JfP}, B_{ScL}), INPs-B_g (INPs-B_{RtP}, INPs-B_{OpL}, INPs-B_{JfP}, INPs-B_{ScL}) and INPs-B_{Che} before and after the reaction with OCPs. The FESEM images of fresh INPs-B_{RtP} (Figure 4.1 b, c), INPs-B_{OpL} (Figure 4.2 b, c), INPs-B_{JfP} (Figure 4.3 b, c), INPs-B_{ScL} (Figure 4.4 b, c) revealed the successful synthesis and deposition of green INPs particles on the bichar surface and inside pores and all types of INPs were found spherical in shape with the diameter ranging from 20-80, 20-60, 10-80 and 15-75 nm, respectively.

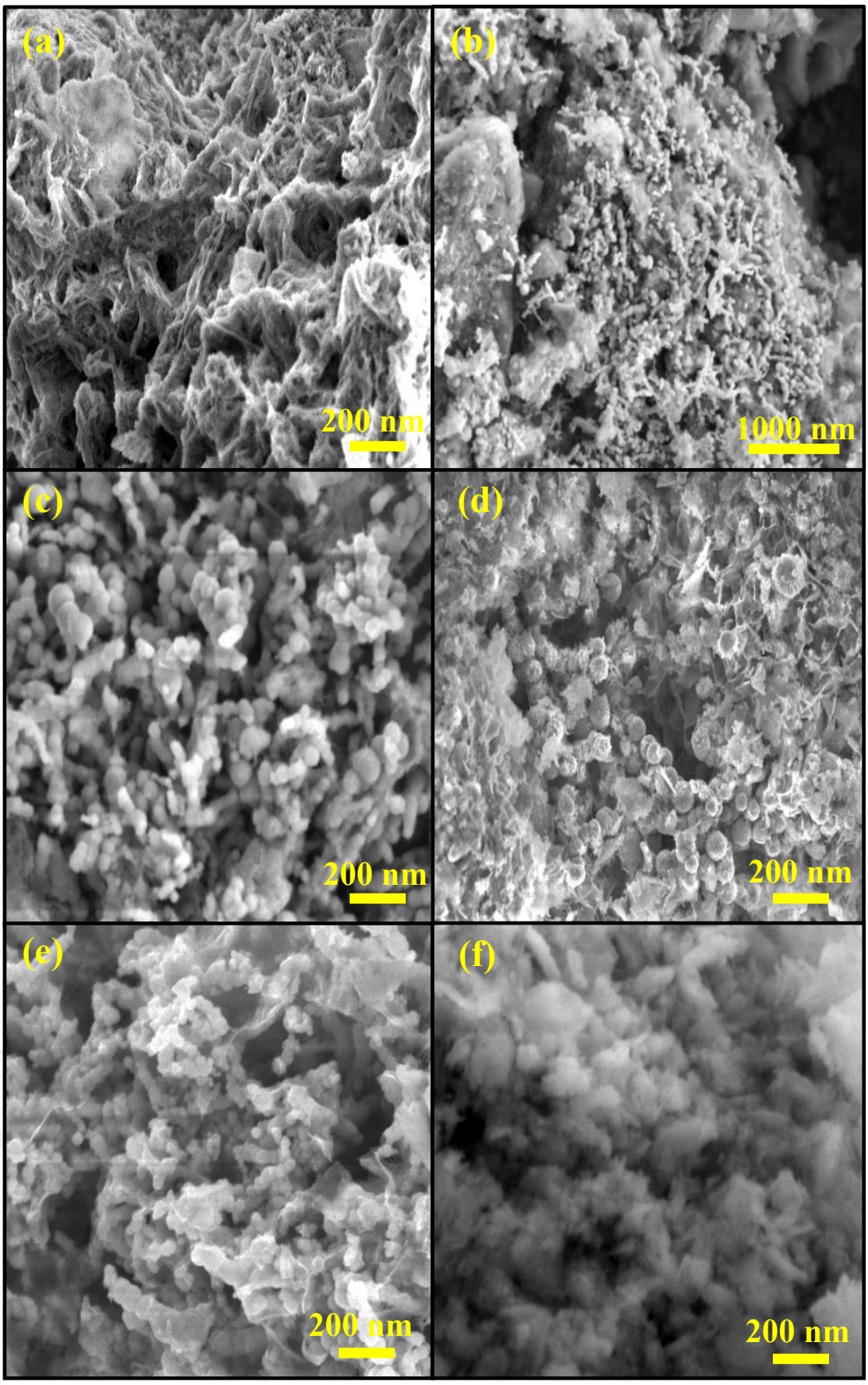

Figure 4.1: FESEM imges of (a) pristine biochar (B_{RtP}), (b, c) INPs supported on biochar (INPs-B_{RtP}) at different magnification times, (d) INPs-B_{RtP} after reaction with OCPs, (e) INPs-B_{Che} before reaction with OCPs, (f) INPs-B_{Che} after reaction with OCPs.

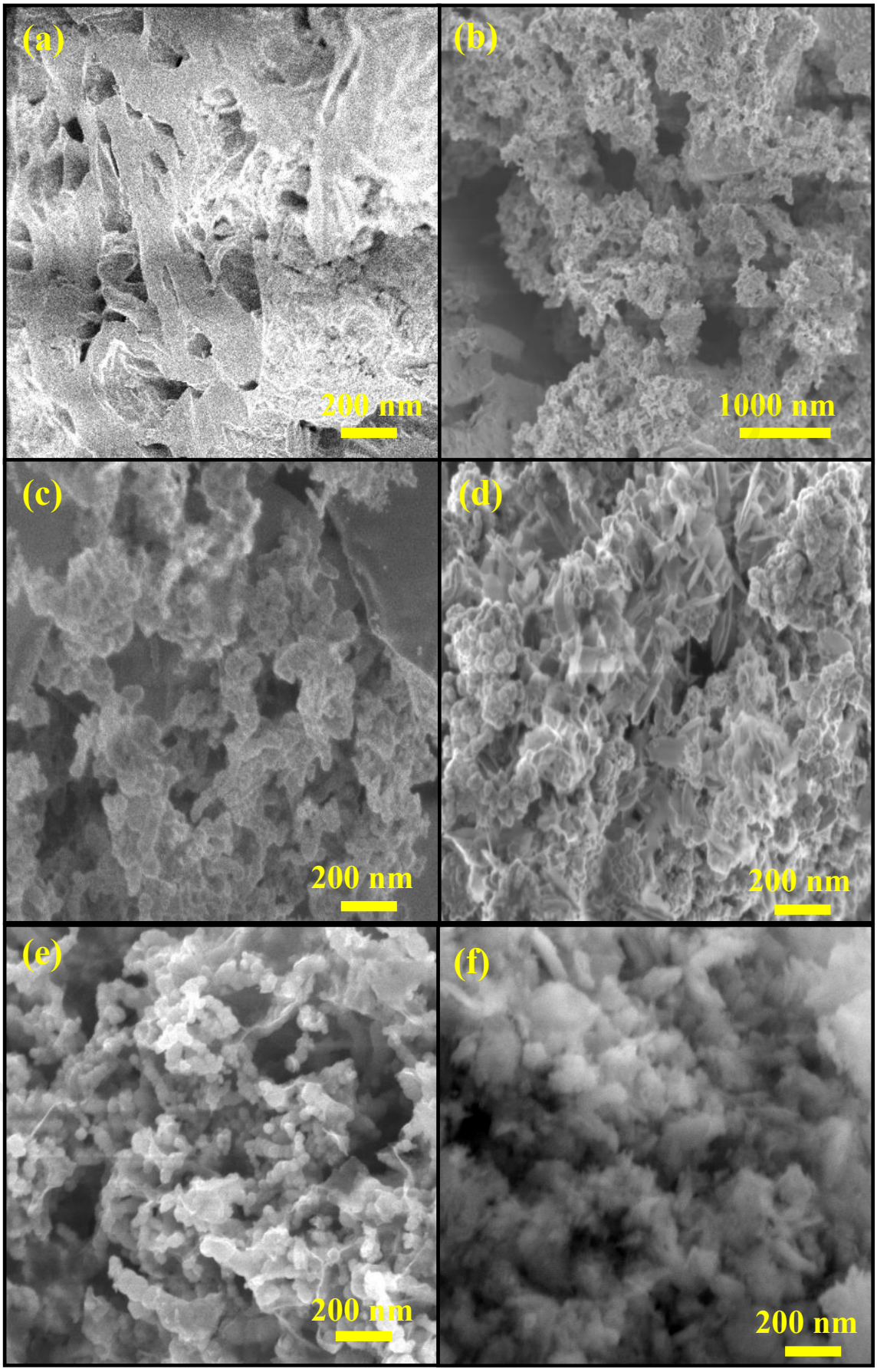

Figure 4.2: FESEM imges of (a) pristine biochar (B_{OpL}), (b, c) INPs supported on biochar (INPs-B_{OpL}) at different magnification times, (d) INPs-B_{OpL} after reaction with OCPs, (e) INPs-B_{Che} before reaction with OCPs, (f) INPs-B_{Che} after reaction with OCPs.

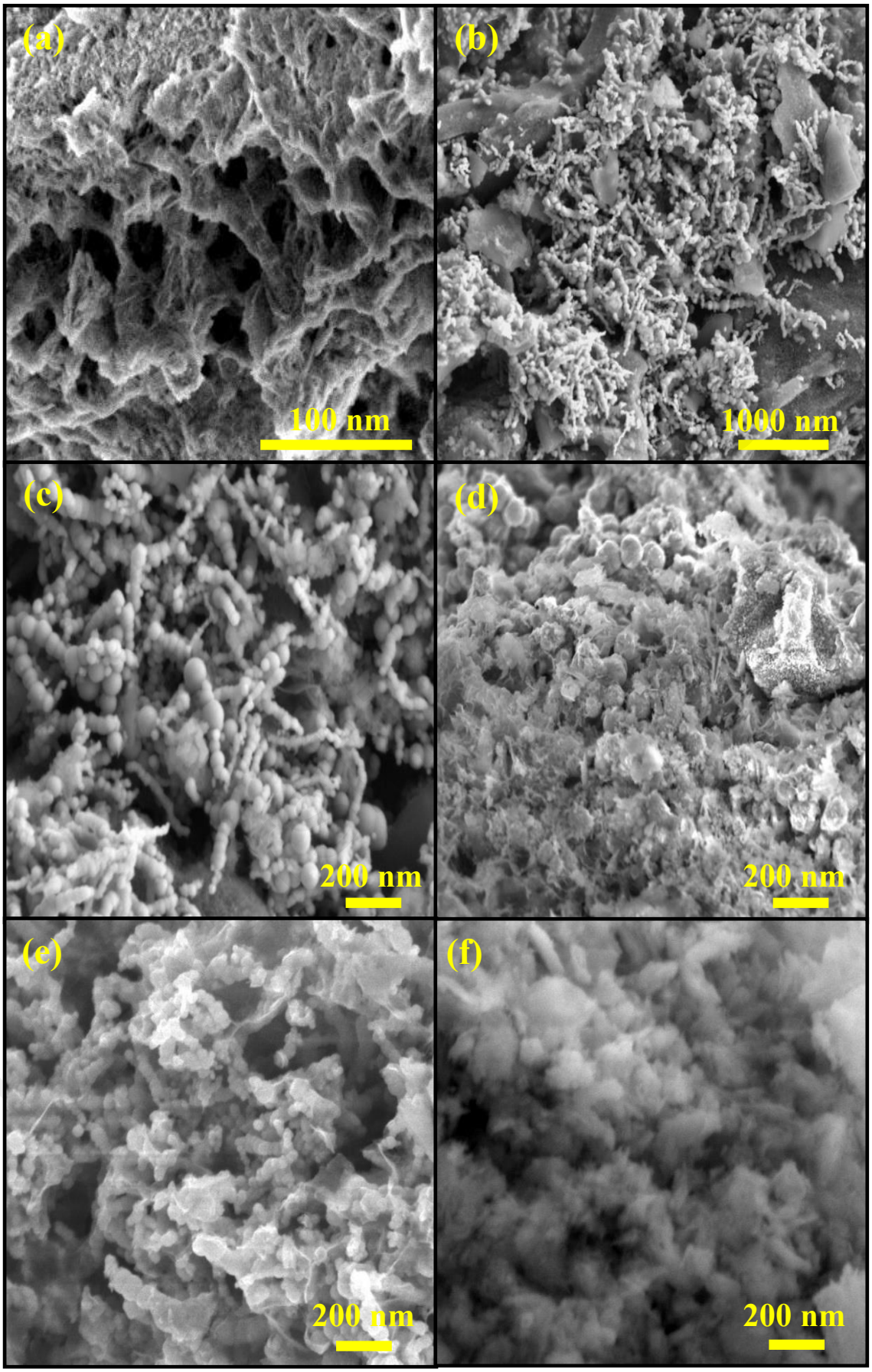

Figure 4.3: FESEM imges of (a) pristine biochar (B_{JfP}), (b, c) INPs supported on biochar (INPs-B_{JfP}) at different magnification times, (d) INPs-B_{JfP} after reaction with OCPs, (e) INPs-B_{Che} before reaction with OCPs, (f) INPs-B_{Che} after reaction with OCPs.

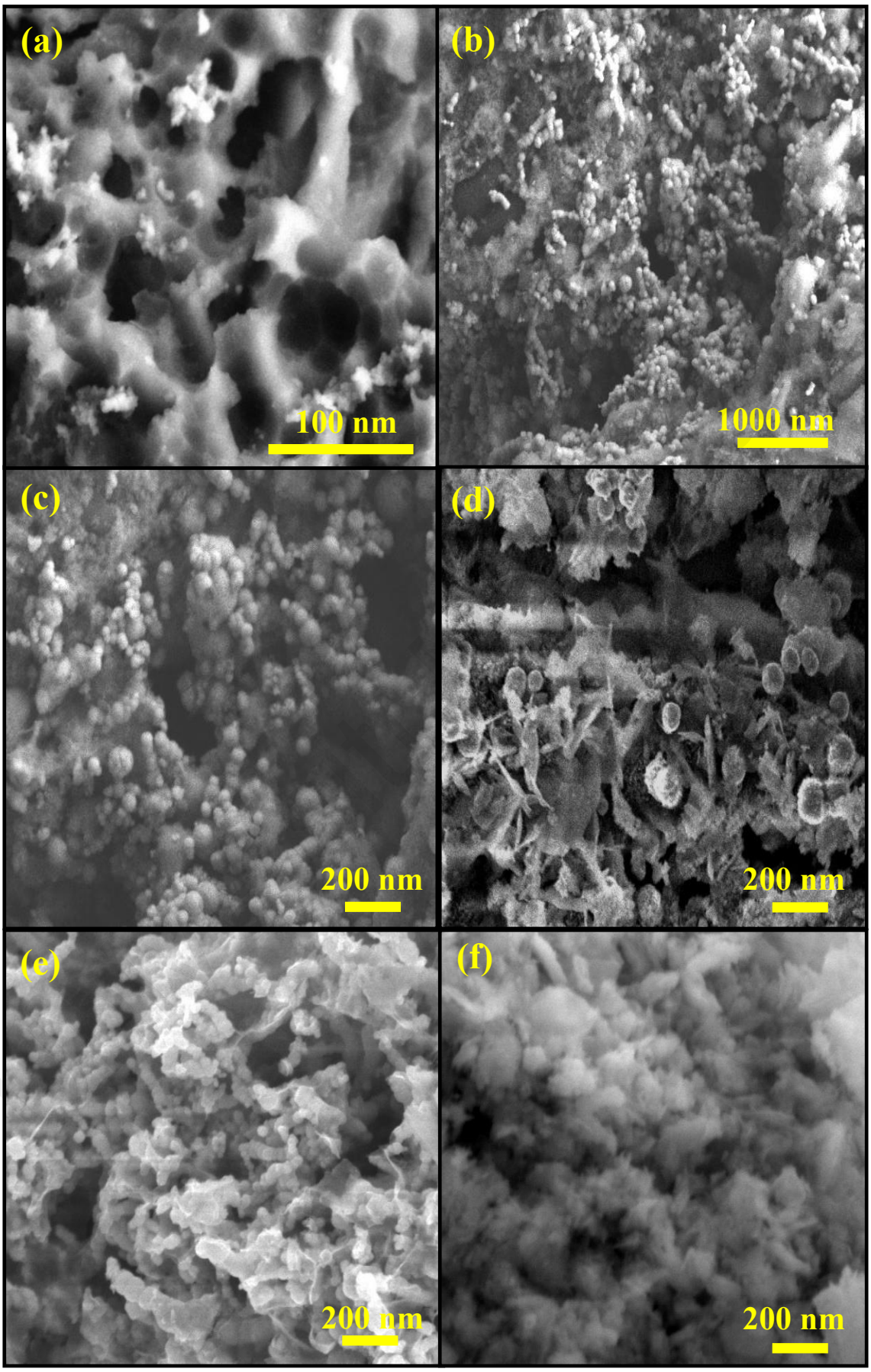

Figure 4.4: FESEM imges of (a) pristine biochar (B_{ScL}), (b, c) INPs supported on biochar (INPs-B_{ScL}) at different magnification times, (d) INPs-B_{ScL} after reaction with OCPs, (e) INPs-B_{Che} before reaction with OCPs, (f) INPs-B_{Che} after reaction with OCPs.

This differs from those INPs synthesized by using chemical (Na_2BH_4 has been used in this study) as a reducing agent which are more efficient in producing narrow dispersal particles i.e. 40-60 nm size in this study (Figure 4.1 to 4.4 e). This fact has also been supported by the findings of Chen et al., 2013. It is probably due to fact that the plant extract is a mixture of various naturally derived compounds with different reducing properties (Roy et al., 2013). After the reaction with OCPs, a quite different appearance of nanocomposite was observed (Figures 4.1 to 4.4 (d) and 4.4 (f), implying that INPs on biochar may be consumed and oxidized during the reductive degradation of OCPs compounds and the biochar almost completely distorted.

4.1.2.2 Energy-dispersive X-ray Spectroscopy

The Energy-dispersive X-ray spectroscopy (EDX) is useful to determine the percentage of the element and atoms in a sample. To further realize the configuration of four types of INPs-B_g nanocomposites and INPs-B_{Che} nanocomposite (for comparison), confined element composition was determined by EDX. As explicated in Figures 4.5 (a), (c), (e) and (g), the EDS pattern showed no peak for Fe in four pristine biochars but only C and O. Conversly, intense peaks Fe along with O and C appeared in Figures 4.5 (b), (d), (f) and (h) approving the production of Fe using green method. The C and O peaks originated predominantly from the polyphenol and other C and O-containing molecules in plant extracts and biochar. Similar peaks of Fe along with O and C were also observed in INPs-B_{Che} nanocomposite as shown in Figure 4.5 (i).

Specifically, the Fe loadings of INPs-B_{RtP} and INPs-B_{OpL} are 82.7 wt% and 70.5 wt%, while they are 63.9 wt% and 51.5 wt% for INPs-B_{JfP}, INPs-B_{ScL}, respectively. Obviously, the weight composition of Fe synthesized by rambutan peel extract is 14% higher than that of oil palm leaf extract whereas it is 22.73% and 37.73% higher than that of jackfruit peel and sugar cane leaf extract, respectively. The observed wt% of Fe was 66.12% in

INPs-B_{Che} nanocomposite. It was found to be 20 % and 6.2% lower than that of INPs-B_{RtP} and INPs-B_{OpL}, respectively while 3.36% and 22% higher than that of INPs-B_{JfP}, INPs-B_{ScL}, respectively. It indicates that INPs-B_{RtP} is superior to INPs-B_{Che} nanocomposite with respect to their wt% of Fe, while INPs-B_{ScL} is inferior to INPs-B_{Che} nanocomposite. The wt% of Fe INPs-B_{OpL} and INPs-B_{JfP} are almost equal to INPs-B_{Che} nanocomposite.

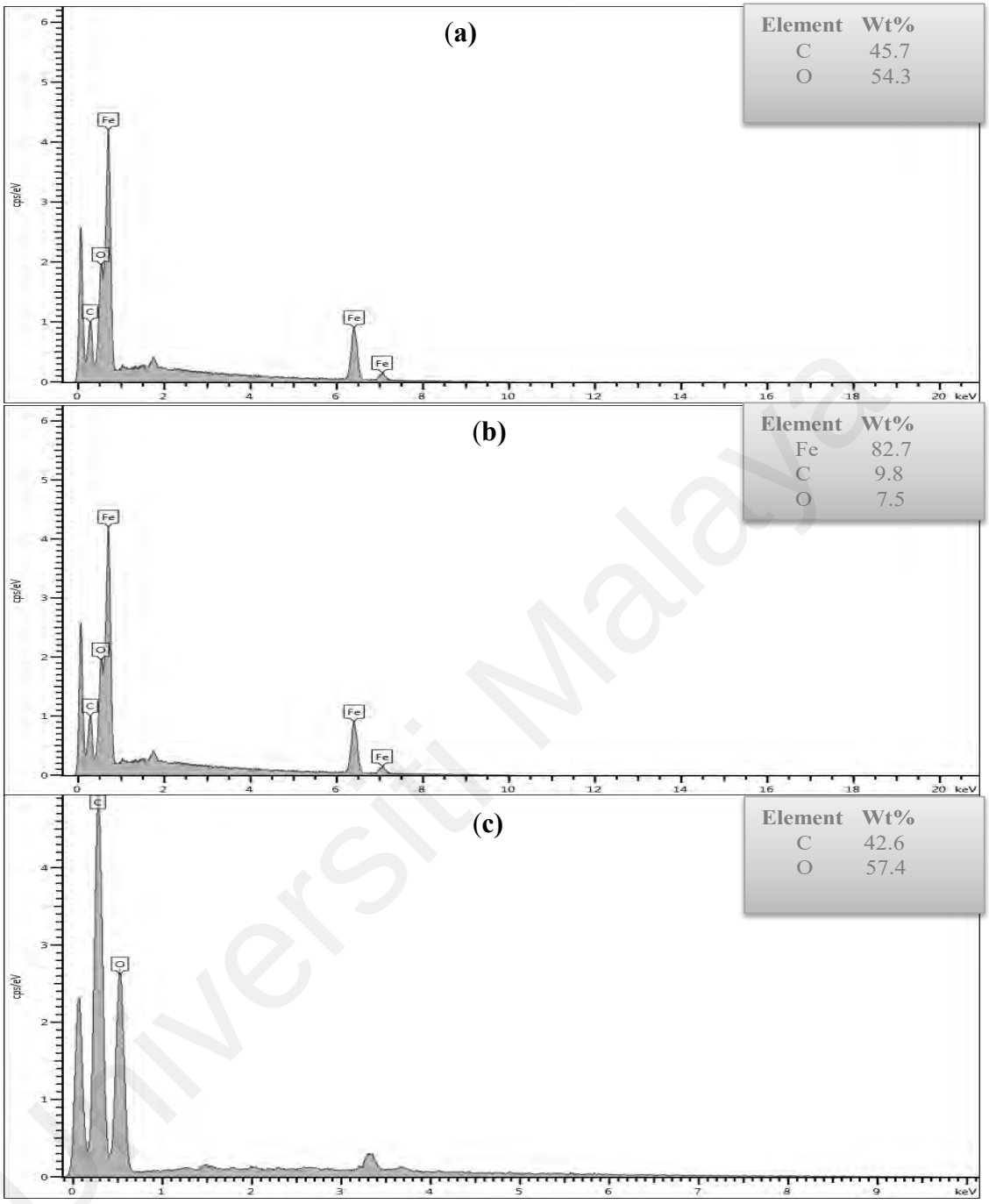

Figure 4.5: EDX spectra of (a) pristine biochar B_{RtP}, (b) INPs-B_{RtP} nanocomposite, (c) B_{OpL}, (d) INPs-B_{OpL} nanocomposite, (e) B_{JfP}, (f) INPs-B_{JfP} nanocomposite, (g) B_{ScL}, (h) INPs-B_{ScL} nanocomposite and (i) INPs-B_{Che} nanocomposite.

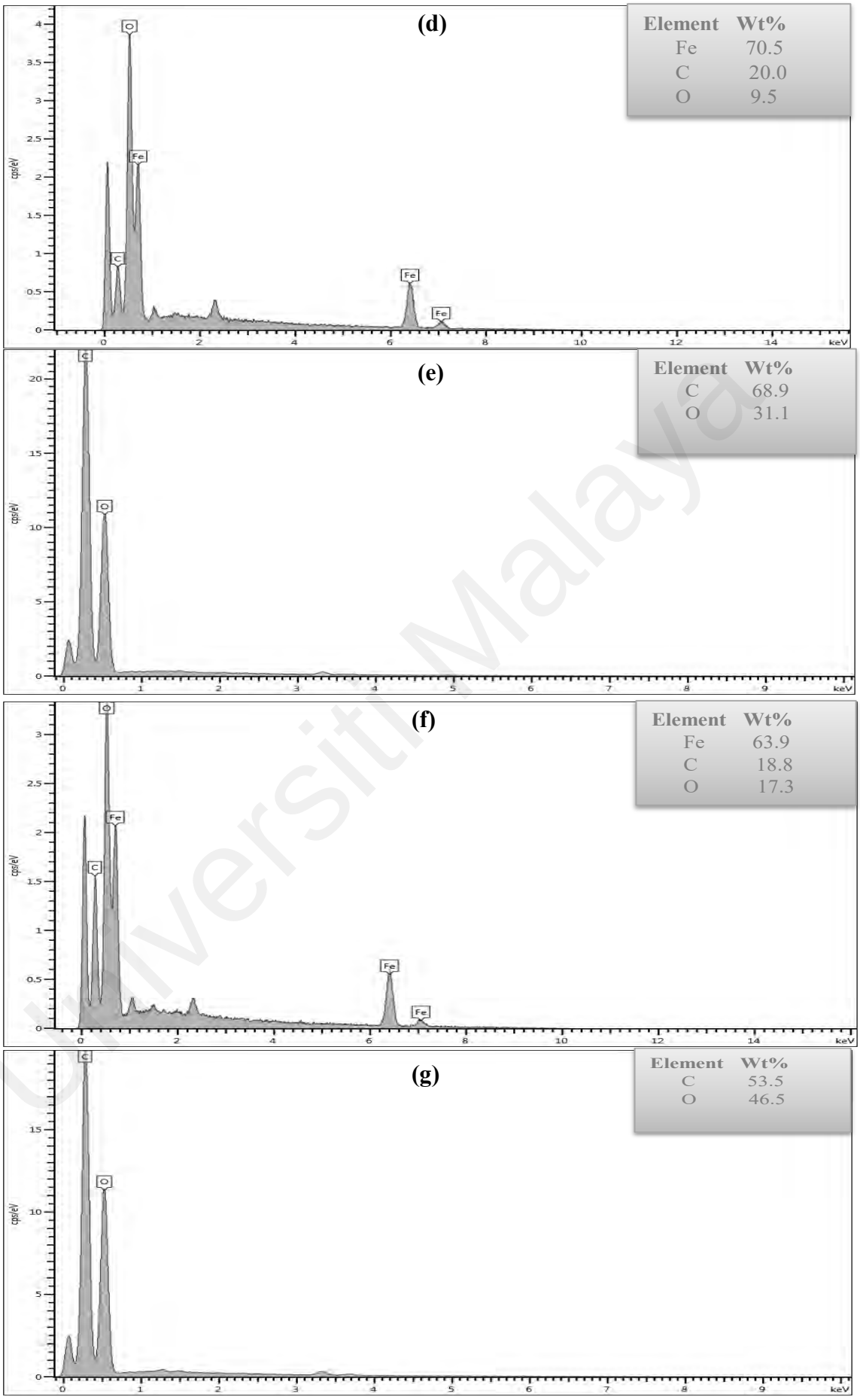

Figure 4.5, continued

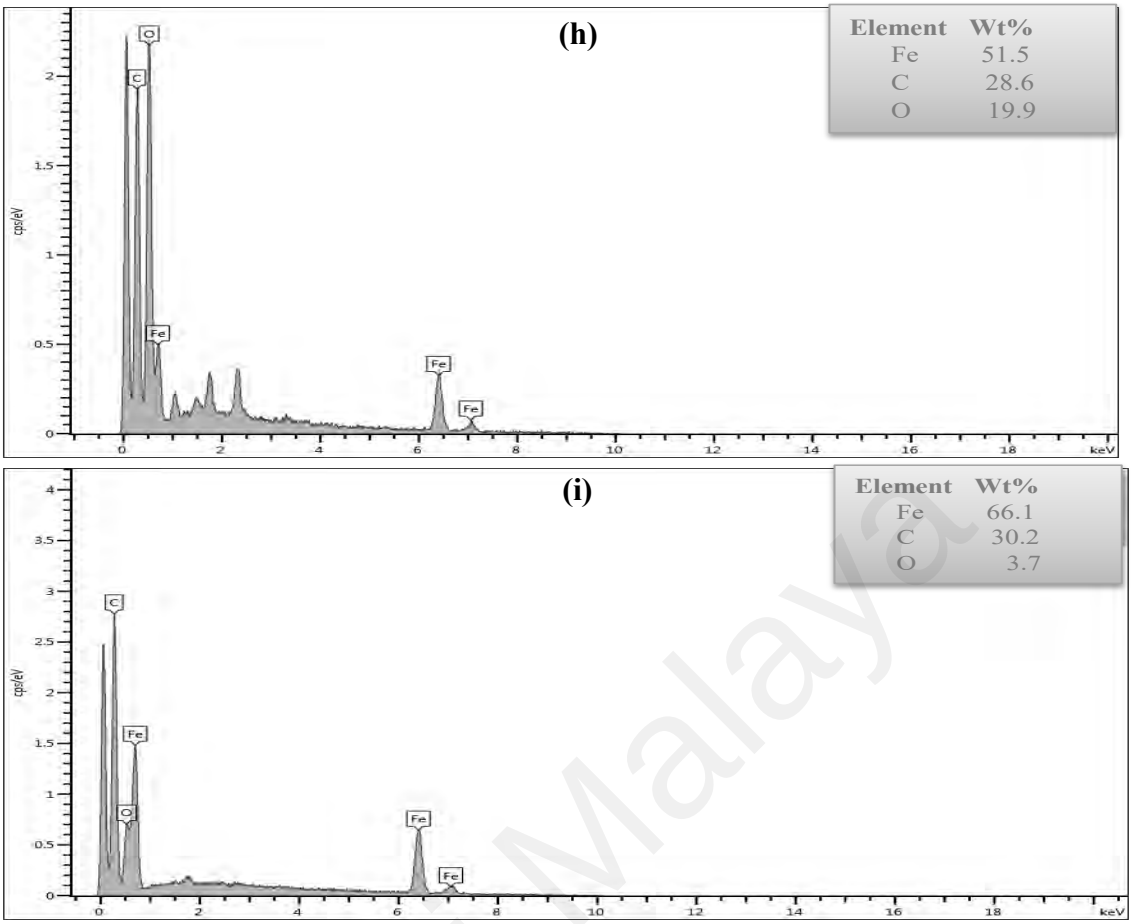

Figure 4.5: continued

4.1.2.3 FTIR Spectra

The FTIR spectra (4000-500 cm^{-1} range) of four types of pristine biochar (B_{RtP}, B_{OpL}, B_{JfP}, B_{ScL}), INPs-B_g (INPs-B_{RtP}, INPs-B_{OpL}, INPs-B_{JfP}, INPs-B_{ScL}) and INPs-B_{Che} (for comparison) before and after reaction with OCPs were employed to analyze the surface functional groups (Figures 4.6). The results of spectra for the four types of biochar supported green INPs nanocomposites of INPs-B_{RtP}, INPs-B_{OpL}, INPs-B_{JfP}, INPs-B_{ScL} and chemical synthesized INPs-B_{Che} have been shown in Table 4.1. Meanwhile, the FTIR spectra of the prepared INPs-B_{RtP}, INPs-B_{OpL}, INPs-B_{JfP}, INPs-B_{ScL} and INPs-B_{Che} (Figures 4.6 (b), (e), (h), (k) and (n), respectively and Table 4.1) displayed the almost similar stretching vibrations as in corresponding biochar B_{RtP}, B_{OpL}, B_{JfP}, B_{ScL} (Figures 4.6 (a), (d), (f), (j) and (m), respectively) and Table 4.1) revealing the presence of biochar constituents in INPs-B_g nanocomposites (Chen et al., 2008). However, the strong peaks

at approximate 584, 561, 568, 539 and 577 cm^{-1} were allocated to –Fe stretching vibration in INPs-B_{RtP}, INPs-B_{OpL}, INPs-B_{JfP}, INPs-B_{ScL} and INPs-B_{Che}, respectively ((Figures 4.6 (b), (e), (h), (k) and (n), respectively and Table 4.1) which reflected the introduction of Fe nanoparticles in all green INPs-B_g and INPs-B_{Che} rather than biochars (Chen et al., 2011; Iram et al., 2010).

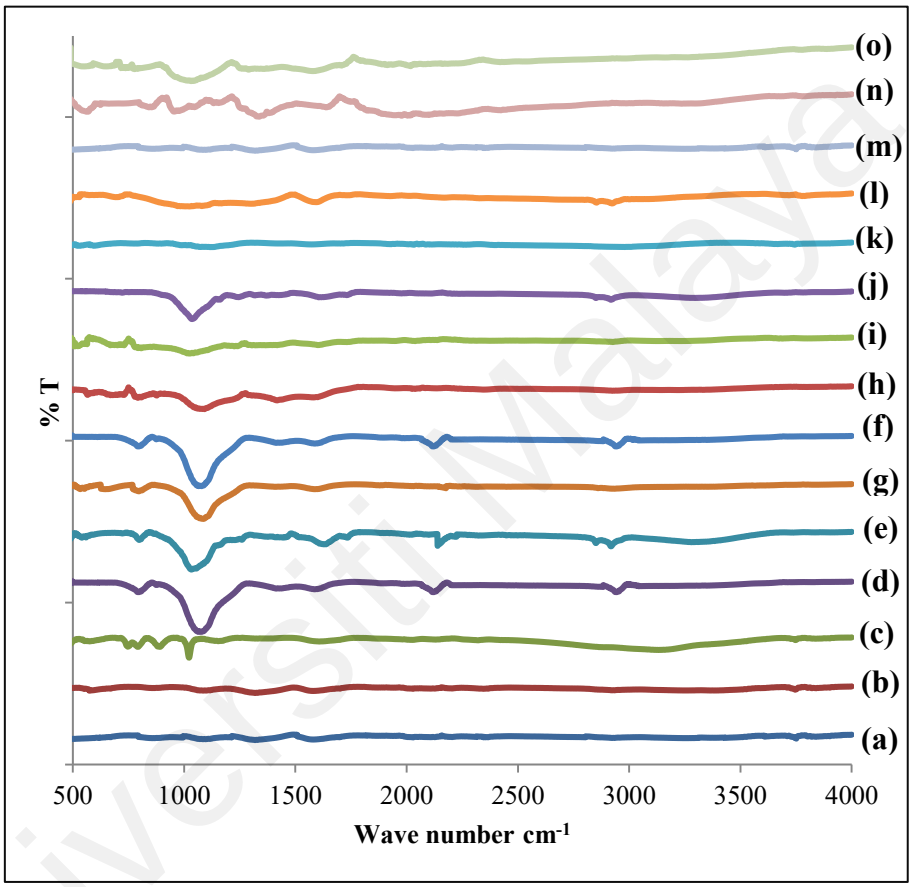

Figure 4.6: FTIR spectra of (a) pristine biochar B_{RtP}, (b) INPs-B_{RtP} nanocomposite before reaction, (c) and after reaction with OCPs, (d) pristine biochar B_{OpL}, (e) INPs-B_{OpL} nanocomposite before reaction, (f) and after reaction, (g) pristine biochar B_{JfP}, (h) INPs-B_{JfP} nanocomposite before reaction, (i) and after reaction, (j) pristine biochar B_{ScL}, (k) INPs-B_{ScL} nanocomposite before reaction, (l) and after reaction, (m) pristine biochar B_{Che}, (n) INPs-B_{Che} nanocomposite before reaction, (o) and after reaction.

Notably, after adsorption and reduction, the peaks at 751, 671, 695, 610 and 746 cm^{-1} were connected with the C–Cl stretching vibration from dechlorination of OCPs by INPs-B_{RtP}, INPs-B_{OpL}, INPs-B_{JfP}, INPs-B_{ScL} and INPs-B_{Che}, respectively ((Figures 4.6 (c), (g), (i), (l) and (o), respectively and Table 4.1). After adsorption and reduction by all types nanocomposite, indicating that the adsorption of these OCPs on to all green INPs-B_g and

INPs-B_{Che} may depend on the functional groups on the matrix surface (Zhang et al., 2015).

Table 4.1: FTIR spectra of all types of biochars and nanocomposites before and after reaction with OCPs.

Samples	Peak position (cm^{-1})	Possible functional groups
B_{RtP}	2952	–OH
	1335	–C-H aromatic
	2244	–C=C aromatic
	1120	–C–N aliphatic amines and nitriles
	1604	–N–H
$INPs\text{-}B_{RtP}$ before reaction	2952	–OH
	1335	–C-H aromatic
	2244	–C=C aromatic
	1120	–C–N aliphatic amines and nitriles
	1604	–N–H
	584	–Fe-O
$INPs\text{-}B_{RtP}$ after reaction	3191	–OH
	1387	–C-H aromatic
	2168	–C=C aromatic
	1023	–C–N aliphatic amines and nitriles
	1637	–N–H
	596	–Fe-O
	751	–Cl
B_{OpL}	2922	–OH
	1467	–C-H aromatic
	2142	–C=C aromatic
	1057	–C–N aliphatic amines and nitriles
	1645	–N–H
$INPs\text{-}B_{OpL}$ before reaction	2922	–OH
	1467	–C-H aromatic
	2142	–C=C aromatic
	1057	–C–N aliphatic amines and nitriles
	1645	–N–H
	561	–Fe-O
$INPs\text{-}B_{OpL}$ after reaction	2969	–OH
	1443	–C-H aromatic
	2177	–C=C aromatic
	1095	–C–N aliphatic amines and nitriles
	1623	–N–H
	555	–Fe-O
	671	–Cl
B_{JfP}	2956	–OH
	1442	–C-H aromatic
	2175	–C=C aromatic
	1097	–C–N aliphatic amines and nitriles
	1604	–N–H
$INPs\text{-}B_{JfP}$ before reaction	2956	–OH
	1442	–C-H aromatic

	2175	–C=C aromatic
	1097	–C–N aliphatic amines and nitriles
	1604	–N–H
	568	–Fe-O

Table 4.1, continued

Samples	Peak position (cm^{-1})	Possible functional groups
$INPs\text{-}B_{IfP}$ after reaction	2941	–OH
	1434	–C-H aromatic
	2146	–C=C aromatic
	1044	–C–N aliphatic amines and nitriles
	1621	–N–H
	527	–Fe-O
	695	–Cl
B_{ScL}	2931	–OH
	1451	–C-H aromatic
	2121	–C=C aromatic
	1143	–C–N aliphatic amines and nitriles
	1609	–N–H
$INPs\text{-}B_{ScL}$ before reaction	2931	–OH
	1451	–C-H aromatic
	2121	–C=C aromatic
	1143	–C–N aliphatic amines and nitriles
	1609	–N–H
	539	–Fe-O
$INPs\text{-}B_{ScL}$ after reaction	3000	–OH
	1326	–C-H aromatic
	2202	–C=C aromatic
	1097	–C–N aliphatic amines and nitriles
	1608	–N–H
	530	–Fe-O
	610	–Cl
B_{Che}	3364	–OH
	868	–C-H aromatic
	2170	–C=C aromatic
	1182,2046	–C–N aliphatic amines and nitriles
	1644	–N–H
$INPs\text{-}B_{Che}$ before reaction	3364	–OH
	868	–C-H aromatic
	2170	–C=C aromatic
	1182,2046	–C–N aliphatic amines and nitriles
	1644	–N–H
	577	–Fe-O
$INPs\text{-}B_{Che}$ after reaction	3353	–OH
	897	–C-H aromatic
	2100	–C=C aromatic
	1250,2041	–C–N aliphatic amines and nitriles
	1603	–N–H
	583	–Fe-O
	746	–Cl

4.1.2.4 XRD-spectra

To well comprehend the crystalline structure and XRD pattern of the as-prepared four types of green INPs-B_g nanocomposites (INPs-B_{RtP}, INPs-B_{OpL}, INPs-B_{JfP}, INPs-B_{ScL}) and chemical synthesized INPs-B_{Che} nanocomposite, XRD configurations of all above samples before and after reaction with OCPs were determined (Figures 4.7 a to j).

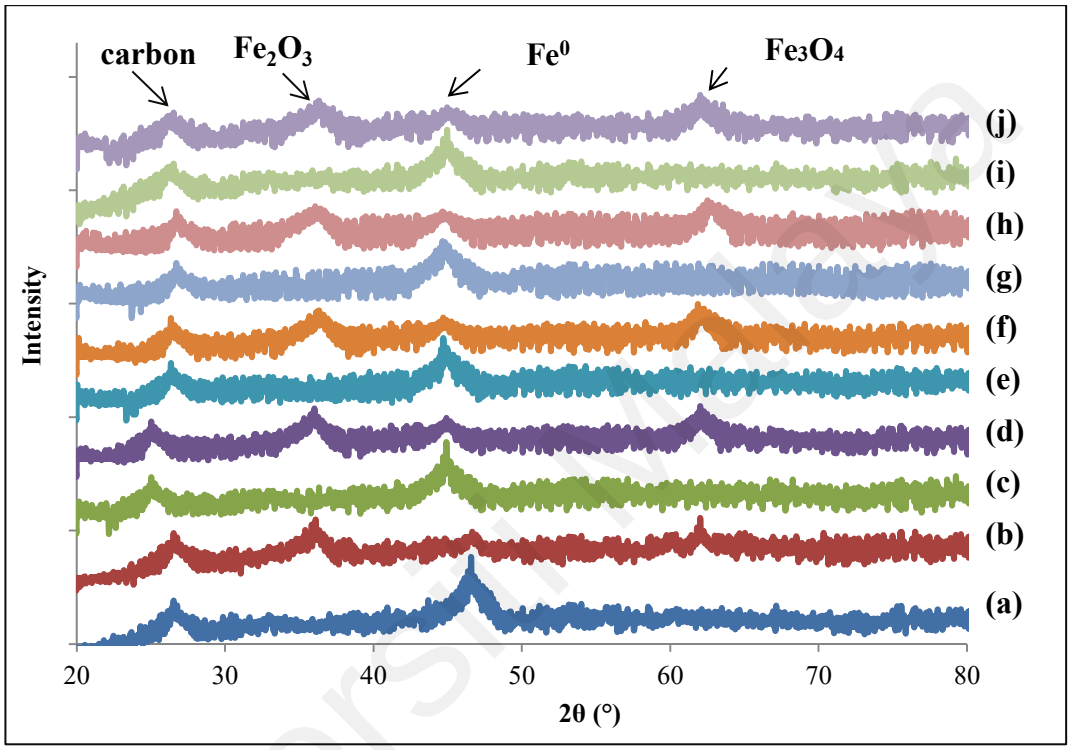

Figure 4.7: XRD spectra of (a) green INPs-B_{RtP} nanocomposite before reaction and (b) after reaction, (c) geen INPs-B_{OpL} nanocomposite before reaction and (d) after reaction, (c) green INPs-B_{JfP} nanocomposite before reaction and (f) after reaction, (g) green INPs-B_{ScL} nanocomposite before reaction and (h) after reaction, (i) chemical synthesized INPs-B_{Che} nanocomposite before reaction and (j) after reaction with OCPs.

The peaks observed in the XRD pattern near 2θ=25-26.53° can be identified as organic material in biochar and polyphenol of plant extracts (Wang et al., 2014B). Moreover, strong reflection peaks appeared at 2θ = 46.58°-44.6° due to green INPs, (Figures 4.7 a, c, e and g) which was found in consistent with the INPs synthesized by Terminalia chebula (Kumar et al., 2013), sorghum bran (Njagi et al., 2011) and green tea (Hoag et al., 2009). Similar intense peaks at 2θ = 45° for INPs on INPs-B_{Che}

nanocomposite synthesized by chemical as a reducing agent (Figure 4.7 i) (Quan et al., 2014)

The XRD spectra of all INPs-B_g nanocomposites and INPs-B_{Che} after reaction demonstrated that the peaks of INPs became less intensified, whereas peaks attributable to Fe_2O_3, Fe_3O_4 at 2θ=36.10° and 2θ=62.02° (Figure 4.7 b, d, f, h and j) showed that redox reaction had been occurred between INPs and OCPs where both green and chemical synthesized INPs acted as reductants.

4.1.2.5 BET Surface Area

The BET surface area of all types of pristine biochar (control sample) gree INPs-B_g nanocomposites and chemical synthesized INPs-B_{Che} (for comparison) were investigated by N_2 adsorption-desorption isotherms at 77 K. According to IUPAC classification (Table 4.1), pore can be distinguished in three groups in terms of their dimensions, i.e macroporous, mesoporous and microporous (Everett, 1986). Also, the pores can be classified according to their width (Sing, 1985). All types of pristine biochar produced in this work are mixed between the micropores and mesopores but the mesopore is higher in all samples. This mesoporous system enables a good dispersion of INPs over biochar support.

As shown in Table 4.2 the surface area, pore volume and pore size of all types of pristine biochar and their respective INPs-B_g nanocomposites existed distinctions. The BET surface area of all types of INPs-B_g nanocomposites (INPs-B_{RtP}, INPs-B_{OpL}, INPs-B_{JfP}, INPs-B_{ScL}) and INPs-B_{Che} were found to be considerably higher (i.e. 59.11, 57.30, 51.22, and 48.68%, respectively and 71.98 of INPs-B_{Che}) than those of their respective pristine biochar (B_{RtP}, B_{OpL}, B_{JfP}, B_{ScL}). All types of INPs-B_g nanocomposites and INPs-B_{Che} possessed larger pore volume and smaller pore size than that of their respective biochar. This was accredited to the formation of small iron stakes between the layers

which could build the micropores and then amplified the surface area. Furthermore, the exterior surface of the medium was layered by the INPs with sizes lager than the diameter of mesopores and micropores also contributed to intensification of surface area (Luo et al., 2013).

Table 4.2: BET surface area, total pore volume and average pore diameter of all the prepared biochar and nanocomposites.

Samples	BET surface area (m^2/g)	Total pore volume (m^2/g)	Average pore diameter (nm)	Wt% of iron
B_{RtP}	14.09	0.077	21.61	0
INPs-B_{RtP}	109.28	0.24	8.84	82.7
B_{OpL}	10.55	0.064	23.82	0
INPs-B_{OpL}	66.18	0.17	10.17	70.9
B_{JfP}	51.44	0.18	14.39	0
INPs-B_{JfP}	193.19	0.34	7.019	63.1
B_{ScL}	22.74	0.098	17.58	0
INPs-B_{ScL}	57.04	0.13	9.02	51
INPs-B_{Che}	71.98	0.33	18.35	66.12

4.2 Application of Nanocomposites for the Removal of OCPs from Water

4.2.1 Individual Removal of OCPs by Nanocomposites

4.2.1.1 Individual Removal of OCPs by Fresh Nanocomposites in Water

*(a) **Effect of Initial Solution pH***

Low pH increases the oxidation and higher pH consequently passivate the INPs grafted on biochar surface (Liuand Lowry, 2006; Songand Carraway, 2006). In this study, therefore, the removal tendencies of pesticides by four types INPs-B_g nanocomposites (INPs-B_{RtP}, INPs-B_{OpL}, INPs-B_{JfP}, INPs-B_{ScL}) under different initial solution pH were studied with the application of 0.25 g/L doses of different adsorbents at ambient temperature. The reactivity of all green synthesized INPs-B_g nanocomposites were also

compared with chemical synthesized INPs-B_{Che} nanocomposite under same experimental conditions as for INPs-B_g nanocomposites. From Figures 4.8 a-f, the removal capacities of INPs-B_{RtP}, INPs-B_{OpL}, INPs-B_{JfP}, INPs-B_{ScL} for pesticides reduced gradually up to 28-46%, 26-41%, 19-25% and 16-26%, respectively with the increase of pH from 5.0 to 12.0, and the adsorption amount for all the pesticides reached the maximum value (80-89%, 77-89%, 63-75% and 52-67%, respectively) at pH 4.0. Almost same trend was observed in case of chemical synthesized INPs-B_{Che} nanocomposite at pH 4.0 to 12.0. Chen et al, (2014) have found the same trend of HCB removal by INPs/AC at pH 5-12. At pH > 4, reduction in removal tendency can be explained by the generation of secondary reductants (Fe(II) or Fe(II)-containing oxides and hydroxides such as $Fe(OH)_3$) on the surface of iron that hinder the access of target contaminants to active sites of iron surface. A weak acidic condition (pH <5) would eliminate these passivating layers from the iron core and render it free for the dechlorination of the organochlorine pesticide molecules (Zhou et al., 2010; Begum and Gautam, 2011).

Moreover, strongly acidic condition promotes the higher production of H^+ ions in the aqueous medium which damage the carbon surface of biochar and oxidize the zero-valent INPs which in turn decrease the removal capacity of organochlorine pesticides (Zhuang et al, 2012). Therefore, pH 4 could be the most reasonable result for the maximum dechlorination of OCPs in a pesticide-INPs-B_g-water system. This result is in accord with that reported by Quan et al, (2014) for the removal of AO7 by chemically synthesized INPs supported on biochar

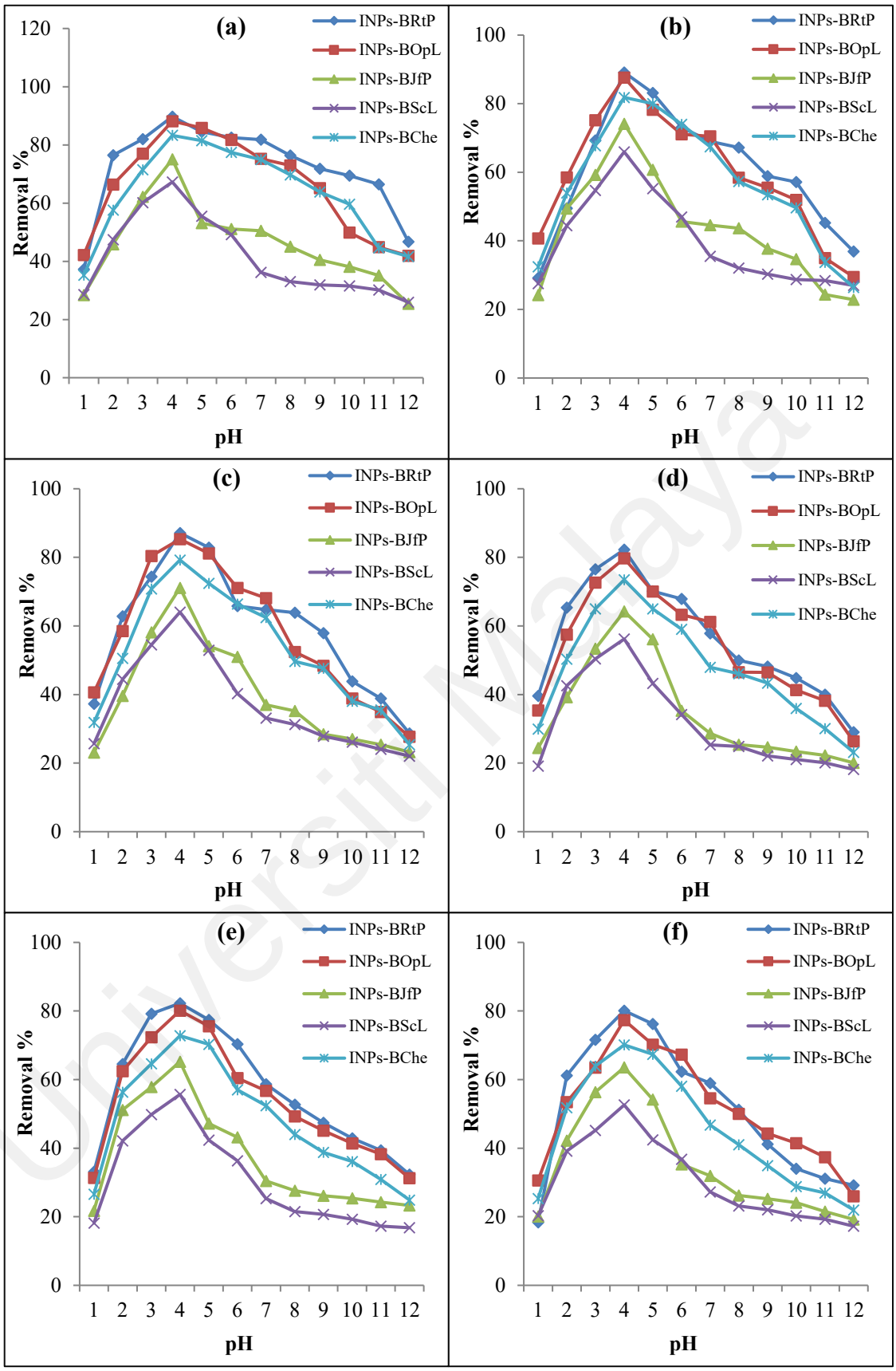

Figure 4.8: Effect of pH on the individual removal of OCPs (a) *p,p′*-DDT, (b) *o,p′*-DDT, (c) aldrin, (d) heptachlor, (e) hexachlorobenzene, and (f) endosulfan I by fresh four green INPs-Bg and INPs-B_{Che} nanocomposites; 2 mg/L of each adsorbate; 0.01 g/L of adsorbent; agitation speed 150 (rpm); agitation time 240 min; at temperature 25±2 °C.

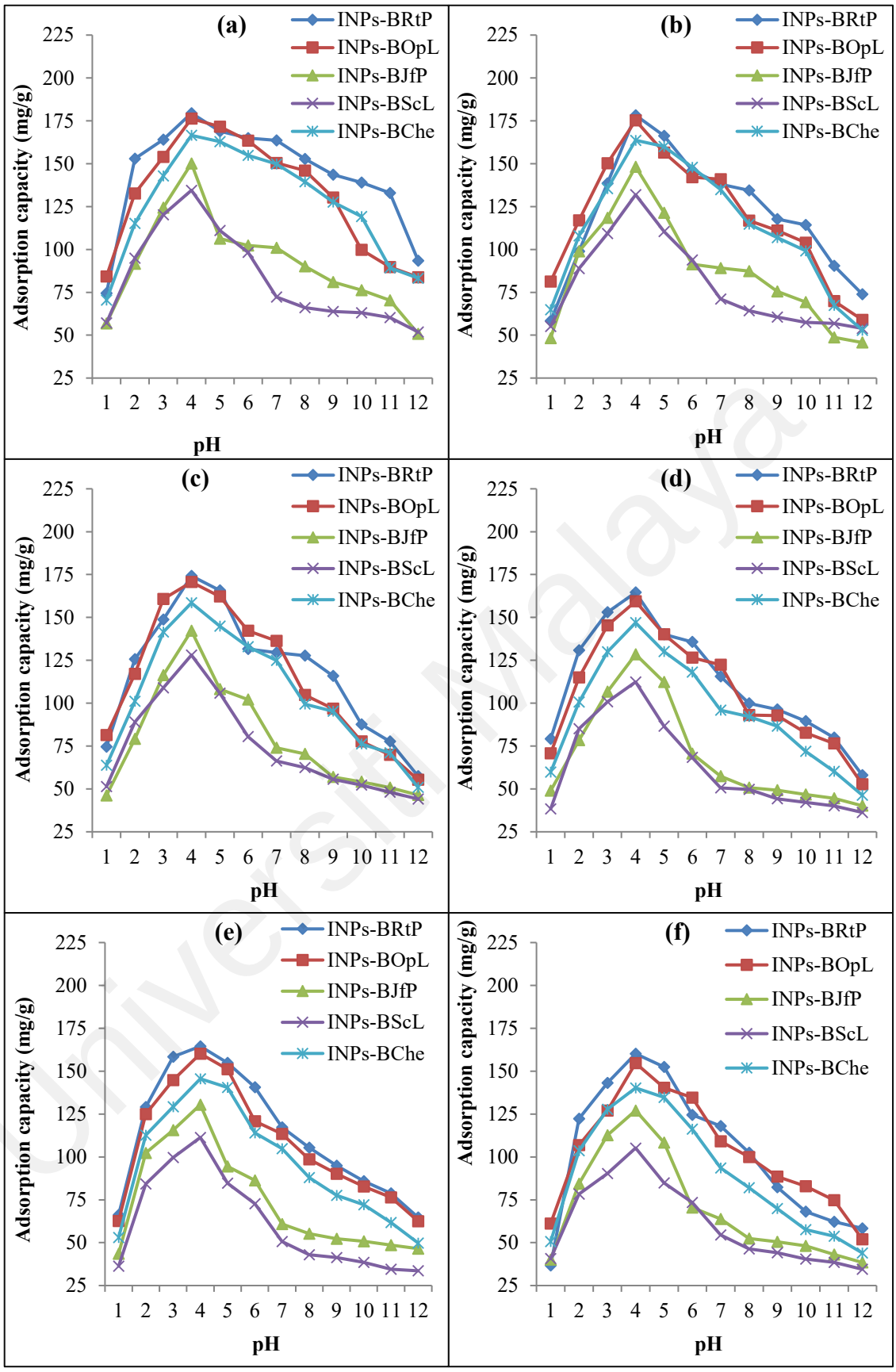

Figure 4.9: Effect of pH on the adsorption capacity of fresh four green INPs-Bg and INPs-B_{Che} nanocomposites for OCPs (a) *p,p′*-DDT, (b) *o,p′*-DDT, (c) aldrin, (d) heptachlor, (e) hexachlorobenzene, and (f) endosulfan I; 2 mg/L of each adsorbate; 0.01 g/L of adsorbent; agitation speed 150 (rpm); agitation time 240 min; at temperature 25±2 °C.

The adsorption capacity decreased with the increase in pH from 5-12 and decrease in pH from 3-1 as well (See Figure 4.9 a-f). In a previous srtudy conducted by Zhang et al, (2015), the same trend was observed for the adsorption of Cr(VI) by chitosan modified magnetic biochar at various range of pH. This trend is obviously expected on account of the fact that the strong acidic and basic condition leads to a decrease in active sites on the surface of the nanoadsorbent which inturn decrease the adsorption of OCP molecules (Zou and Khan, 2016). The adsorption capacity of chemically synthesized INPs-B_{Che} at pH 4 (140.2-166.5 mg/g for all OCPs) were found to be only 7.2% and 5.6% lower than that of green B_{RtP} and INPs-B_{OpL} nanocomposites (160.2-179.5 and 154.7-176.3 mg/g, respectively for all OCPs) whereas it was found to be only 9.8% higher than that of INPs-B_{JfP} (127.1-150.2 mg/g for all OCPs) and considerably higher than that of INPs-B_{ScL} (105.2-134.5 mg/g for all OCPs). As the pH increased from 5-12, the adsorption capacity of all types of nanocomposites decreased in the range of 51-83%. Therefore, maximum adsorption capacity of all OCPs were found at pH 4 with all types of nanocomposites which is in consistent with the result findings of a researcher Shih et al, (2011) for the removal of HCB by chemically synthesized INP-AC.

(b) Effect of Initial Dosage of Nanocomposites

The influence of all INPs-B_g nanocomposite dosages on removal of organochlorine pesticides (OCPs) with 2 mg/L concentration at pH 4.0 was also investigated. The reactivity of all green INPs-B_g nanocomposites were also compared with chemical synthesized INPs-B_{Che} nanocomposite under same experimental conditions as for all INPs-B_g nanocomposites and the results are illustrated in Figures 4.10 a-f. The removal tendency of OCPs is increased considerably with increasing adsorbent dosage from 0.01-0.15 g/L of INPs-B_{RtP}, INPs-B_{OpL}, INPs-B_{Che} and 0.01-0.2 g/L of INPs-B_{JfP}, INPs-B_{ScL}. The positive correlation between adsorbent dose and OCPs removal can be attributed to an increase in the adsorption surface area and availability of more active sites. The

maximum adsorption (100%) is achieved when 0.1 g/L of INPs-B_{RtP}, INPs-B_{OpL} nanocomposites and 0.15 g/L of INPs-B_{JfP}, INPs-B_{ScL} nanocomposites.

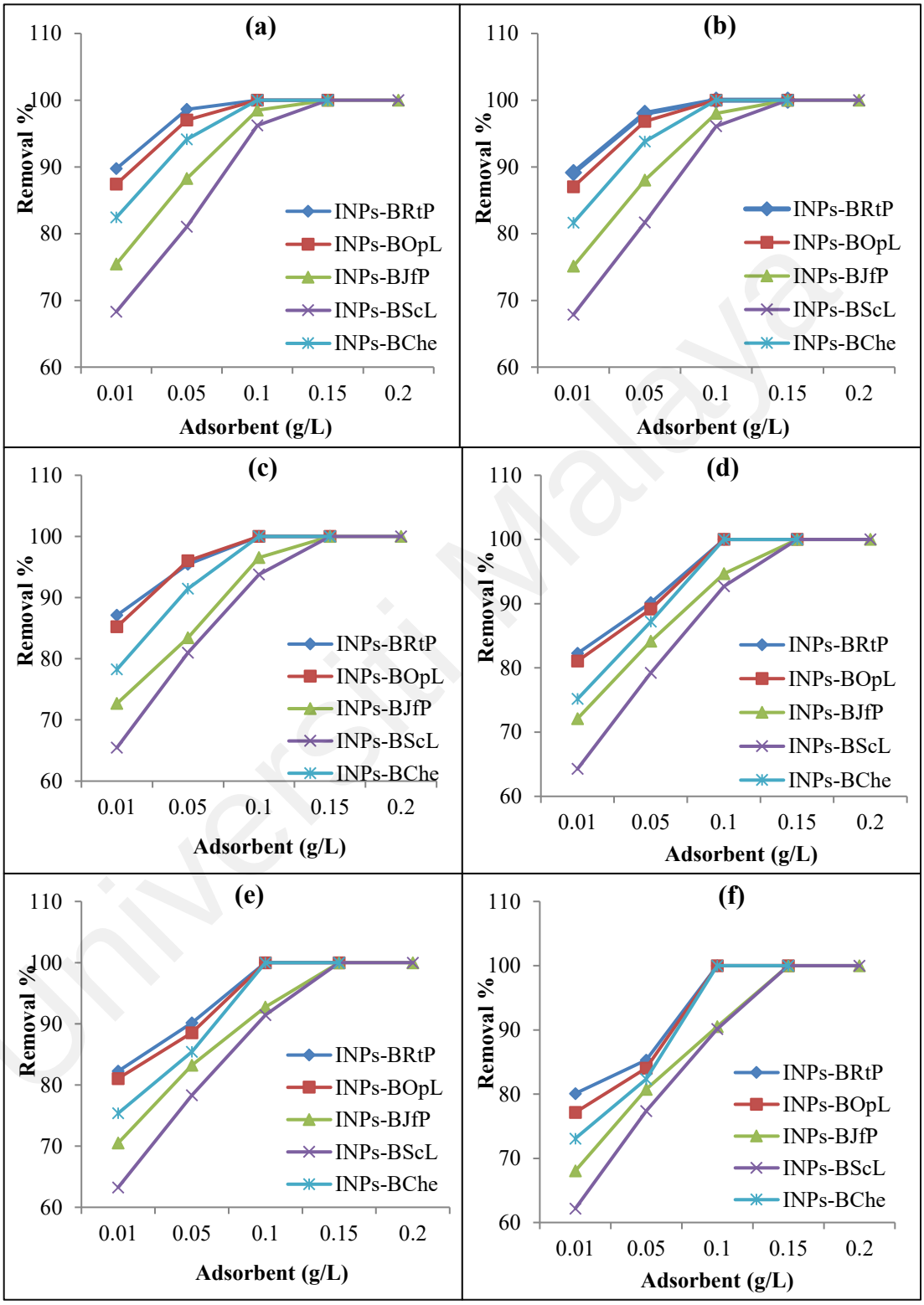

Figure 4.10: Effect of initial concentration of fresh four green INPs-Bg and INPs-B_{Che} nanocomposites on individual removal of OCPs (a) *p,p′*-DDT, (b) *o,p′*-DDT, (c) aldrin, (d) heptachlor, (e) hexachlorobenzene, and (f) endosulfan I; 2 mg/L of each adsorbate; agitation speed 150 (rpm); agitation time 240 min; at temperature 25±2 °C and pH 4

As the concentration of adsorbent dose (g/L) applied and OCPs removal percentage both are associated with wt% of iron of nanocomposites, therefore, both INPs-B_{RtP} and INPs-B_{OpL} having higher wt% (83% and 71%, respectively) of iron than other nanocomposites has given maximum removal % of OCPs with only 0.1 g/L of nanocomposite.

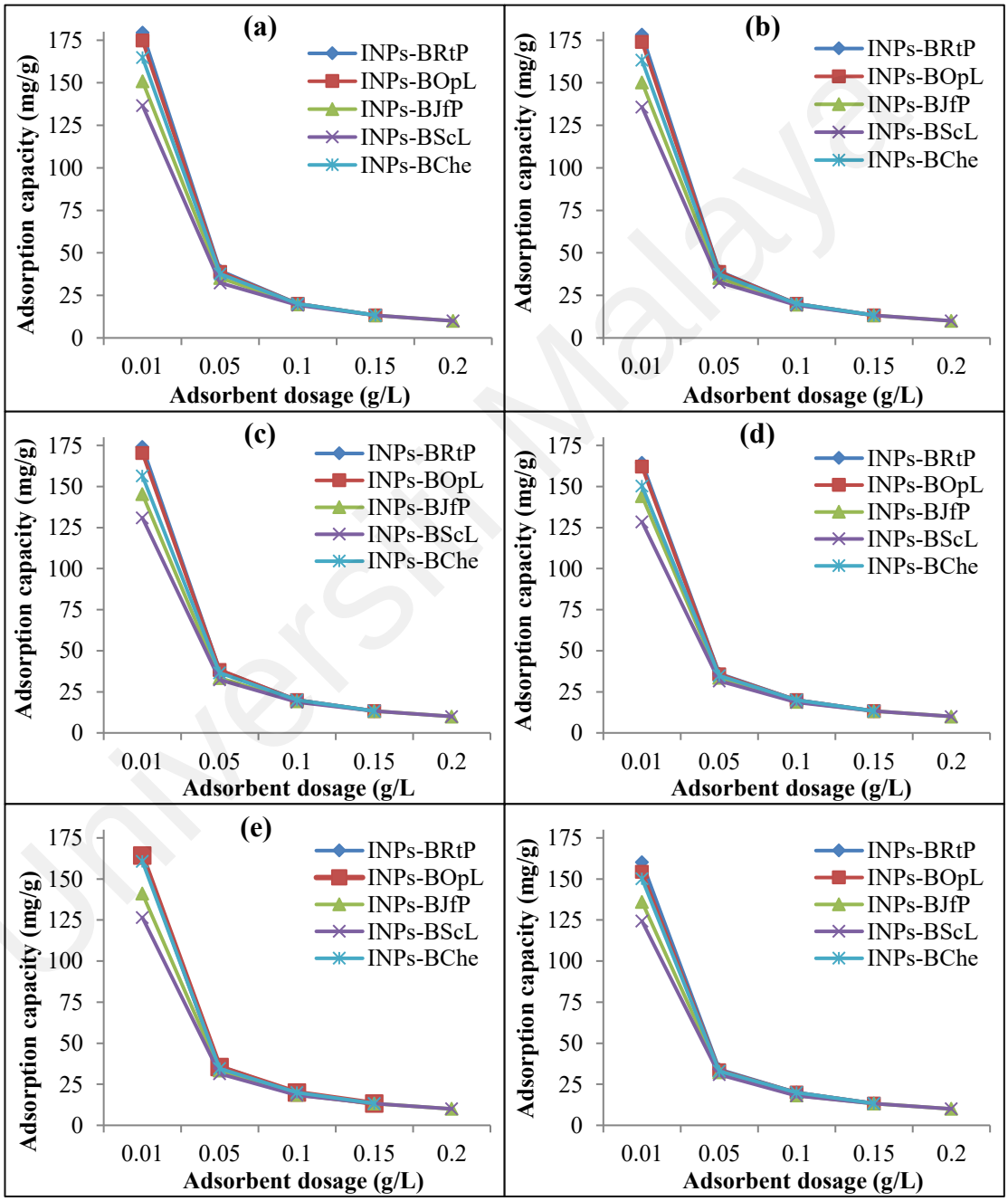

Figure 4.11: Effect of initial concentration of fresh four green INPs-B_g and INPs-B_{Che} nanocomposites on their adsorption capacity for OCPs (a) *p,p′*-DDT, (b) *o,p′*-DDT, (c) aldrin, (d) heptachlor, (e) hexachlorobenzene, and (f) endosulfan I; 2 mg/L of each adsorbate; agitation speed 150 (rpm); agitation time 240 min; at temperature 25±2 °C and pH 4.

In comparison, chemically synthesized INPs-B_{Che} nanocomposite gave 100% removal efficiency using only 0.1 g/L as with INPs-B_{RtP} and INPs-B_{OpL} nanocomposites, meanwhile 0.15 g/L of INPs-B_{JfP} and INPs-B_{ScL} gave 100% removal of OCPs. A similar study was conducted by Han et al, (2015) in which they developed the biochar supported INPs using chemical method and applied for the removal of methyl orange (MO) dye in aqueous solution. Only 38.6% removal of MO was obtained with 0.3 g/L within 15 min. while, removal % increased upto 97.3 % with 0.9 g/L dose of MO within 15 min. This shows that all INPs-B_g nanocomposite synthesized in this study are highly efficient for the removal of OCPs.

As seen in Figures 4.11 a-f, an opposite trend of adsorption capacity at equilibrium was observed for all OCPs with all types of nanocomposites. The adsorption capacity of all types of nanocomposites decreased by 91-94% which was in the range of 124-174mg/g at the lowest adsorbent dose (0.01 g/L) and 10 mg/g at highest adsorbent concentration (0.2 g/L) for all types of nanocomposites. This may be attributed to aggregation of the nanocomposites which reduce the active sites contributing to the low adsorption capacity by increasing the adsorbent dose (Pourtedal & Sadegh, 2002). The highest adsorption capacity of INPs-B_{RtP}, INPs-B_{OpL}, INPs-$B_{Che,}$ INPs-B_{JfP} and INPs-B_{ScL} at 0.1-0.15 g/L dose of nanocomposites were found to be in the following order: $20 \approx 20 \approx 20 > 13$ and ≈ 13 (mg/g), respectively. Higher concentration of polyphenol content in rambutan peel extract may attribute to the higher wt% of iron in rambutan peel based synthesized INPs supported on rambutan peel biochar which in turn gave highest range of adsorption capacity for OCPs than those of other nanocomposites.

(c) Effect of Initial Concentration of Adsorbate

The rate of adsorption is a function of the initial concentration of the adsorbate, which is a significant factor to be considered for effective adsorption. Figures 4.12 a-f reveal

that removal capacity of OCPs decreased with increment of the OCPs. However, with the increase in the concentration of adsorbates from 4 to 20 mg/L, a considerable decrease in removal efficiency of all INPs-B_g nanocomposites was observed.

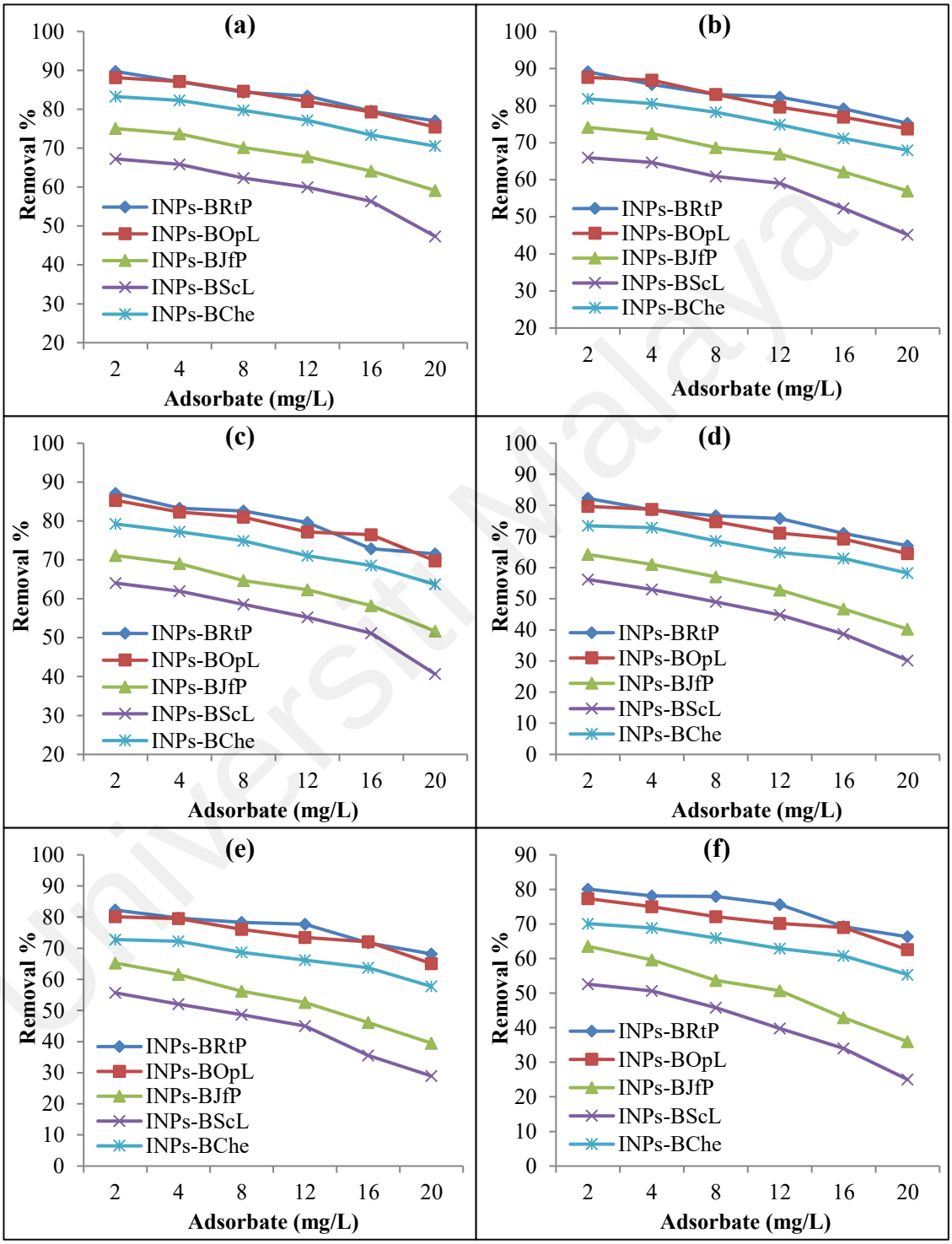

Figure 4.12: Effect of initial pesticide concentration on individual removal of OCPs (a) *p,p′*-DDT, (b) *o,p′*-DDT, (c) aldrin, (d) heptachlor, (e) hexachlorobenzene, and (f) endosulfan I by 0.10-0.15 g/L of fresh four green INPs-B_g and INPs-B_{Che} nanocomposites; agitation speed 150 (rpm); agitation time 240 min; at temperature 25±2 °C and pH 4

The reactivity of all green INPs-B_g nanocomposites were also compared with chemical synthesized INPs-B_{Che} nanocomposite under same experimental conditions as for green INPs-B_g nanocomposites. At initial concentration 2 mg/L of adsorbates, maximum removal % (range of % removal of all OCPs i.e 80-89%, 77-88%, 64-75%, 53-67% and 70-83%) was achieved with the application of INPs-B_{RtP}, INPs-$B_{OpL,}$ INPs-B_{JfP}, INPs-B_{ScL} and INPs-B_{Che}, respectively.

However, in case of higher initial concentrations up to 20 mg/L of adsorbate, the lower % removal 66-77%, 63-75%, 36-59%, 25-47% and 55-71% was achieved with INPs-B_{RtP}, INPs-$B_{OpL,}$ INPs-B_{JfP}, INPs-B_{ScL} and INPs-B_{Che}, respectively. Our research findings are in consistent with the results of Pourtedal and Sadeg (2014) in which they removed four antibiotics simultaneously i.e., Amoxicilline, Cephalexin, Tetracycline and Pencillin G in the mixture and observed the decrease in removal % with increase in adsorbate concentration. In case of INPs-B_{JfP} and INPs-B_{ScL}, a considerable decline in removal % (up to 44 and 53%, respectively) with increase in adsorbate concentration may attribute to the less wt% of Fe^0 in these nanocomposites because of less polyphenol concentration in the extracts of jackfruit peel and sugar cane leaf, respectively responsible for the less production of INPs on biochar surface. The effect of higher dose on removal efficiency can be explained by considering that dechlorination of previously adsorbed OCPs provide sorption sites for the OCPs in the solution even at higher concentrations. Moreover, dechlorination of OCPs generates the chloride ions in the solution that adsorb on nanocmposites (Shih et al., 2011).

The adsorption capacity of green INPs-B_{RtP}, INPs-$B_{OpL,}$ for all OCPs (at 2 mg/L of adsorbates) were found to be in range of 16.0-18.0 mg/g and 15.5-17.6 mg/g, respectively and it was found to be almost similar to that of INPs-B_{Che} which was 14.0-16.7 mg/g, whereas, the adsorption capacity of green INPs-B_{JfP} and INPs-B_{ScL} was found to be considerably lower (39 and 50%, respectively) than that of INPs-B_{Che} which was 8.5-

10.0 and 7.0-9.0 mg/g, respectively. By further increase in adsorbate concentration, chloride ions were produced in abundant amount in solution which can compete with OCP molecules for the available active sites on the surface of INPs-B_g nanocomposites and make less availability of active sites for dechlorination process.

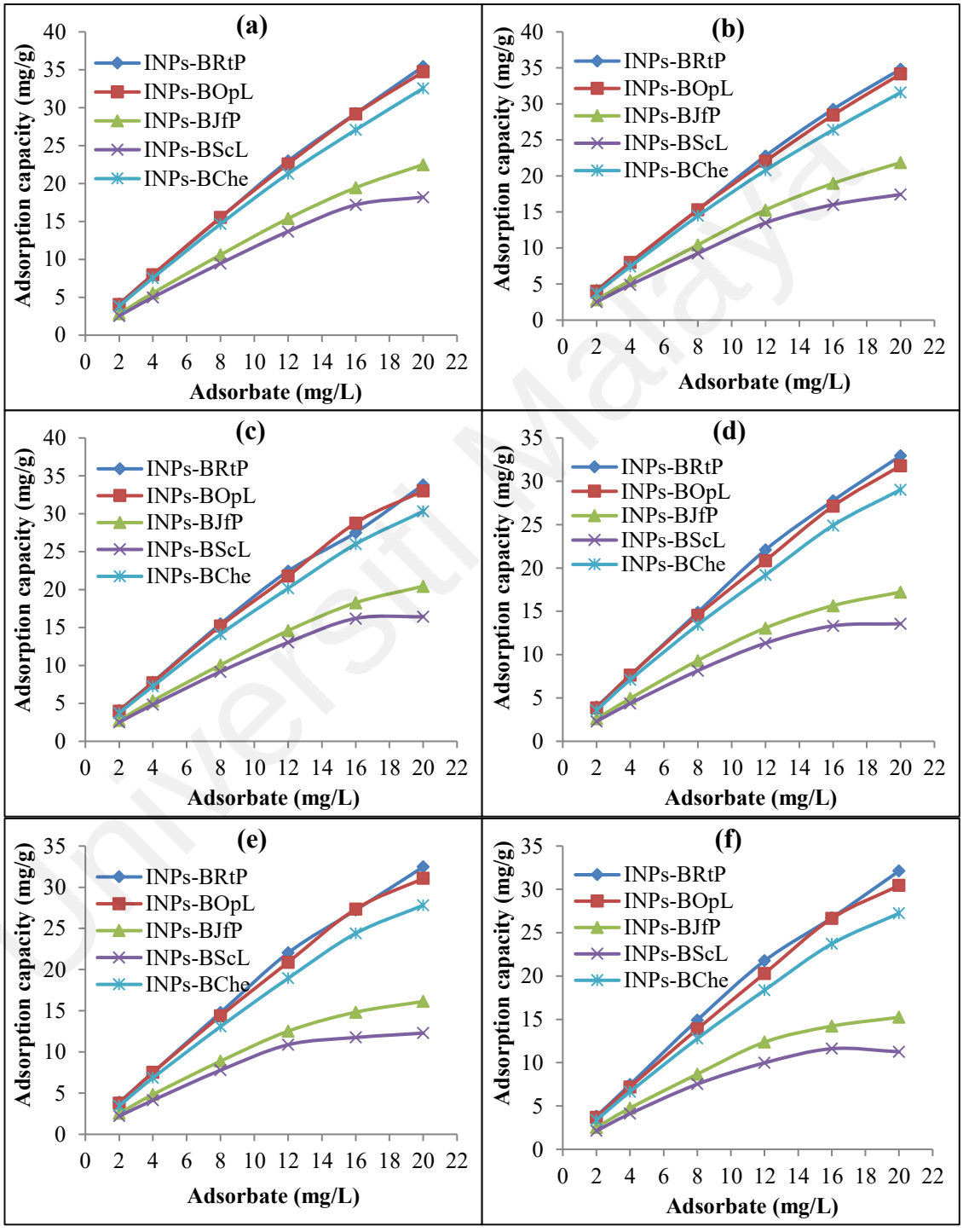

Figure 4.13: Effect of initial pesticide concentration of OCPs (a) *p,p′*-DDT, (b) *o,p′*-DDT, (c) aldrin, (d) heptachlor, (e) hexachlorobenzene, and (f) endosulfan I on adsorption capacity of 0.10-0.15 g/L of fresh four green INPs-B_g and INPs-B_{Che} nanocomposites; agitation speed 150 (rpm); agitation time 240 min; at temperature 25±2 °C and pH 4.

These are the reasons for the decrease of sorption and dechlorination capacity at higher adsorbate concentrations (Pouretedal and Saedi, 2014). Conversely, the adsorption capacity at equilibrium is amplified with an increase in initial level of OCPs (Figures 4.13 a-f) which is in consistent with the research finding of the Pouretedal and Sadegh (2014). This is attributed to an increasing concentration gradient, which acts as a driving force to overcome the resistances to mass transfer of OCPs between the aqueous phase and the nanoadsorbents (Sirzad et al., 2011).

(d) ***Effect of Time***

The effect of various agitation time (5, 10, 15, 20, 25, 30, 35, 40, 45, 50, 55, 60 min) on the individual removal of all 6 OCPs (2 mg/L each OCP) by different green INPs-B_g nanocomposites, INPs-B_{RtP}, INPs-$B_{OpL,}$ INPs-B_{JfP} and INPs-B_{ScL} and chemical synthesized INPs-B_{Che}, at pH 4 and ambient temperature as shown in Figures 4.14 a-f. In all cases, the amount of % removal of all OCPs increased with the increase in agitation time until the equilibrium is reached at 40, 45, 50, 55 and 45 min for B_{RtP}, INPs-B_{OpL}, INPs-B_{JfP}, INPs-B_{ScL} and chemical synthesized INPs-B_{Che}, respectively. Over time, the adsorption process decreased due to the active sites being occupied by adsorbate molecules (Tan et al., 2009). The equilibrium time of OCPs adsorption with various green INPs-B_g nanocomposites was different because of different wt% iron loading on biochar surface and in turn, the efficiency of each INPs-B_g nanocomposite was in the Following order INPs-B_{RtP} > INPs-B_{OpL} > INPs-B_{Che} > INPs-B_{JfP} and INPs-B_{ScL}. As seen from Figures 4.14 a-f, the removal % yield of 6 OCPs by INPs-B_g nanocomposites increased with the increased contact time up to their equilibrium time. Afterwards, adsorption of OCPs remained constant. The high adsorption rate at the initial stage may be explained by high availability in the number of active sites on the adsorbent surface which was later occupied by contaminants contributing to less availability of these sites.

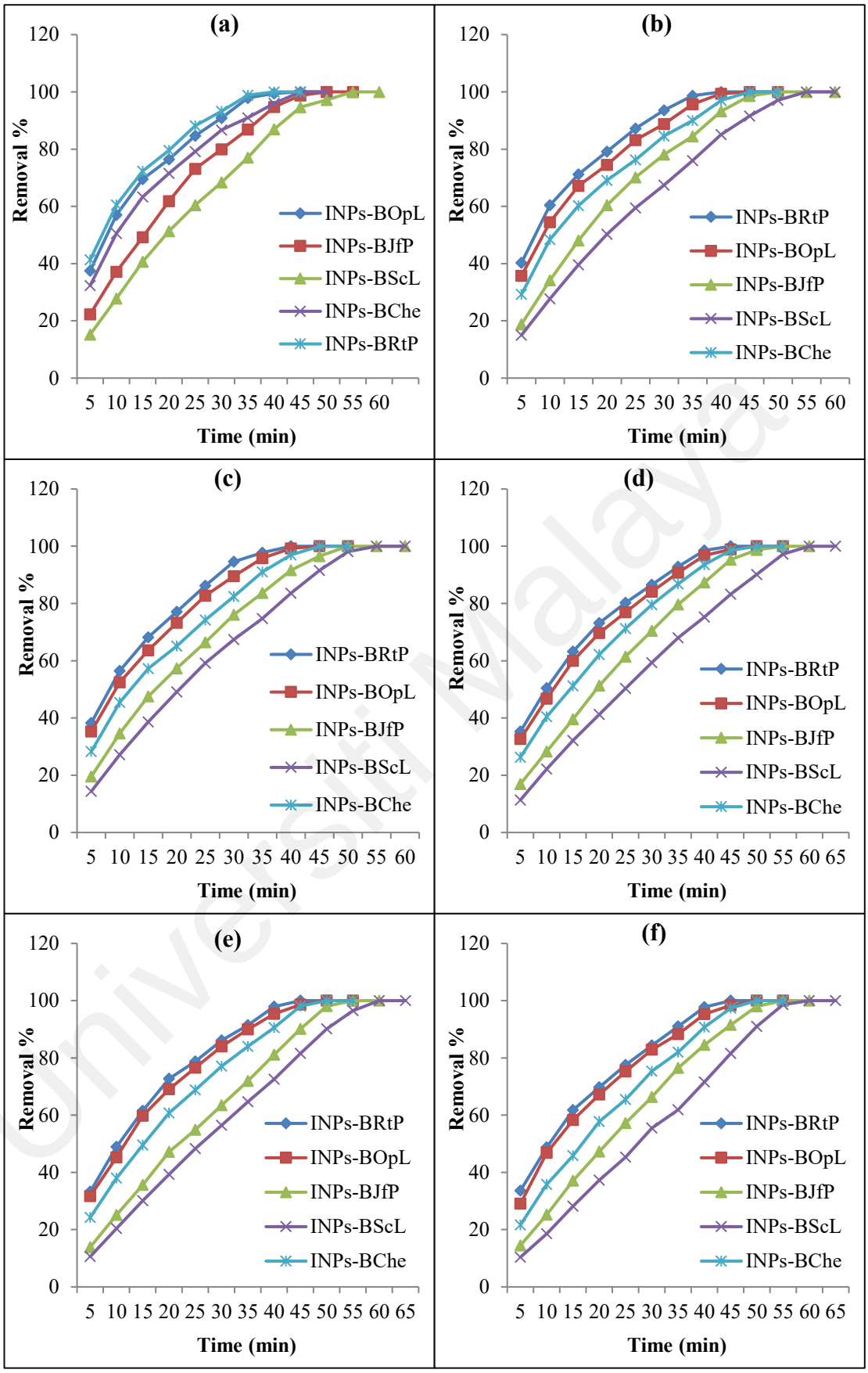

Figure 4.14: Effect of time on individual removal of OCPs (a) *p,p′*-DDT, (b) *o,p′*-DDT, (c) aldrin, (d) heptachlor, (e) hexachlorobenzene, and (f) endosulfan I by fresh four green INPs-B_g and INPs-B_{Che} nanocomposites; 2 mg/L of each adsorbate; 0.1-0.15 g/L of adsorbent; agitation speed 150 (rpm); at temperature 25±2 °C and pH 4.

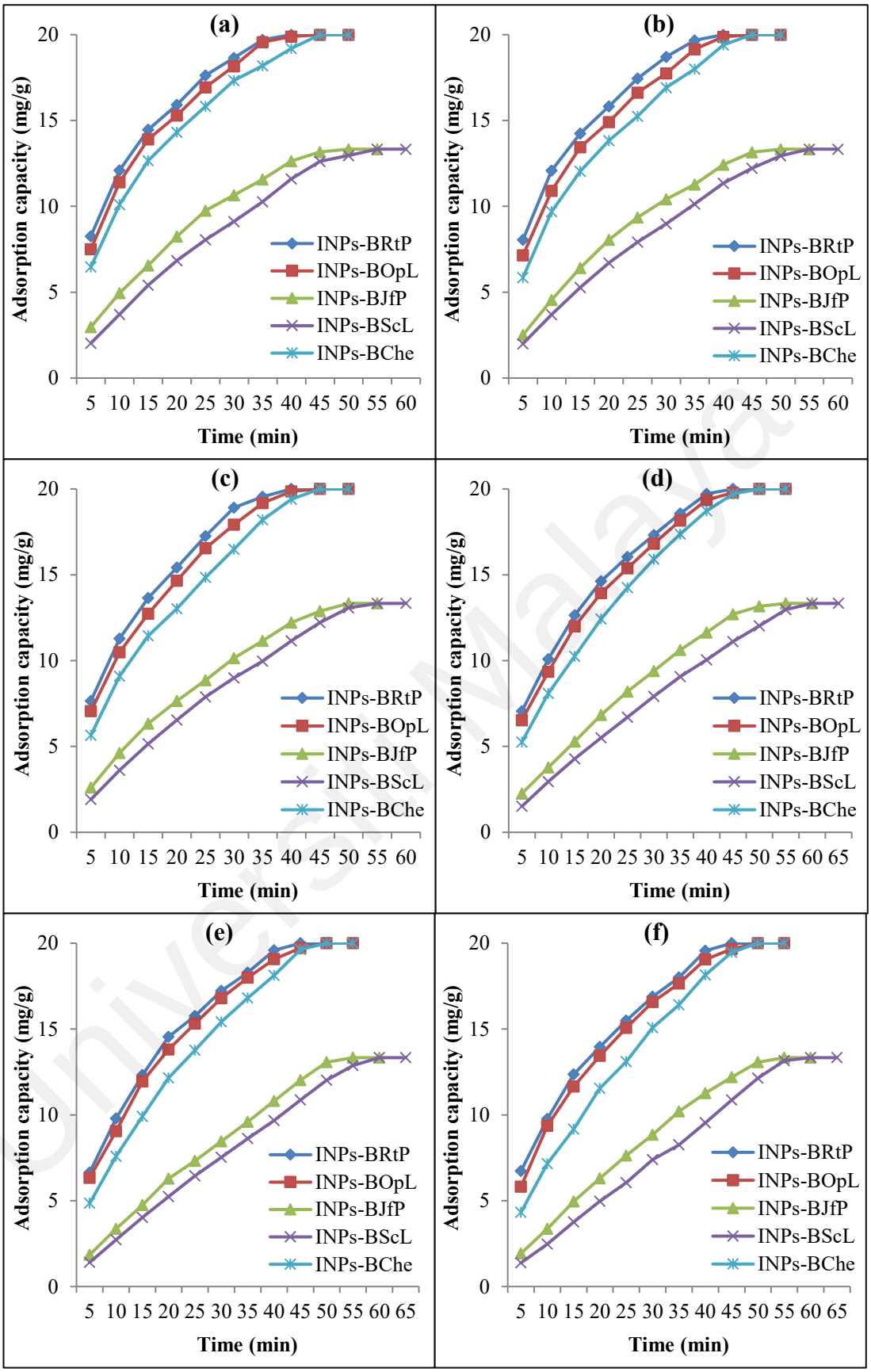

Figure 4.15: Effect of time on adsorption capacity of fresh four green INPs-B_g and INPs-B_{Che} nanocomposites for OCPs (a) *p,p′*-DDT, (b) *o,p′*-DDT, (c) aldrin, (d) heptachlor, (e) hexachlorobenzene, and (f) endosulfan I; 2 mg/L of each adsorbate; 0.1-0.15 g/L of adsorbent; agitation speed 150 (rpm); at temperature 25±2 °C and pH 4.

The adsorption capacity of all types of nanocomposites i.e. INPs-B_{RtP}, INPs-B_{OpL}, INPs-B_{JfP}, INPs-B_{ScL} and INPs-B_{Che} increased by 67, 71, 85, 90 and 79%, respectively with the increase in time until their respective equilibrium time is reached and it was recorded in the following range; 20, 20, 13, 13 and 20 (mg/g), respectively for all OCPs in the individual solution (Figures 4.15 a-f). Over the equilibrium time, the adsorption capacity remained constant. This may be attributed to the more availability of active sites in the initial time which were occupied later by the OCP molecules which in turn lead to the blockage of further adsorption process at their equilibrium.

Quan et al (2014) prepared the biochar supported INPs using toxic chemical as a reducing agent and applied for the removal of 20 mg/L of AO7 dye in aqueous solution. They removed 100% AO7 dye within 15 min by application of 3.2 g/L of nanocomposite. The higher wt% of Fe^0, compared to those in our case, can be attribute to the higher removal rate of AO7 within less equilibrium time. Conversely, in the current research four types of INPs supported on biochar using various green extracts rich in polyphenol (used as a reducing agent). Based on the various concentrations of polyphenol in each extract of biomass waste, four types of nanocomosites with different mprphology and different wt% of Fe^0 were obtained. Nanoocomposites INPs-B_{OpL}, INPs-B_{JfP} and INPs-B_{ScL} prepared from oil palm leaf, jackfruit peel and sugar cane leaf extract have less wt% of Fe^0 (73%, 63% and 51%, respectively) compared to that of INPs-B_{RtP} which have 83% wt% of Fe^0. On the basis of this difference in morphology, INPs-B_{ScL} has given100% removal within 55-60 min, whereas, INPs-B_{RtP} with highest wt% of Fe^0 has given the 100% removal 40-45 min for all OCPs. Study proves that, INPs-B_{RtP} synthesized by using rambutan peel waste is a very cheep, environmentally friendly and highly efficient source for the removal of lethal elements from water system.

Tian et al, (2015) prepared magnetic mesoporous silica nanocomposites by chemical method and applied for the removal of DDT in water using 2 g/L of nanocomposite. 97%

of DDT removed within 1 hr. Similarly, another study performed by Chen et al, (2014) in which they synthesized INPs/AC by chemical method and removed 98% of HCB in water within 48 hr. Pillai and Kottekottil, (2016) prepared cellulose supported INPs and applied for the removal of endosulfan. 82% removal was achieved within 5 hrs. Simkovik et al, (2015) also prepared INPs/AC by chemical method and removed heptachlore 100% within 24 hrs. Meanwhile, in this study 100% removal was achieved within range of 40-55 min by all types of nanocomposites prepared by green method. By comparing the maximum capacity of OCP removal with the previous studies revealed that green synthesized nanocomposites in this study showed better efficiency compared to other chemically synthesized iron based materials reported in the literature.

4.2.1.2 Individual Removal of OCPs by Aged Nanocomposites in Water

Reactivity of all types of aged green INPs-B_g nanocomposites, i.e. INPs-B_{RtP}, INPs-$B_{OpL,}$ INPs-B_{JfP} and INPs-B_{ScL} and aged synthesized chemically i.e. INPs-B_{Che} was compared after being completely exposed to air for one month. The removal % was determined at pH 4 and room temperature (2 mg/L each OCP in individually contaminated water) as shown in Figures 4.16 a-f. In all cases, the amount of % removal of all OCPs increased with the increase in agitation time until the equilibrium is reached at 40, 45, 50 and 55 min for INPs-B_{RtP}, INPs-B_{OpL}, INPs-B_{JfP} and INPs-B_{ScL} same as before aging. However, the equilibrium time for INPs-B_{Che} was increased from 45 to 60 min after being aged. The removal efficiency of INPs-B_{Che} was dropped considerably up to 52.2-55.6% (declined by 44-48%) after being aged for all OCPs. Whereas, the removal efficiency of all aged green INPs-B_g nanocomposites INPs-B_{RtP}, INPs-$B_{OpL,}$ INPs-B_{JfP} and INPs-B_{ScL} was retained same as before their aging i.e. 100% removal for all OCPs.

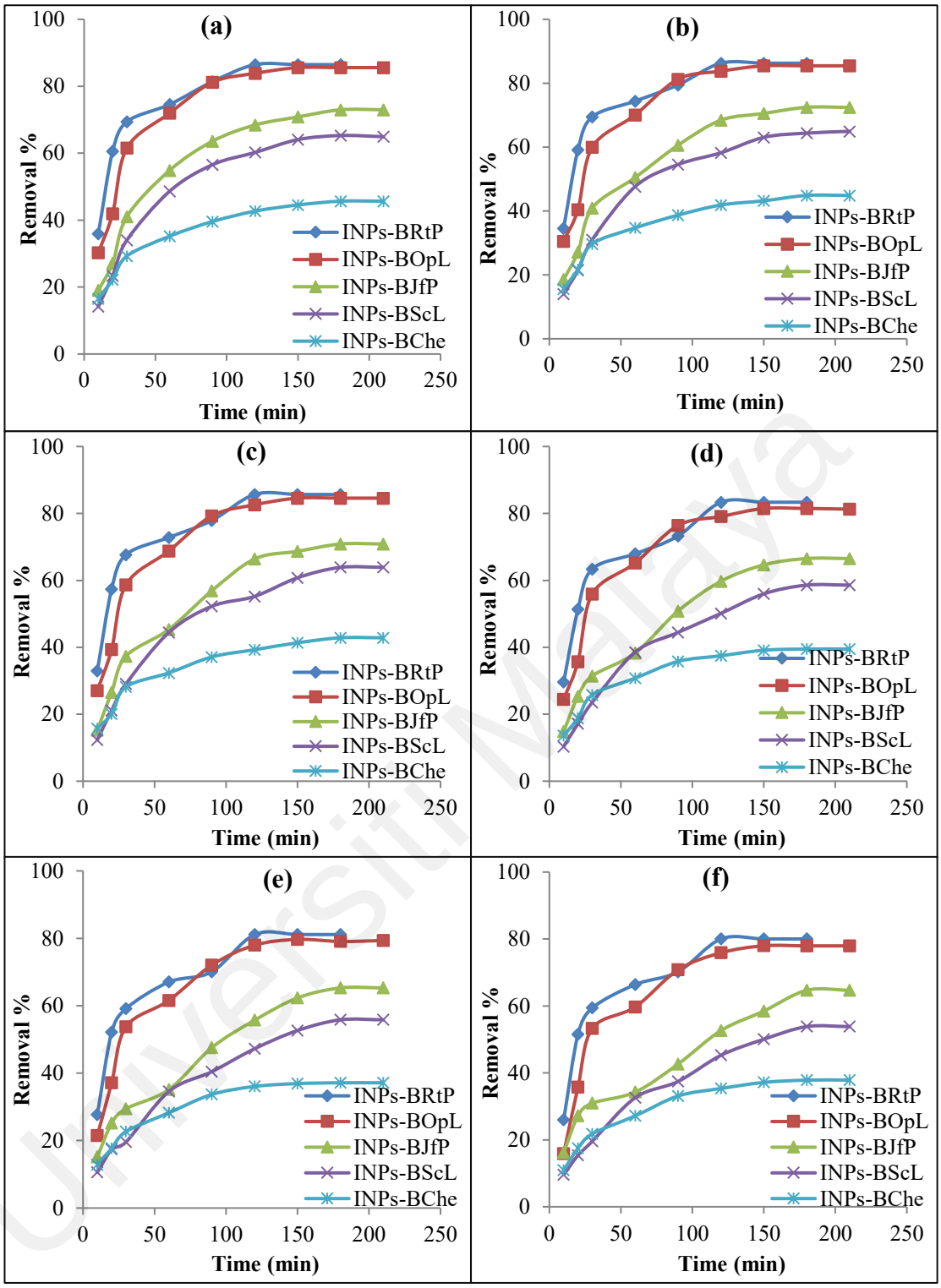

Figure 4.16: Removal efficiency of individual OCPs (a) *p,p′*-DDT, (b) *o,p′*-DDT, (c) aldrin, (d) heptachlor, (e) hexachlorobenzene, and (f) endosulfan I by aged four green INPs-B_g and INPs-B_{Che} nanocomposites; 2 mg/L of each adsorbate, 0.1-0.15 g/L of adsorbent, agitation speed 150 (rpm); at temperature 25±2 °C and pH 4

It can be concluded that green INPs supported on biochar were stayed relatively stable in air because of the outer covering of polyphenols in plant extract. Whereas, INPs synthesized by chemical method get oxidized in air during aging process due to lack of

protective coating of plyphenol and it is in agreement with Wang et al, (2014) and O' Caroll et al, (2013) who observed the same phenomenon for chemical and green synthesized INPs. Over the equilibrium time, the adsorption process decreased due to the active sites being occupied by adsorbate molecules (Tan et al., 2009).

4.2.2 Removal of Mixed OCPs by Nanocomposites

4.2.2.1 Removal of Mixed OCPs by Fresh Nanocomposites in Water

*(a) **Effect of Initial Dosage of Nanocomposites***

The influence of all INPs-B_g nanocomposite dosages on removal of organochlorine pesticides (OCPs) with 2 mg/L concentration at pH 4.0 was also investigated. The reactivity of all green INPs-B_g nanocomposites were also compared with chemical synthesized INPs-B_{Che} nanocomposite under same experimental conditions as for all INPs-B_g nanocomposites and the results are illustrated in Figures 4.17 a-f. The removal tendency of OCPs is increased considerably with increasing adsorbent dosage from 0.1-0.65 g/L of INPs-B_{RtP}, INPs-B_{OpL}, INPs-B_{Che} and 0.1-0.75 g/L of INPs-B_{JfP}, INPs-B_{ScL}. The positive correlation between adsorbent dose and OCPs removal can be attributed to an increase in the adsorption surface area and availability of more active sites. The maximum adsorption (86-91%, 83-91%) is achieved when 0.45 g/L of INPs-B_{RtP}, INPs-B_{OpL} adsorbent was used while 69-77% and 59-69% removal was achieved with 0.55 g/L of INPs-B_{JfP}, INPs-B_{ScL} adsorbent respectively. As the concentration of adsorbent dose (g/L) applied and OCPs removal percentage both are associated with wt% of iron of nanocomposites, therefore, INPs-B_{RtP} having higher wt% (83%) of iron than other nanocmosites has given higher removal % of OCPs. After a dose of 0.45 g/L dose of INPs-B_{RtP}, INPs-B_{OpL} and INPs-B_{Che} and 0.55 g/L dose of INPs-B_{JfP}, INPs-B_{ScL} nanoadsorbent, the removal % is almost stable. This is due to non-availability of active sites on the adsorbents and establishment of equilibrium between the OCP molecules on

the adsorbents and in the solution. This result is in agreement with the findings of Han et al, (2015).

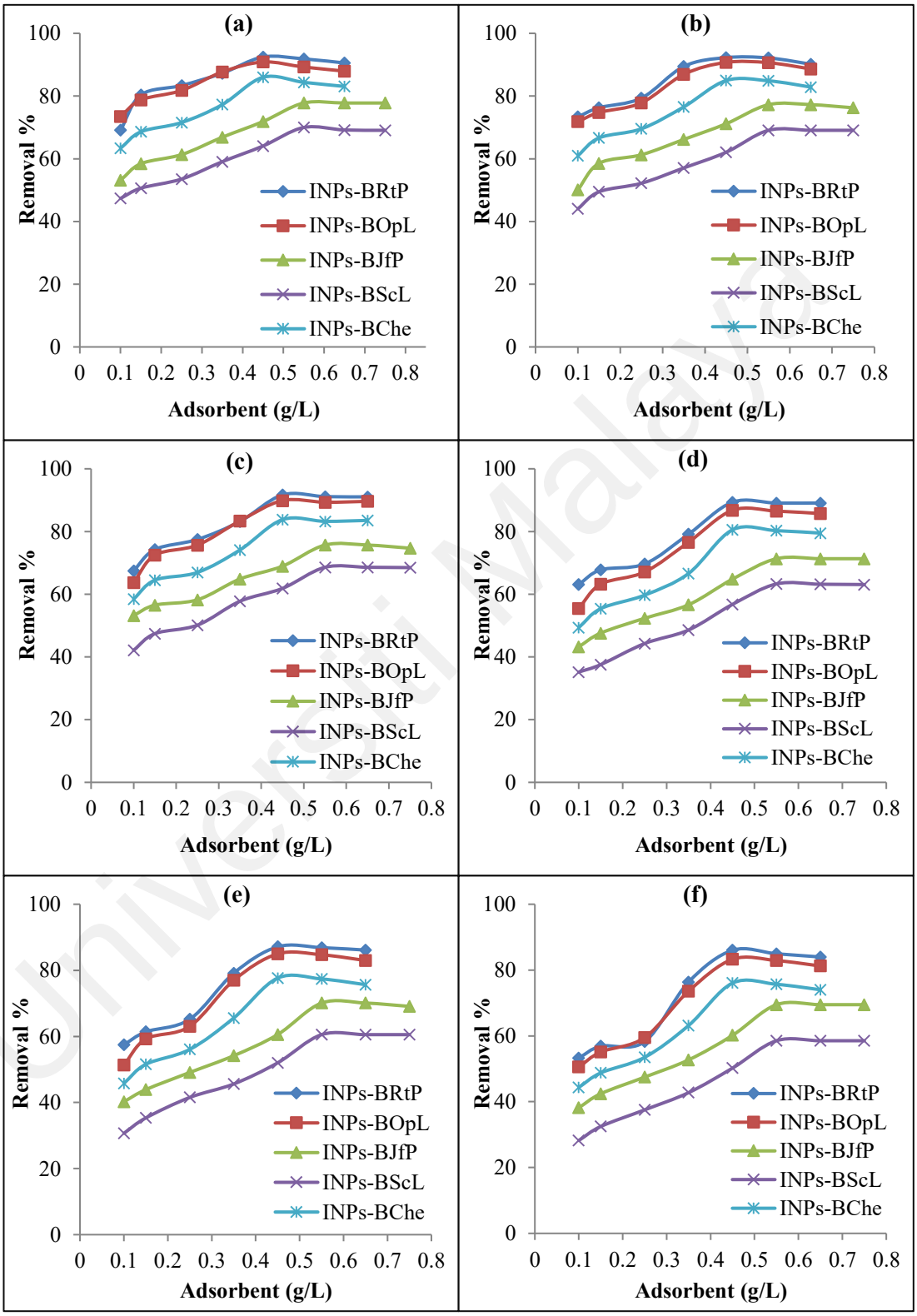

Figure 4.17: Effect of initial concentration of fresh four green INPs-B_g and INPs-B_{Che} nanocomposites on removal of mixed OCPs (a) *p,p'*-DDT, (b) *o,p'*-DDT, (c) aldrin, (d) heptachlor, (e) hexachlorobenzene, and (f) endosulfan I; 2 mg/L of each adsorbate, agitation speed 150 (rpm), agitation time 240 min, at temperature 25±2 °C and pH 4.

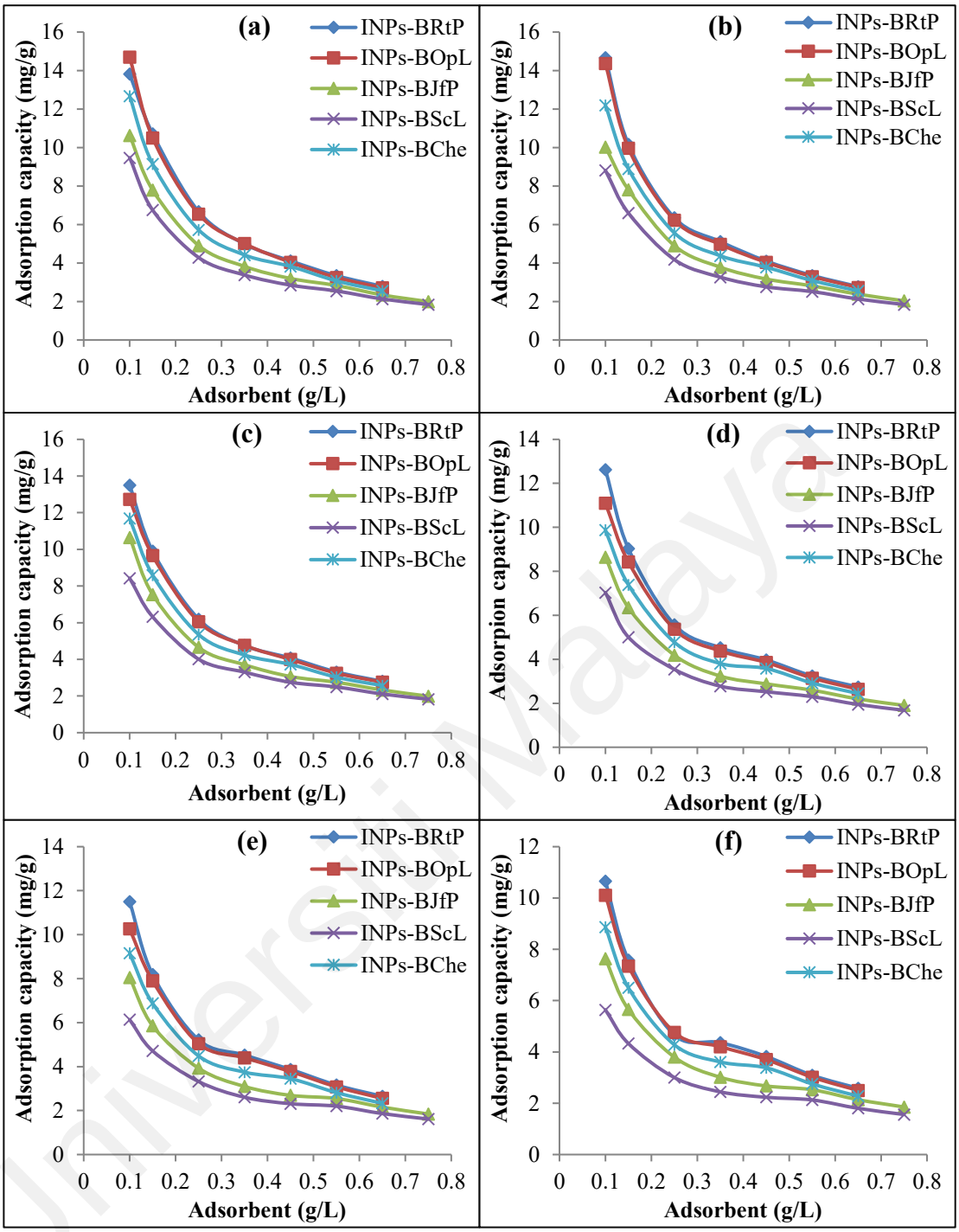

Figure 4.18: Effect of initial concentration of fresh four green INPs-B_g and INPs-B_{Che} nanocomposites on their adsorption capacity for mixed OCPs (a) *p,p'*-DDT, (b) *o,p'*-DDT, (c) aldrin, (d) heptachlor, (e) hexachlorobenzene, and (f) endosulfan I; 2 mg/L of each adsorbate, agitation speed 150 rpm, agitation time 240 min, at temperature 25±2 °C and pH 4.

As seen in Figures 4.18 a-f, an opposite trend of adsorption capacity at equilibrium was observed for all OCPs with all types of nanocomposites. The adsorption capacity of all types of nanocomposites decreased by 69-72% when dosage of nanocomposite increased from 0.1-0.65 g/L. This may be attributed to the less availability of active sites

for the adsorption of OCP compounds resulting from aggregation or overlapping of active sites (Shukla et al., 2002). The highest adsorption capacity of INPs-B_{RtP}, INPs-B_{OpL}, INPs-$B_{Che,}$ INPs-B_{JfP} and INPs-B_{ScL} at 0.45-0.55 g/L dose of nanocomposites were found to be in the following order: 10.7-14.7 > 10.1-13.8 > 8.9-12.7 > 7.6-10.6 and > 5.6-9.8 (mg/g), respectively. Higher concentration of polyphenol content in rambutan peel extract may attribute to the higher wt% of iron in rambutan peel based synthesized INPs supported on rambutan peel biochar which in turn gave highest range of adsorption capacity for OCPs than those of other nanocomposites.

(b) ***Effect of Time***

The removal of all 6 OCPs (2 mg/L each OCP in a mixture) by different green INPs-B_g nanocomposites, INPs-B_{RtP}, INPs-$B_{OpL,}$ INPs-B_{JfP} and INPs-B_{ScL} and chemical synthesized INPs-B_{Che}, at various time intervals, at pH 4 and ambient temperature as shown in Figures 4.19 a-f. In all cases, the amount of % removal of all OCPs increased with the increase in agitation time until the equilibrium is reached at 120 min for INPs-B_{RtP} , 150 min for INPs-B_{OpL} and chemical synthesized INPs-B_{Che}, respectively using 0.45 g/L of nanocomposites and 180 min for both adsorbents INPs-B_{JfP} and INPs-B_{ScL} using 0.55 g/L of respective nanocomposites. Over time, the adsorption process decreased due to the active sites being occupied by adsorbate molecules (Tan et al., 2009). The equilibrium time of OCPs adsorption with various green INPs-B_g nanocomposites was different because of different wt% iron loading on biochar surface and in turn, the efficiency of each INPs-B_g nanocomposite was in the Following order INPs-B_{RtP} > INPs-B_{OpL} > INPs-B_{Che} > INPs-B_{JfP} and INPs-B_{ScL}.

As seen from Figures 4.17 a-f, the removal % yield of 6 OCPs by INPs-B_g nanocomposites increased with the increased contact time up to their equilibrium time. Afterwards, adsorption of OCPs remained constant. The rate of OCPs removal was

higher at the beginning. A dramatic removal 65-76%, 60-65%, 46-56%, 35-41% and 24-52% was obtained with INPs-B_{RtP}, INPs-B_{OpL}, INPs-B_{Che}, INPs-BJ_{fP} and INPs-B_{ScL}, respectively within first 30 min.

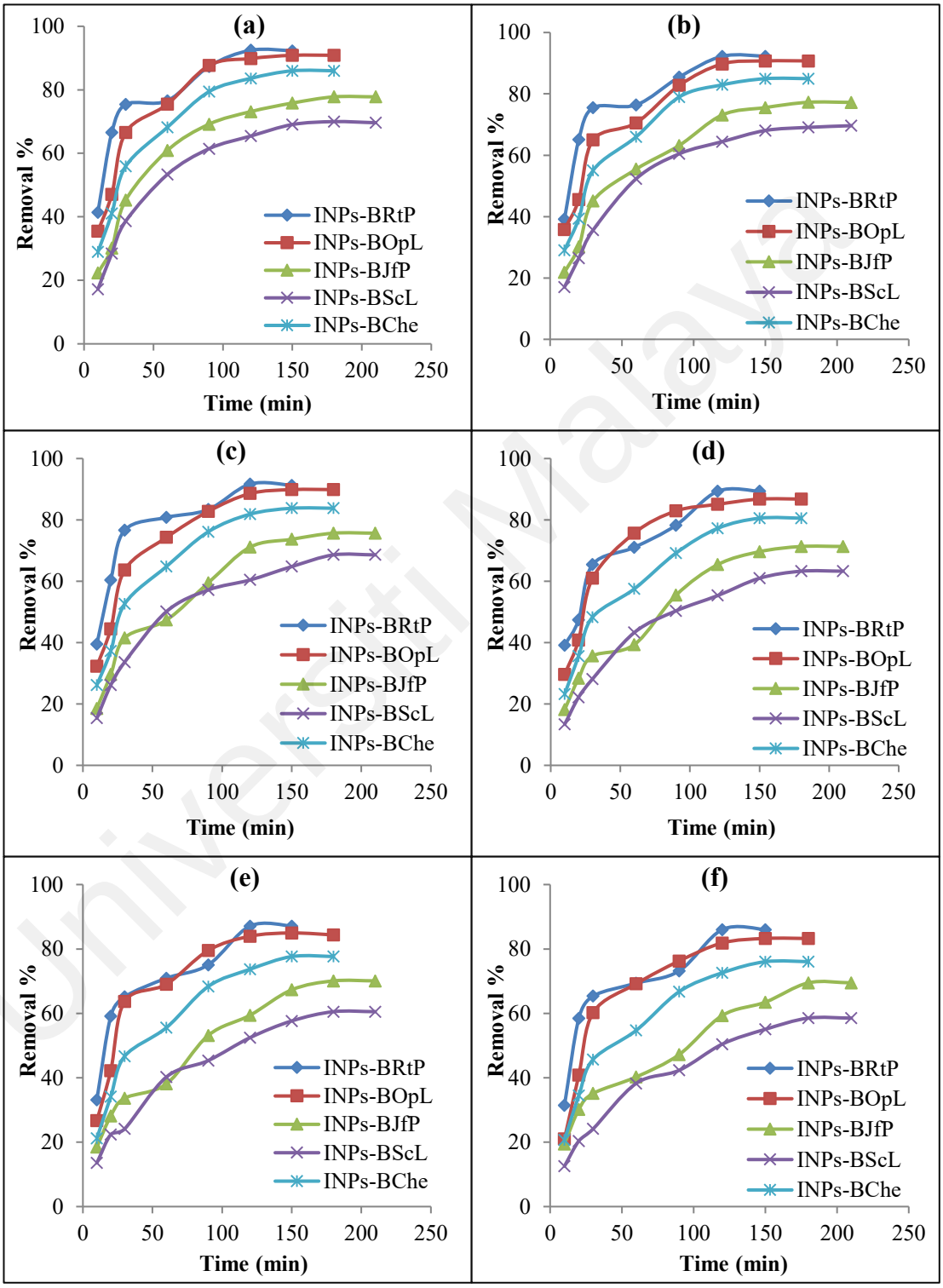

Figure 4.19: Effect of time on the removal of mixed OCPs (a) *p,p′*-DDT, (b) *o,p′*-DDT, (c) aldrin, (d) heptachlor, (e) hexachlorobenzene, and (f) endosulfan I by fresh four green INPs-B_g and INPs-B_{Che} nanocomposites; 2 mg/L of each adsorbate; 0.45-0.55 g/L of adsorbent, agitation speed 150 rpm; at temperature 25±2 °C and pH 4

However, the removal rate was gradually reduced after 30 min till the end of experiment which was 86-92%, 83-91%, 76-86%, 69-78% and 59-70%, respectively within their respective equilibrium time. The high adsorption rate at the initial stage may be explained by high availability in the number of active sites on the adsorbent surface which was later occupied by contaminants contributing to less availability of these sites.

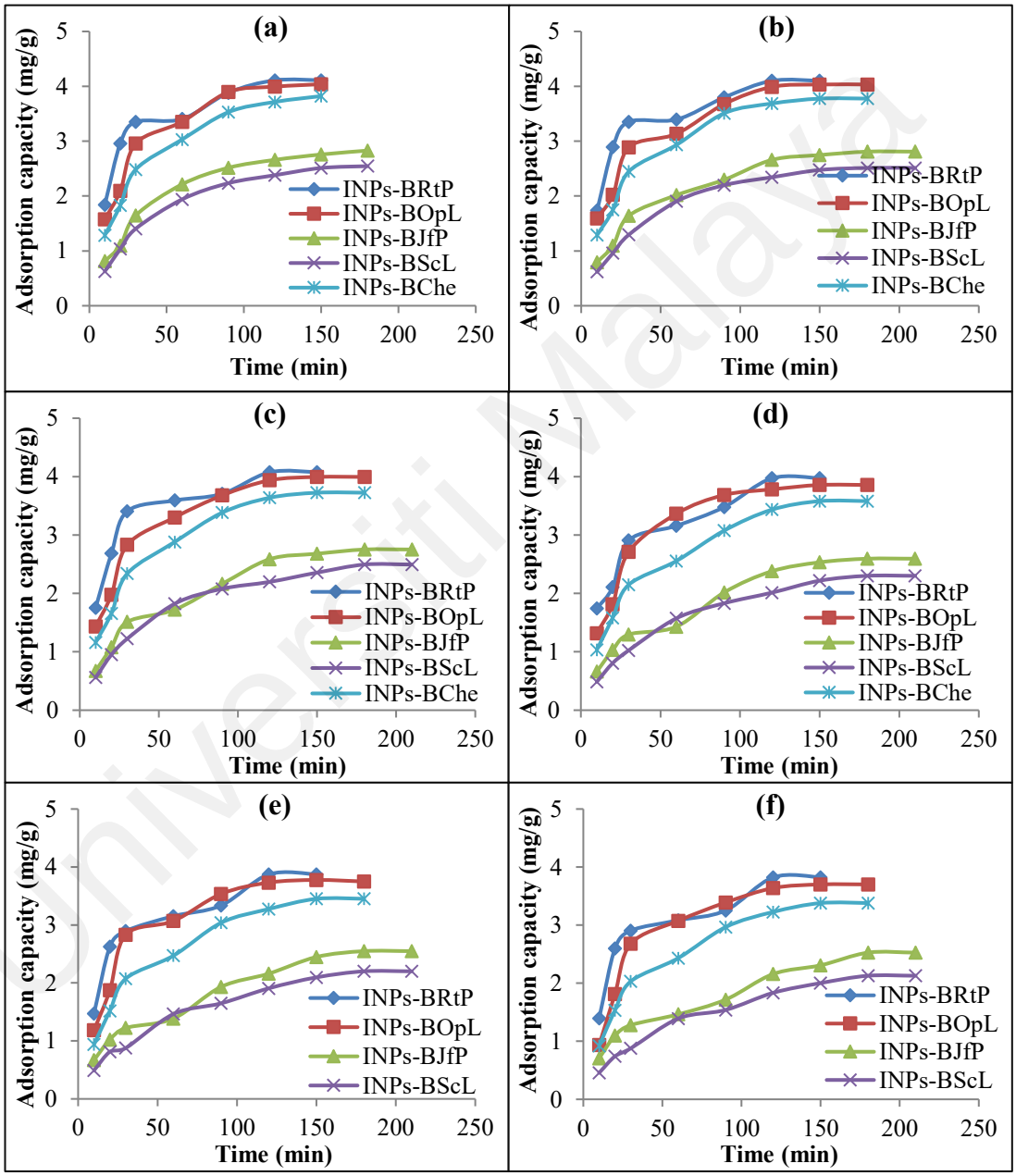

Figure 4.20: Effect of time on adsorption capacity of fresh four green INPs-B_g and INPs-B_{Che} nanocomposites for mixed OCPs (a) *p,p′*-DDT, (b) *o,p′*-DDT, (c) aldrin, (d) heptachlor, (e) hexachlorobenzene, and (f) endosulfan I; 2 mg/L of each adsorbate, 0.45-0.55 g/L of adsorbent, agitation speed 150 rpm; at temperature 25±2 °C and pH 4.

The adsorption capacity of all types of nanocomposites i.e. INPs-B_{RtP}, INPs-B_{OpL}, INPs-B_{JfP}, INPs-B_{ScL} and INPs-B_{Che} increased by 55.23, 60.89, 71.38, 75.20 and 66.23%, respectively with the increase in time until their respective equilibrium time is reached and it was recorded in the following range; 3.8-4.1, 3.7-4.04, 2.5-2.8, 2.1-2.5 and 3.4-3.9 (mg/g), respectively for all OCPs in the mixture solution (Figures 4.20 a-f). Over the equilibrium time, the adsorption capacity remained constant. This may be attributed to the more availability of active sites in the initial time which were occupied later by the OCP molecules which in turn lead to the blockage of further adsorption process at their equilibrium.

Quan et al (2014) prepared the biochar supported INPs using toxic chemical as a reducing agent and applied for the removal of 20 mg/L of AO7 dye in aqueous solution. They removed 100% AO7 dye within 15 min by application of 3.2 g/L of nanocomposite. The higher wt% of Fe^0, compared to those in our case, can be attribute to the higher removal rate of AO7 within less equilibrium time. Conversely, in the current research four types of INPs supported on biochar using various green extracts rich in polyphenol (used as a reducing agent). Based on the various concentrations of polyphenol in each extract of biomass waste, four types of nanocomosites with different mprphology and different wt% of Fe^0 were obtained. Nanoocomposites INPs-B_{OpL}, INPs-B_{JfP} and INPs-B_{ScL} prepared from oil palm leaf, jackfruit peel and sugar cane leaf extract have less wt% of Fe^0 (73%, 63% and 51%, respectively) compared to that of INPs-B_{RtP} which have 83% wt% of Fe^0. On the basis of this difference in morphology, INPs-B_{ScL} has given lowest % removal i.e. 59-70%, whereas, INPs-B_{RtP} with highest wt% of Fe^0 has given the maximum removal % in range between 86-92% for all OCPs. Study proves that, INPs-B_{RtP} synthesized by using rambutan peel waste is a very cheep, environmentally friendly and highly efficient source for the removal of lethal elements from water system.

4.2.2.2 Removal of Mixed OCPs by Aged Nanocomposites in Water

Reactivity of all types of aged green INPs-B_g nanocomposites, i.e. INPs-B_{RtP}, INPs-$B_{OpL,}$ INPs-B_{JfP} and INPs-B_{ScL} and aged synthesized chemically i.e. INPs-B_{Che} was compared after being completely exposed to air for one month. The removal % was determined at pH 4 and room temperature (2 mg/L each OCP in a mixture) as shown in Figures 4.21 a-f. In all cases, the amount of % removal of all OCPs increased with the increase in agitation time until the equilibrium is reached at 120 min and 150 min for INPs-B_{RtP} INPs-B_{OpL}, respectively and 180 min for both adsorbents INPs-B_{JfP} and INPs-B_{ScL} same as before aging. However, the equilibrium time for INPs-B_{Che} was increased from 150 to 180 min after being aged. The removal efficiency of INPs-B_{Che} was dropped considerably up to 45.66-37.84 % (declined by 46.90-50.24 %) after being aged for all OCPs. Whereas, the removal efficiency of all aged green INPs-B_g nanocomposites INPs-B_{RtP}, INPs-$B_{OpL,}$ INPs-B_{JfP} and INPs-B_{ScL} was retained almost same as before their aging i.e. 81.02-87.46 %,78-86 %, 64.68-72.98 % and 53.83-66.28 %, respectively (dropping only 5.49-6.58 %, 5.83-6.36 %, 6.17-6.91 % and 6.72-8.03 %, respectively for all OCPs).

It can be concluded that green INPs supported on biochar were stayed relatively stable in air because of the outer covering of polyphenols in plant extract. Whereas, INPs synthesized by chemical method get oxidized in air during aging process and it is in agreement with Wang et al, (2014) and O' Caroll et al, (2013) who observed the same phenomenon for chemical and green synthesized INPs. Over the equilibrium time, the adsorption process decreased due to the active sites being occupied by adsorbate molecules (Tan et al., 2009).

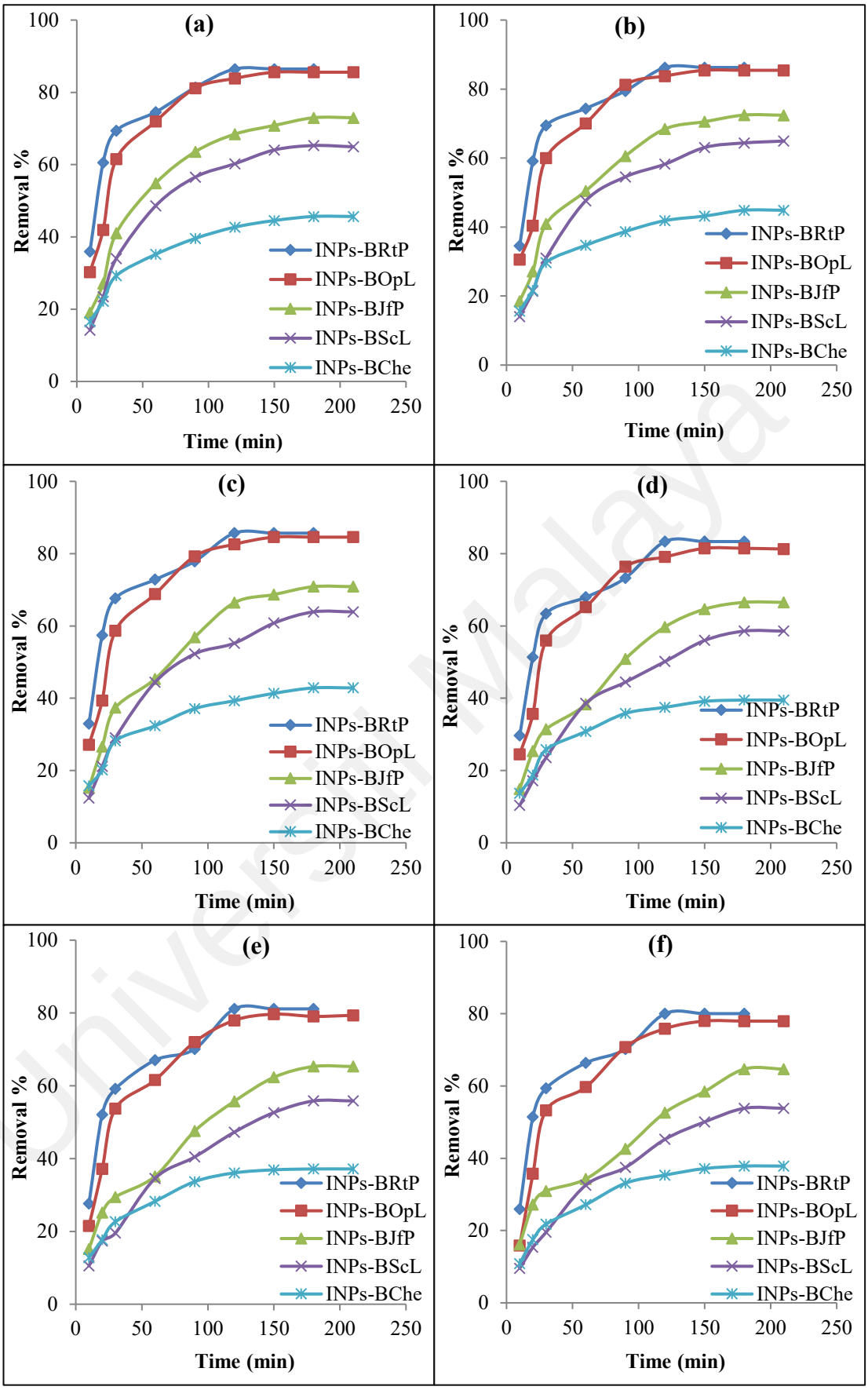

Figure 4.21: Removal efficiency of mixed OCPs (a) *p,p′*-DDT, (b) *o,p′*-DDT, (c) aldrin, (d) heptachlor, (e) hexachlorobenzene, and (f) endosulfan I by aged four green INPs-B_g and INPs-B_{Che} nanocomposites; 2 mg/L of each adsorbate; 0.45-0.55 g/L of adsorbent; agitation speed 150 rpm; at temperature 25±2 °C and pH 4

4.2.3 Removal of OCPs in Oil Palm Plantation Drainage (OPPD) Water Samples

4.2.3.1 Physicochemical Characteristics of OPPD Water Samples

Physic-chemical characteristics of OPPD water samples are presented in Table 4.3 and Appendix F. The pH, temperature, conductivity, TDS, DO, TSS and salinity values were found within the range of water quality standards values for land irrigation water which are 5.5-8.4, 18-30 °C, 0.75-2.5 dS/m, 500-2000 mg/L, 5-25 mg/L, 512-1600 mg/L, 50 mg/L, respectively. The levels of detected cations (K^+ and Mg^+) and anions (NO_3^{-1} and PO_4^{-2}) were found higher than that of the desired range (20-50, 6-24, < 50, < 1.2-2.5 mg/L, respectively) for the land irrigation water because of the excessive application of the fertilizers comprising K, N, P as a macronutrients and Mg as a secondary macronutrient. However, other detected cations (Na^+, Ca^+ and Fe^+) and anions (Cl^- and SO_4^{-2}) were found within the acceptable limits (46-102, 40-120, 2-5, 70-140, < 400 mg/L, respectively) required for the land irrigation water.

Organochlorine pesticides (*p,p'*-DDT, *o,p'*-DDT, endosulfan, aldrin, heptachlore and hexachlorobenzene) were detected and quantified in OPPD water (Table 4.3, Figure F.1 (Appendix F)). *p,p'*-DDT, *o,p'*-DDT and heptachlor were found in very low concentrations in all OPPD water samples i.e. 1.052-1.773, 1.051-1.114 and 1.186-1.528 µg/L a little higher than the acceptable limits (1 µg/L). However, endosulfan I, aldrin and hexachlorocyclobenzene were detected in higher concentrations than those of the above mentioned OCPs. The calculated concentrations of endosulfan I, aldrin and hexachlorocyclobenzene were 2.568-3.136, 2.02-2.528 and 3.531-3.832 µg/L higher than permissible limits (1 µg/L) (Fipps, 2015). The presence of OCPs in the drainage water coming from irrigation runoff restrict its re-use for the irrigation of crops and also have caused the downstream water quality problems.

Table 4.3: Physicochemical characteristics of OPPD water samples.

Parameters	Drainage water samples	Acceptable limits
pH	5.7-6.9	5.5-8.4
Temperature (°C)	26.3-27.5	18-30
Conductivity (dS/m)	0.94-1.1	0.75-2.5
TDS (mg/L)	590-631	500-2000
DO (mg/L)	10-12	5-25
Salinity (mg/L)	613-694	512-1600
TSS	6.4-7.2	50
Na^+ (mg/L)	98-105	46-102
K^+ (mg/L)	103-167	20-50
Ca^+ (mg/L)	65-80	40-120
Mg^+ (mg/L)	34-48	6-24
Fe^+ (mg/L)	3.5-4.4	2-5
Cl^- (mg/L)	106-112	70-140
NO_3^{-1} (mg/L)	126-189	< 50
PO_4^{-2} (mg/L)	10-18	< 1.2-2.5
SO_4^{-2} (mg/L)	14-20	< 400

Table 4.4: Detected and quantified OCPs in OPPD water samples

OCPs	Concentration (µg/L)
p,p'-DDT	1.052-1.773
o,p'-DDT	1.051-1.114
Endosulfan I	2.568-3.136
Aldrin	2.02-2.528
Heptachlor	1.186-1.528
Hexachlorocyclobenzene	3.531-3.832

4.2.3.2 Removal of OCPs in OPPD Water Samples by Fresh Nanocomposites

*(a) **Effect of Adsorbent Dosage on Removal of OCPs in OPPD Water Samples***

Adsorbent dosage is an important parameter in OPPD water samples treatment. In contrast with green INPs-B_{RtP} composits, chemical synthesized INPs-B_{Che} composits were also applied for comparison under same experimental conditions. The amount of adsorbent required for the different OPPD water samples are shown in Figure 4.22 a-f to 4.24 a-f. It can be seen from the Figures 4.22 a-f to 4.24 a-f that there is an incredible increase in the percentage removal of all OCPs for all the OPPD water samples with increasing adsorbent dosage of green INPs-B_{RtP} and chemical synthesized INPs-B_{Che} nanocomposites and then reach saturation. This increase in the removal of OCPs from

OPPD water samples can be attributed to the availability of increased number of active sites for the adsorption with increased adsorbent dosage.

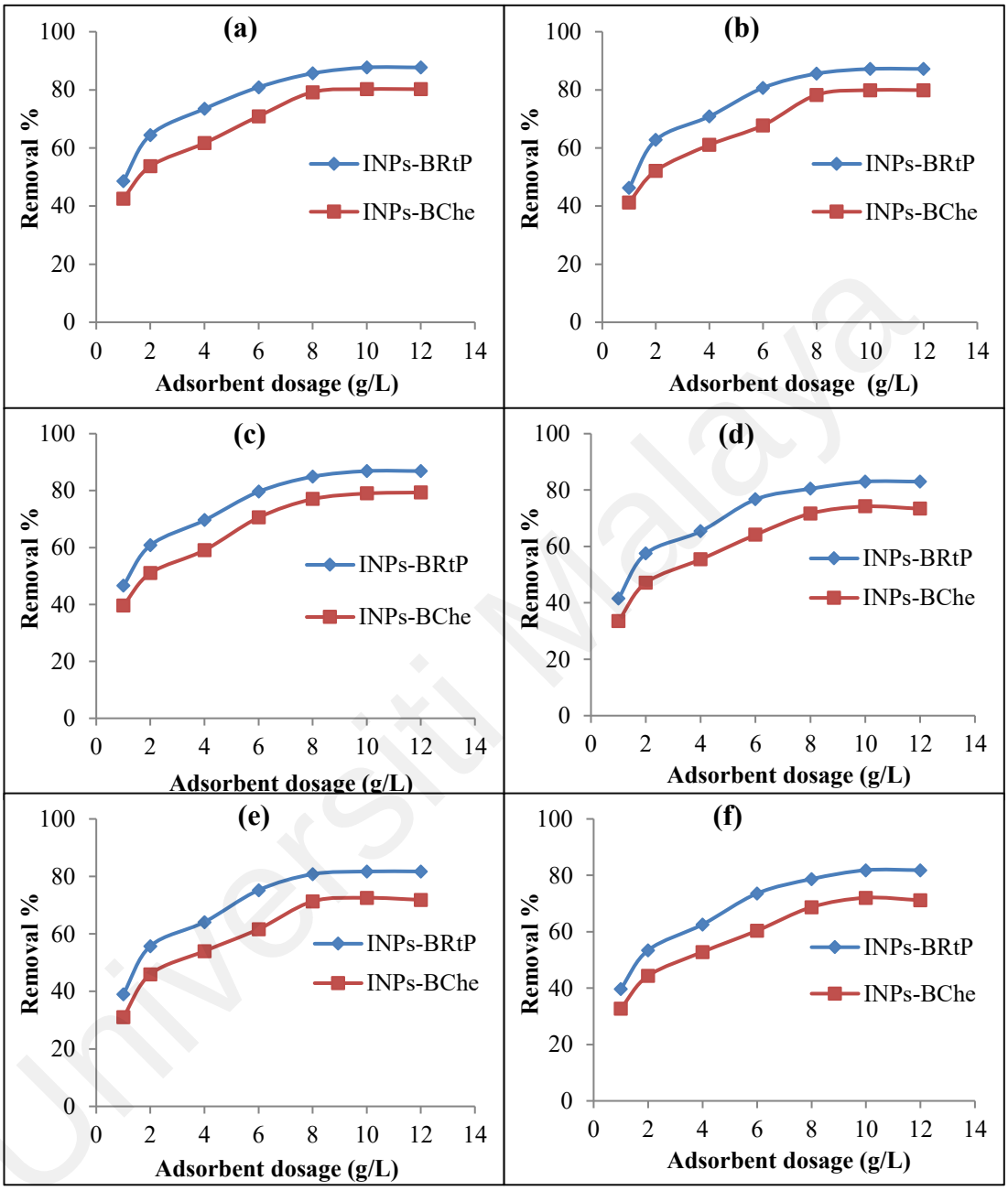

Figure 4.22: The effect of adsorbent dosage (g/L) of fresh INPs-B_g and INPs-B_{Che} nanocomposites on the the removal of OCPs (a) *p,p′*-DDT, (b) *o,p′*-DDT, (c) aldrin, (d) heptachlor, (e) hexachlorobenzene, and (f) endosulfan I in OPPD water samples PE1; 2 mg/L of each adsorbate; agitation speed 150 (rpm); agitation time 240 min, at temperature 25±2 °C and pH 4.

In distinction with the removal efficiency of both green INPs-B_{RtP} and chemical synthesized INPs-B_{Che} composits for all OCPs in synthetic solutions (mixture form), an incredible higher amount of adsorbents i.e. 10 g/L have been needed for the removal of

all OCPs in OPPD water samples in comparison with synthetic solution (mixture form) which was only 0.45 g/L. It may be attributed to the presence of other impurities in drainage water samples that tend to adsorb on the prepared nanoadsorbents in competition with the OCPs of interest in this study.

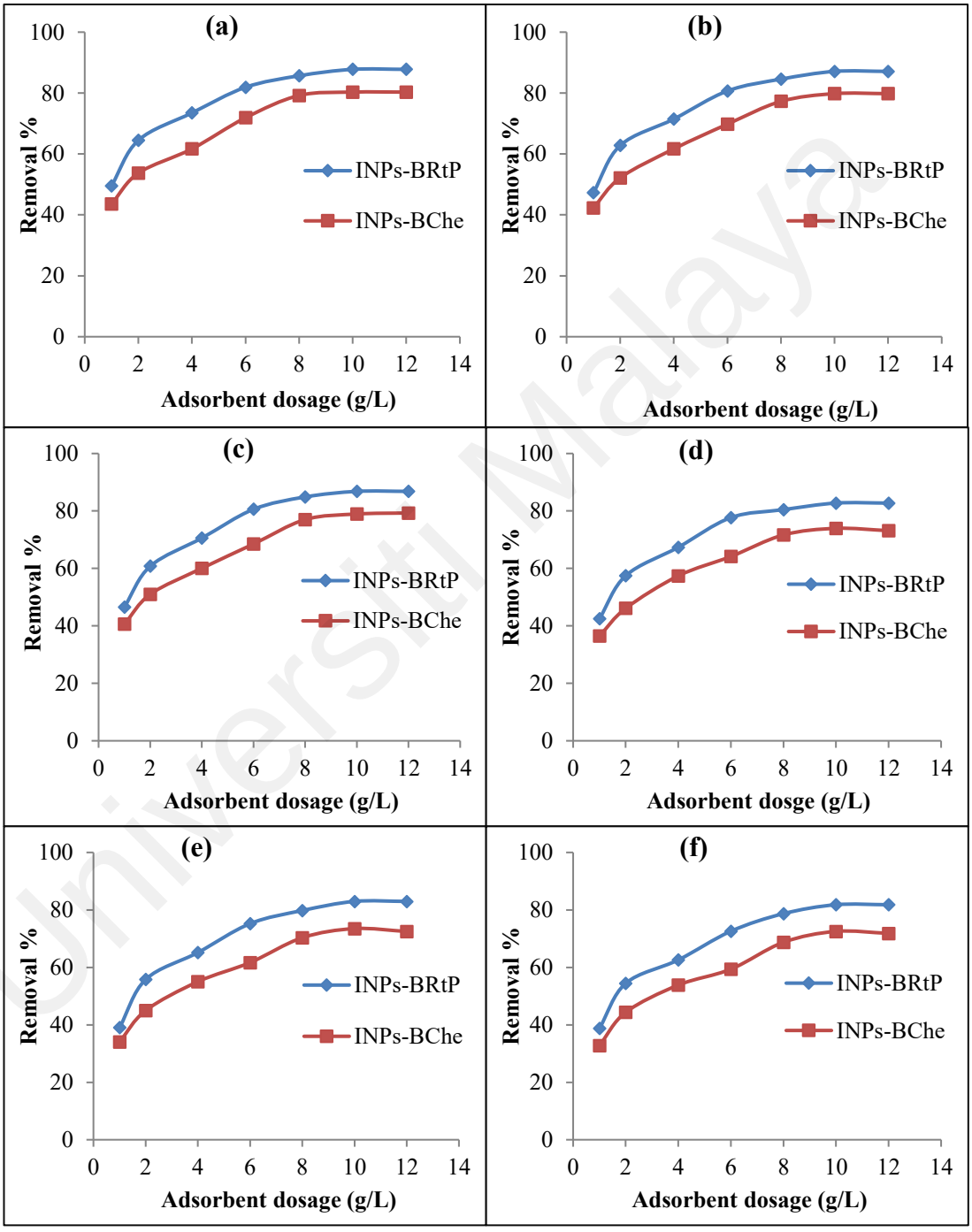

Figure 4.23: The effect of adsorbent dosage (g/L) of fresh INPs-B_g and INPs-B_{Che} nanocomposites on the the removal of OCPs (a) *p,p′*-DDT, (b) *o,p′*-DDT, (c) aldrin, (d) heptachlor, (e) hexachlorobenzene, and (f) endosulfan I in OPPD water samples PMD2; 2 mg/L of each adsorbate; agitation speed 150 (rpm); agitation time 240 min, at temperature 25±2 °C and pH 4

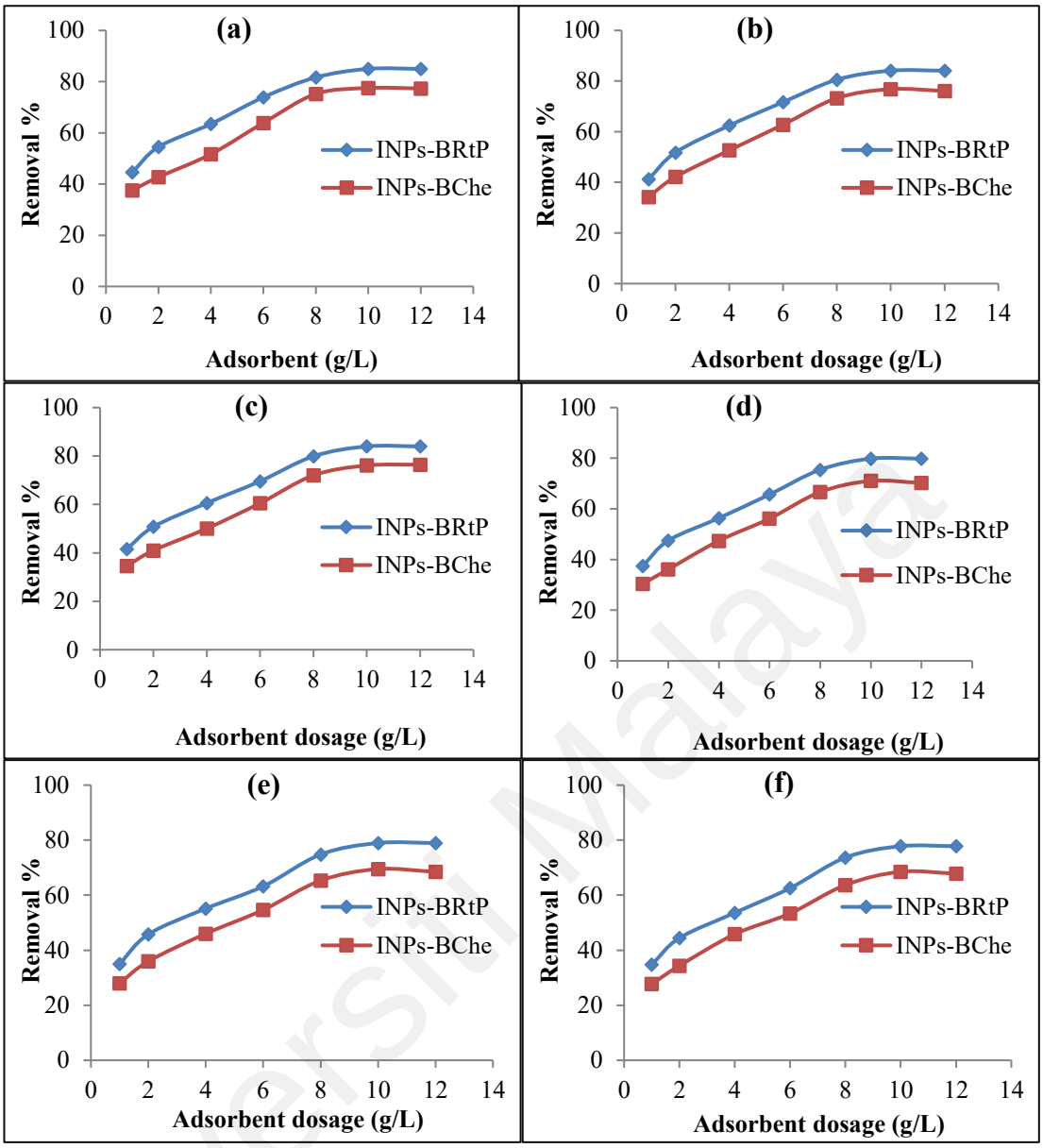

Figure 4.24: The effect of adsorbent dosage (g/L) of fresh INPs-B_g and INPs-B_{Che} nanocomposites on the the removal of OCPs (a) *p,p′*-DDT, (b) *o,p′*-DDT, (c) aldrin, (d) heptachlor, (e) hexachlorobenzene, and (f) endosulfan I in OPPD water samples PMD3; 2 mg/L of each adsorbate; agitation speed 150 (rpm); agitation time 240 min, at temperature 25±2 °C and pH 4.

(b) Effect of Agitation Time on Removal of OCPs in OPPD Water Samples

The effect of agitation time on the removal of OCPs from OPPD water samples by the adsorbent is shown in the Figures 4.25 a-f to 4.27 a-f. It shows that the uptake of OCPs using green INPs-B_{RtP} increased with increase in agitation time and attained the equilibrium at 150 minutes with overall 77-87% removal in all wasterwater samples. Meanwhile, chemical synthesized INPs-B_{Che} composit has given only 8-13% less removal than that of green INPs-B_{RtP} which was 67-80% within same equilibrium time 150 min.

The increase in agitation time can be attributed to the increase in the intera prticle diffusion occurring at increased agitation time and breakdown of adsorbed OCP compounds with iron nanoparticles in their vicinity also make some free sites for the adsorption of OCPs in the solution during incubation time may also contribute to the increased removal of OCPs with adsorbent.

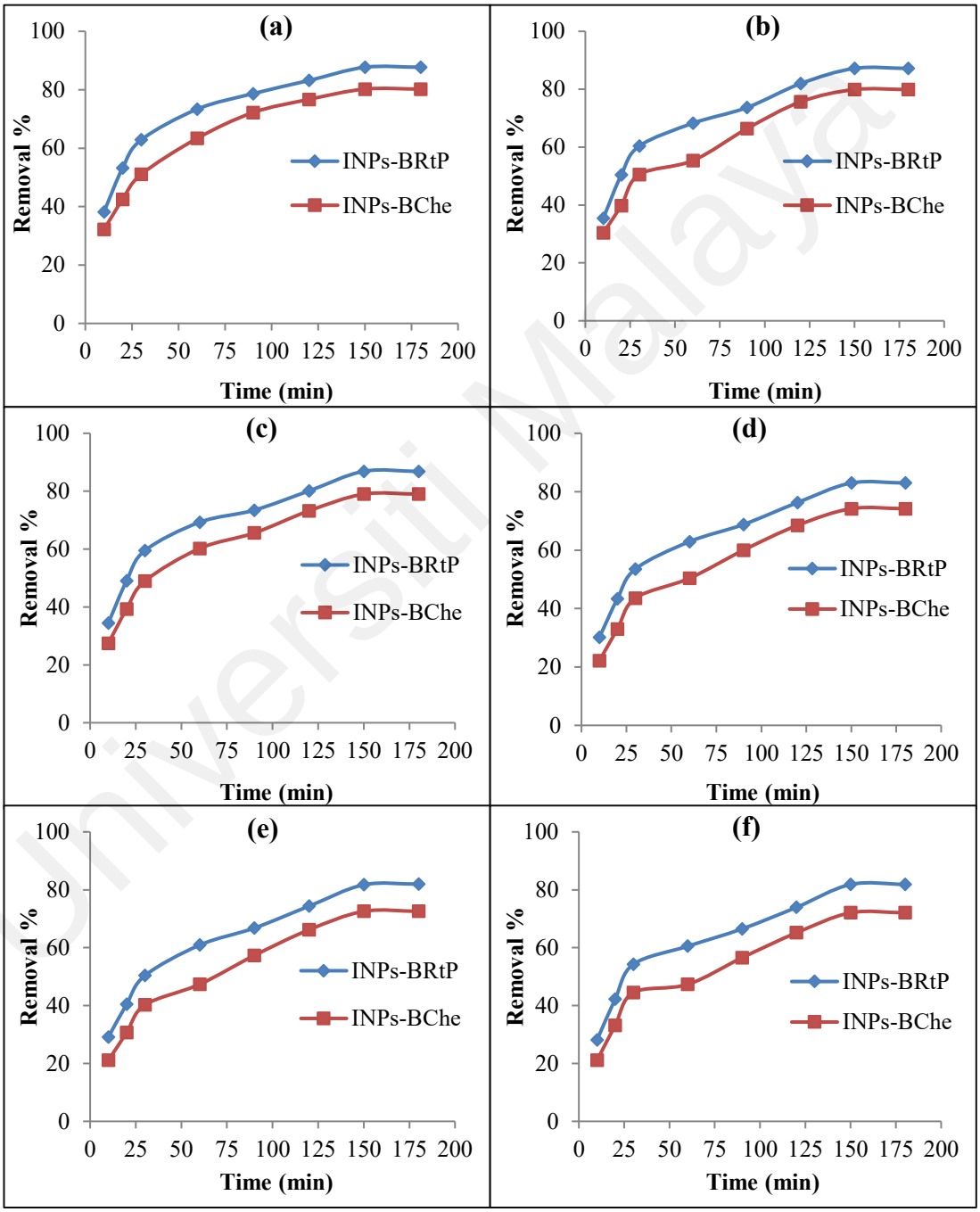

Figure 4.25: The effect of time (min) on the the removal of OCPs (a) *p,p′*-DDT, (b) *o,p′*-DDT, (c) aldrin, (d) heptachlor, (e) hexachlorobenzene, and (f) endosulfan I by 10g/L of fresh INPs-B_g and INPs-B_{Che} nanocomposites in OPPD water samples PE1; 2 mg/L of each adsorbate; agitation speed 150 (rpm);, at temperature 25±2 °C and pH 4.

In contrast with the removal efficiency of both green INPs-B_{RtP} and chemical synthesized INPs-B_{Che} composit for all OCPs in OPPD water samples, in synthetic solution of OCPs (mixture form) it was found to be only 5% higher however an extensive amount of nanocomposites (22 fold higher amount) needed to applied for the removal of OCPs from OPPD water samples thay may be attributed to the occurence of other impurities in OPPD water samples causing the competition with OCPs of interest in this study.

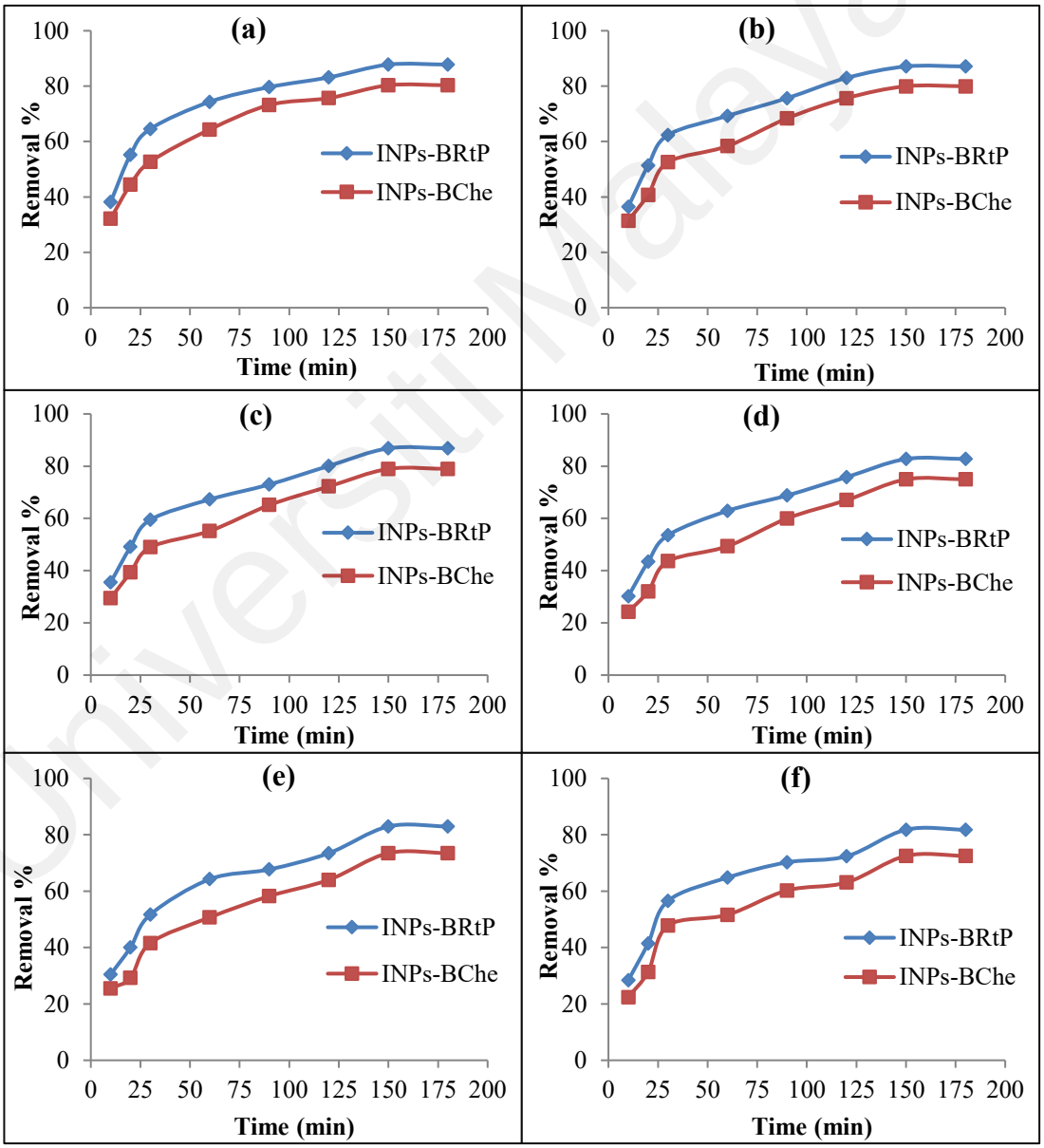

Figure 4.26: The effect of time (min) on the the removal of OCPs (a) *p,p′*-DDT, (b) *o,p′*-DDT, (c) aldrin, (d) heptachlor, (e) hexachlorobenzene, and (f) endosulfan I by 10 g/L of fresh INPs-B_g and INPs-B_{Che} nanocomposites in OPPD water samples PMD2; 2 mg/L of each adsorbate; agitation speed 150 (rpm); at temperature 25±2 °C and pH 4.

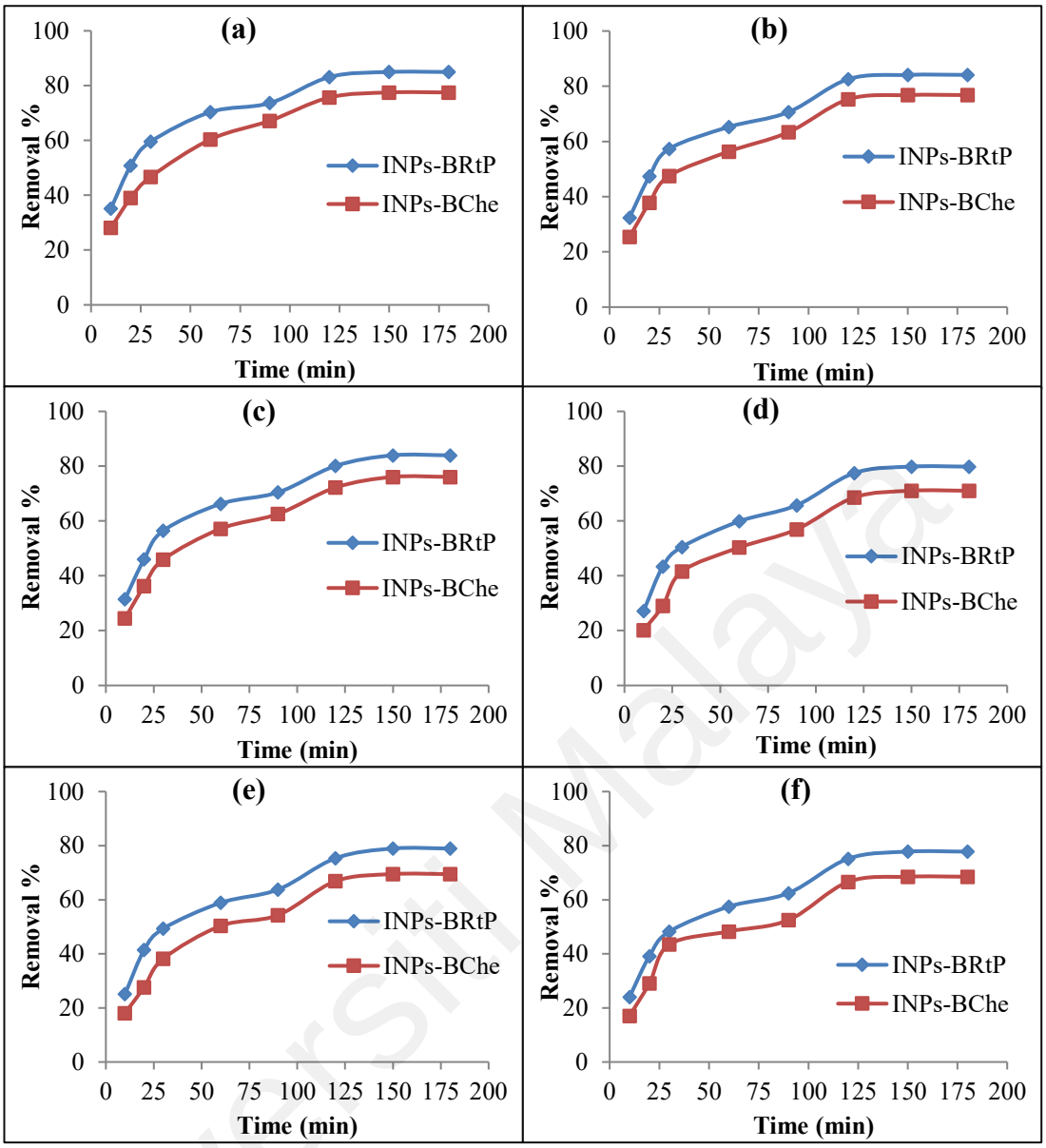

Figure 4.27: The effect of time (min) on the the removal of OCPs (a) p,p'-DDT, (b) o,p'-DDT, (c) aldrin, (d) heptachlor, (e) hexachlorobenzene, and (f) endosulfan I by 10 g/L of fresh INPs-B_g and INPs-B_{Che} nanocomposites in OPPD water samples PMD3; 2 mg/L of each adsorbate; agitation speed 150 (rpm); at temperature 25±2 °C and pH 4.

4.2.3.3 Removal of OCPs in OPPD Water Samples by Aged Nanocomposites

Aged green and chemical synthesized nanocomposites were also applied for the removal of OCPs in oil palm OPPD water samples in order to compare the removal efficiency with fresh green and chemical synthesized nanocomposites. Figures 4.28 a-f, 4.29 a-f and 4.30 a-f show that 76.53-83.70%, 83.78-77.80% and 80.09-72.18% removal was achieved within 150 min in three oil palm OPPD water samples i.e. PE1, PMD2 and PMD3, respectively with aged green INPs-B_{RtP} which showed that slower decline in terms

of removal % compared to fresh which was 81.83-87.70, 81.80-87.78 and 77.80-84.99% (dropping only 4.56-6.48%, 4.41-5.31% and 5.77-7.22%, respectively) .

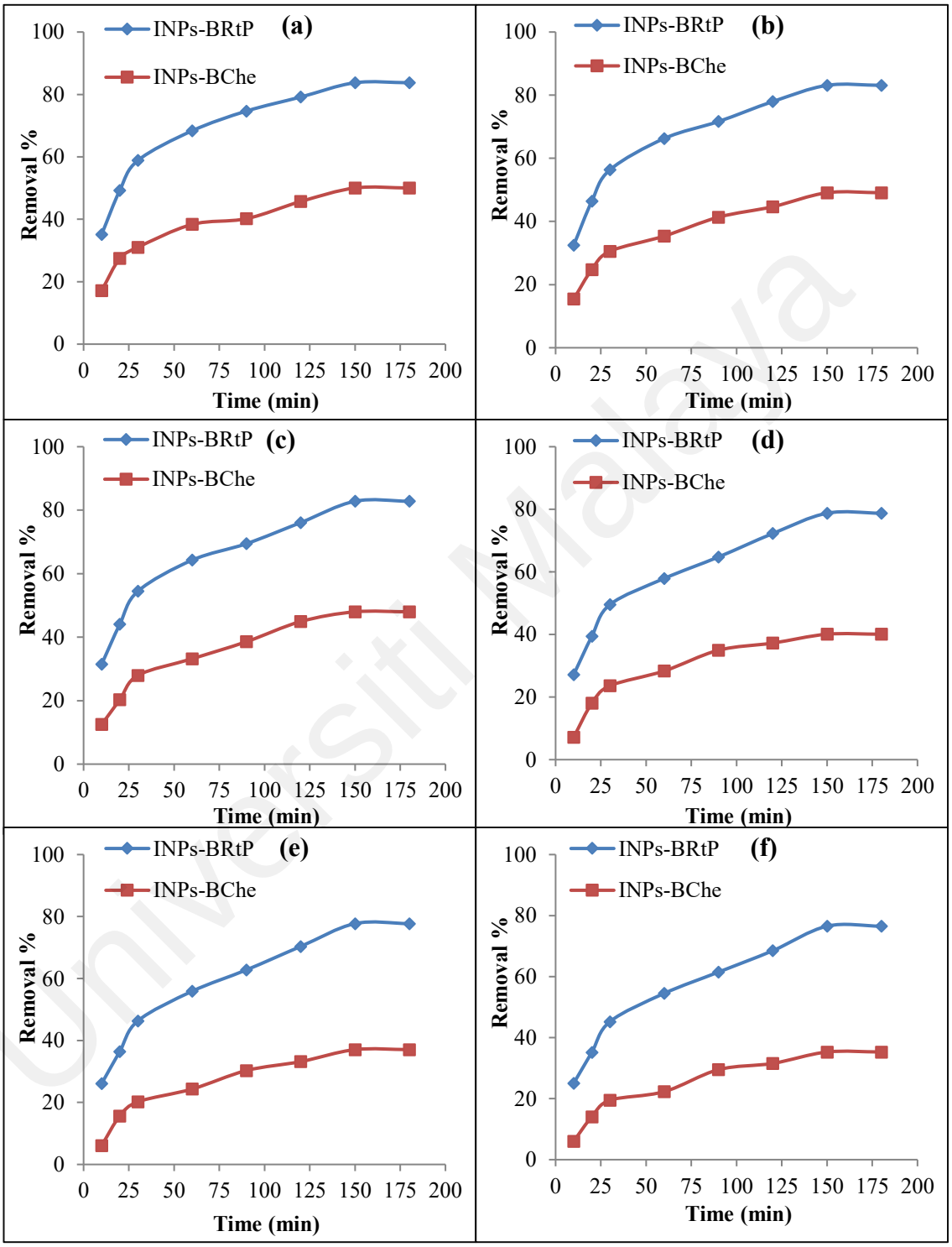

Figure 4.28: Removal efficiency of OCPs (a) *p,p′*-DDT, (b) *o,p′*-DDT, (c) aldrin, (d) heptachlor, (e) hexachlorobenzene, and (f) endosulfan I in OPPD water samples PE1 by 10 g/L of aged green INPs-B_g and INPs-B_{Che} nanocomposites; 2 mg/L of each adsorbate; agitation speed 150 (rpm); at temperature 25±2 °C and pH 4.

Meanwhile, after being aged for one month the removal % of chemical synthesized INPs-B_{Che} declined to 35.29-50.03%, 37.55-52.03% and 32.35-47.73%, in three OPPD samples i.e. PE1, PMD2 and PMD3 respectively dropping about 37.64-50.41%, 35.21-47.72% and 38.29-52.31%, respectively in contrast to the fresh INPs-$B_{Che.}$within same time period i.e. 150 min.

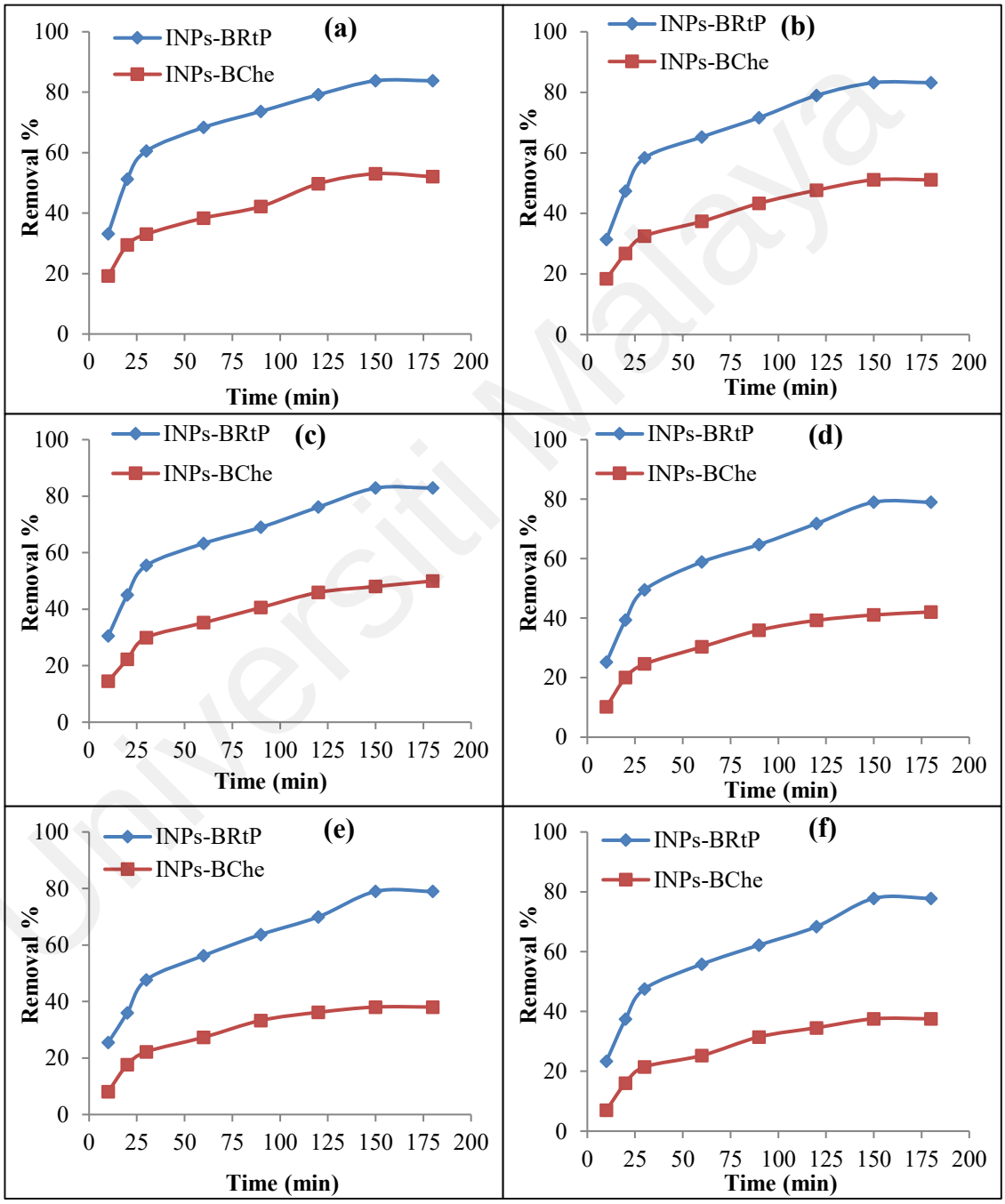

Figure 4.29: Removal efficiency of OCPs (a) *p,p′*-DDT, (b) *o,p′*-DDT, (c) aldrin, (d) heptachlor, (e) hexachlorobenzene, and (f) endosulfan I in OPPD water samples PMD2 by 10 g/L of aged green INPs-B_g and INPs-B_{Che} nanocomposites; 2 mg/L of each adsorbate; agitation speed 150 (rpm); at temperature 25±2 °C and PH 4.

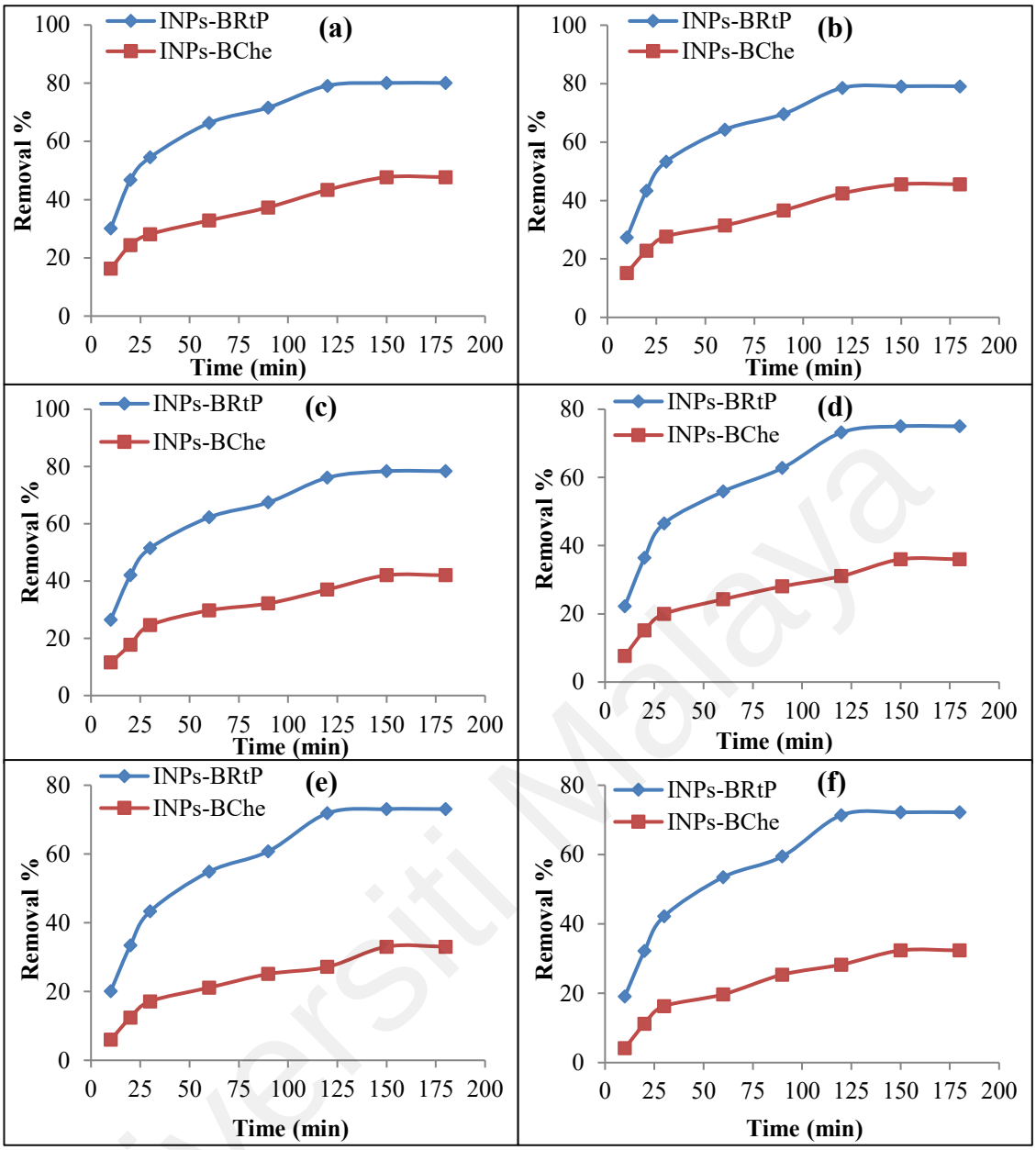

Figure 4.30: Removal efficiency of OCPs (a) *p,p′*-DDT, (b) *o,p′*-DDT, (c) aldrin, (d) heptachlor, (e) hexachlorobenzene, and (f) endosulfan I in OPPD water samples PMD3 by 10 g/L of aged INPs-B_g and INPs-B_{Che} nanocomposites after being aged; 2 mg/L of each adsorbate; agitation speed 150 (rpm); at temperature 25±2 °C and pH 4.

4.2.4 Desorption Studies

The amount of OCPs concentrated on the four types of exhausted green INPs-B_g nanocomposites were determined using n-hexane as a solvent and the concentration of OCPs on all exhausted green INPs-B_g nanocomposites (INPs-B_{RtP}, INPs-B_{OpL}, INPs-B_{JfP} and INPs-B_{ScL}) were found to be in range of 0.20-0.23 mg/L, 0.27-0.25 mg/L, 0.35-0.36 mg/L and 0.40-0.41 mg/L respectively. The initial concentration of OCPs in the solution was 2 mg/L and removal efficiency of all OCPs obtained by INPs-B_{RtP}, INPs-B_{OpL}, INPs-

B_{JfP} and INPs-B_{ScL} were found to be in range of 96-99%, 91-95%, 78-82% and 69-73%, respectively. It can be concluded that 88-99%, 86-87%, 74-78% and 71-72% of the adsorbed OCPs were dechlorinated by the INPs-B_{RtP}, INPs-$B_{OpL,}$ INPs-B_{JfP} and INPs-B_{ScL}, respectively. The dechlorination of OCPs leads to the formation of dechlorinated byproducts (as shown in Figures 4.31 a-f). The intermediate byproducts and the final byproducts present in the solution due to the dechlorination of OCPs were detected at various time intervals and the results has indicated that dechlorinated byproducts of each OCP was found to be detected with the contact time till 120 hr, 150 hr, 180 hr and 180 hr, by INPs-B_{RtP}, INPs-$B_{OpL,}$ INPs-B_{JfP} and INPs-B_{ScL}, respectively, after which no further production of new byproducts in the solution was observed.

4.2.5 Dechlorination Intermediates of OCPs by Nanocomposites

Because dechlorination reactions may occur during the OCP removal in particular with green INPs supported on biochar, potential degradation products of OCPs (*p,p'*-DDT, *o,p'*-DDT, aldrin, heptachlor, hexachlorobenzene and endosulfan I) were monitored. Figures 4.31 a-f show the various dechlorination byproducts of each OCP at different time intervals for green INPs-B_g nanocomposites. A rapid dechlorination of OCPs was observed during the experiment time (as shown in Figure E.1 a-e in appendix with respective retention time (RT), min of each OCP and their produced metabolites). During the initial reaction period (First 10 min as shown in Figure E.1 b), *p,p'*-DDD and *p,p'*-DDE ($C_{14}H_{10}Cl_4$, $C_{14}H_8Cl_4$, respectively), *o,p'*-DDD and *o,p'*-DDE ($C_{14}H_{10}Cl_4$, $C_{14}H_8Cl_4$, respectively), monodechloroaldrin ($C_{12}H_9Cl_5$), chlordane ($C_{10}H_6Cl_6$), pentachlorobenzene (C_6HCl_5O) and [(3a, alpha,7beta,7a alpha,8s)-4,5,6,7,8 Pentachloro 3a,4,7,7a-tetrahydro] ($C_9H_3Cl_5O_3$), were detected as an intermediates of *p,p'*-DDT, *o,p'*-DDT, aldrin, heptachlor, hexachlorobenzene and endosulfan I, respectively. The detection of various intermediates in the solution proved that reductive dechlorination

reaction by the loss of chloride atoms occurred with green INPs supported on biochar (as shown in Figure E.1 a-f).

Subsequent degradation of byproducts was continued (see Figure E.1 c) and after 30 min (Figure E.1 d) tetrachlorobenzene ($C_6H_2Cl_4$) and trichlorobenzene ($C_6H_3Cl_3$) (intermediates of hexachlorobenzene), DDMS ($C_{14}H_{11}Cl_3$) (intermediate of *p,p'*-DDT and *o,p'*-DDT) and Benzofuran,4,5,7-trichloro-2,3-dihydro-2-methyl ($C_9H_7Cl_3O$) (intermediate of endosulfan I) were detected. However, no further dechlorinated byproducts were detected till the end of the experiment for aldrin and heptachlor (Figures 4.31 c-d and E.1 d-e). The end products of *p,p'*-DDT and *o,p'*-DDT and hexachlorobenzene were found to be dichlorobenzophenone ($C_{13}H_8Cl_2O$) and dichlorobenzene ($C_6H_4Cl_2$), respectively (Figures 4.31 a,b,f and E.1 e). It indicated that green INPs supported on biochar have higher dechlorination reactivity.

Different distributions of byproducts were observed by using green INPs-B_g nanocomposites although the reduction was not completed at the end of these experiments (Figure E.1 e). However, no further production of new byproducts were observed even after 180 min of incubation (See Figure E.1 f). It is in agreement with Shih et al, (2009). The reductive dechlorination by successive loss of chloride atoms is confirmed as the main pathway of the degradation of OCPs with green INPs supported on biochar. It is in agreement with several reduction studies of chlorinated compounds with INPs (Mathesan & Tratnyek, 1994; Lowry & Johnson, 2004; Lien & Zhang, 2001).

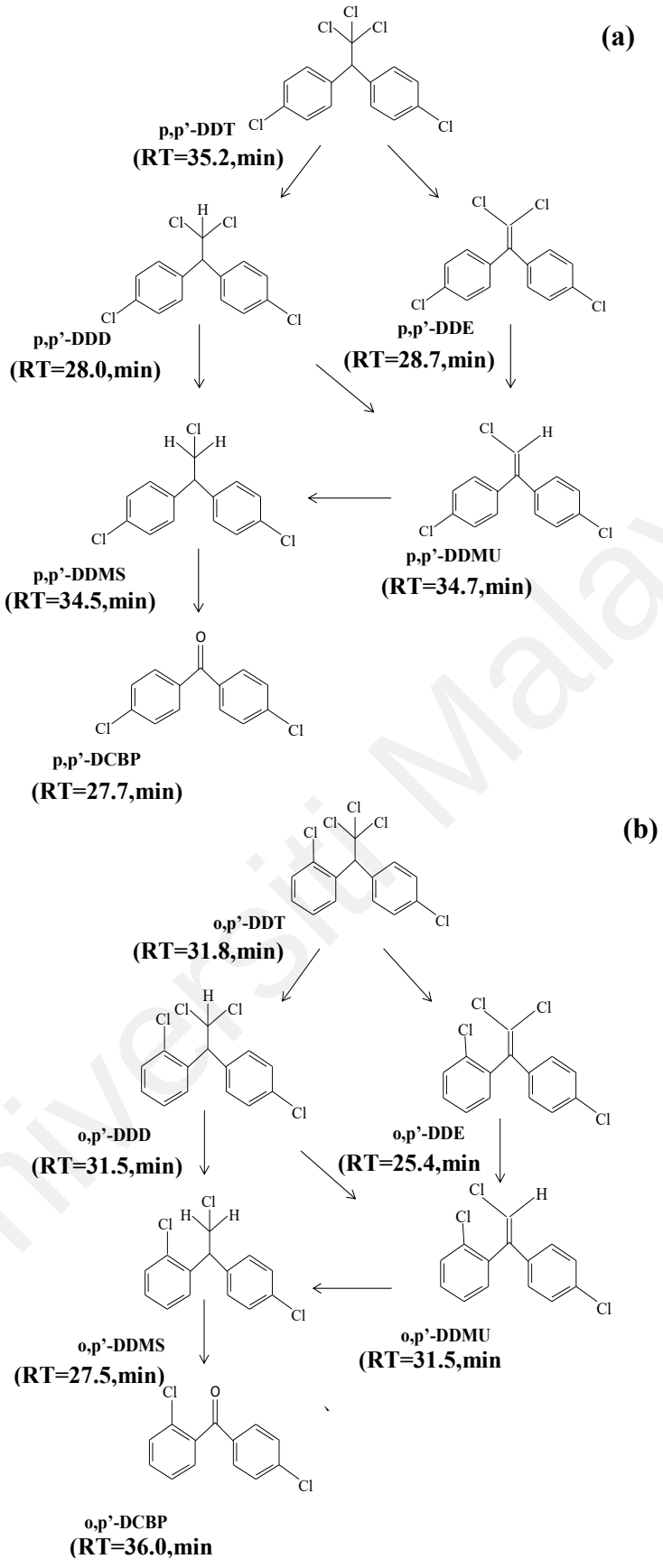

Figure 4.31: Proposed reductive dechlorination pathway (a) *p,p′*-DDT, (b) *o,p′*-DDT, (c) aldrin, (d) endosulfan I, (e) heptachlor and (f) hexachlorobenzene. by green INPs-B_g nanocomposites.

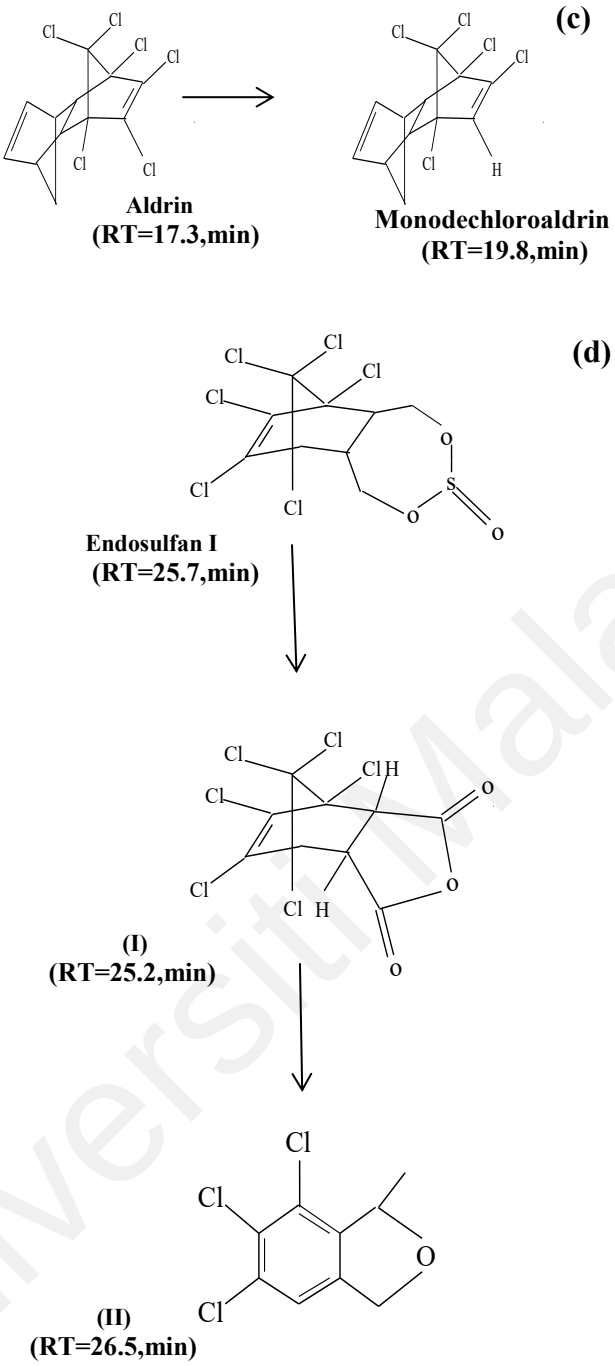

I Benzofuran,4,5,7-trichloro-2,3-dihydro-2-methyl

II [(3a, alpha,7beta,7a alpha,8s)-4,5,6,7,8 Pentachloro 3a,4,7,7a-tetrahydro]

Figure 4.31, continued

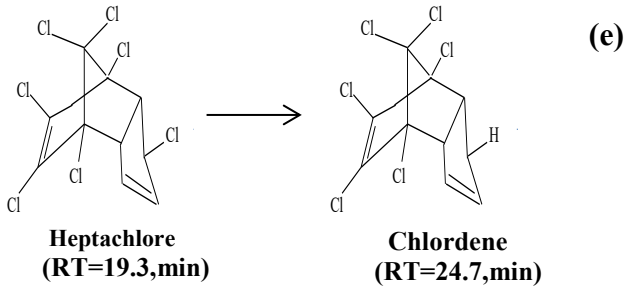

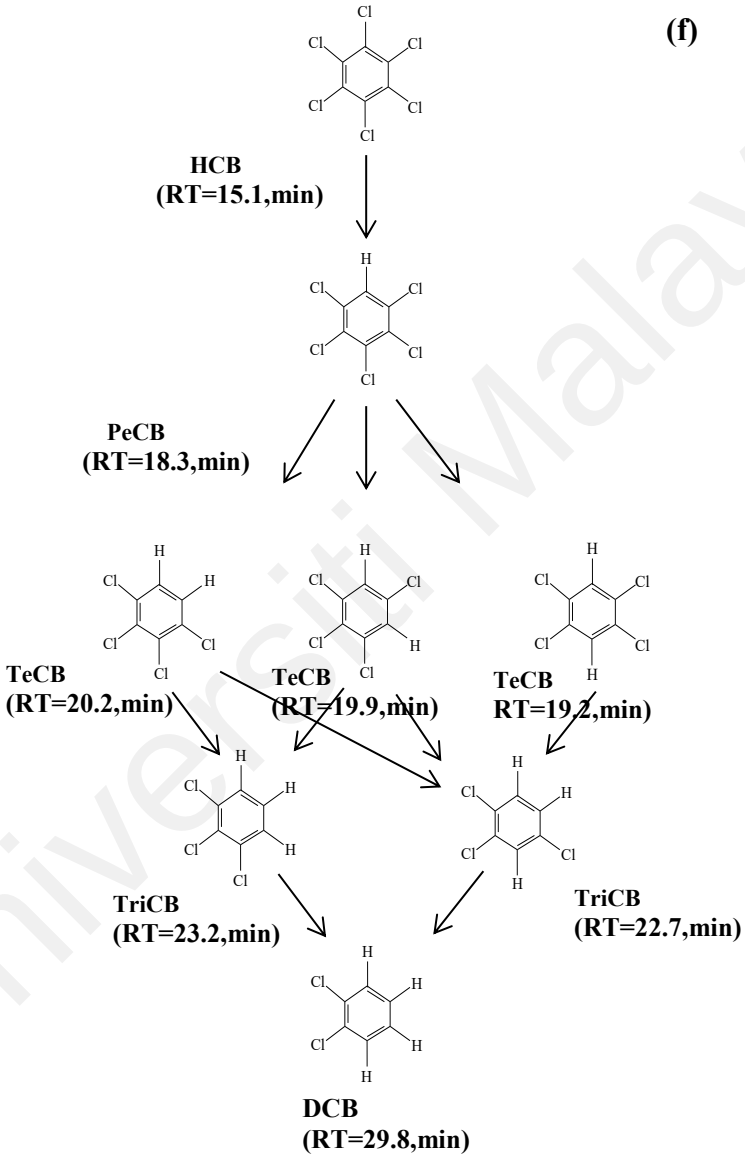

Figure 4.31, continued

4.3 Adsorption Isotherms and Adsorption Kinetic Studies

4.3.1 Adsorption Isotherms

In this study, the most commonly used models i.e. Langmuir and Freundlich models were implemented to analyze the experimental data, and thus illustrate the adsorption characteristics between adsorbent and OCPs.

4.3.1.1 Freundlich Isotherm

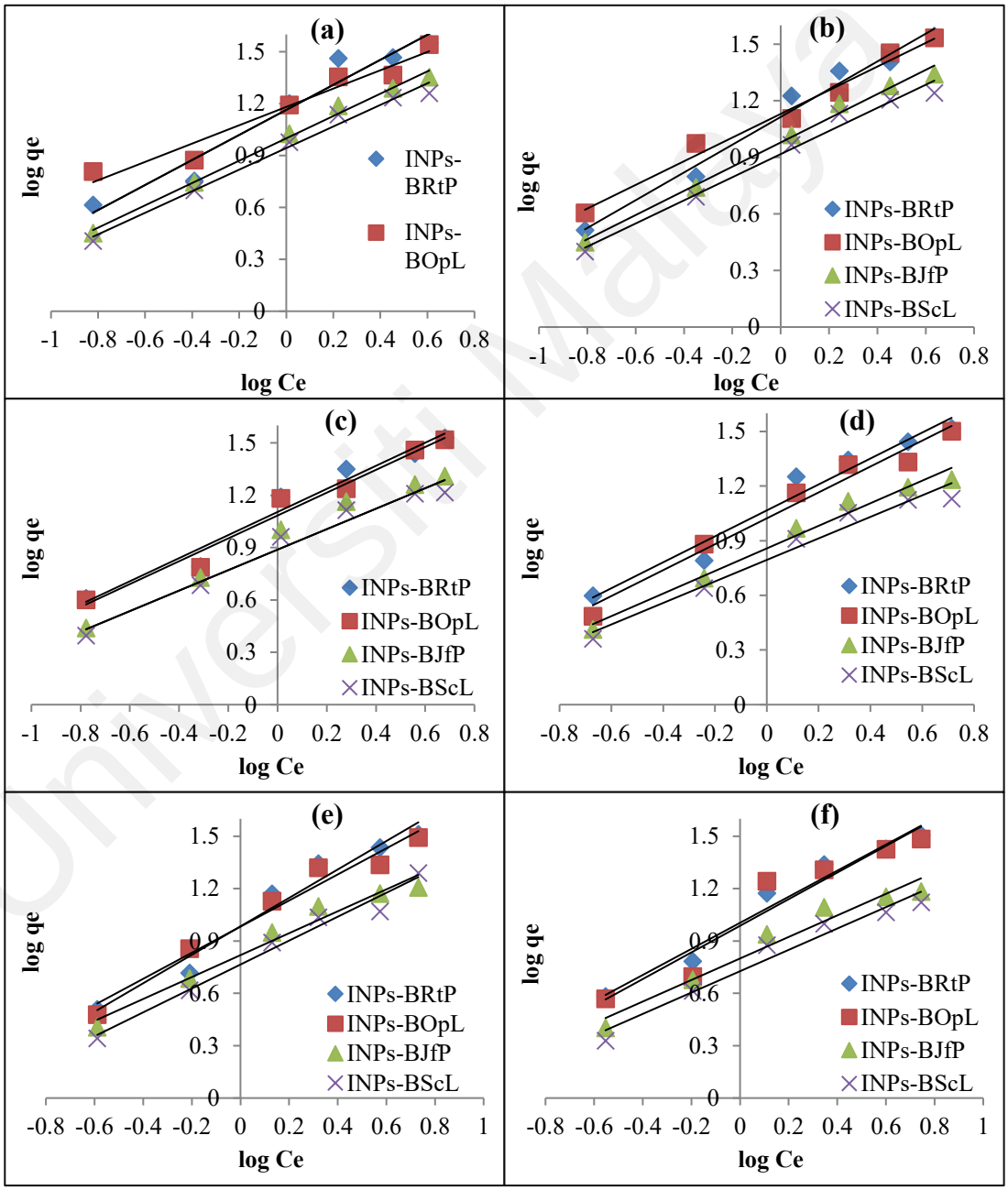

Figure 4.32: Freundlich isotherm plots of OCPs (a) *p,p′*-DDT, (b) *o,p′*-DDT, (c) aldrin, (d) heptachlor, (e) hexachlorobenzene, and (f) endosulfan I by four green INPs-B_g and INPs-B_{Che} nanocomposites.

The points of the plots of the linear form of Freundlich model of the adsorption isotherms of 6 OCPs on the four INPs-B_g nanocomposites and INPs-B_{Che} obtained at room temperature are described in Figure 4.32 and Table 4.5 shows the values of the parameters of the Freundlich isotherm model calculated from Figure 4.32 a-f for OCPs on the four types of the INPs-B_g nanocomposites, INPs-B_{RtP}, INPs-$B_{OpL,}$ INPs-B_{JfP} and INPs-B_{ScL} and chemical synthesized INPs-B_{Che}. It is indicated that correlation coefficient (R^2) values of Freundlich of all OCPs were lower (not above 0.98) than that of Langmuir model for all the adsorbents, consequently, less multilayer heterogenous adsorption on all adsorbents mentioned above. This observation is in agreement with previous work by Erto et al, (2010) who investigated TCE adsorption onto activated carbon and reported that Freundlich model was the best fitting model for this system. In the Freundlich isotherms, $\frac{1}{n}$ is a significant parameter of exchange intensity or surface heterogeneity and the values range between 0 and 1. As seen in Table 4.5, the values of $\frac{1}{n}$ at all the adsorbents samples were between 0 and 1, representing that surface of both types of nanocomposites is favorable for the adsorption of OCPs (Devi and Saroha, 2014). It is manifested that in this study, the suitability of adsorption for Freundlich model was less adequate. It indicated that monolayer adsorption and heterogeneous surface conditions might coexist under the experimental conditions, but heterogenous adsorption was less dominant (Li et al., 2014). The high values of K_f for all the adsorbents mentioned before indicate the favorable adsorption conditions for all OCPs in aqueous solution.

4.3.1.2 Langmuir Isotherm

The Langmuir model parameters for 6 OCPs adsorption by the four adsorbents namely INPs-B_{RtP}, INPs-$B_{OpL,}$ INPs-B_{JfP} and INPs-B_{ScL} are shown in Table 4.5. These parameters (q_{max} and b) were calculated from Figures 4.33 a-f. The values of R^2 of the adsorption of all OCPs were higher (0.99 >) than those of the Freundlich isotherms by all adsorbents,

which confirms that Langmuir model is the best model to describe the adsorption process of OCPs on all green INPs-B_g and chemical synthesized INPs-B_{Che}.

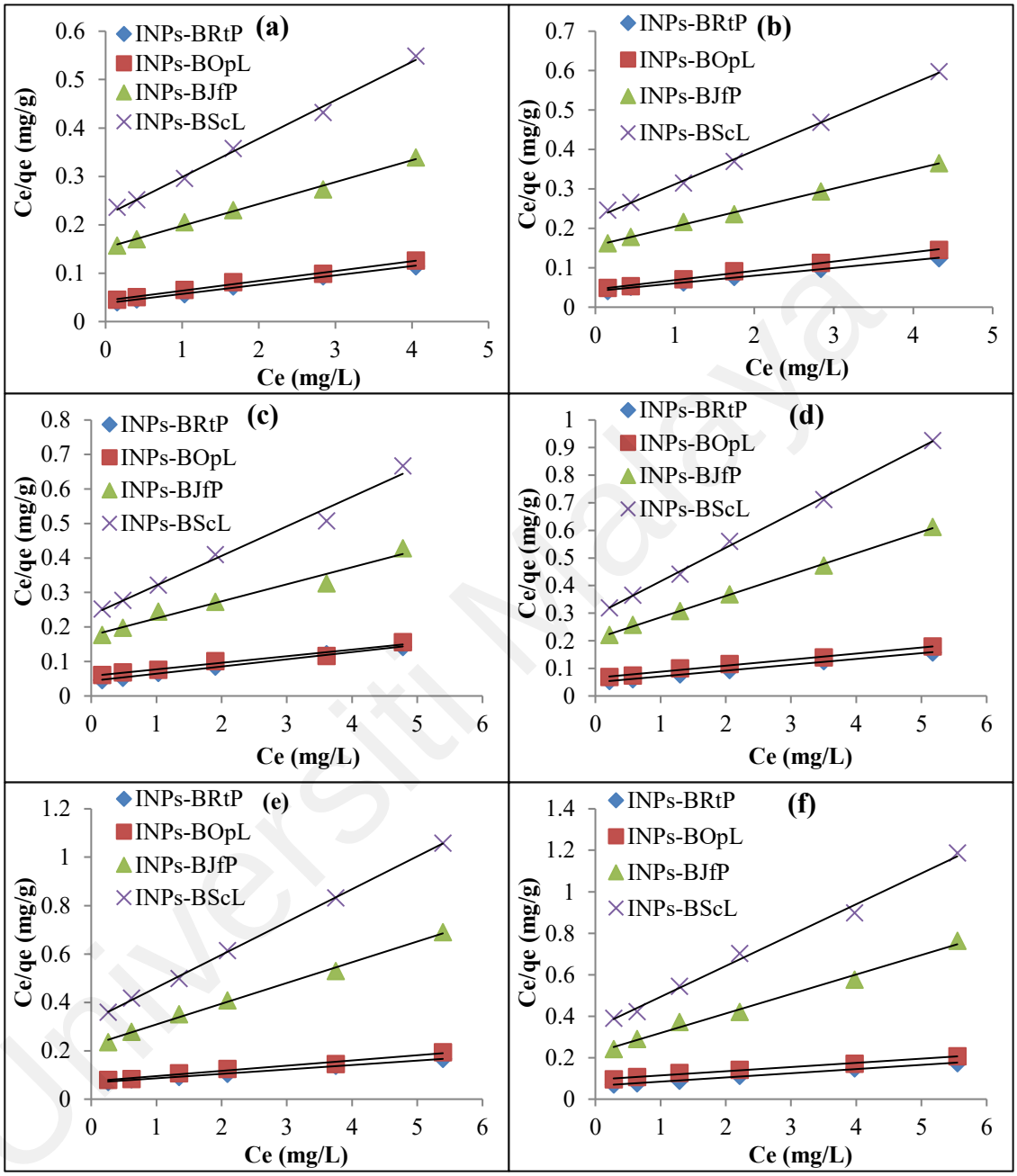

Figure 4.33: Langmuir isotherm plots of OCPs (a) *p,p′*-DDT, (b) *o,p′*-DDT, (c) aldrin, (d) heptachlor, (e) hexachlorobenzene, and (f) endosulfan I by four green INPs-B_g and INPs-B_{Che} nanocomposites.

Consequently, more monolayer homogenous adsorption on all adsorbents mentioned above. Moreover, from the equation above we can see that $0 < R_L < 1$ favorable. The values of $\frac{1}{n} < 1$ also represent that surface of both types of nanocomposites is favorable for the adsorption of OCPs (Devi and Saroha, 2014).

Table 4.5: The calculated Langmuir and Freundlich constants and correlation coefficients of isotherm models in the individual removal of OCPs by all four green INPs-B_g and INPs-B_{Che} nanocomposites.

Adsorbents	Adsorbates	Langmuir			Freundlich		
		q_{max}	b	R^2	K_f	$\frac{1}{n}$	R^2
INPs-B_{RtP}	*p,p'*-DDT	270.2	0.2992	0.9971	49.3628	0.8819	0.9919
	o,p'-DDT	263.3	0.2570	0.9986	57.4116	0.7105	0.9911
	Aldrin	250.0	0.2312	0.9976	49.7851	0.6142	0.9922
	Heptachlor	250.0	0.1762	0.9978	40.5508	0.7527	0.9934
	Hexachlorobenzene	238.1	0.2080	0.9994	36.8231	0.7214	0.9932
	Endosulfan	222.2	0.2143	0.9989	38.6011	0.6809	0.9915
INPs-B_{OpL}	*p,p'*-DDT	243.9	0.2063	0.9984	49.9919	0.7070	0.9880
	o,p'-DDT	250.0	0.2614	0.9975	55.4242	0.6372	0.9914
	Aldrin	222.2	0.2744	0.9975	47.1411	0.7636	0.9929
	Heptachlor	212.8	0.1992	0.9982	35.8591	0.6881	0.9906
	Hexachlorobenzene	227.3	0.1889	0.9978	34.6577	0.7575	0.9910
	Endosulfan	243.9	0.1395	0.9994	35.3590	0.6778	0.9911
INPs-B_{JfP}	*p,p'*-DDT	144.9	0.1494	0.9979	18.2725	0.7661	0.9912
	o,p'-DDT	135.1	0.1520	0.9986	17.8936	0.7097	0.9918
	Aldrin	112.4	0.1595	0.9997	15.5230	0.6143	0.9919
	Heptachlor	80.7	0.1676	0.9990	11.7842	0.5600	0.9928
	Hexachlorobenzee	76.3	0.1825	0.9966	12.5487	0.7641	0.9910
	Endosulfan	67.6	0.1971	0.9980	12.2462	0.7650	0.9913
INPs-B_{ScL}	*p,p'*-DDT	104.2	0.1484	0.9986	13.6584	0.7484	0.9917
	o,p'-DDT	86.2	0.2079	0.9988	12.7174	0.6928	0.9906
	Aldrin	74.6	0.2172	0.9998	11.7598	0.5470	0.9915
	Heptachlor	57.5	0.1716	0.9987	8.7559	0.5824	0.9919
	Hexachlorobenzene	53.8	0.1824	0.9987	9.8175	0.7146	0.9912
	Endosulfan	40.3	0.3464	0.9989	9.0970	0.6442	0.9900
INPs-B_{Che}	*p,p'*-DDT	256.4	0.2063	0.9967	42.7070	0.8630	0.9946
	o,p'-DDT	238.1	0.2019	0.9984	44.0149	0.6730	0.9905
	Aldrin	227.3	0.1606	0.9992	36.3329	0.7153	0.9917
	Heptachlor	217.4	0.1341	0.9998	29.9847	0.7819	0.9923
	Hexachlorobenzene	200.0	0.1623	0.9971	27.6566	0.8819	0.9919
	Endosulfan	195.7	0.1168	0.9986	22.3306	0.7105	0.9911

It is manifested that the adsorption in this study was suitable for Langmuir model more adequately. It indicated that monolayer adsorption and heterogeneous surface conditions might coexist under the experimental conditions, but monolayer adsorption was more dominant (Li et al., 2014). The monolayer adsorption also confirms chemisorption for OCP removal via the INPs-B_{RtP} and INPs-B_{Che} (Pouretedal and Sadegh, 2014).

The q_{max} values were found in range of 40.3-270.2 mg/g, indicating the monolayer adsorption was much favorable to the surface of all the adsorbents. The values of the b were between 0 and 1 indicating that the adsorption energy was favorable. Based on the correlation coefficient values of the aadsorption isother model, Langmuir model fitted well for all OCPs by all types of nanocomposites. The monolayer adsorption was dominant for all types of nanocomposites indicating that adsorption of OCPs was chemisorption.

4.3.2 Adsorption Kinetics Studies

4.3.2.1 Adsorption Kinetics of Individual OCPs by Fresh Nanocomposites

There are several kinetic models used to identify the rate of the adsorption process such as chemical reaction and mass transfer. Two kinetic models such as Pseudo-first order and Pseudo-second order models were used to determine the individual adsorption process of OCPs on the green INPs-B_g nanocomposites. A series of contact time experiments were carried out with their respective dosages of the four different INPs-B_g nanocomposites and constant temperature (room temperature, 25±2 °C) at initial OCPs concentrations of 2 mg/L. For comparison, same models were also applied for chemical synthesized INPs-B_{Che} nanocomposite under same experimental conditions.

Figures 4.34 a-f to 4.35 a-f shows the plots of the linearized form of the pseudo-first order and pseudo-second order model equations, respectively. The kinetic parameters calculated from the two models have been listed in Table 4.6. The correlation coefficient (R^2) values of INPs-B_{RtP}, INPs-$B_{OpL,}$ INPs-B_{JfP}, INPs-B_{ScL} and INPs-B_{Che} were above 0.98 for the pseudo-first order reduction kinetic model and above 0.99 for the pseudo-second order adsorption kinetic model, indicating that the individual removal of OCPs using green INPs-B_g and chemical synthesized INPs-B_{Che} fitted well to both the reduction and adsorption kinetic models. The adsorbed OCPs onto biochar and INPs were then

reduced by Fe^0 which is confirmed by the previous study conducted by Chen et al, (2014) in which they use chemically synthesized INPs supported on activated carbon for the removal of HCB. INPs successfully reduced the HCB. According to their adsorption kinetic analysis, the removal of HCB using INPs supported on activated carbon fitted well to both the reduction and adsorption kinetic models.

Table 4.6: Kinetic parameters for the individual OCPs removal by fresh four green INPs-B_g and INPs-B_{Che} nanocomposites.

Adsorbents	Pseudo first-order model			Pseudo second-order model			
	Adsorbates	k_{obs} (min^{-1})	R^2	q_e (g/mg)	k_2	h(g/mmin^{-1})	R^2
INPs-B_{RtP}	*p,p'*-DDT	0.1096	0.9861	27.47	0.0035	2.2852	0.9970
	o,p'-DDT	0.1083	0.9806	27.10	0.0033	2.2080	0.9966
	Aldrin	0.1067	0.9827	27.03	0.0026	1.9459	0.9931
	Heptachlor	0.0944	0.9794	26.95	0.0023	1.6683	0.9916
	Hexachlorobenzene	0.0868	0.9788	25.91	0.0021	1.5667	0.9925
	Endosulfan	0.0830	0.9780	25.64	0.0025	1.5625	0.9946
INPs-B_{OpL}	*p,p'*-DDT	0.1008	0.9805	26.20	0.0028	1.9708	0.9963
	o,p'-DDT	0.0994	0.838	25.83	0.0025	1.8155	0.9959
	Aldrin	0.0983	0.9809	25.68	0.0022	1.6872	0.9926
	Heptachlor	0.0866	0.9811	25.79	0.0019	1.4633	0.9907
	Hexachlorobenzene	0.0799	0.9843	24.61	0.0018	1.4180	0.9920
	Endosulfan	0.0763	0.9773	24.46	0.0016	1.2598	0.9939
INPs-B_{jfP}	*p,p'*-DDT	0.0526	0.9808	19.33	0.0011	0.6340	0.9900
	o,p'-DDT	0.0514	0.9749	19.24	0.00082	0.5523	0.9955
	Aldrin	0.0517	0.9885	19.21	0.00069	0.5582	0.9928
	Heptachlor	0.0453	0.9782	18.99	0.00030	0.4188	0.9926
	Hexachlorobenzene	0.0425	0.9785	18.13	0.00022	0.3228	0.9943
	Endosulfan	0.0392	0.9676	18.02	0.00017	0.3677	0.9909
INPs-B_{ScL}	*p,p'*-DDT	0.0412	0.9827	17.28	0.00040	0.4274	0.9960
	o,p'-DDT	0.0406	0.9805	17.07	0.00036	0.4173	0.9941
	Aldrin	0.0395	0.9760	17.03	0.00029	0.3994	0.9951
	Heptachlor	0.0359	0.9806	16.98	0.00017	0.3101	0.9955
	Hexachlorobenzene	0.0330	0.9830	16.32	0.00011	0.2847	0.9900
	Endosulfan I	0.0324	0.9804	16.15	0.00007	0.2514	0.9943
INPs-B_{Che}	*p,p'*-DDT	0.0811	0.9826	24.49	0.0023	1.6181	0.9975
	o,p'-DDT	0.0809	0.9820	23.85	0.0018	1.4148	0.9934
	Aldrin	0.0805	0.9815	23.47	0.0012	1.2071	0.9958
	Heptachlor	0.0794	0.9843	22.59	0.00069	0.9411	0.9996
	Hexachlorobenzene	0.0738	0.9871	22.04	0.00051	0.8896	0.9959
	Endosulfan	0.0716	0.9838	21.83	0.00045	0.7906	0.9936

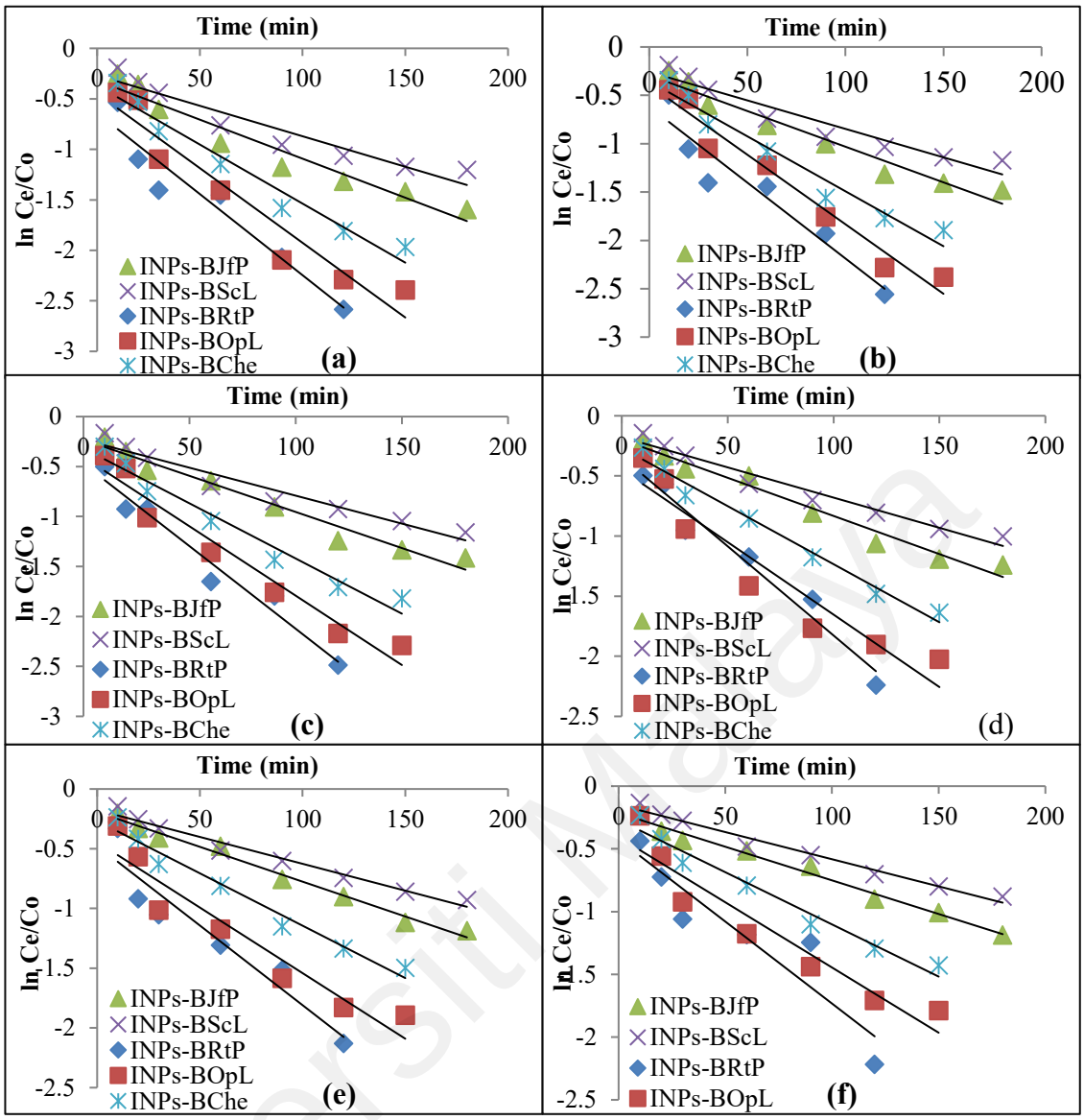

Figure 4.34: Pseudo-first-order reduction rate model fittings to the experimental data for the individual removal of OCPs (a) *p,p′*-DDT, (b) *o,p′*-DDT, (c) aldrin, (d) heptachlor, (e) hexachlorobenzene, and (f) endosulfan I by fresh four green INPs-B_g and INPs-B_{Che} nanocomposites.

The high R^2 values of OCPs with all nanocomposites indicated that it is in good agreement with the previous studies on carbon-supported INPs (Quan et al., 2014; Pouretedal & Saedi, 2014; Su et al., 2013). For all types of nanocomposites the observed reaction rate constant (k_{obs}) were found in the following order INPs-B_{RtP} (0.0830-0.1096 min^{-1}) > INPs-B_{OpL} (0.0763-0.1008 min^{-1}) > INPs-B_{JfP} (0.0392-0.0526 min^{-1}) and INPs-B_{ScL} (0.0324-0.0406 min^{-1}). The observed reaction rate constant values indicated that reduction of OCPs occurs at INPs interface (Wang et al., 2017). The observed reaction rate constant (k_{obs}) values of all OCPs for INPs-B_{RtP} adsorbent was found slightly higher

(up to 8.1 %) than that for INPs-B_{OpL}, while incredibly higher (up to 53 and 61 %) in case of INPs-B_{JfP} and INPs-B_{ScL}. It may be attributed to the higher wt% of INPs on the B_{RtP} (82.7%) and B_{OpL} (70.5%) biochar rather than that of B_{JfP} (63.9%) B_{ScL} (51.5%) biochar. The reactivity of chemically synthesized INPs-B_{Che} was found only 14% and 6% lower than that of the green synthesized INPs-B_{RtP} and INPs-B_{OpL}, respectively however it was found to be incredibly higher i.e. 45% and 55% than that of the INPs-B_{JfP} and INPs-B_{ScL}, respectively and calculated k_{obs} value was ranged between 0.0716-0.0811 min^{-1} for all OCPs. The reactivities of all INPs-B nanocomposites were found in the following order: INPs-B_{RtP} > INPs-B_{OpL} > INPs-B_{Che} > INPs-B_{JfP} and > INPs-B_{ScL}.

The results are in good agreement with the observations reported by Chen et al, (2014) who studied the removal of HCB with two samples of activated carbon loaded with various cocentrations of INPs i.e. INPs/AC-A containing 72% higher INPs than that of INPs/AC-1. Therefore, the k_{obs} value of INPs/AC-A was found 25% higher than that of INPs/AC-1. In our study, the calculated k_{obs} values which is the same order of the magnitude but has a considerably larger values than the values reported by chen et al, (2014) which are 0.0010 and 0.0013 min^{-1} for INPs/AC-1 and INPs/AC-A. The larger values of K_{obs} indicated that nanocomposites prepared by green method in our study have high reactivity for OCPs.

In all cases, on the basis of specific log Kow values of each OCP molecule, the observed reaction rate constant (k_{obs}) values were always found in the following order *o,p'*-DDT > *p,p'*-DDT > aldrin > heptachlor > hexachlorobenzene and endosulfan I. For all types of adsorbents, the *p,p'*-DDT compound was found with highest observed reaction rate constant (k_{obs}) values (range between 0.0406-0.1096 min^{-1}) as compared to the rest of the 5 OCP compounds in this study. The observed reaction rate constant (k_{obs}) values of *p,p'*-DDT was found slightly higher (up to 2 and 4%) than that of *o,p'*-DDT

and aldrin, respectively. Whereas, it was found to be considerably higher (up to 13, 20 and 24%) than that of heptachloe, hexachlorobenzene and endosulfan, respectively.

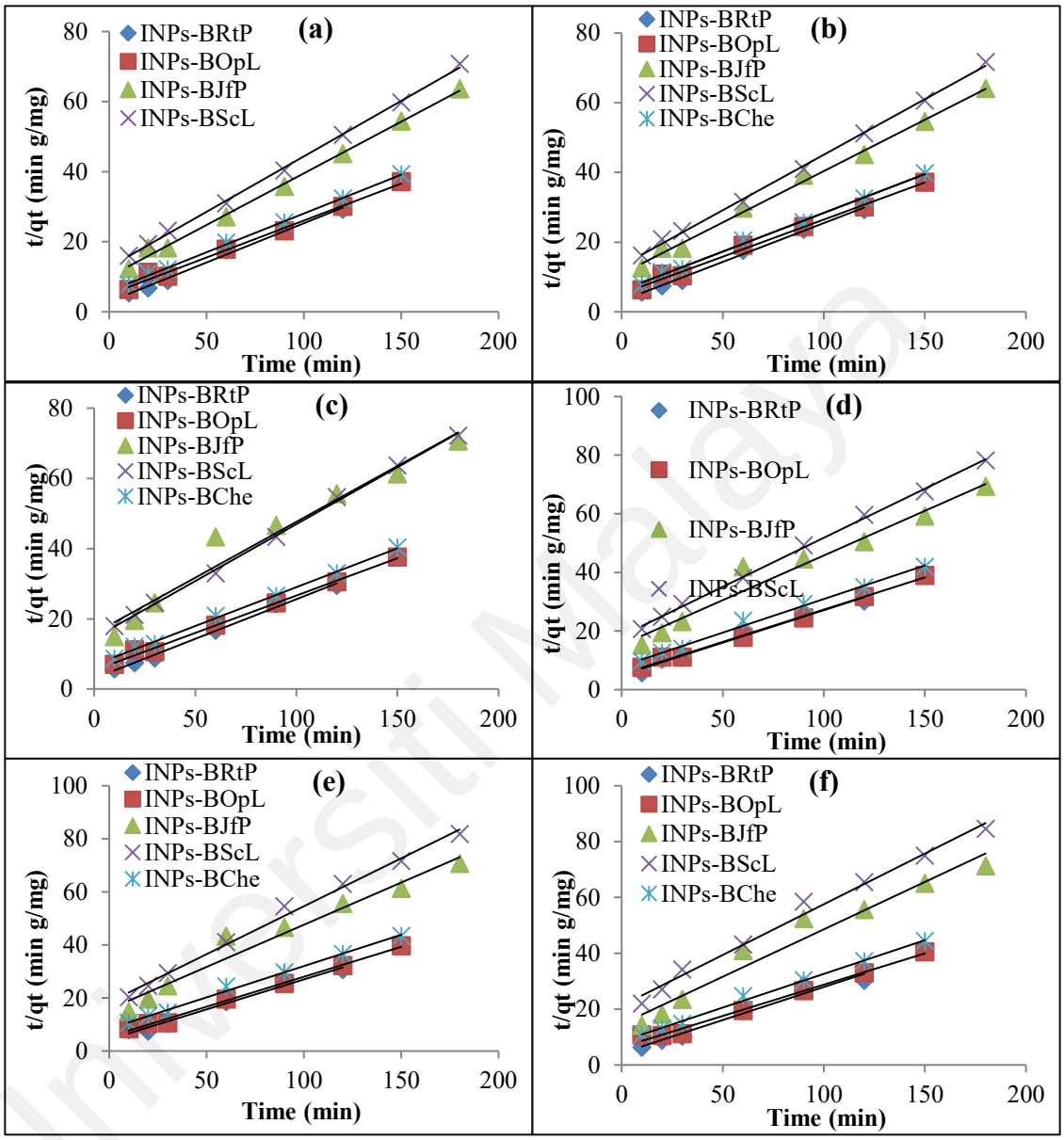

Figure 4.35: Pseudo-second-order absorption model fittings to the experimental data for the individual removal of OCPs (a) *p,p′*-DDT, (b) *o,p′*-DDT, (c) aldrin, (d) heptachlor, (e) hexachlorobenzene, and (f) endosulfan I by fresh four green INPs-B_g and INPs-B_{Che} nanocomposites.

A similar study was conducted by Elliot et al, (2016) in which they remove they prepared supported INPs by chemical method and applied same concentrations (2.2 mg/L) for the removal of aldrin, atrazine and heptachlore. The adsorbates aldrine and heptachlor with higher log Kow values (6.5 and 5.44, respectively) showed higher reactivity than than that of atrazine which have lower log Kow value (2.61). The k_{obs}

values of aldrine and heptachlor were found to be 36 and 31% higher than that of the atrazine which is in agreement with our observations that higher the log Kow higher is the k_{obs} value of adsorbate.

4.3.2.1 Adsorption Kinetics of Individual OCPs by Aged Nanocomposites

The linearized form of the pseudo-first order and pseudo-second order model equations have been plotted for all types of green and chemical synthesized nanocomposites used for the individual removal of OCPs (Figures 4.36 a-f and 4.37 a-f, respectively). The kinetic parameters calculated from the two models have been listed in Table 4.7.

Table 4.7: The kinetic parameters for individual OCPs removal by aged four green INPs-B_g and INPs-B_{Che} nanocomposites

Adsorbents	Pseudo first-order model			Pseudo second-order model			
	Adsorbates	k_{obs} (min^{-1})	R^2	q_e (g/mg)	k_2	(g/mg min^{-1})	R^2
INPs-B_{RtP}	*p,p'*-DDT	0.0967	0.9861	24.52	0.0032	1.9376	0.9933
	o,p'-DDT	0.0955	0.9806	24.39	0.0032	1.8997	0.9943
	Aldrin	0.0941	0.9827	24.10	0.0029	1.6949	0.9905
	Heptachlor	0.0833	0.9794	23.25	0.0027	1.4633	0.9902
	Hexachlorobenzene	0.0766	0.9788	23.41	0.0025	1.3716	0.9946
	Endosulfan	0.0735	0.9780	22.82	0.0026	1.3289	0.9955
INPs-B_{OpL}	*p,p'*-DDT	0.0880	0.9799	23.20	0.0024	1.7170	0.9946
	o,p'-DDT	0.0874	0.9860	22.83	0.0020	1.5888	0.9988
	Aldrin	0.0859	0.9782	22.68	0.0014	1.3075	0.9976
	Heptachlor	0.0750	0.9848	22.79	0.0013	1.1818	0.9991
	Hexachlorobenzene	0.0699	0.9853	21.61	0.0012	1.1561	0.9980
	Endosulfan	0.0665	0.9863	21.46	0.0011	1.0928	0.9980
INPs-B_{JfP}	*p,p'*-DDT	0.0464	0.9759	16.38	0.00084	0.5788	0.9900
	o,p'-DDT	0.0439	0.9854	16.18	0.00045	0.4853	0.9969
	Aldrin	0.0414	0.9808	16.14	0.00038	0.4674	0.9970
	Heptachlor	0.0358	0.9825	15.94	0.00015	0.3695	0.9978
	Hexachlorobenzene	0.0314	0.9814	15.11	0.00010	0.3154	0.9951
	Endosulfan	0.0301	0.9825	15.02	0.00008	0.3237	0.9903
I	*p,p'*-DDT	0.0348	0.9753	14.29	0.00019	0.3763	0.9970
	o,p'-DDT	0.0315	0.9751	14.10	0.00013	0.3477	0.9960

	Aldrin	0.0320	0.9765	14.00	0.00012	0.3457	0.9931
	Heptachlor	0.0267	0.9848	13.99	0.00009	0.2704	0.9951
	Hexacyclobenzene	0.0248	0.9780	13.41	0.00007	0.2698	0.9986

Table 4.8, continued

Adsorbents	**Pseudo first-order model**			**Pseudo second-order model**			
	Adsorbates	k_{obs} **(min^{-1})**	R^2	q_e **(g/mg)**	k_2	**(g/mg min^{-1})**	R^2
	Endosulfan I	0.0221	0.9804	13.03	0.00006	0.1998	0.9924
INPs-B_{Che}	*p,p'*-DDT	0.0112	0.9826	12.37	0.0038	0.9463	0.9911
	o,p'-DDT	0.0111	0.9820	12.04	0.0041	0.8989	0.9822
	Aldrin	0.0108	0.9815	11.81	0.0036	0.7445	0.9913
	Heptachlor	0.0104	0.9843	11.41	0.0030	0.5848	0.9926
	Hexachlorobenzene	0.0100	0.9871	11.13	0.0026	0.4966	0.9906
	Endosulfan	0.0098	0.9838	10.96	0.0023	0.4294	0.9923

The correlation coefficient (R^2) values of INPs-B_{RtP}, INPs-$B_{OpL,}$ INPs-B_{JfP}, INPs-B_{ScL} and INPs-B_{Che} were between 0.98 for the pseudo-first order reduction kinetic model and above 0.98 for the pseudo-second order adsorption kinetic model, indicating that the individual removal of OCPs using nanocomposites fitted well to both the reduction and adsorption kinetic models. The adsorbed OCPs onto biochar and INPs were then reduced by Fe^0 which is confirmed by the previous studies (Kassaee et al., 2011 & Kim et al., 2012).

After aging of all types of green INPs-B_g nanocomposites (INPs-B_{RtP}, INPs-$B_{OpL,}$ INPs-B_{JfP}, INPs-B_{ScL}), the observed reaction rate constant (k_{obs}) values decreased slightly up to 11%, 13%, 23% and 32%, respectively for all OCPs, whereas in case of aged chemical synthesized INPs-B_{Che}, a considerable decrease in reaction rate constant values were observed i.e. up to 86% for all OCPs in the mixture solution. It can be decided that green INPs supported on biochar were persisted quite unchanged in air due to the outer coating of polyphenols from plant extract. Whereas, INPs synthesized by chemical

method get oxidized in air during aging process and it is in agreement with Wang et al, (2014) who observed the same phenomenon for chemical and green synthesized INPs using green tea and eucalyptus leaf ectract used for the removal of nitrate. After being aged in air for two months, k_{obs} of chemically synthesized INPs dropped about 74% in contrast to the fresh INPs. Whereas, the k_{obs} values of INPs synthesized using green tea and eucalyptus leaf ectracts remained almost same. Thus, it can be confirmed that in this study green nanocomposites are highly stable as compared to the chemically synthesized nanocomposites.

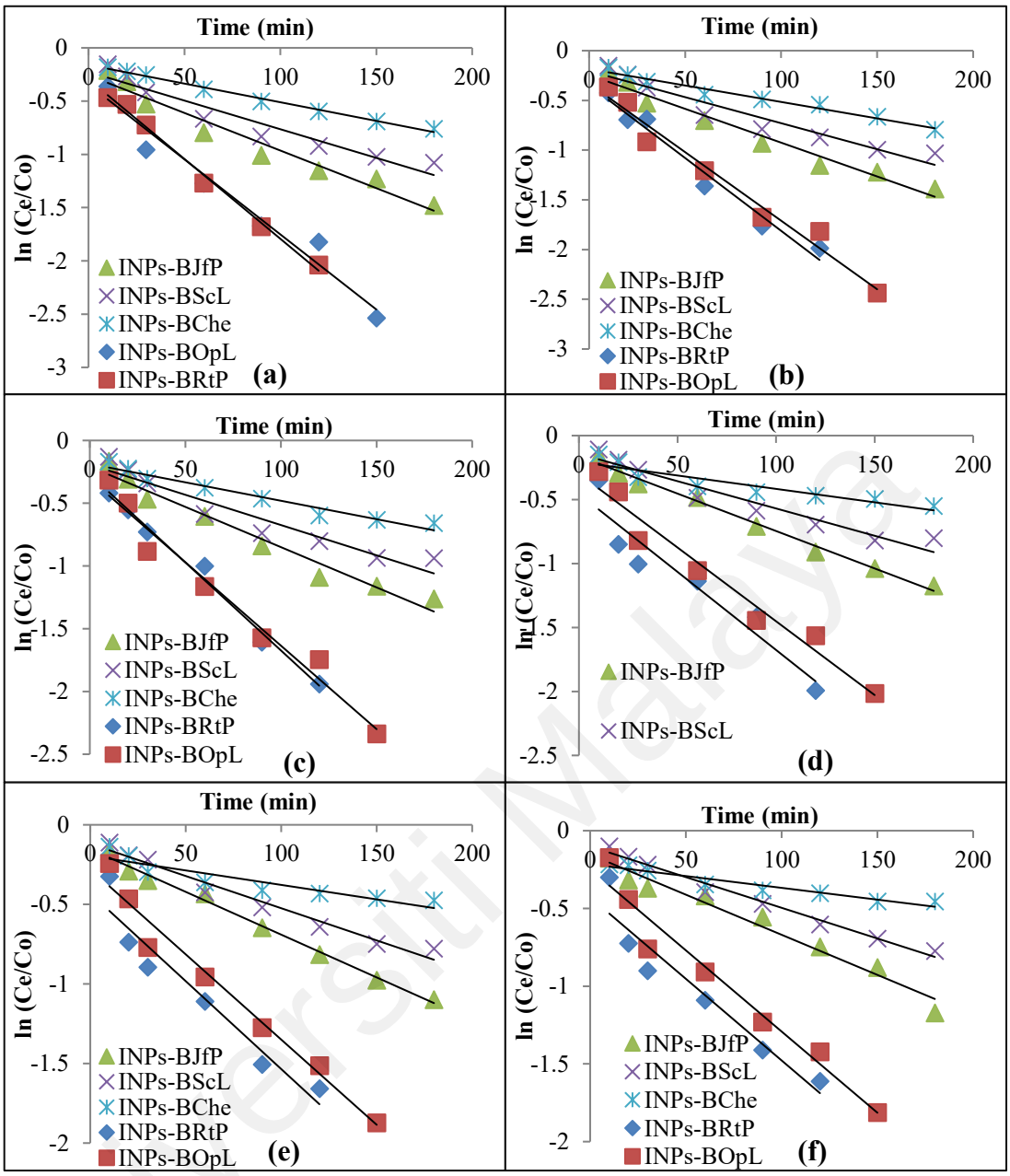

Figure 4.36: Pseudo-first-order model fittings to the experimental data for the individual removal of OCPs (a) *p,p′*-DDT, (b) *o,p′*-DDT, (c) aldrin, (d) heptachlor, (e) hexachlorobenzene, and (f) endosulfan I by aged four green INPs-B_g and INPs-B_{Che} nanocomposites.

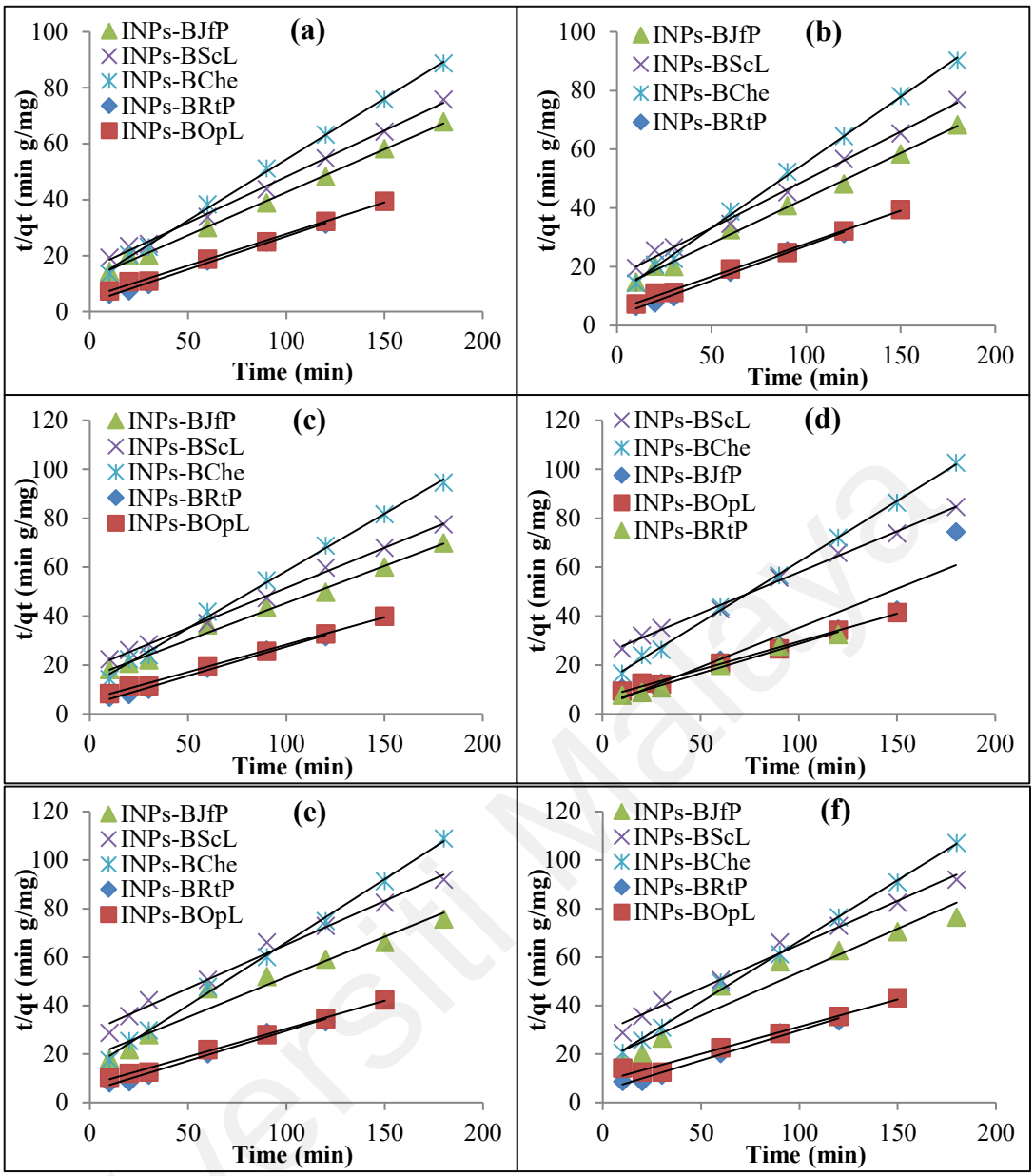

Figure 4.37: Pseudo-second-order model fittings to the experimental data for the individual removal of OCPs (a) *p,p'*-DDT, (b) *o,p'*-DDT, (c) aldrin, (d) heptachlor, (e) hexachlorobenzene, and (f) endosulfan I by aged four green INPs-B_g and INPs-B_{Che} nanocomposites.

4.3.2.2 Adsorption Kinetics of Mixed OCPs by Fresh Nanocomposites

Figures 4.38 a-f to 4.39 a-f represents the plots of linearized form of the pseudo-first order and pseudo-second order model equations for green and chemical synthesized nanocomposites used for the removal of mixed OCPs in the solution using the 0.45-0.55 g/L of nanocomposites at pH 4 and room temperature.

Table 4.9: Kinetic parameters for the removal of mixed OCPs by fresh four green INPs-B_g and INPs-B_{Che} nanocomposites.

Adsorbents	Pseudo first-order model			Pseudo second-order model			
	Adsorbates	k_{obs} (min^{-1})	R^2	q_e (g/mg)	k_2	h (g/mg min^{-1})	R^2
INPs-B_{RtP}	*p,p'*-DDT	0.0161	0.9266	4.74	0.0174	0.3909	0.9938
	o,p'-DDT	0.0157	0.9129	4.70	0.0170	0.3755	0.9929
	Aldrin	0.0151	0.8881	4.69	0.0165	0.3629	0.9948
	Heptachlor	0.0132	0.8665	4.54	0.0131	0.2700	0.9833
	Hexachlorobenzene	0.0120	0.8958	4.46	0.0116	0.2307	0.9855
	Endosulfan	0.0113	0.8687	4.43	0.0099	0.1943	0.9701
INPs-B_{OpL}	*p,p'*-DDT	0.0148	0.9251	4.51	0.0096	0.1946	0.9906
	o,p'-DDT	0.0144	0.9615	4.49	0.0092	0.1854	0.9921
	Aldrin	0.0139	0.9533	4.42	0.0090	0.1758	0.9948
	Heptachlor	0.0121	0.9056	4.31	0.0088	0.1635	0.9955
	Hexachlorobenzene	0.011	0.9121	4.25	0.0085	0.1535	0.9953
	Endosulfan	0.0104	0.9086	4.23	0.0079	0.1414	0.9902
INPs-B_{JfP}	*p,p'*-DDT	0.0077	0.8933	3.30	0.0091	0.0996	0.9968
	o,p'-DDT	0.0074	0.9434	3.25	0.0087	0.0916	0.9952
	Aldrin	0.0072	0.9560	3.23	0.0066	0.0684	0.9617
	Heptachlor	0.0063	0.9644	3.12	0.0067	0.0655	0.9645
	Hexachlorobenzene	0.0058	0.9855	3.02	0.0054	0.0633	0.9617
	Endosulfan	0.0054	0.9809	2.79	0.0052	0.0633	0.9596
INPs-B_{ScL}	*p,p'*-DDT	0.006	0.9206	3.07	0.0084	0.0840	0.9912
	o,p'-DDT	0.0059	0.9741	3.05	0.0081	0.0757	0.9984
	Aldrin	0.0056	0.9672	3.03	0.0075	0.0689	0.9988
	Heptachlor	0.0050	0.9663	2.98	0.0061	0.0546	0.9984
	Hexachlorobenzene	0.0045	0.9535	2.84	0.0067	0.0543	0.9936
	Endosulfan	0.0043	0.9492	2.77	0.0061	0.0471	0.9891
INPs-B_{Che}	*p,p'*-DDT	0.0117	0.9616	4.52	0.1838	0.1690	0.9985
	o,p'-DDT	0.0114	0.9574	4.50	0.1771	0.1627	0.9968
	Aldrin	0.0110	0.9642	4.46	0.1603	0.1458	0.9976
	Heptachlor	0.0097	0.9805	4.36	0.1460	0.1251	0.9943
	Hexachlorobenzene	0.0088	0.9701	4.24	0.1467	0.1186	0.9957
	Endosulfan	0.0083	0.9679	4.14	0.1525	0.1178	0.9959

Figures 4.38 a-f to 4.39 a-f shows the plots of the linearized form of the pseudo-first order and pseudo-second order model equations, respectively. The kinetic parameters calculated from the two models have been listed in Table 4.8. The correlation coefficient (R^2) values of INPs-B_{RtP}, INPs-B_{OpL}, INPs-B_{JfP}, INPs-B_{ScL} and INPs-B_{Che} were between 0.98-0.99 for the pseudo-first order reduction kinetic model and above 0.99 for the

pseudo-second order adsorption kinetic model, indicating that the removal of OCPs using green INPs-B_g and chemical synthesized INPs-B_{Che} fitted well to both the reduction and adsorption kinetic models. The adsorbed OCPs onto biochar and INPs particles were then reduced by Fe^0 which is confirmed by the previous study conducted by Chen et al, (2014) in which they use chemically synthesized INPs supported on activated carbon for the removal of HCB. INPs successfully reduced the HCB. Accoroding to their adsorption kinetic analysis, the removal of HCB using INPs supported on activated carbon fitted well to both the reduction and adsorption kinetic models.

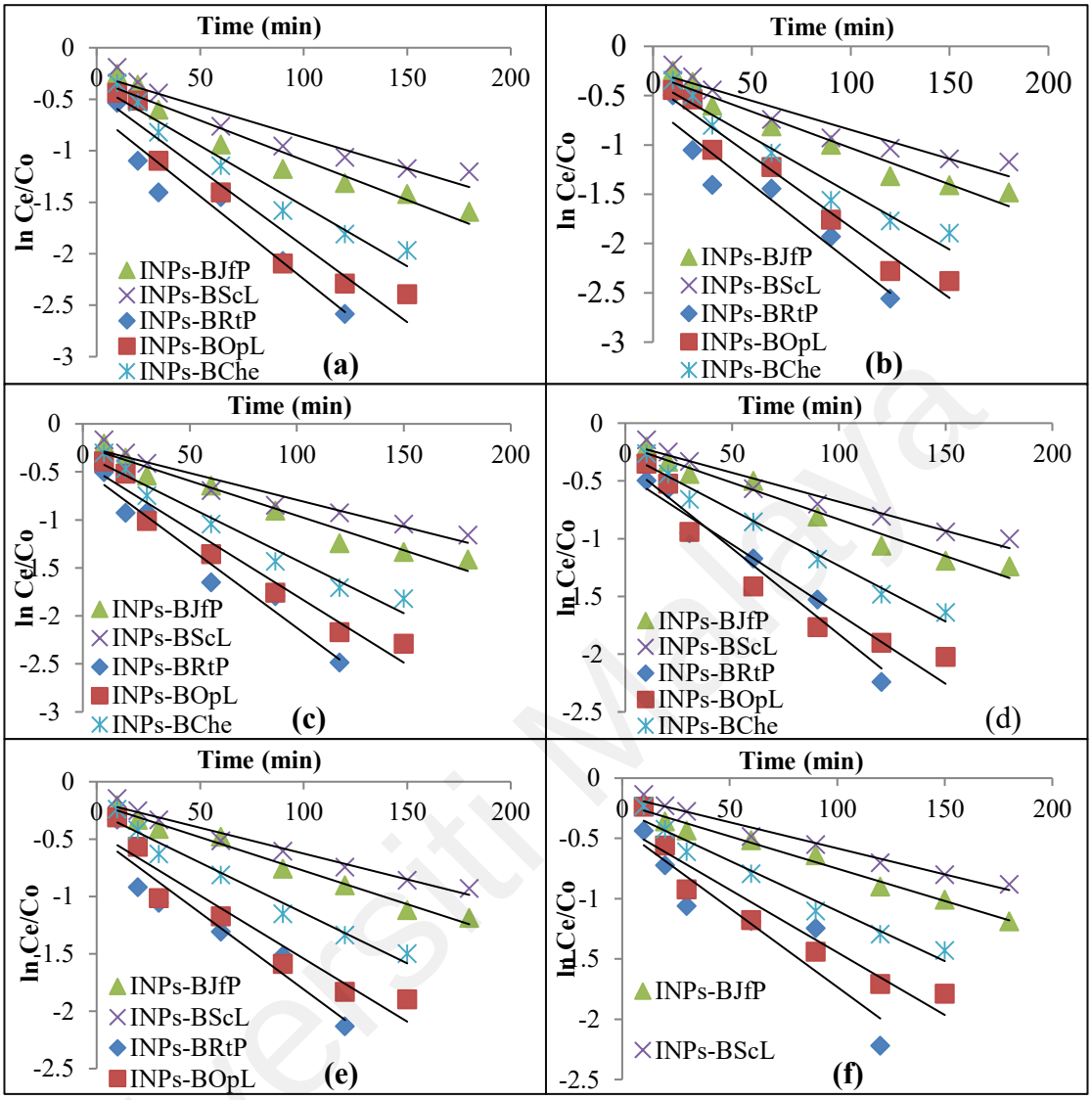

Figure 4.38: Pseudo-first-order model fittings to the experimental data using fresh INPs-B_g and INPs-B_{Che} nanocomposites for the removal of mixed OCPs (a) *p,p′*-DDT, (b) *o,p′*-DDT, (c) aldrin, (d) heptachlor, (e) hexachlorobenzene, and (f) endosulfan I.

The high R^2 values of OCPs with all nanocomposites indicated that it is in good agreement with the previous studies on carbon-supported INPs (Quan et al., 2014; Pouretedal & Saedi, 2014; Su et al., 2013). For all types of nanoadsorbents the observed reaction rate constant (k_{obs}) were found in the following order INPs-B_{RtP} (0.0113-0.0161 min^{-1}) > INPs-B_{OpL} (0.0104-0.0148 min^{-1}) > INPs-B_{JfP} (0.0054-0.0077 min^{-1}) and INPs-B_{ScL} (0.0043-0.0060 min^{-1}). The observed reaction rate constant values indicated that reduction of OCPs occurs at INPs interface (Wang et al., 2017). The observed reaction

rate constant (k_{obs}) values of all OCPs for INPs-B_{RtP} adsorbent was found slightly higher (up to 8 %) than that for INPs-B_{OpL}, while incredibly higher (up to 52 and 62 %) in case of INPs-B_{JfP} and INPs-B_{ScL}. It may be attributed to the higher wt% of INPs on the B_{RtP} (82.7%) and B_{OpL} (70.5%) biochar rather than that of B_{JfP} (63.9%) B_{ScL} (51.5%) biochar. The reactivity of chemically synthesized INPs-B_{Che} was found only 26% and 20% lower than that of the green synthesized INPs-B_{RtP} and INPs-B_{OpL}, respectively however it was found to be incredibly higher i.e. 35% and 49% than that of the INPs-B_{JfP} and INPs-B_{ScL}, respectively and calculated k_{obs} value was ranged between 0.0083-0.0117 min^{-1} for all OCPs. The reactivities of all types nanocomposites were found in the following order: INPs-B_{RtP} > INPs-B_{OpL} > INPs-B_{Che} > INPs-B_{JfP} and > INPs-B_{ScL}. The results are in good agreement with the observations reported by Chen et al, (2014) who studied the removal of HCB with two samples of activated carbon loaded with various cocentrations of INPs i.e. INPs/AC-A containing 72% higher INPs than that of INPs/AC-1. Therefore, the k_{obs} value of INPs/AC-A was found 25% higher than that of INPs/AC-1. In our study, the calculated k_{obs} values which is the same order of the magnitude but has a considerably larger values than the values reported by chen et al, (2014) which are 0.0010 and 0.0013 min^{-1} for INPs/AC-1 and INPs/AC-A. The larger values of k_{obs} indicated that nanocomposites prepared by green method in our study have high reactivity for OCPs.

In all cases, on the basis of specific log Kow values of each OCP molecule, the observed reaction rate constant (k_{obs}) values were always found in the following order *p,p'*-DDT > *o,p'*-DDT > aldrin > heptachlor > hexachlorobenzene and endosulfan I. For all types of adsorbents, the *p,p'*-DDT compound was found with highest observed reaction rate constant (k_{obs}) values (range between 0.006-0.0161 min^{-1}) as compared to the rest of the 5 OCP compounds in this study. The observed reaction rate constant (k_{obs}) values of *p,p'*-DDT was found slightly higher (up to 2 and 6%) than that of *o,p'*-DDT and

aldrin, respectively. Whereas, it was found to be considerably higher (up to 8, 25 and 30%) than that of heptachloe, hexachlorobenzene and endosulfan, respectively.

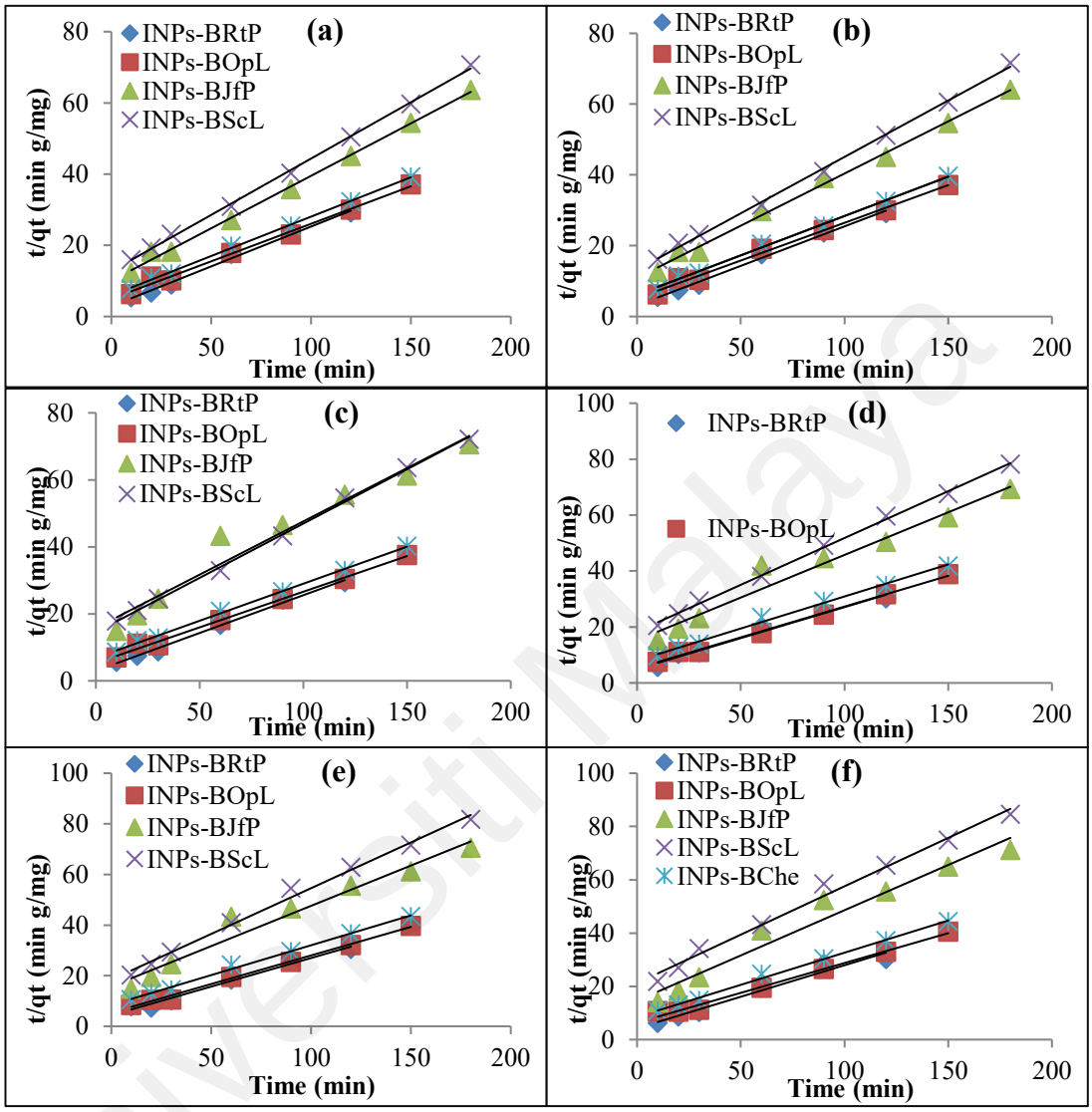

Figure 4.39: Pseudo-second-order model fittings to the experimental data using fresh INPs-B_g and INPs-B_{Che} nanocomposites for the removal of mixed OCPs (a) *p,p′*-DDT, (b) *o,p′*-DDT, (c) aldrin, (d) heptachlor, (e) hexachlorobenzene, and (f) endosulfan I.

A similar study was conducted by Elliot et al, (2016) in which they remove they prepared supported INPs by chemical method and applied same concentrations (2.2 mg/L) for the removal of aldrin, atrazine and heptachlore. The adsorbates aldrine and heptachlor with higher log Kow valuese (6.5 and 5.44, respectively) showed higher reactivity than than that of atrazine which have lower log Kow value (2.61). The k_{obs} values of aldrine and heptachlor were found to be 36 and 31% higher than that of the

atrazine which is in agreement with our observations that higher the log Kow higher is the k_{obs} value of adsorbate.

In case of removal of mixed OCPs, the pseudo-first-order reaction rate constant (k_{obs} min^{-1}) values were found to be incredibly lower (up to 86%) than those of the OCP compounds in the individual solution. It may be attributed to the absence of other competent compounds in the aqueous solution during the individual removal of OCPs.

4.3.2.3 Adsorption Kinetics of Mixed OCPs by Aged Nanocomposites

The linearized form of the pseudo-first order and pseudo-second order model equations have been plotted for all types of green and chemical synthesized nanocomposites used for the removal of OCPs in the mixture (Figures 4.40 a-f and 4.41 a-f, respectively). The kinetic parameters calculated from the two models have been listed in Table 4.9. The correlation coefficient (R^2) values of all types of nanocomposites were found between 0.98-0.99 for the pseudo-first order reduction kinetic model and above 0.99 for the pseudo-second order adsorption kinetic model, indicating that the removal of OCPs using nanocomposites fitted well to both the reduction and adsorption kinetic models. The adsorbed OCPs onto biochar and INPs were then reduced by Fe^0 which is confirmed by the previous studies (Kassaee et al., 2011 & Kim et al., 2012).

After aging of all types of green INPs-B_g nanocomposites (INPs-B_{RtP}, INPs-B_{OpL}, INPs-B_{JfP}, INPs-B_{ScL}), the observed reaction rate constant (k_{obs}) values decreased slightly up to 6.83%, 4.73%, 7.79% and 13.33%, respectively for all OCPs, whereas in case of aged chemical synthesized INPs-B_{Che}, a considerable decrease in reaction rate constant values were observed i.e. up to 70.09% for all OCPs in the mixture solution. It can be decided that green INPs supported on biochar were persisted quite unchanged in air due to the outer coating of polyphenols from plant extract.

Table 4.10: The kinetic parameters for removal of mixed OCPs by aged four green INPs-B_g and INPs-B_{Che} nanocomposites.

Adsorbents	Pseudo first-order model			Pseudo second-order model			
	Adsorbates	k_{obs} (min^{-1})	R^2	q_e (g/mg)	k_2	h (g/mg min^{-1})	R^2
INPs-B_{RtP}	*p,p'*-DDT	0.0150	0.9930	4.47	0.0152	0.3037	0.9965
	o,p'-DDT	0.0148	0.9735	4.45	0.0147	0.2918	0.9951
	Aldrin	0.0144	0.9902	4.42	0.0137	0.2683	0.9937
	Heptachlor	0.0136	0.9436	4.38	0.0115	0.2205	0.9893
	Hexachlorobenzene	0.0131	0.9537	4.32	0.0118	0.2099	0.9868
	Endosulfan	0.0129	0.9905	4.30	0.0109	0.2020	0.9869
INPs-B_{OpL}	*p,p'*-DDT	0.0141	0.9661	4.24	0.0106	0.1912	0.9971
	o,p'-DDT	0.0138	0.9729	4.22	0.0104	0.1849	0.9963
	Aldrin	0.0133	0.9723	4.21	0.0095	0.1683	0.9966
	Heptachlor	0.0115	0.9635	4.14	0.0087	0.1488	0.9945
	Hexachlorobenzene	0.0107	0.9724	4.03	0.0084	0.1372	0.9952
	Endosulfan	0.0104	0.9580	4.02	0.0070	0.1135	0.9777
INPs-B_{JfP}	*p,p'*-DDT	0.0071	0.9570	3.12	0.0086	0.0842	0.9972
	o,p'-DDT	0.0068	0.9654	3.15	0.0080	0.0792	0.9960
	Aldrin	0.0064	0.9643	2.93	0.0078	0.0666	0.9926
	Heptachlor	0.0059	0.9893	2.86	0.0070	0.0570	0.9795
	Hexachlorobenzene	0.0054	0.9917	2.75	0.0074	0.0535	0.9617
	Endosulfan	0.0052	0.9676	2.58	0.0080	0.0559	0.9411
INPs-B_{ScL}	*p,p'*-DDT	0.0054	0.9241	2.86	0.0080	0.0656	0.9973
	o,p'-DDT	0.0052	0.9276	2.83	0.0075	0.0597	0.9962
	Aldrin	0.0048	0.9224	2.77	0.0070	0.0534	0.9980
	Heptachlor	0.0043	0.9374	2.65	0.0058	0.0410	0.9970
	Hexachlorobenzene	0.0040	0.9690	2.38	0.0066	0.0375	0.9835
	Endosulfan	0.0039	0.9834	2.36	0.0062	0.0344	0.9873
INPs-B_{Che}	*p,p'*-DDT	0.0035	0.9920	2.29	0.0177	0.0928	0.9986
	o,p'-DDT	0.0033	0.9729	2.24	0.0183	0.0917	0.9985
	Aldrin	0.0029	0.9590	2.14	0.0188	0.0862	0.9973
	Heptachlor	0.0021	0.8627	2.01	0.0199	0.0802	0.9988
	Hexachlorobenzene	0.0017	0.8106	1.99	0.0180	0.0713	0.9980
	Endosulfan	0.0016	0.9549	1.92	0.0165	0.0610	0.9982

Whereas, INPs synthesized by chemical method get oxidized in air during aging process and it is in agreement with Wang et al, (2014) who observed the same phenomenon for chemical and green synthesized INPs using green tea and eucalyptus leaf ectract used for the removal of nitrate. After being aged in air for two months, k_{obs} of chemically synthesized INPs dropped about 74% in contrast to the fresh INPs. Whereas, the k_{obs}

values of INPs synthesized using green tea and eucalyptus leaf ectracts remained almost same. Thus, it can be confirmed that in this study green nanocomposites are highly stable as compared to the chemically synthesized nanocomposites.

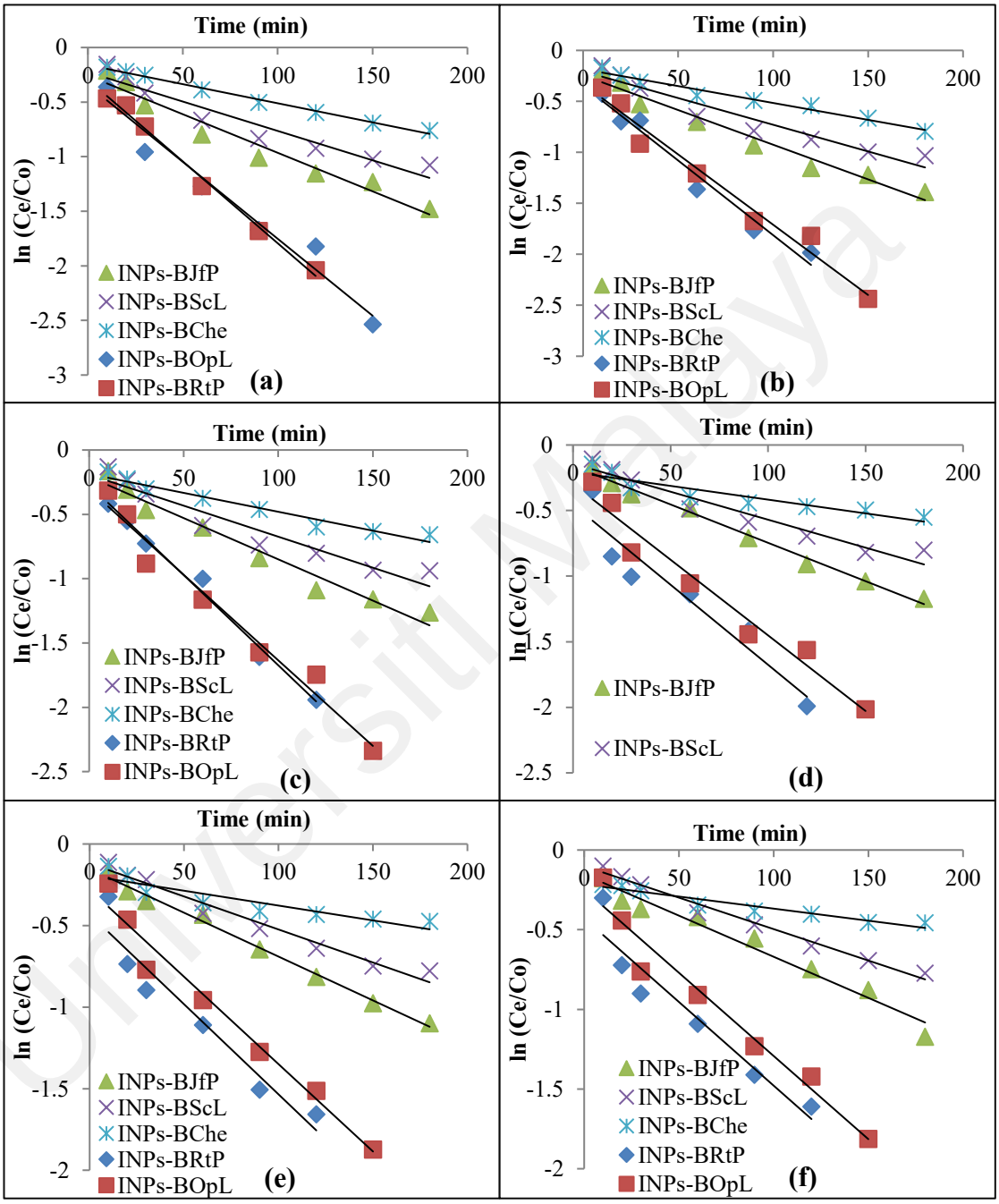

Figure 4.40: Pseudo-first-order model fittings to the experimental data for the removal of mixed OCPs (a) *p,p′*-DDT, (b) *o,p′*-DDT, (c) aldrin, (d) heptachlor, (e) hexachlorobenzene, and (f) endosulfan I by aged INPs-B_g and INPs-B_{Che} nanocomposites.

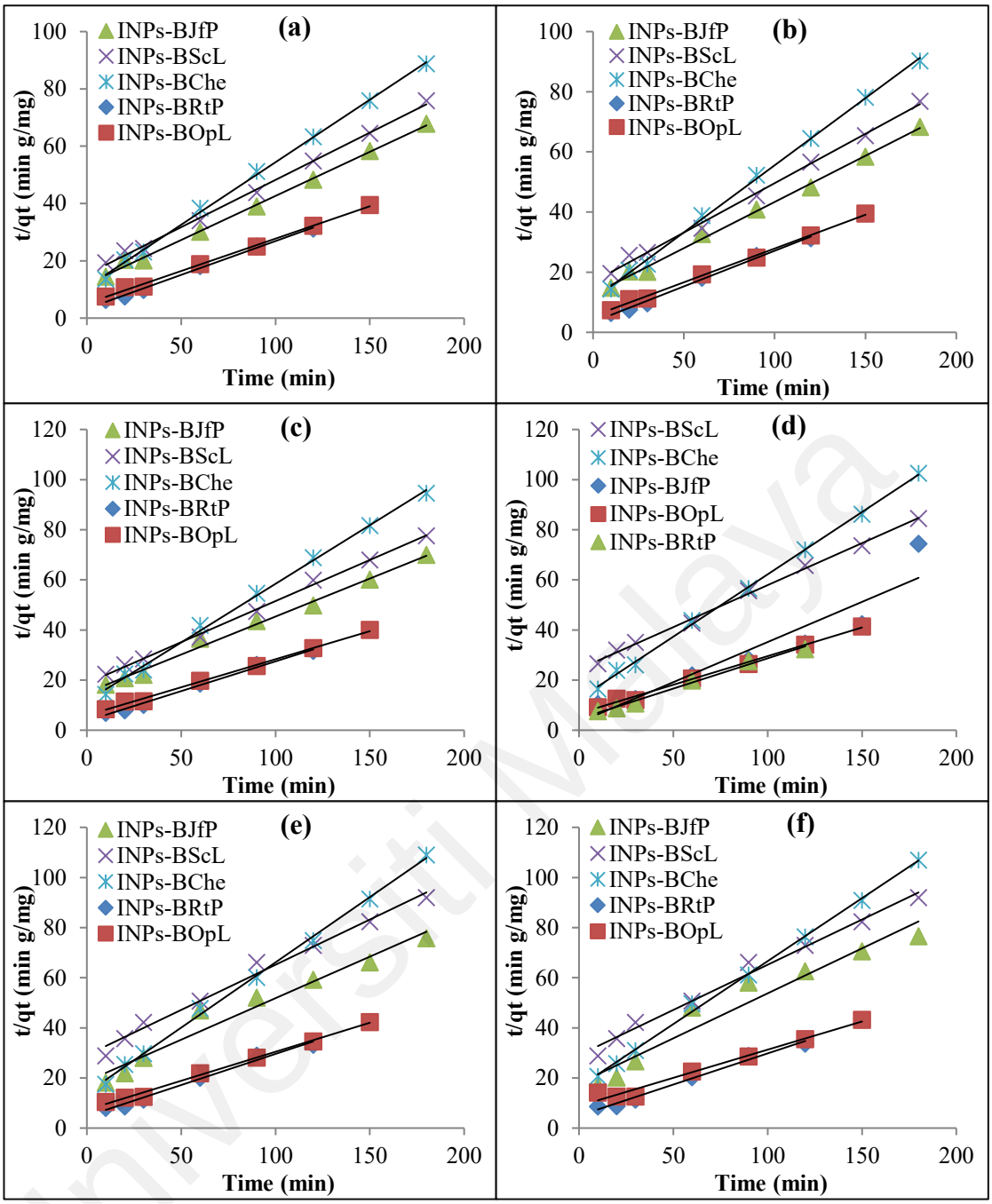

Figure 4.41: Pseudo-second-order model fittings to the experimental data for the removal of mixed OCPs (a) *p,p′*-DDT, (b) *o,p′*-DDT, (c) aldrin, (d) heptachlor, (e) hexachlorobenzene, and (f) endosulfan I by aged INPs-B_g and INPs-B_{Che} nanocomposites..

4.3.2.4 Adsorption Kinetics of OCPs in the OPPD Water Samples by Fresh Nanocomposites

The plots of linearized form of the pseudo-first order and pseudo-second order model equations for fresh green INPs-B_{RtP} and chemical synthesized INPs-B_{Che} nanocomposites used for the removal of all OCPs removed from three OPPD water samples samples PE1, PMD2 and PMD3, have been represented in Figures 4.42 to 4.47.

Table 4.11: Kinetic parameters for the removal of OCPs from OPPD water samples using fresh INPs-B_g and INPs-B_{Che} nanocomposites.

Water Samples	Adsorbents	Adsorbates	Pseudo first-order model		Pseudo second-order model			
			k_{obs} (min^{-1})	R^2	q_e (g/mg)	k_2	h (g/mg min^{-1})	R^2
PE1	INPs-B_{RtP}	*p,p'*-DDT	0.0107	0.9749	0.1917	0.3074	0.0113	0.9986
		o,p'-DDT	0.0105	0.9679	0.1908	0.2685	0.0098	0.9935
		Aldrin	0.0102	0.9777	0.1896	0.2677	0.0096	0.9943
		Heptachlor	0.0091	0.9777	0.1851	0.2255	0.0077	0.9922
		Hexachlorobenzene	0.0089	0.9794	0.1838	0.2096	0.0071	0.9912
		Endosulfan I	0.0086	0.9603	0.1816	0.2253	0.0074	0.9892
	INPs-B_{Che}	*p,p'*-DDT	0.0084	0.9797	0.1809	0.2476	0.0081	0.9977
		o,p'-DDT	0.0084	0.9810	0.1806	0.2087	0.0068	0.9838
		Aldrin	0.0081	0.9871	0.1780	0.2153	0.0068	0.9937
		Heptachlor	0.0072	0.9855	0.1751	0.1659	0.0051	0.9857
		Hexachlorobenzene	0.0069	0.9817	0.1747	0.1489	0.0045	0.9800
		Endosulfan I	0.0065	0.9769	0.1687	0.1757	0.0050	0.9763
PMD2	INPs-B_{RtP}	*p,p'*-DDT	0.0107	0.9623	0.1913	0.3213	0.0118	0.9988
		o,p'-DDT	0.0105	0.9722	0.1908	0.2878	0.0105	0.9957
		Aldrin	0.0101	0.9740	0.1891	0.2669	0.0095	0.9926
		Heptachlor	0.0092	0.9788	0.1853	0.2253	0.0077	0.9927
		Hexachlorobenzene	0.0090	0.9837	0.1839	0.2189	0.0074	0.9895
		Endosulfan I	0.0087	0.9841	0.1820	0.2480	0.0082	0.992
	INPs-B_{Che}	*p,p'*-DDT	0.0087	0.9728	0.1822	0.2624	0.0087	0.9983
		o,p'-DDT	0.0086	0.9839	0.1821	0.2258	0.0075	0.9909
		Aldrin	0.0082	0.9784	0.1797	0.2073	0.0067	0.9857
		Heptachlor	0.0072	0.9892	0.1758	0.1654	0.0051	0.9790
		Hexachlorobenzene	0.0087	0.9783	0.1742	0.1659	0.0050	0.9787
		Endosulfan I	0.0067	0.9670	0.1672	0.1983	0.0055	0.9847
PMD3	INPs-B_{RtP}	*p,p'*-DDT	0.0100	0.9608	0.1892	0.2834	0.0101	0.9963
		o,p'-DDT	0.0099	0.9619	0.1885	0.2448	0.0087	0.9915
		Aldrin	0.0096	0.9699	0.1878	0.2420	0.0085	0.9940
		Heptachlor	0.0087	0.9683	0.1832	0.2106	0.0071	0.9898
		Hexachlorobenzene	0.0084	0.9686	0.1819	0.1985	0.0066	0.9888
		Endosulfan I	0.0083	0.9653	0.1819	0.1856	0.0061	0.9873
	INPs-B_{Che}	*p,p'*-DDT	0.0081	0.9810	0.1806	0.2087	0.0068	0.9961
		o,p'-DDT	0.0080	0.9810	0.1799	0.1906	0.0062	0.9892
		Aldrin	0.0076	0.9871	0.1778	0.1891	0.0060	0.9931
		Heptachlor	0.0065	0.9855	0.1746	0.1503	0.0046	0.9867
		Hexachlorobenzene	0.0063	0.9817	0.1696	0.1512	0.0043	0.9865
		Endosulfan I	0.0061	0.9669	0.1651	0.1525	0.0042	0.9736

The kinetic parameters calculated from the two models using the 10 g/L of nanocomposites at pH 4 and room temperature that have been listed in Table 4.10. The correlation coefficient (R^2) values of both aged INPs-B_{RtP}, and INPs-B_{Che} in three OPPD water samples samples i.e. PE1, PMD2 and PMD3 were between 0.9603-0.9794, 0.9623-0.9841, 0.9608-0.9699, respectively and 0.9769-0.9871, 0.9670-0.9892 and 0.9669-0.9855, respectively for the pseudo-first order reduction kinetic model and above 0.98 for the pseudo-second order adsorption kinetic model, indicating that the removal of OCPs using fresh nanocomposites fitted well to both the reduction and adsorption kinetic models. The adsorbed OCPs onto biochar and INPs were then reduced by Fe^0 which is confirmed by the previous studies (Kassaee et al., 2011 & Kim et al., 2012).

Table 4.10 represents the calculated pseudo-first-order reaction rate constant (k_{obs} min^{-1}) of all OCPs removed from three OPPD water samples samples PE1, PMD2 and PMD3 using both fresh green INPs-B_g and INPs-B_{Che} nanocomposites at pH 4 and room temperature. The pseudo-first-order reaction rate constant (k_{obs} min^{-1}) values for all OCPs were found in the following order 0.0107, 0.0107, 0.0100 (*p,p'*-DDT) > 0.0105, 0.0105, 0.0099 (*o,p'*-DDT) > 0.0102, 0.0101, 0.0096 (aldrin) > 0.0091, 0.0092. 0.0087 (heptachlor) > 0.0089, 0.0090, 0.0084 (hexachlorobenzene) and 0.0086, 0.0087, 0.0083 (endosulfan I) in samples PE1, PMD2 and PMD3, respectively. In all OPPD water samples samples, out of 6 OCP compounds, *p,p'*-DDT showed the highest k_{obs} value than that of other OCP compounds and it was found to be slightly higher (1-1.87%, and 4-5.61%) higher than those of *o,p'*-DDT and aldrin, respectively and relatively higher (13.05-14.95%, 15.89-16.82% and 17-19.63%) than those of heptachlor, hexachlorobenzene and endosulfan I, respectively. In comparison with removal of OCPs in individual removal and in mixture solution, the pseudo-first-order reaction rate constant (k_{obs} min^{-1}) values in OPPD water samples were found to be considerably lower up to 89.64 -90.44%, and 23.89-33.54%, than those of the OCP compounds in the

individual solutions and mixture solution of OCPs, respectively. It may be attributed to the presence of other competent compounds in the OPPD water samples during the removal of OCPs in OPPD water samples. In comparison with reactivity of fresh green INPs-B_{RtP}, the calculated k_{obs} values of fresh chemical synthesized INPs-B_{Che} nanocomposite were found to be 19-23% lower than that of fresh green INPs-B_{RtP} nanocomposite.

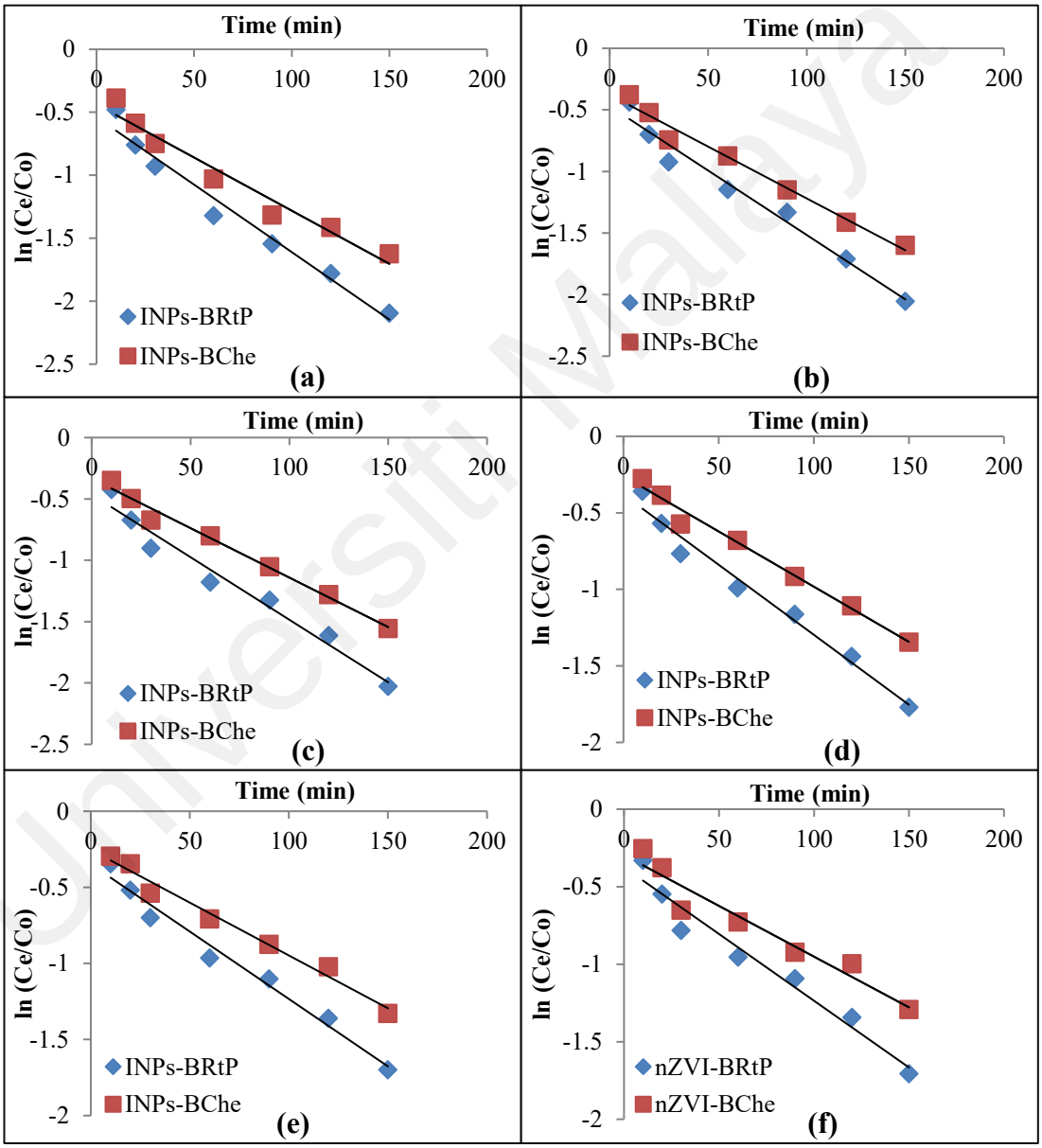

Figure 4.42: Pseudo-first-order model fittings to the experimental data using fresh INPs-B_g and INPs-B_{Che} nanocomposites for the removal of OCPs (a) *p,p′*-DDT, (b) *o,p′*-DDT, (c) aldrin, (d) heptachlor, (e) hexachlorobenzene, and (f) endosulfan I from OPPD water samples PE1.

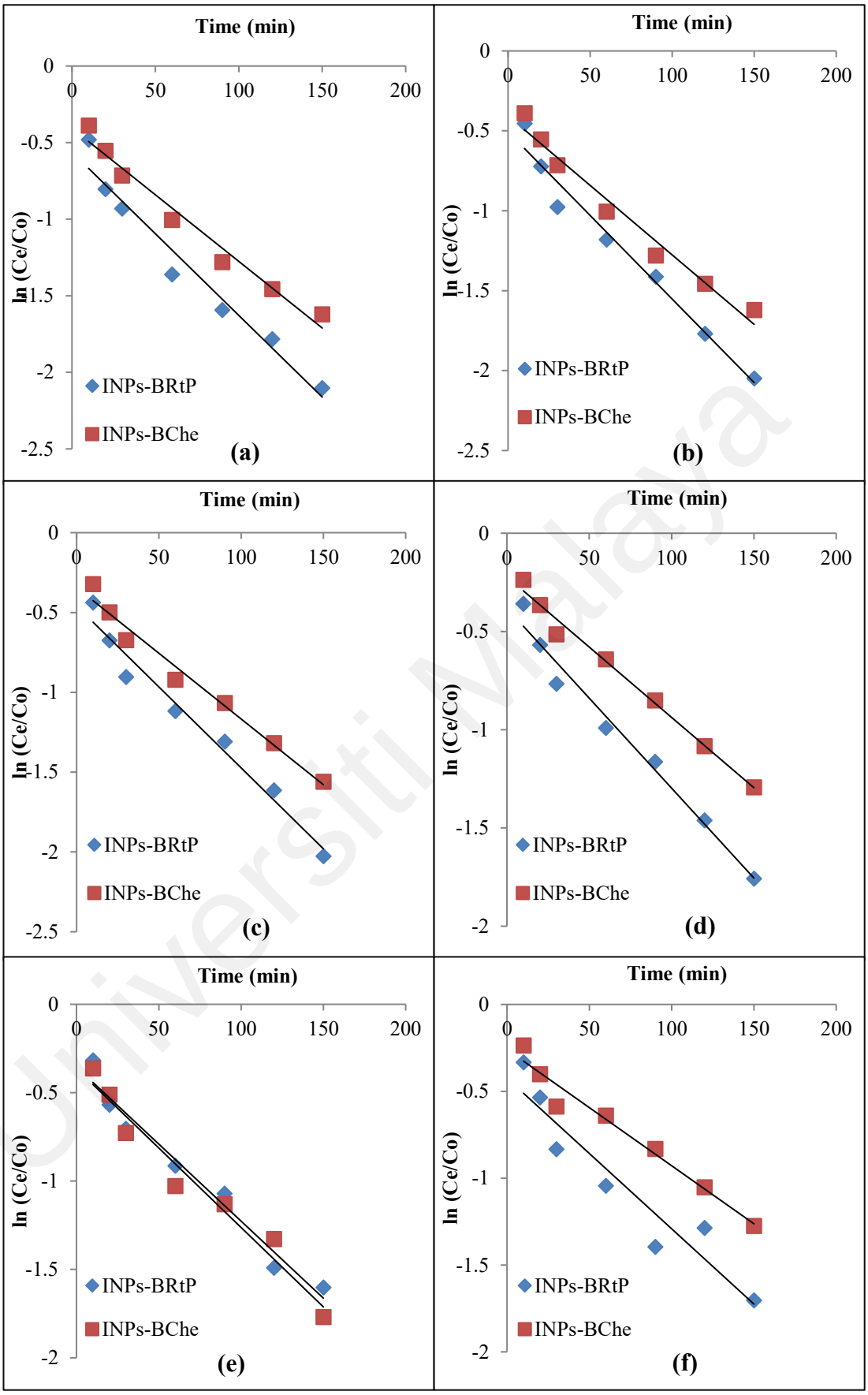

Figure 4.43: Pseudo-first-order model fittings to the experimental data using fresh INPs-B_g and INPs-B_{Che} nanocomposites for the removal of OCPs (a) *p,p′*-DDT, (b) *o,p′*-DDT, (c) aldrin, (d) heptachlor, (e) hexachlorobenzene, and (f) endosulfan I from OPPD water samples PMD2.

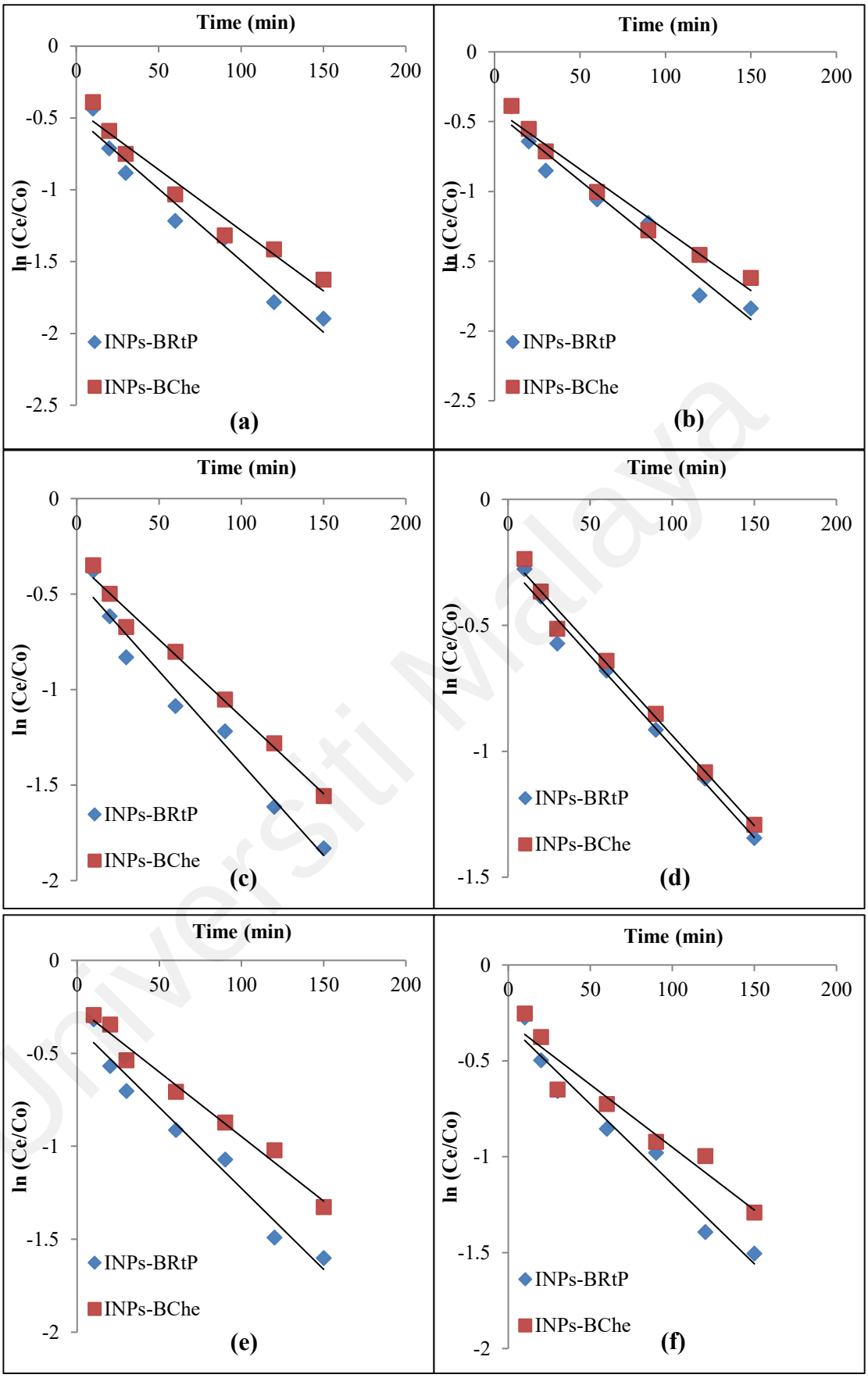

Figure 4.44: Pseudo-first-order model fittings to the experimental data using fresh INPs-B_g and INPs-B_{Che} nanocomposites for the removal of OCPs (a) *p,p′*-DDT, (b) *o,p′*-DDT, (c) aldrin, (d) heptachlor, (e) hexachlorobenzene, and (f) endosulfan I from OPPD water samples PMD3.

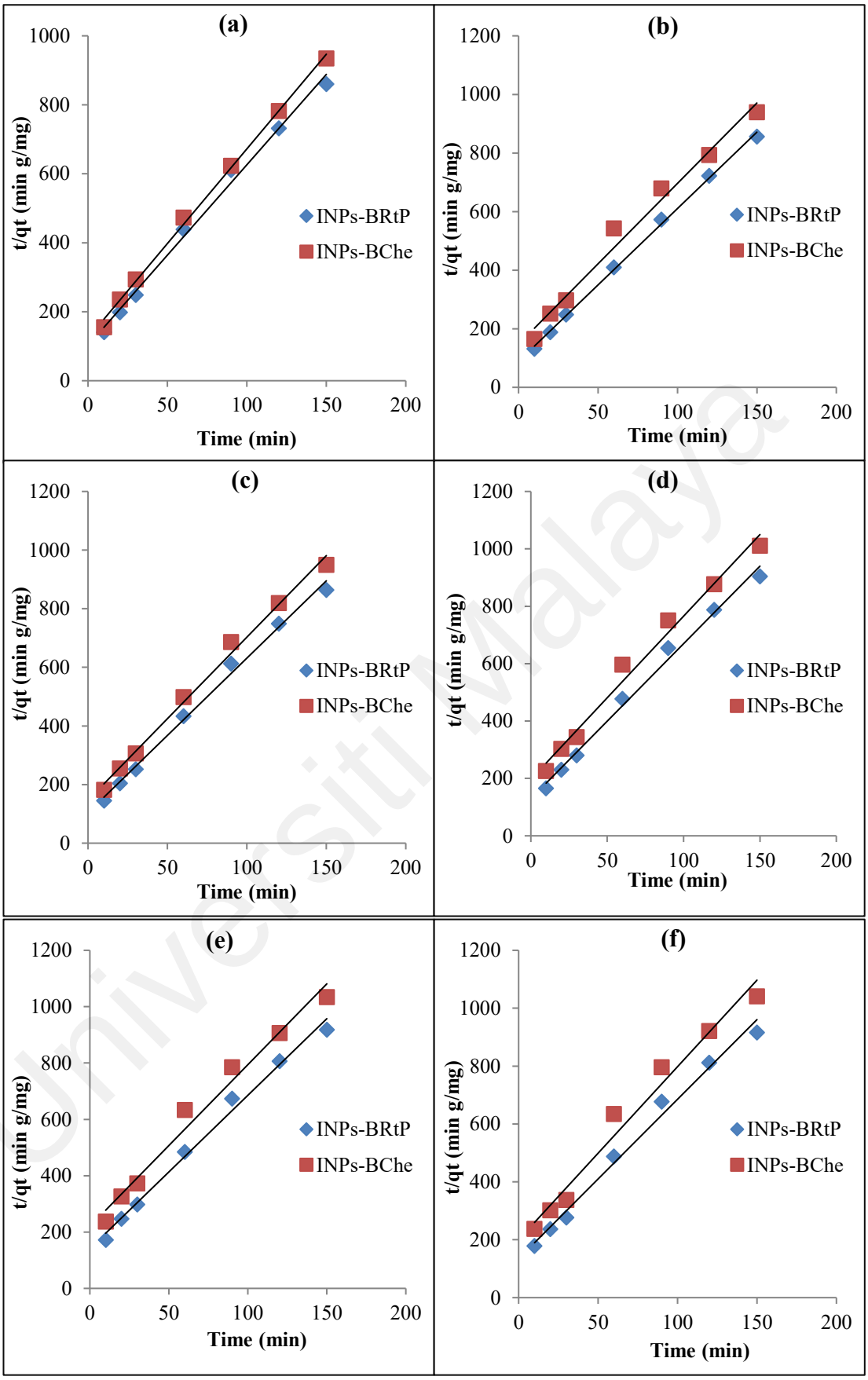

Figure 4.45: Pseudo-second-order model fittings to the experimental data using fresh INPs-B_g and INPs-B_{Che} nanocomposites for the removal of OCPs (a) *p,p′*-DDT, (b) *o,p′*-DDT, (c) aldrin, (d) heptachlor, (e) hexachlorobenzene, and (f) endosulfan I from OPPD water samples PE1.

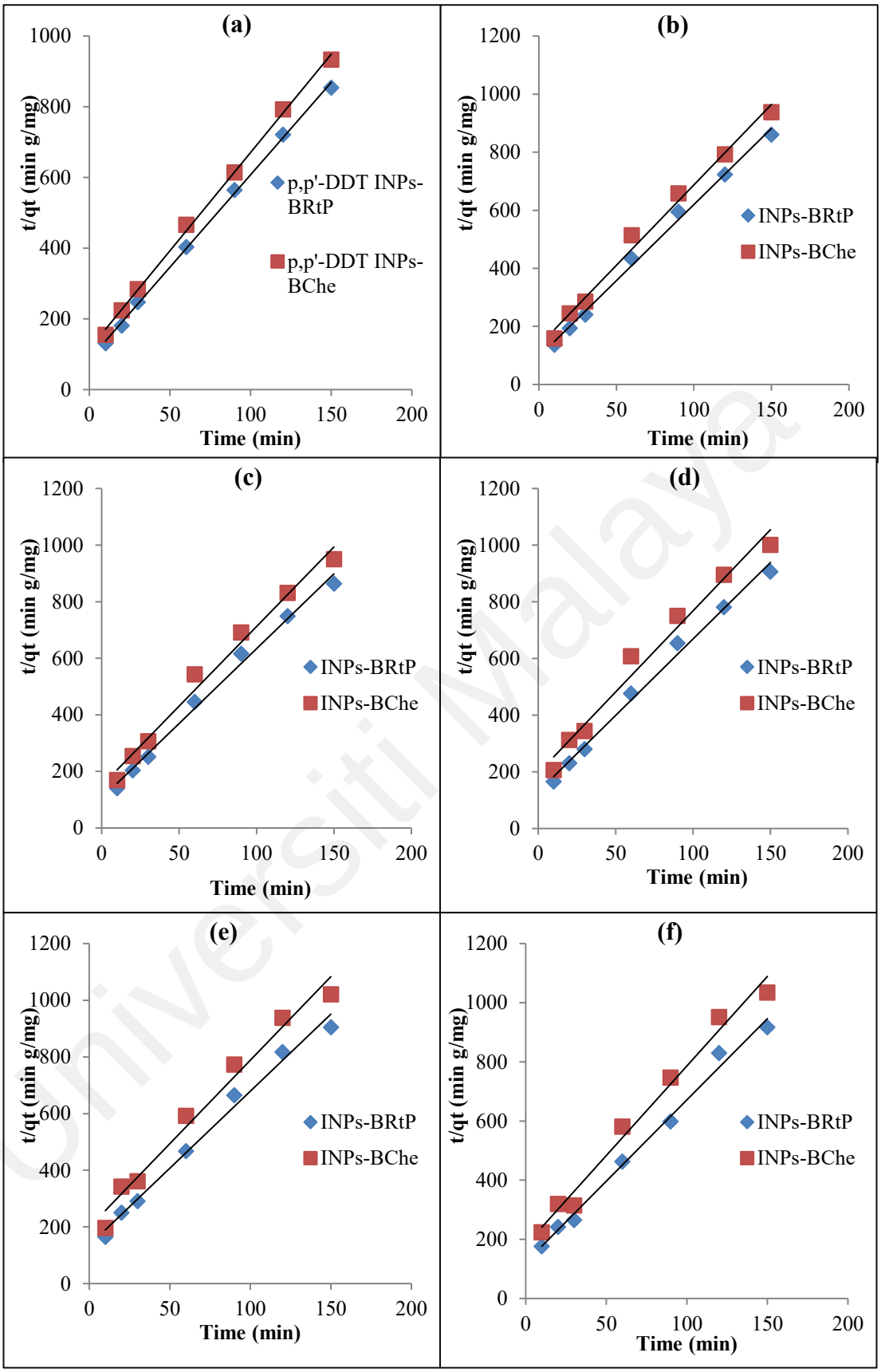

Figure 4.46: Pseudo-second-order model fittings to the experimental data using fresh INPs-B_g and INPs-B_{Che} nanocomposites for the removal of OCPs (a) *p,p′*-DDT, (b) *o,p′*-DDT, (c) aldrin, (d) heptachlor, (e) hexachlorobenzene, and (f) endosulfan I from OPPD water samples PMD2.

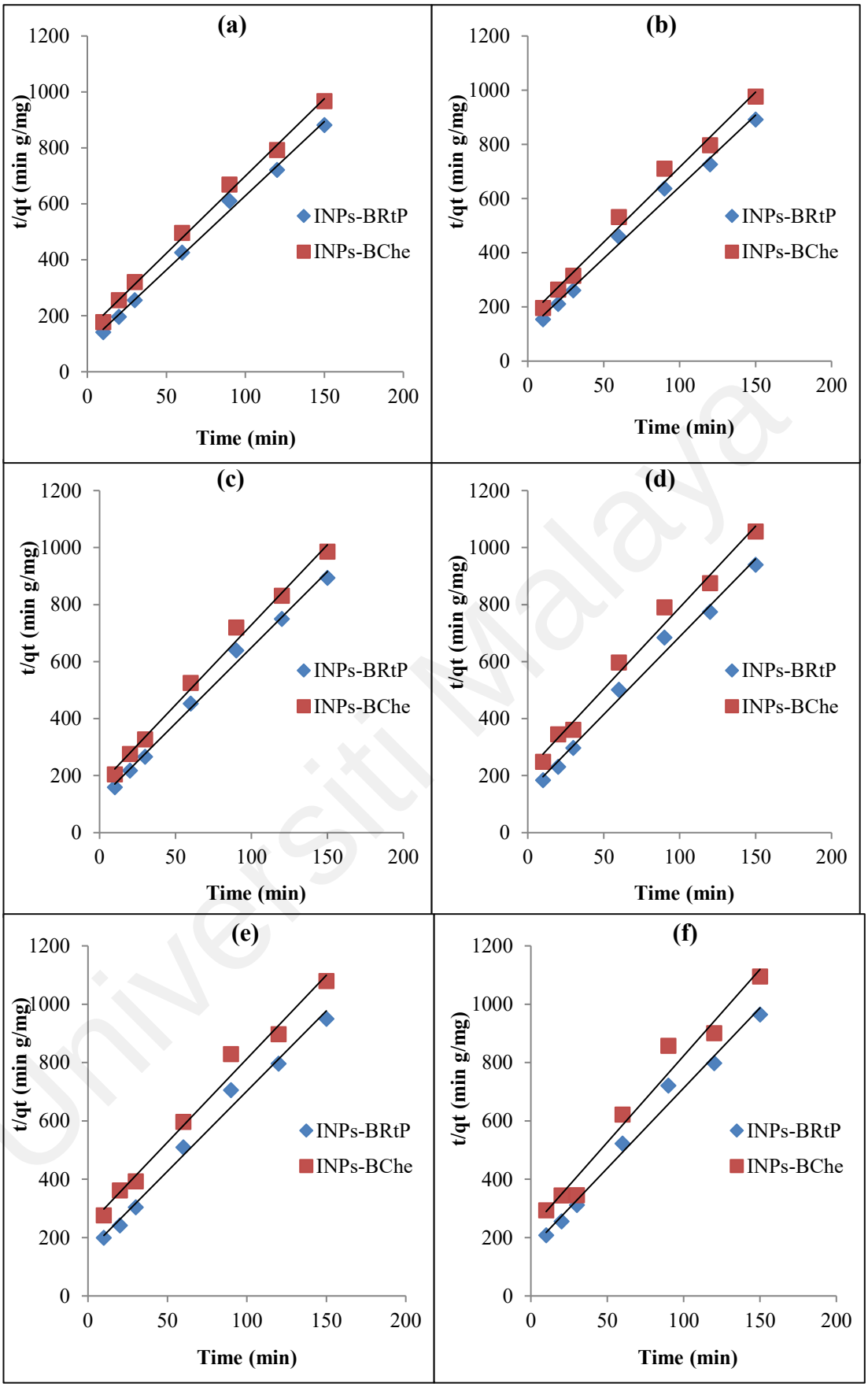

Figure 4.47: Pseudo-second-order model fittings to the experimental data using fresh INPs-B_g and INPs-B_{Che} nanocomposites for the removal of OCPs (a) *p,p′*-DDT, (b) *o,p′*-DDT, (c) aldrin, (d) heptachlor, (e) hexachlorobenzene, and (f) endosulfan I from OPPD water samples PMD3.

4.3.2.5 Adsorption Kinetics of OCPs in the OPPD Water Samples by Aged Nanocomposites

The plots of linearized form of the pseudo-first order and pseudo-second order model equations for aged green INPs-B_{RtP} and chemically synthesized INPs-B_{Che} nanocomposites have been represented in Figures 4.48 a-f to 4.50 a-f and 4.51 a-f to 4.53 a-f, respectively used for the removal of all OCPs removed from three OPPD water samples PE1, PMD2 and PMD3.

The kinetic parameters calculated from the two models using the 10 g/L of nanocomposites at pH 4 and room temperature that have been listed in Table 4.11 represents that the correlation coefficient (R^2) values of both aged INPs-B_{RtP}, and INPs-B_{Che} in three OPPD water samples i.e. PE1, PMD2 and PMD3 were between 0.9626-0.9844, 0.9624-0.9765, 0.9625-0.9888, respectively and 0.9604-0.9785, 0.9614-0.873 and 0.9604-0.9888, respectively for the pseudo-first order reduction kinetic model and above 0.98 for the pseudo-second order adsorption kinetic model, indicating that the removal of OCPs using aged nanocomposites also fitted well to both the reduction and adsorption kinetic models same as in case of fresh nanocomposites. The adsorbed OCPs onto biochar and INPs were then reduced by Fe^0 which is confirmed by the previous studies (Kassaee et al., 2011 & Kim et al., 2012).

After being aged in air for one month, observed reaction rate constant (k_{obs}) values of INPs-B_{Che} declined to 0.0024-0.0033 min^{-1}, 0.0025-0.0035 min^{-1} and 0.0020-0.0030 min^{-1} in drainage samples PE1, PMD2 and PMD3, respectively, dropping about 60.71-63.08%, 59.77-62.69% and 64.29-69.23%, respectively in contrast to the fresh INPs-B_{Che}, which is due to fast corrosion of INPs. Meanwhile, the aged INPs-B_{RtP} showed slight decline in terms of k_{obs}, which were 0.0077-0.0091 min^{-1}, 0.0078-0.0091 min^{-1} and 0.0075-0.0086 min^{-1} compared to the fresh INPs-B_{RtP} (dropping only 10.47-14.95%, 10.34-14.95% and 9.64-13.82%, respectively).

Table 4.12: The kinetic parameters for OCPs removal by aged INPs-B_g and INPs-B_{Che} nanocomposites from OPPD water samples.

Water Samples	Adsorbents	Adsorbates	Pseudo first-order model		Pseudo second-order model			
			k_{obs} (min^{-1})	R^2	q_e (g/mg)	k_2	h (g/mg min^{-1})	R^2
PE1	INPs-B_{RtP}	*p,p'*-DDT	0.0091	0.9626	0.1841	0.3033	0.0103	0.9981
		o,p'-DDT	0.0091	0.9702	0.1836	0.2660	0.0090	0.9963
		Aldrin	0.009	0.9737	0.1834	0.2443	0.0082	0.9935
		Heptachlor	0.0081	0.9791	0.1785	0.2101	0.0067	0.9904
		Hexachlorobenzene	0.0079	0.9844	0.1777	0.1912	0.0060	0.9885
		Endosulfan I	0.0078	0.9807	0.1771	0.184	0.0057	0.9847
	INPs-B_{Che}	*p,p'*-DDT	0.0033	0.9604	0.1177	0.3238	0.0045	0.9890
		o,p'-DDT	0.0032	0.9604	0.1124	0.3155	0.0040	0.9920
		Aldrin	0.0031	0.9656	0.1113	0.2432	0.0030	0.9890
		Heptachlor	0.0028	0.9785	0.1058	0.1966	0.0022	0.9731
		Hexachlorobenzene	0.0025	0.9675	0.0996	0.1794	0.0018	0.9648
		Endosulfan I	0.0024	0.9773	0.0952	0.1854	0.0017	0.9823
PMD2	INPs-B_{RtP}	*p,p'*-DDT	0.009	0.9685	0.1845	0.3050	0.0104	0.9971
		o,p'-DDT	0.0091	0.9624	0.1831	0.2691	0.0090	0.9955
		Aldrin	0.0089	0.9690	0.1830	0.2450	0.0082	0.9923
		Heptachlor	0.0081	0.9706	0.1800	0.2024	0.0066	0.9923
		Hexachlorobenzene	0.0082	0.9764	0.1791	0.1867	0.0060	0.9872
		Endosulfan I	0.0077	0.9655	0.1764	0.1911	0.0059	0.9865
	INPs-B_{Che}	*p,p'*-DDT	0.0035	0.9653	0.1185	0.3380	0.0047	0.9834
		o,p'-DDT	0.0034	0.9614	0.1156	0.3445	0.0046	0.9922
		Aldrin	0.0031	0.9823	0.1143	0.2783	0.0036	0.9943
		Heptachlor	0.0028	0.9703	0.1011	0.2799	0.0029	0.9954
		Hexachlorobenzene	0.0026	0.9873	0.0984	0.2408	0.0023	0.9900
		Endosulfan I	0.0025	0.9685	0.0973	0.2113	0.0020	0.9797
PMD3	INPs-B_{RtP}	*p,p'*-DDT	0.0086	0.9625	0.1825	0.2680	0.0089	0.9984
		o,p'-DDT	0.0086	0.9823	0.1815	0.2390	0.0079	0.9973
		Aldrin	0.0083	0.9658	0.1802	0.2271	0.0074	0.9968
		Heptachlor	0.0078	0.9625	0.1797	0.1781	0.0058	0.9932
		Hexachlorobenzene	0.0076	0.9795	0.1793	0.1594	0.0051	0.9937
		Endosulfan I	0.0075	0.9888	0.1792	0.1498	0.0048	0.9918
	INPs-B_{Che}	*p,p'*-DDT	0.0030	0.9694	0.1076	0.3251	0.0038	0.9794
		o,p'-DDT	0.0029	0.9607	0.1045	0.3284	0.0036	0.9833
		Aldrin	0.0027	0.9724	0.0986	0.2838	0.0028	0.9822
		Heptachlor	0.0023	0.9657	0.0983	0.2076	0.0020	0.9808
		Hexachlorobenzene	0.0021	0.9791	0.0883	0.1994	0.0016	0.9673
		Endosulfan I	0.0020	0.9604	0.0842	0.1676	0.0012	0.9200

It can be decided that green INPs supported on biochar were persisted quite unchanged in air due to the outer coating of polyphenols from plant extract. Whereas, INPs synthesized by chemical method get oxidized in air during aging process and it is in agreement with Wang et al, (2014) and O' Caroll et al, (2013) who observed the same phenomenon for chemical and green synthesized INPs.

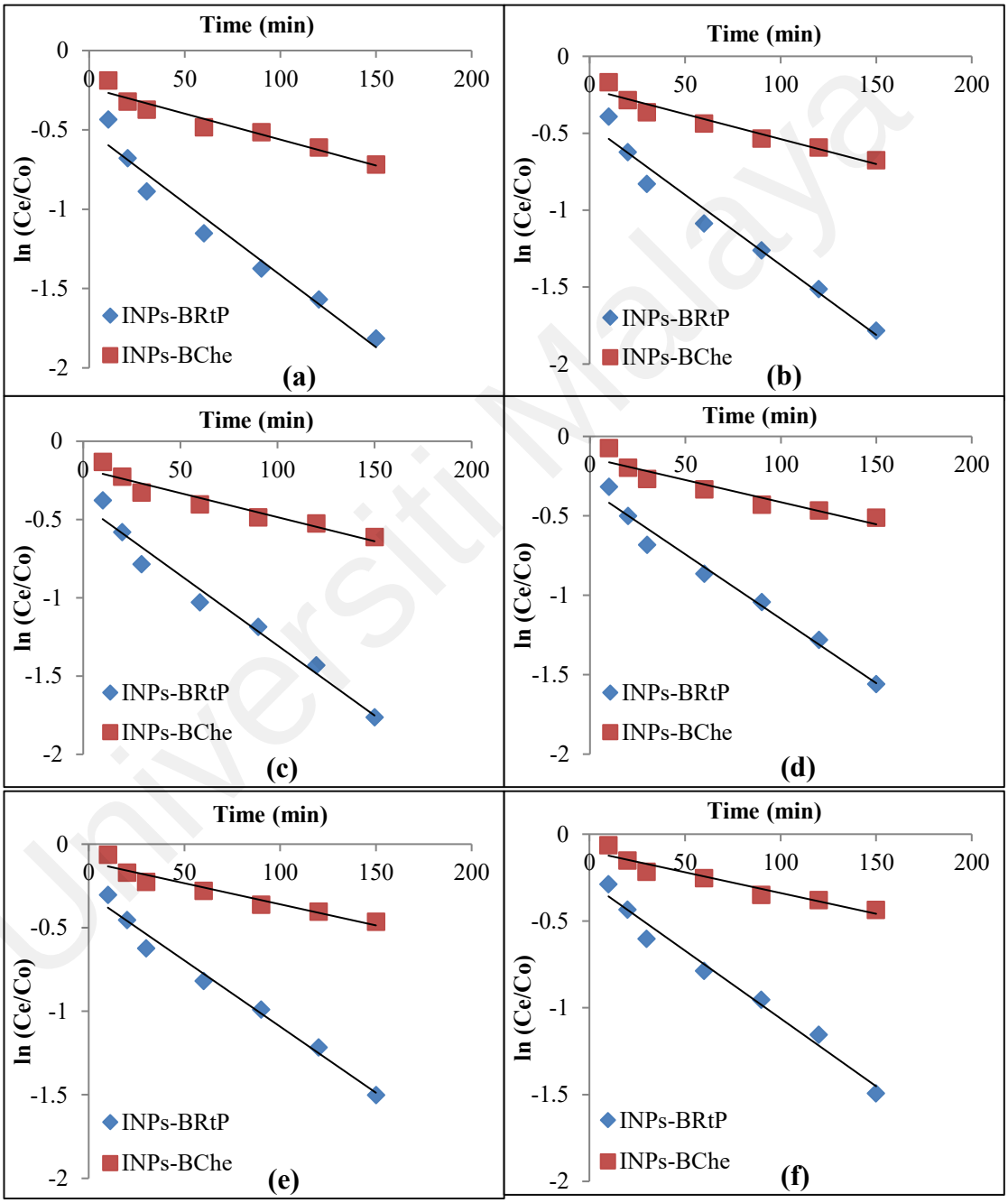

Figure 4.48: Pseudo-first-order model fittings to the experimental data for the removal of OCPs (a) *p,p'*-DDT, (b) *o,p'*-DDT, (c) aldrin, (d) heptachlor, (e) hexachlorobenzene, and (f) endosulfan I in OPPD water samples PE1 by aged INPs-B_g and INPs-B_{Che} nanocomposites.

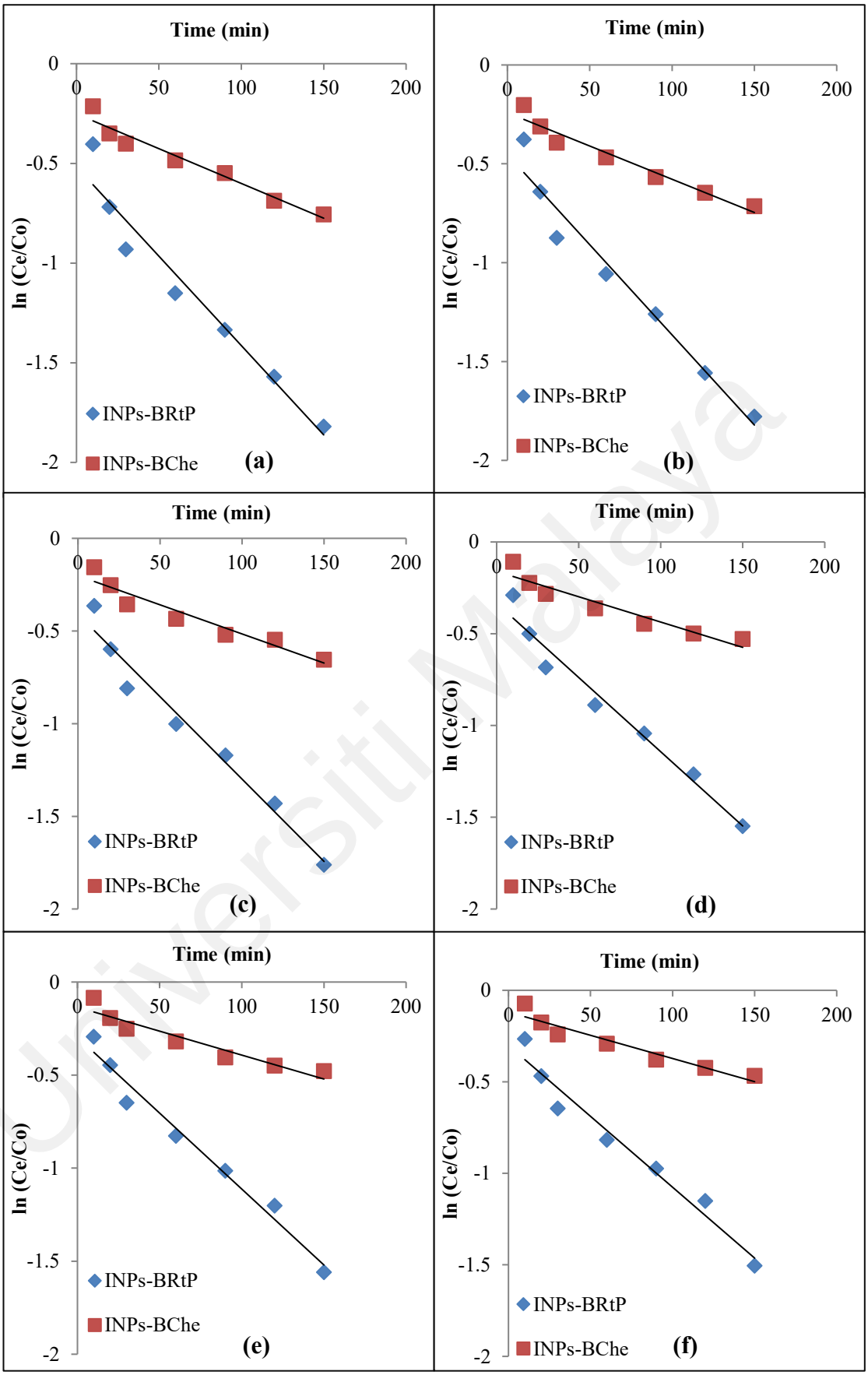

Figure 4.49: Pseudo-first-order model fittings to the experimental data for the removal of OCPs (a) *p,p′*-DDT, (b) *o,p′*-DDT, (c) aldrin, (d) heptachlor, (e) hexachlorobenzene, and (f) endosulfan I in OPPD water samples PMD2 by aged INPs-B_g and INPs-B_{Che} nanocomposites.

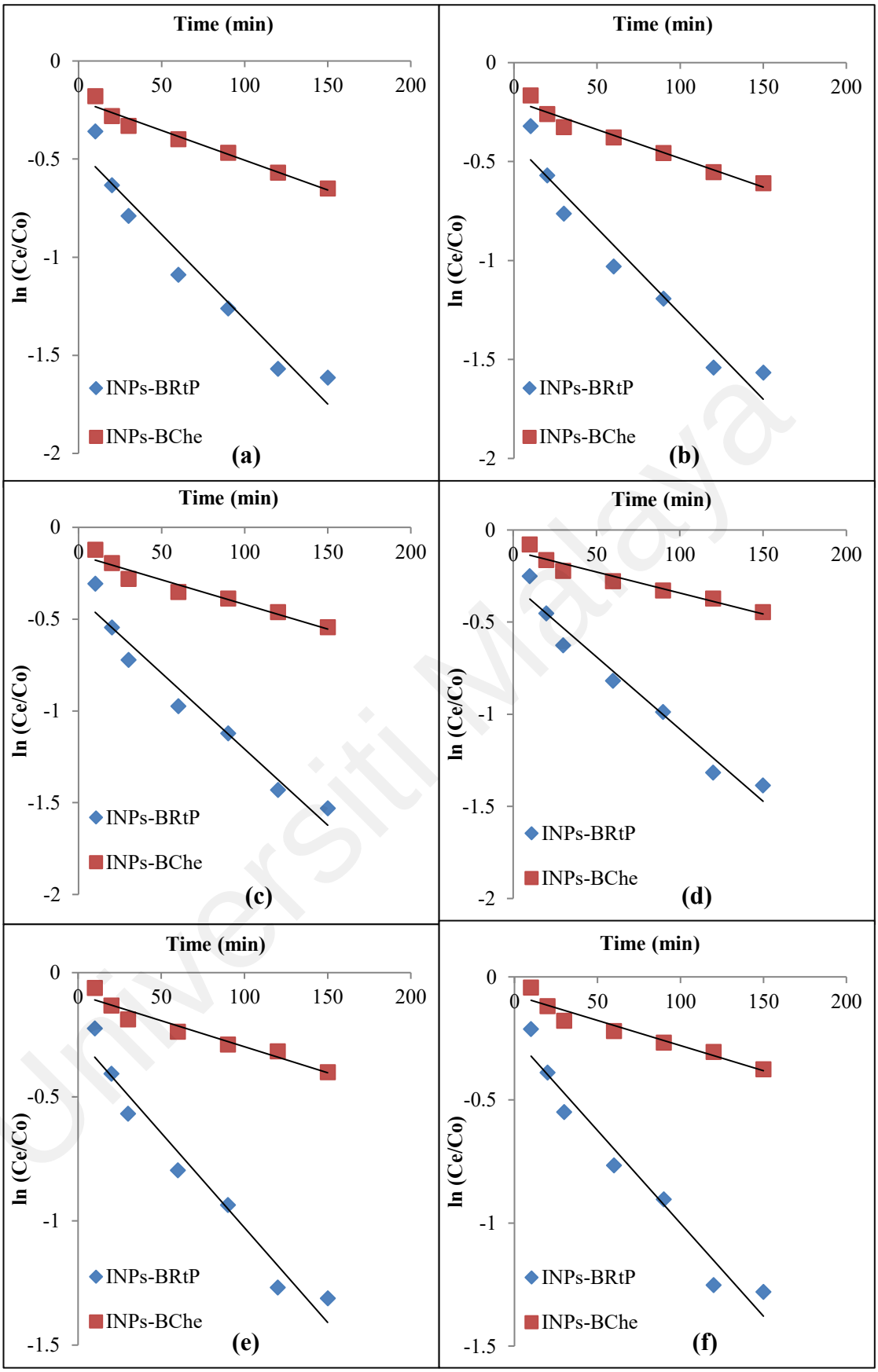

Figure 4.50: Pseudo-first-order model fittings to the experimental data for the removal of OCPs (a) *p,p′*-DDT, (b) *o,p′*-DDT, (c) aldrin, (d) heptachlor, (e) hexachlorobenzene, and (f) endosulfan I in OPPD water samples PMD3 by aged INPs-B_g and INPs-B_{Che} nanocomposites.

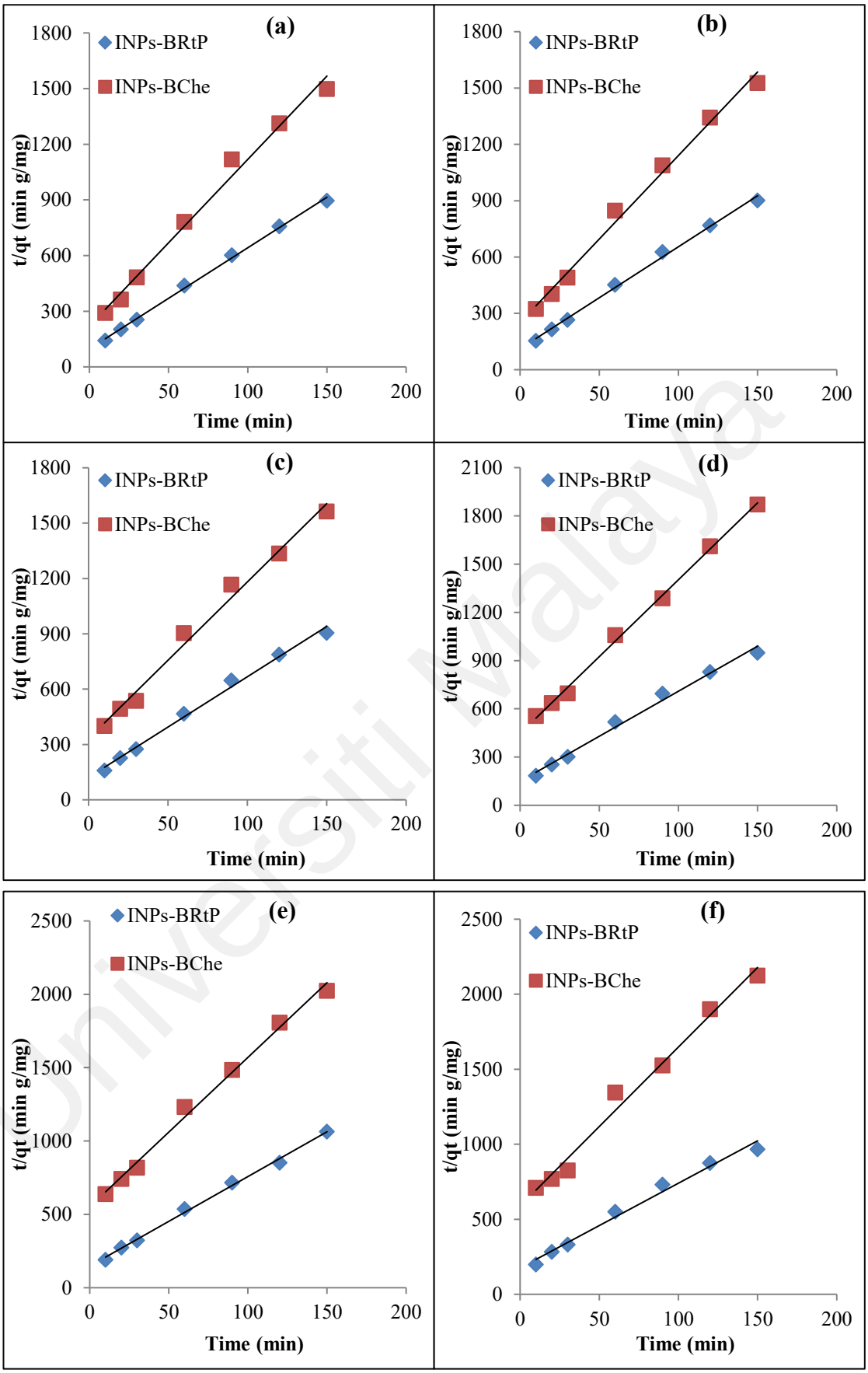

Figure 4.51: Pseudo-second-order model fittings to the experimental data for the removal of OCPs (a) *p,p′*-DDT, (b) *o,p′*-DDT, (c) aldrin, (d) heptachlor, (e) hexachlorobenzene, and (f) endosulfan I in OPD water samples PE1 by aged INPs-B_g and INPs-B_{Che} nanocomposites.

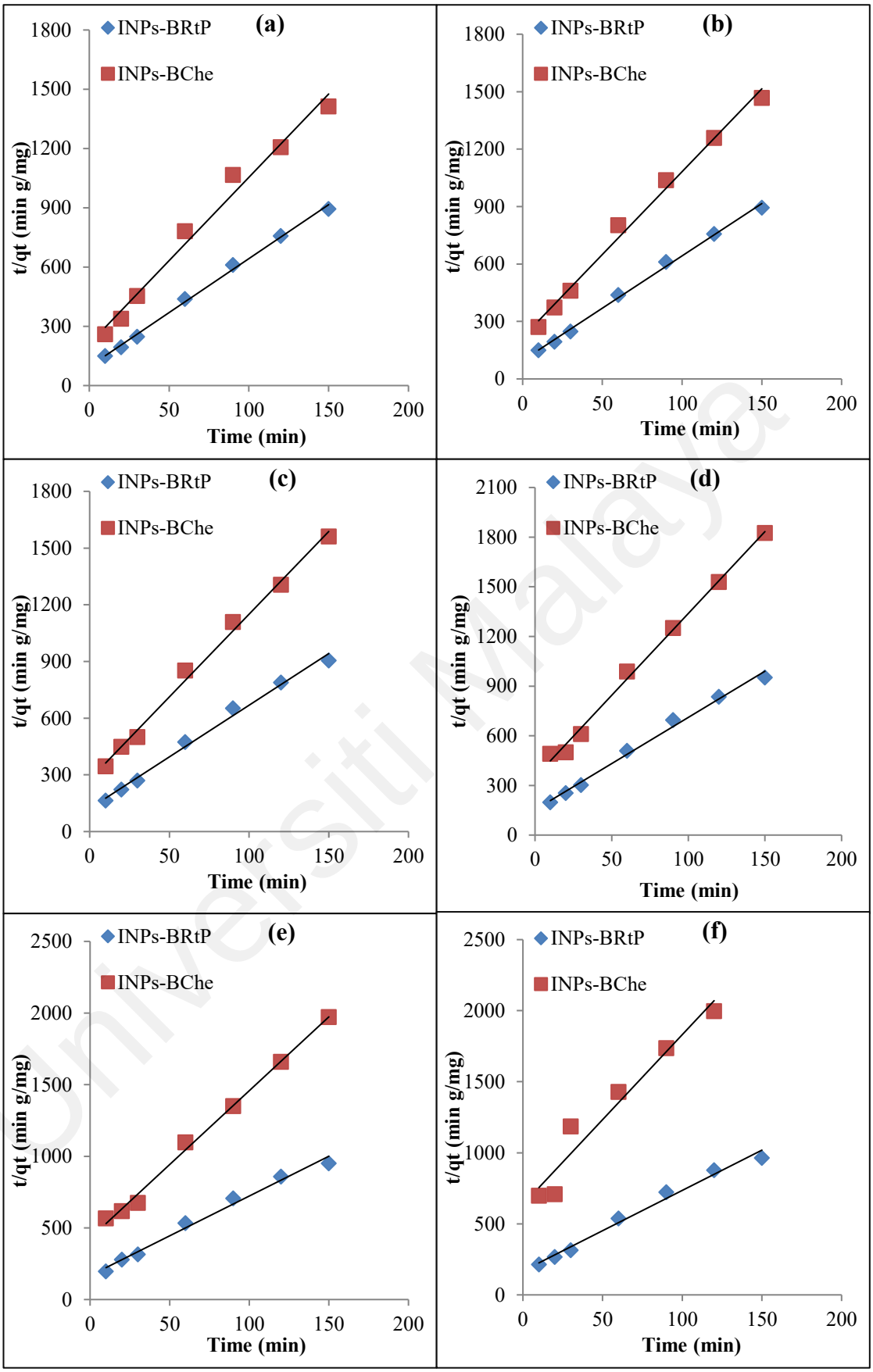

Figure 4.52: Pseudo-second-order model fittings to the experimental data for the removal of OCPs (a) *p,p′*-DDT, (b) *o,p′*-DDT, (c) aldrin, (d) heptachlor, (e) hexachlorobenzene, and (f) endosulfan I in OPPD water samples PMD2 by aged INPs-B_g and INPs-B_{Che} nanocomposites.

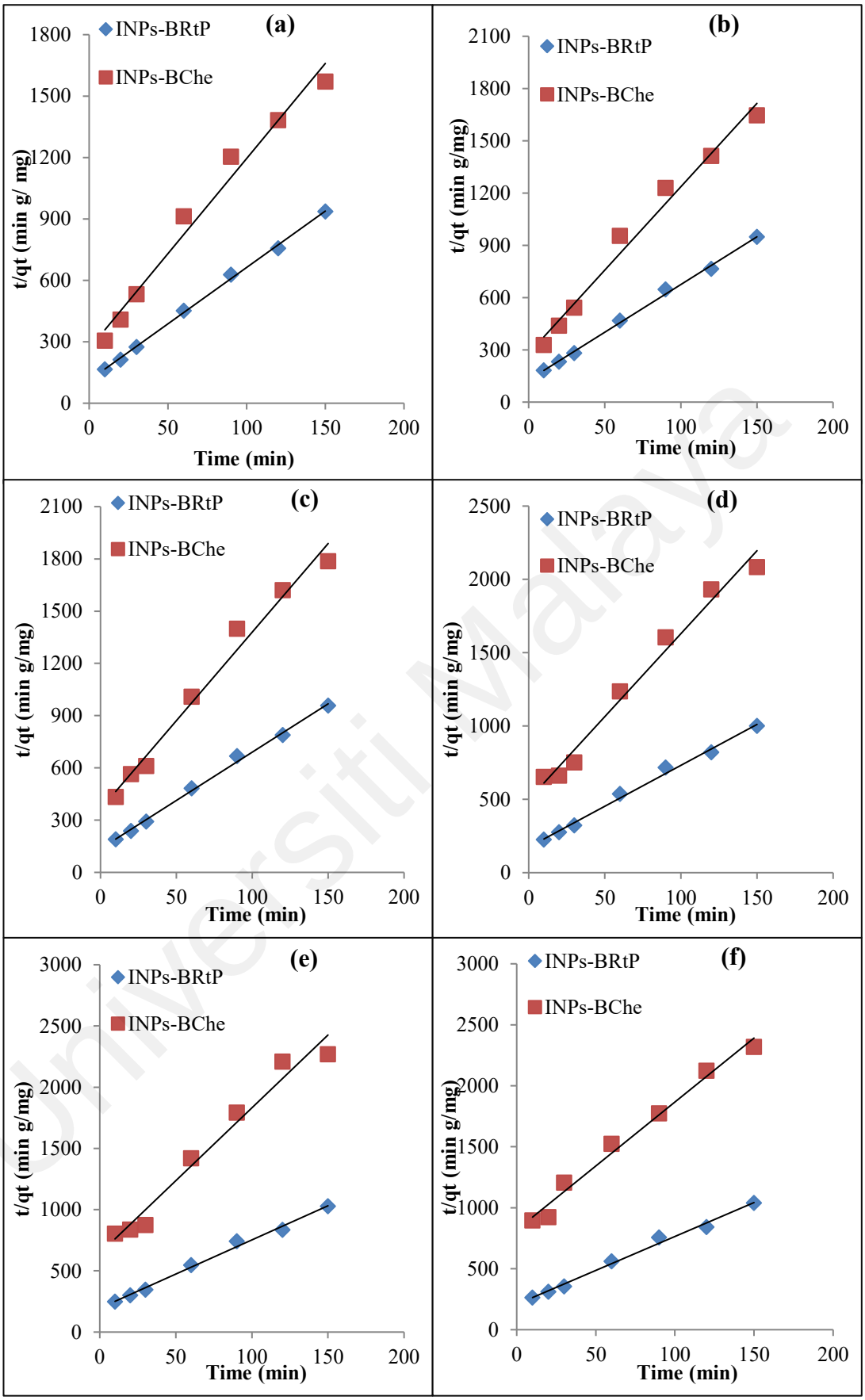

Figure 4.53: Pseudo-second-order model fittings to the experimental data for the removal of OCPs (a) *p,p′*-DDT, (b) *o,p′*-DDT, (c) aldrin, (d) heptachlor, (e) hexachlorobenzene, and (f) endosulfan I in OPPD water samples PMD3 by aged INPs-B_g and INPs-B_{Che} nanocomposites.

CHAPTER 5: CONCLUSION

In this study, we have developed four unique types of biochar supported green iron particles (INPs-B_{RtP}, INPs-B_{OpL}, INPs-B_{JfP}, INPs-B_{ScL} nanocomposites) from rambutan (*N. lappaceum*) fruit peel waste, oil palm (*E. guineensis*) leaf waste, jackfruit (*A. heterophyllus*) peel waste and sugar cane (*S. officinarum*) leaf waste for the simultaneous adsorption and dechlorination of OCPs in water. The green INPs-B_g nanocomposites were synthesized and deposited onto and inside of biochar pores using biodegradable and non-toxic polyphenol contents of extracts of rambutan fruit peel, oil palm leaf, jackfruit peel and sugar cane leaf as the green reducing mediator to reduce ferrous oxide (Fe(II)) to zerovalent iron (Fe^0), instead of eminent, toxic and highly expensive sodium borohydride and potassium borohydride. With respect to the polyphenol concentrations in the extracts of used plant material obtained at their best optimized conditions were found in the following order: rambutan fruit peel > oil palm leaf > jackfruit peel and > sugar cane leaf. For comparison, nanocomposites were also prepared by chemical method.

Field emission scanning electron microscopy (FESEM) and energy dispersive spectroscopy (EDX) confirmed the successful synthesis and dispersion of iron nanoparticles on the surface of biochar. FESEM images indicated that all types of biochar supported INPs are spherical in shape and non-uniform in size distribution. The EDX analysis showed that with respect to wt% of Fe, the nanocomposites were found in the following order: INPs-B_{RtP} (82.70%) > INPs-B_{OpL} (70.5%) > INPs-B_{Che} (66.12%), INPs-B_{JfP} (63.9%) and INPs-B_{ScL} (51.5%). BET surface area analysis of all types of pristine biochar, INPs-B_g nanocomposites and INPs-B_{Che} nanocomposite before and after reactions indicates that BET surface area of all types of nanocomposites were considerably higher than those of their respective pristine biochar and become lower after the reaction with OCPs. The deposition of INPs onto and inside of the mesopores of

bichar may contributed to the increased surface area and after reaction the OCPs adsorbed on biochar surface and INPs get oxidized causing the reduced BET surface area.

XRD analysis of all types of green INPs-B_g nanocomposites indicated that all types of green INPs successfully deposited on their respective bichar surface. The strong peaks for carbon and Fe^0 at around 2θ=25-26 and 2θ=44-46, respectively confirmed the deposition of green INPs on biochar. XRD analysis of all nanocomposites after reaction with OCPs showed the Fe^0 peaks of low intensity and formation of some new peaks for Fe_2O_3 at 2θ=36 and Fe_3O_4 at 2θ=62 indicating the consumption of green INPs and production of Fe_2O_3 and Fe_3O_4 as a result of the oxidation of green INPs during the dechlorination of OCPs. FTIR analysis of all pristine biochar and nanocomposites before and after reaction indicated that green Fe^0 has been successfully introduced into the biochar and after reaction the Cl^- peaks confirmed the adsorption of OCPs on biochar surface

The reasonable pH value was found to be 4 for the maximum removal of all OCPs by all types of nanocomposites. The removal percentage decreased with an increase of OCPs solution pH from 4-12. This may be result of the increased concentration of OH^- ions in the solution generating the secondary reductants (Fe^{2+} or Fe^{3+}-containing oxides and hydroxides such as $Fe(OH)_3$) on the surface of iron that impede the contact of target compounds to active sites of iron surface. Moreover, the pH > 4 gives higher concentration of H^+ ions in the solution damaging the carbon and oxidation of INPs and consequently removal capacity of organochlorine pesticide decreases. Increase in removal efficiency of all OCPs with the increase in adsorbent dose of all types of nanocomposites showed that the active sites for the adsorption and reduction of OCPs have increased.

In case of individual removal of OCPs, 100% removal was achievd with 0.1 g/L dose of INPs-B_{RtP}, INPs-B_{OpL} and INPs-B_{Che} nanocomposite within 40, 45 and 50 min, respectively and with 0.15 g/L dose of INPs-B_{JfP} and INPs-B_{ScL} within 50 and 55 min, respectively. Optimum contact time for equilibrium to be achieved for all OCPs (2 mg/L initial concentration) in the synthetic solution (mixture) was found to be 120 min for INPs-B_{RtP} (86-92% removal with 0.45 g/L of nanoadsorbent), 150 min for INPs-B_{OpL} (83-91% removal with 0.45 g/L of nanoadsorbent) and INPs-B_{Che} (76-86% removal with 0.45 g/L of nanoadsorbent), 180 min for INPs-B_{JfP} (69-78% removal with 0.55 g/L of nanoadsorbent) and INPs-B_{ScL} (59-70% removal with 0.55 g/L of nanoadsorbent). On the basis of these removal experiments it has been concluded that INPs-B_{RtP} nanocomosite synthesized using rambutan peel extract was found to be highly effiecient in OCPs removal as compared to other nanocomposites synthesized using oil palam leaf, jackfruit peel and sugarcane leaf extracts. The superlative removal efficiency of rambutan peel extract-based INPs-B_{RtP} nanocomosite is attributed to its higher Wt% of Fe which obtained because of higher polyphenol content in rambutan peel extrct than those of others mentioned above. The best one found nanoadsorbent i.e. INPs-B_{RtP} was also applied for the removal of OCPs in the OPPD water samples which gave 81-87% removal in 150 min by 10 g /L of nanoadsorbent.

Based on the correlation coefficient (R^2) values of the aadsorption isother model, Langmuir model fitted well for all OCPs by all types of nanocomposites. Also based on the values of the correlation coefficient of adsorption kinetic models, it was fitted well first to the pseudo-second-order model and then to the to pseudo-first-order model. With respect to the removal percentage, adsorption capacity and reaction rate constant (k_{obs}) values, the order of adsorption was described as follows: *p,p'*-DDT > *o,p'*-DDT > aldrin > heptachlor > hexachlorobenze and endosulfan I in all cases. The removal percentage and reaction rate constant (k_{obs} min^{-1}) values of the four different types of green INPs-

B_g nanocomposites as mentioned above and INPs-B_{Che} for OCPs (mixture) in the following order: INPs-B_{RtP} > INPs-B_{OpL} > INPs-B_{Che} > INPs-B_{JfP} and INPs-B_{ScL}. The k_{obs} values of all OCPs removed with all nanoadsorbent were found to be in the following order: individual solution (0.0830-0.1096 min^{-1}) > mixture solution (0.0113-0.0161 min^{-1}) > OPPD water samples (0.0083-0.0107 min^{-1}). The k_{obs} values of OCPs in the mixture was found to be 34% higher than those of OCPs in the OPPD water samples, whereas it was found to be 85% higher than those of OCPs in the individual solution.

Nonetheless, removal efficiency of INPs-B_{Che} decreased by more than 50 % after being aged in air for one month, whereas green INPs-B_g nanocomposites remained almost same. The experimental findings here in illustrate that the application of these as-prepared INPs-B_g nanocomposites could signify a potential functional material for adsorption and subsequent dechlorination of OCPs in aquatic system and it is an eco-friendly and highly cost effective environmental pollution controlling technique for the OCPs removal from aquatic system.

REFERENCES

Agrafioti, E., Kalderis, D., & Diamadopoulos, E. (2014). Arsenic and chromium removal from water using biochars derived from rice husk, organic solid wastes and sewage sludge. *Journal of Environmental Management*, *133*, 309-314.

Agrawal, A., Sahu, K. K., & Pandey, B. D. (2005). Systematic studies on adsorption of lead on sea nodule residues. *Journal of Colloid and Interfacescience*, 281, 291-298.

Al-Asheh, S., Banat, F., & Abu-Aitah, L. (2003). Adsortion of phenol using different types of activated bentonites. *Searation and Purification technology*, 33, 1-10.

Allabaksh, M. B., Mandal, B. K., Kesarla, M. K., Kumar, K. S., & Reddy, P. S. (2010). Preparation of Stable Zero Valent Iron Nanoparticles using Different Chelating Agents. *Journal of Chemical and Pharmaceutical Research*. *2*(5): 67-74.

Aktar, W., Sengupta, D., & Chowdhury, A. (2009). Impact of pesticides use in agriculture: their benefits and hazards. *Interdisciplinary toxicology*, *2*(1), 1-12.

Anesini, C., Ferraro, G. E., & Filip, R. (2008). Total polyphenol content and antioxidant capacity of commercially available tea (Camellia sinensis) in Argentina. *Journal of Agricultural and Food Chemistry*, *56*(19), 9225-9229.

Arancibia-Miranda, N., Baltazar, S. E., García, A., Munoz-Lira, D., Sepúlveda, P., Rubio, M. A., & Altbir, D. (2016). Nanoscale zero valent supported by zeolite and montmorillonite: template effect of the removal of lead ion from an aqueous solution. *Journal of Hazardous Materials*, *301*, 371-380.

Arivoli, S., Sundaravadivelu, M., & Elango, K. P. (2008). Removal of basic and acidic dyes from aqueous solution by adsorption on a low cost activated carbon: Kinetic and thermodynamic study. *Indian Journal of Chemical Technology, 15*, 130-139.

Atieh, M. A. (2011). Removal of chromium (VI) from polluted water using carbon nanotubes supported with activated carbon. *Procedia Environmental Sciences*, *4*, 281-293.

Baccar, R., Bouzid, J., Feki, M., & Montiel, A. (2009). Preparation of activated carbon from Tunisian olive-waste cakes and its application for adsorption of heavy metal ions.*Journal of Hazardous Materials*, *162*(2), 1522-1529.

Bansiwal, A., Pillewan, P., Biniwale, R. B., & Rayalu, S. S. (2010). Copper oxide incorporated mesoporous alumina for defluoridation of drinking water. *Microporous and Mesoporous Materials*, *129*(1), 54-61.

Barnes, R. J., Riba, O., Gardner, M. N., Scott, T. B., Jackman, S. A., & Thompson, I. P. (2010). Optimization of nano-scale nickel/iron particles for the reduction of high concentration chlorinated aliphatic hydrocarbon solutions.*Chemosphere*, *79*(4), 448-454.

Barau, A., Budarin, V., Caragheorgheopol, A., Luque, R., Macquarrie, D. J., Prelle, A., & Zaharescu, M. (2008). A simple and efficient route to active and dispersed silica supported palladium nanoparticles. *Catalysis Letters*, *124*(3-4), 204-214.

Baseri, J. R., Palanisamy, P. N., & Kumar, P. S. (2012). Adsorption of basic dyes from synthetic textile effluent by activated carbon prepared from Thevetia peruviana. *Indian Journal of Chemical Technology*, *19*(5): 311-321.

Begum, S.k., 2011. Dechlorination of endocrine disrupting chemicals using $Mg^0/ZnCl_2$ bimetallic system. *Water Research*, *45*, 2383–2391.

Behrooz, R. D., Esmaili-Sari, A., Ghasempouri, S. M., Bahramifar, N., & Covaci, A. (2009). Organochlorine pesticide and polychlorinated biphenyl residues in feathers of birds from different trophic levels of South-West Iran. *Environment international*, *35*(2), 285-290.

Bhowmick, S., Chakraborty, S., Mondal, P., Van Renterghem, W., Van den Berghe, S., Roman-Ross, G., & Iglesias, M. (2014). Montmorillonite-supported nanoscale zero-valent iron for removal of arsenic from aqueous solution: Kinetics and mechanism. *Chemical Engineering Journal*, *243*, 14-23.

Borja, J. Q., Ngo, M. A. S., Saranglao, C. C., Tiongco, R. P. M., Roque, E. C., & Dugos, N. P. (2015). Synthesis of green zero-valent iron using polyphenols from dried green tea extract. *Journal of Engineering Science and Technology*, *10*, 22-31.

Brooks, G. T. (1980). The preparation of some reductively dechlorinated analogues of dieldrin, endosulfan and isobenzan. *Journal of Pesticide Science*, *5*(4), 565-574.

Cao, J., Xu, R., Tang, H., Tang, S., & Cao, M. (2011). Synthesis of monodispersed CMC-stabilized Fe–Cu bimetal nanoparticles for in situ reductive dechlorination of 1, 2, 4-trichlorobenzene. *Science of the Total Environment*, *409*(11), 2336-2341.

Chen, B., Zhou, D., & Zhu, L. (2008). Transitional adsorption and partition of nonpolar and polar aromatic contaminants by biochars of pine needles with different pyrolytic temperatures.*Environmental Science and Technology*, *42*(14), 5137-5143.

Chiang, Y. C., Lee, C. C., & Lee, H. C. (2007). Characterization of microstructure and surface properties of heat-treated PAN-and rayon-based activated carbon fibers.*Journal of Porous Materials*, *14*(2), 227-237.

Chemizmu, K., & Fentona, R. (2009). Fenton reaction-controversy concerning the chemistry. *Ecological chemistry and engineering*, *16*, 347-358.

Chen, Z., Wang, T., Jin, X., Chen, Z., Megharaj, M., & Naidu, R. (2013). Multifunctional kaolinite-supported nanoscale zero-valent iron used for the adsorption and degradation of crystal violet in aqueous solution. *Journal of Colloid and Interface Science*, *398*, 59-66.

Chen, M. Y., Su, Y. F., & Shih, Y. H. (2014). Effect of geochemical properties on degradation of trichloroethylene by stabilized zerovalent iron nanoparticle with Na-acrylic copolymer. *Journal of Environmental Management*, *144*, 88-92.

Chen, W. F., Pan, L., Chen, L. F., Wang, Q., & Yan, C. C. (2014). Dechlorination of hexachlorobenzene by nano zero-valent iron/activated carbon nanocomposite: iron loading, kinetics and pathway. *Rsc Advances*, *4*(87), 46689-46696.

Cheng, S. F., & Wu, S. C. (2000). The enhancement methods for the degradation of TCE by zero-valent metals.*Chemosphere*, *41*(8), 1263-1270.

Choe, S., Chang, Y. Y., Hwang, K. Y., & Khim, J. (2000). Kinetics of reductive denitrification by nanoscale zero-valent iron. *Chemosphere*, *41*(8), 1307-1311.

Choe, S., Lee, S. H., Chang, Y. Y., Hwang, K. Y., & Khim, J. (2001). Rapid reductive destruction of hazardous organic compounds by nanoscale Fe 0. *Chemosphere*, *42*(4), 367-372.

Choi, H., Al-Abed, S. R., Agarwal, S., & Dionysiou, D. D. (2008). Synthesis of reactive nano-Fe/Pd bimetallic system-impregnated activated carbon for the simultaneous adsorption and dechlorination of PCBs. *Chemistry of Materials*, *20*(11), 3649-3655.

Chrysochoou, M., Johnston, C. P., & Dahal, G. (2012). A comparative evaluation of hexavalent chromium treatment in contaminated soil by calcium polysulfide and green-tea nanoscale zero-valent iron. *Journal of Hazardous Materials*,*201*, 33-42.

Chu, B. S., Baharin, B. S., Che Man, Y. B., & Quek, S. Y. (2004). Separation of vitamin from alm fatty acid distillate using silica; I Equilibrium of batch adsorption. *Journal of Food Engineering*, 62, 97-103.

Crane, R. A., & Scott, T. B. (2012). Nanoscale zero-valent iron: future prospects for an emerging water treatment technology. *Journal of Hazardous Materials*, *211*, 112-125.

Craggs, R., Cooke, J., Mathieson, T., & Park, J. (2010). Potential of Mussel Shell as a Biosorbent for Stormwater Treatment. ISSN 1179-0512.

Devi, P., & Saroha, A. K. (2014). Risk analysis of pyrolyzed biochar made from paper mill effluent treatment plant sludge for bioavailability and eco-toxicity of heavy metals. *Bioresource Technology*, *162*, 308-315.

Cushing, B. L., Kolesnichenko, V. L., & O'Connor, C. J. (2004). Recent advances in the liquid-phase syntheses of inorganic nanoparticles. *Chemical Reviews*, *104*(9), 3893-3946.

Daniel, S.C.G.K., Vinothini, G., Subramanian, N., Nehru, K., Sivakumar, M., 2013. Biosynthesis of Cu, ZVI, and Ag nanoparticles using Dodonaea viscosa extract for antibacterial activity against human pathogens. *Journal of. Nanoparticle Research*. 15(1): 1319-2013.

Danish, M., Gu, X., Lu, S., & Naqvi, M. (2016). Degradation of chlorinated organic solvents in aqueous percarbonate system using zeolite supported nano zero valent iron (Z-INPs) nanocomposite. *Environmental Science and Pollution Research*, *23*(13), 13298-13307.

Deng B, Burniss DR, Campbell TJ (1999) Reductive vinyl chloride in metallic iron–water systems. *Environtal Sciences Technology*, 33:2651–2656

Devi, P., Saroha, A.K., 2014. Synthesis of the magnetic biochar nanocomposites for use as an adsorbent for the removal of pentachlorophenol from the effluent. *Bioresource and. Technology*. 169, 525–531.

Dien, N. T., De Windt, W., Buekens, A., & Chang, M. B. (2013). Application of bimetallic iron (BioCAT slurry) for pentachlorophenol removal from sandy soil. *Journal of hazardous materials*, *252*, 83-90.

Doong, R. A., Saha, S., Lee, C. H., & Lin, H. P. (2015). Mesoporous silica supported bimetallic Pd/Fe for enhanced dechlorination of tetrachloroethylene. *RSC Advances*, *5*(110), 90797-90805.

Djebbar, M., Djafri, F., Bouchekara, M., & Djafri, A. (2012). Adsorption of phenol on natural clay. *Applied Water Science*,*2*(2), 77-86.

Dorathi, P. J., & Kandasamy, P. (2012). Dechlorination of chlorophenols by zero valent iron impregnated silica. *Journal of Environmental Sciences*, *24*(4), 765-773.

Domínguez-Domínguez, S., Arias-Pardilla, J., Berenguer-Murcia, Á., Morallón, E., & Cazorla-Amorós, D. (2008). Electrochemical deposition of platinum nanoparticles on different carbon supports and conducting polymers. *Journal of Applied Electrochemistry*, *38*(2), 259-268.

ElBayoumi, T. A., Torchilin, V. P, Weissig, V. (2010). Liposomes: Methods and Protocols, Pharmaceutical Nanocarriers *1*.

Elliott, D. W., Lien, H. L., & Zhang, W. X. (2009). Degradation of lindane by zero-valent iron nanoparticles. *Journal of Environmental Engineering*, *135*(5), 317-324.

Erto, A. (2010). *Chem. Eng*., 156, 353-359.

El-Temsah, Y. S., Sevcu, A., Bobcikova, K., Cernik, M., & Joner, E. J. (2016). DDT degradation efficiency and ecotoxicological effects of two types of nano-sized zero-valent iron (INPs) in water and soil. *Chemosphere*, *144*, 2221-2228.

Everett, D. H. (1986). Reporting data on adsorption from solution at the solid/solution interface (Recommendations 1986). *Pure and Applied Chemistry*, *58*(7), 967-984.

Euorpeon Commission, DG-SANCO. Method validation and quality control procedures for pesticide residues analysis in food and feed, Document No. SANCO/12495/2011 (2012)

Fan, G., Cang, L., Qin, W., Zhou, C., Gomes, H. I., & Zhou, D. (2013). Surfactants-enhanced electrokinetic transport of xanthan gum stabilized nanoPd/Fe for the remediation of PCBs contaminated soils. *Separation and Purification Technology*, *114*, 64-72.

Figueroa, I. D. C., & Simmons, M. S. (1991). Structure-activity relationships of chlorobenzenes using DNA measurement as a toxicity parameter in algae. *Environmental Toxicology and Chemistry*, *10*(3), 323-329.

Fipps, G. (2003). Irrigation water quality standards and salinity management strategies. *Texas Farmer Collection*.

Ghadiri, S. K., Nabizadeh, R., Mahvi, A. H., Nasseri, S., Kazemian, H., Mesdaghinia, A. R., & Nazmara, S. (2010). Methyl tert-butyl ether adsorption on surfactant

modified natural zeolites. *Iranian Journal of Environmental Health Science and Engineering*, *7*(3), 241.

Glaspell, G., Hassan, H. M., Elzatahry, A., Abdalsayed, V., & El-Shall, M. S. (2008). Nanocatalysis on supported oxides for CO oxidation. *Topics in Catalysis*, *47*(1-2), 22-31.

Grieger, K. D., Linkov, I., Hansen, S. F., & Baun, A. (2012). Environmental risk analysis for nanomaterials: review and evaluation of frameworks. *Nanotoxicology*, *6*(2), 196-212.

Guo, H., Jin, Y., Cheng, Y., Leaderer, B., Lin, S., Holford, T. R., Qiu, J., Zhang, Y., Shi, K., Zhu, Y., Niu, J., Bassig, B. A., Xu, S., Zhang, B., Li, Y., Hu, X., Chen, Q., Zheng, T. (2014). Prenatal exposure to organochlorine pesticides and infant birth weight in China. *Chemosphere*, *110*, 1-7.

Haruta, M., Tsubota, S., Kobayashi, T., Kageyama, H., Genet, M. J., & Delmon, B. (1993). Low-temperature oxidation of CO over gold supported on TiO2, α-Fe_2O_3, and $Co3O_4$. *Journal of Catalysis*, *144*(1), 175-192.

He, F., Zhao, D., & Paul, C. (2010). Field assessment of carboxymethyl cellulose stabilized iron nanoparticles for in situ destruction of chlorinated solvents in source zones. *Water Research*, *44*(7), 2360-2370.

Hider, R. C., Liu, Z. D., & Khodr, H. H. (2001). Metal chelation of polyphenols. *Methods in Enzymology*, *335*, 190-203.

Hoag, G. E., Collins, J. B., Holcomb, J. L., Hoag, J. R., Nadagouda, M. N., & Varma, R. S. (2009). Degradation of bromothymol blue by 'greener'nano-scale zero-valent iron synthesized using tea polyphenols. *Journal of Materials Chemistry*, *19*(45), 8671-8677.

Hossain, M. A., & Rahman, M. A. (2013). Removal of basic violet 10 from neutral aqueous solution by adsorption on used black tea leaves. *International Journal of Chemistry*, *2*(2), 83-94.

Huang, L., Weng, X., Chen, Z., Megharaj, M., & Naidu, R. (2014). Synthesis of iron-based nanoparticles using oolong tea extract for the degradation of malachite green. *Spectrochimica Acta Part A: Molecular and Biomolecular Spectroscopy*, *117*, 801-804.

Ignat, I., Volf, I., & Popa, V. I. (2011). A critical review of methods for characterisation of polyphenolic compounds in fruits and vegetables. *Food chemistry*, *126*(4), 1821-1835.

Iravani, S. (2011). Green synthesis of metal nanoparticles using plants. *Green Chemistry*, *13*(10), 2638-2650.

ISO 14502-1:2005(E). Determination of substances characteristic of green and black tea — Part 1: Content of total polyphenols in tea — Colorimetric method using Folin- Ciocalteu reagent.

Ivashechkin, P., Corvini, P. X., & Dohmann, M. (2004). Behaviour of endocrine disrupting chemicals during the treatment of municipal sewage sludge. *Water Science and Technology*, *50*(5), 133-140.

Iwata, H. and Matsuda, T., P., A hand book of membrane separation: chemical, pharmaceutical, food and biotechnological separation. *Journal of. Membrane Scienc, 38* (2), 185–199, 1998

Jortner, J., & Rao, C. N. R. (2002). Nanostructured advanced materials. Perspectives and directions. *Pure and Applied Chemistry*, *74*(9), 1491-1506.

Jovanovic, G. N., Žnidaršič Plazl, P., Sakrittichai, P., & Al-Khaldi, K. (2005). Dechlorination of p-chlorophenol in a microreactor with bimetallic Pd/Fe catalyst. *Industrial and Engineering Chemistry Research*, *44*(14), 5099-5106.

Johnson, R. L., Nurmi, J. T., O'Brien Johnson, G. S., Fan, D., O'Brien Johnson, R. L., Shi, Z., & Lowry, G. V. (2013). Field-scale transport and transformation of carboxymethylcellulose-stabilized nano zero-valent iron.*Environmental Science and Technology*, *47*(3), 1573-1580.

Ju-Nam, Y., & Lead, J. R. (2008). Manufactured nanoparticles: an overview of their chemistry, interactions and potential environmental implications. *Science of the Total Environment*, *400*(1), 396-414.

Kahru, A., & Dubourguier, H. C. (2010). From ecotoxicology to nanoecotoxicology. *Toxicology*, *269*(2), 105-119.

Kanel, S. R., Nepal, D., Manning, B., & Choi, H. (2007). Transport of surface-modified iron nanoparticle in porous media and application to arsenic (III) remediation. *Journal of Nanoparticle Research*, *9*(5), 725-735.

Khan, Z., AL-Thabaiti, S. A., & Hussain, S. (2015). Nanoscale water soluble self-assembled zero-valent iron: role of stabilizers in their morphology. *RSC Advances*, *6*(9), 7267-7278.

Kharisov, B. I., Dias, H. R., Kharissova, O. V., Jiménez-Pérez, V. M., Pérez, B. O., & Flores, B. M. (2012). Iron-containing nanomaterials: synthesis, properties, and environmental applications. *Rsc Advances*, *2*(25), 9325-9358.

Kong, K. W., Mat-Junit, S., Aminudin, N., Ismail, A., & Abdul-Aziz, A. (2012). Antioxidant activities and polyphenolics from the shoots of Barringtonia racemosa (L.) Spreng in a polar to apolar medium system. *Food Chemistry*, *134*(1), 324-332.

Kumar, K. M., Mandal, B. K., Kumar, K. S., Reddy, P. S., & Sreedhar, B. (2013). Biobased green method to synthesise palladium and iron nanoparticles using Terminalia chebula aqueous extract. *Spectrochimica Acta Part A: Molecular and Biomolecular Spectroscopy*, *102*, 128-133.

Kumar, K. M., Mandal, B. K., Kumar, K. S., Reddy, P. S., & Sreedhar, B. (2013). Biobased green method to synthesise palladium and iron nanoparticles using Terminalia chebula aqueous extract. *Spectrochimica Acta Part A: Molecular and Biomolecular Spectroscopy*, *102*, 128-133.

Kusvuran, E., & Erbatur, O. (2004). Degradation of aldrin in adsorbed system using advanced oxidation processes: comparison of the treatment methods. *Journal of hazardous materials*, *106*(2-3), 115-125.

Laumann, S., Micić, V., Lowry, G. V., & Hofmann, T. (2013). Carbonate minerals in porous media decrease mobility of polyacrylic acid modified zero-valent iron nanoparticles used for groundwater remediation. *Environmental Pollution*, *179*, 53-60.

Laura, B. H., Elizabeth, J.M. and Bianca, W.H., *Environtal Sciences and Technology*., 42, 2600-2605, 2008

Laurent, S., Forge, D., Port, M., Roch, A., Robic, C., Vander Elst, L., & Muller, R. N. (2008). Magnetic iron oxide nanoparticles: synthesis, stabilization, vectorization, physicochemical characterizations, and biological applications. *Chemical reviews*, *108*(6), 2064-2110.

Li, X. Q., Elliott, D. W., & Zhang, W. X. (2006). Zero-valent iron nanoparticles for abatement of environmental pollutants: materials and engineering aspects. *Critical Reviews in Solid State and Materials Sciences*, *31*(4), 111-122.

Li, H., Qiu, Y. F., Wang, X. L., Yang, J., Yu, Y. J., & Chen, Y. Q. (2017). Biochar supported Ni/Fe bimetallic nanoparticles to remove 1, 1, 1-trichloroethane under various reaction conditions. *Chemosphere*, *169*, 534-541.

Li, T. T., Liu, Y. G., Peng, Q. Q., Hu, X. J., Liao, T., Wang, H., & Lu, M. (2013). Magnetic responsive microbial cells for metal ions removal and detection. *Chemical. Engineering. Journal*, 214, 189–197.

Lillo-Ródenas, M. A., Cazorla-Amorós, D., & Linares-Solano, A. (2003). Understanding chemical reactions between carbons and NaOH and KOH: an insight into the chemical activation mechanism. *Carbon*, *41*(2), 267-275.

Lin, D., & Xing, B. (2007). Phytotoxicity of nanoparticles: inhibition of seed germination and root growth. *Environmental Pollution*, *150*(2), 243-250.

Lin, X. M., & Samia, A. C. (2006). Synthesis, assembly and physical properties of magnetic nanoparticles. *Journal of Magnetism and Magnetic Materials*, *305*(1), 100-109.

Lin, C. J., Lo, S. L., & Liou, Y. H. (2008). Dechlorination of trichloroethylene in aqueous solution by noble metal-modified iron. *Journal of Hazardous Materials*, *116*(3), 219-228.

Ling, D., & Hyeon, T. (2013). Chemical design of biocompatible iron oxide nanoparticles for medical applications. *Small*, *9*(9-10), 1450-1466.

Liu, C., & Huang, P. M. (2003). Kinetics of lead adsorption by iron oxides formed under the influence of citrate. *Geochimica et Cosmochimica Acta*, *67*(5), 1045-1054.

Liu, Y., Majetich, S. A., Tilton, R. D., Sholl, D. S., & Lowry, G. V. (2005). TCE dechlorination rates, pathways, and efficiency of nanoscale iron particles with different properties.*Environmental Science and Technology*, *39*(5), 1338-1345.

Liu, T., Wang, Z. L., Zhao, L., & Yang, X. (2012). Enhanced chitosan/Fe 0-nanoparticles beads for hexavalent chromium removal from wastewater. *Chemical Engineering Journal*, *189*, 196-202.

Liu, X., Peng, P. A., Fu, J., & Huang, W. (2003). Effects of FeS on the transformation kinetics of γ-hexachlorocyclohexane. *Environmental Science and Technology*, *37*(9), 1822-1828.

Lowry, G. V., & Johnson, K. M. (2004). Congener-specific dechlorination of dissolved PCBs by microscale and nanoscale zerovalent iron in a water/methanol solution. *Environmental Science and Technology*, *38*(19), 5208-5216.

Luborsky, F. E. (1957). The kinetics of growth of spherical iron crystallites in mercury. *The Journal of Physical Chemistry*, *61*(10), 1336-1340.

Luo, S., Qin, P.F., Shao, J.H., Peng, L., Zeng, Q.R., Gu, J.D., 2013. Synthesis of reactive nanoscale zero valent iron using rectorite supports and its application for orange II removal. *Journal of. Chemical. Engineering*,. 223, 1–7.

Masciangioli, T., & Zhang, W. X. (2003). Peer reviewed: environmental technologies at the nanoscale. *Environmental Science and Technology,* 102-108.

Matheson, L. J., & Tratnyek, P. G. (1994). Reductive dehalogenation of chlorinated methanes by iron metal.*Environmental Science and Technology*, *28*(12), 2045-2053.

Mimmo, T., Panzacchi, P., Baratieri, M., Davies, C. A., & Tonon, G. (2014). Effect of pyrolysis temperature on miscanthus (Miscanthus× giganteus) biochar physical, chemical and functional properties. *Biomass and Bioenergy*, *62*, 149-157.

Miyake, Y., & Suzukit, M. (1993). Removal of trichloroethylene from air stripping off-gas by adsorption on activated carbon fibre. *Gas Separation and Purification*, *7*(4), 229.

Mohan, D., Singh, K. P., & Singh, V. K. (2006). Trivalent chromium removal from wastewater using low cost activated carbon derived from agricultural waste material and activated carbon fabric cloth. *Journal of Hazardous Materials*, *135*(1), 280-295.

Murgueitio, E., Debut, A., Landivar, J., Cumbal, L., 2016. Synthesis of Iron Nanoparticles through Extracts of Native Fruits of Ecuador, as Capuli (*Prunus serotina*) and Mortiño (*Vaccinium floribundum*). *Biol. Med*, 8, 282.

Mystrioti, C., Sparis, D., Papassiopi, N., Xenidis, A., Dermatas, D., & Chrysochoou, M. (2012). Hexavalent chromium reduction with polyphenolcoated nano zero valent iron. *International Conference on Industrial and Hazardous Waste Management.* 12-14 September 2012, Chania, Crete, Greece.

Nadagouda, M. N., Castle, A. B., Murdock, R. C., Hussain, S. M., & Varma, R. S. (2010). In vitro biocompatibility of nanoscale zerovalent iron particles (INPS) synthesized using tea polyphenols. *Green Chemistry*, *12*(1), 114-122.

Nardini, M., Cirillo, E., Natella, F., & Scaccini, C. (2002). Absorption of phenolic acids in humans after coffee consumption. *Journal of Agricultural and Food Chemistry*, *50*(20), 5735-5741.

Njagi, E. C., Huang, H., Stafford, L., Genuino, H., Galindo, H. M., Collins, J. B., & Suib, S. L. (2010). Biosynthesis of iron and silver nanoparticles at room temperature using aqueous sorghum bran extracts. *Langmuir*, *27*(1), 264-271.

Nemecek, J., Lhotský, O., & Cajthaml, T. (2014). Nanoscale zero-valent iron application for in situ reduction of hexavalent chromium and its effects on indigenous microorganism populations. *Science of the Total Environment*, *485*, 739-747.

Machado, S., Pinto, S. L., Grosso, J. P., Nouws, H. P. A., Albergaria, J. T., & Delerue-Matos, C. (2013). Green production of zero-valent iron nanoparticles using tree leaf extracts. *Science of the Total Environment*, *445*, 1-8.

Mueller, N. C., Braun, J., Bruns, J., Černík, M., Rissing, P., Rickerby, D., & Nowack, B. (2012). Application of nanoscale zero valent iron (INPS) for groundwater remediation in Europe.*Environmental Science and Pollution Research*, *19*(2), 550-558.

Ng, L. Y., Mohammad, A. W., Leo, C. P., & Hilal, N. (2013). Polymeric membranes incorporated with metal/metal oxide nanoparticles: a comprehensive review. *Desalination*, *308*, 15-33.

Novak, J. M., Lima, I., Xing, B., Gaskin, J. W., Steiner, C., Das, K. C., & Schomberg, H. (2009). Characterization of designer biochar produced at different temperatures and their effects on a loamy sand. *Annals of Environmental Science*, *3*(1), 195-206.

Ok, Y. S., Yang, J. E., Zhang, Y. S., Kim, S. J., & Chung, D. Y. (2007). Heavy metal adsorption by a formulated zeolite-Portland cement mixture. *Journal of Hazardous Materials*, *147*(1), 91-96.

Pan, X.; Niu, G.; and Liu, H. (2003). Microwave-assisted extraction of tea polyphenols and tea caffeine from green tea leaves. *Chemical Engineering Processing*, 42, 129-133

Parshetti, G. K., & Doong, R. A. (2012). Dechlorination of chlorinated hydrocarbons by bimetallic Ni/Fe immobilized on polyethylene glycol-grafted microfiltration membranes under anoxic conditions. *Chemosphere*, *86*(4), 392-399.

Patil, S., Renukdas, S., & Patel, N. (2011). Removal of methylene blue, a basic dye from aqueous solutions by adsorption using teak tree (Tectona grandis) bark powder. *International Journal of Environmental Sciences*, *1*(5), 711.

Pattanayak, M., Mohapatra, D., & Nayak, P. L. (2013). Green synthesis and characterization of zero valent iron nanoparticles from the leaf extract of coffea Arabica (Coffee). *American-Eurasian Journal of Scientific Research*, *8*(4): 184-187.

Petala, E., Dimos, K., Douvalis, A., Bakas, T., Tucek, J., Zbořil, R., & Karakassides, M. A. (2013). Nanoscale zero-valent iron supported on mesoporous silica:

characterization and reactivity for Cr (VI) removal from aqueous solution. *Journal of Hazardous Materials*, *261*, 295-306.

Phenrat, T., Saleh, N., Sirk, K., Tilton, R. D., & Lowry, G. V. (2007). Aggregation and sedimentation of aqueous nanoscale zerovalent iron dispersions. *Environmental Science and Technology*, *41*(1), 284-290.

Pillai, H. P., & Kottekottil, J. (2016). Nano-phytotechnological remediation of endosulfan using zero valent iron nanoparticles. *Journal of Environmental Protection*, *7*(05), 734.

Pooja, D., Panyaram, S., Kulhari, H., Rachamalla, S. S., & Sistla, R. (2014). Xanthan gum stabilized gold nanoparticles: characterization, biocompatibility, stability and cytotoxicity.*Carbohydrate Polymers*, *110*, 1-9.

Pouretedal, H. R., & Saedi, E. (2014). Dechlorination of 2, 4-dichlorophenol by zero-valent iron nanoparticles impregnated MCM-48. *International Journal of Industrial Chemistry*, *5*(3-4), 77-83.

Pouretedal, H. R., & Hasanali, M. A. (2013). Photocatalytic degradation of some β-lactam antibiotics in aqueous suspension of ZnS nanoparticles. *Desalination and Water Treatment*, *51*(13-15), 2617-2623.

Pouretedal, H. R., & Sadegh, N. (2014). Effective removal of Amoxicillin, Cephalexin, Tetracycline and Penicillin G from aqueous solutions using activated carbon nanoparticles prepared from vine wood. *Journal of Water Process Engineering*, *1*, 64-73.

Quan, G., Sun, W., Yan, J., & Lan, Y. (2014). Nanoscale zero-valent iron supported on biochar: characterization and reactivity for degradation of acid orange 7 from aqueous solution. *Water, Air, & Soil Pollution*, *225*(11), 2195.

Raichur, A. M., & Panvekar, V. (2002). Removal of As (V) by adsorption onto mixed rare earth oxides. *Separation Science and Technology*, *37*(5), 1095-1108.

Ray, J. R., Lee, B., Baltrusaitis, J., & Jun, Y. S. (2012). Formation of iron (III)(hydr) oxides on polyaspartate-and alginate-coated substrates: effects of coating hydrophilicity and functional group. *Environmental Science & Technology*, *46*(24), 13167-13175.

Remor, A. P., Totti, C. C., Moreira, D. A., Dutra, G. P., Heuser, V. D., & Boeira, J. M. (2009). Occupational exposure of farm workers to pesticides: biochemical parameters and evaluation of genotoxicity. *Environment international*, *35*(2), 273-278.

Roberts, A. L., Totten, L. A., Arnold, W. A., Burris, D. R., & Campbell, T. J. (1996). Reductive elimination of chlorinated ethylenes by zero-valent metals. *Environmental Science & Technology*, *30*(8), 2654-2659.

Roy, N., Mondal, S., Laskar, R. A., Basu, S., Mandal, D., & Begum, N. A. (2010). Biogenic synthesis of Au and Ag nanoparticles by Indian propolis and its constituents. *Colloids and Surfaces B: Biointerfaces*, *76*(1), 317-325.

Rudge, S. R., Kurtz, T. L., Vessely, C. R., Catterall, L. G., & Williamson, D. L. (2000). Preparation, characterization, and performance of magnetic iron–carbon nanocomposite microparticles for chemotherapy. *Biomaterials*, *21*(14), 1411-1420.

Saif, S., Tahir, A., & Chen, Y. (2016). Green synthesis of iron nanoparticles and their environmental applications and implications. *Nanomaterials*, *6*(11), 209.

Saleh, N., Phenrat, T., Sirk, K., Dufour, B., Ok, J., Sarbu, T., & Lowry, G. V. (2005). Adsorbed triblock copolymers deliver reactive iron nanoparticles to the oil/water interface. *Nano Letters*, *5*(12), 2489-2494.

Schrick, B., & Hydutsky, F. A. (2004). *Chem. Mater.,* 16, 2187-2193.

Shih, Y. H., & Gschwend, P. M. (2011). Evaluating activated carbon− water sorption coefficients of organic compounds using a linear solvation energy relationship approach and sorbate chemical activities. *Environmental Science & Technology*, *43*(3), 851-857.

Shih, Y. H., Chen, Y. C., Chen, M.Y., Tai, Y. T., & Tso, C. P. (2009). Dechlorination of hex- achlorobenzene by using nanoscale Fe and nanoscale Pd/Fe bimetallic particles, Colloid Surf. A: Physicochem. *Eng. Asp., 332*, 84–89.

Sing, K. S. (1985). Reporting physiosorption data for gas/solid systems with special reference to the determination of surface area and porosity. *Pure and applied chemistry*, 57, 603-619.

Sirk, K. M., Saleh, N. B., Phenrat, T., Kim, H. J., Dufour, B., Ok, J., Golas, P. L., Matyjaszewski, K., Lowry, G. V., & Tilton, R. D. (2009). Effect of adsorbed polyelectrolytes on nanoscale zero valent iron particle attachment to soil surface models. *Environmental Science & Technology*, *43*(10), 3803-3808.

Siskova, K. M., Straska, J., Krizek, M., Tucek, J., Machala, L., & Zboril, R. (2013). Formation of zero-valent iron nanoparticles mediated by amino acids. *Procedia Environmental Sciences*, *18*, 809-817.

Serp, P., Kalck, P., & Feurer, R. (2002). Chemical vapor deposition methods for the controlled preparation of supported catalytic materials. *Chemical reviews*, *102*(9), 3085-3128.

Simkovic, K., Derco, J., & Valičková, M. (2015). Removal of selected pesticides by nano zero-valent iron. *Acta Chimica Slovaca*, *8*(2), 152-155.

Sirk, K. M., & Saleh, N. B. 2009. *Environtal. Science and Technol.,* 43, 3803-3808.

Smith, M. B., & March, J. (2001). Eliminations. *March's Advanced Organic Chemistry: Reactions, Mechanisms, and Structure, Sixth Edition*, 1477-1558.

Smuleac, V., Varma, R., Sikdar, S., & Bhattacharyya, D. (2011). Green synthesis of Fe and Fe/Pd bimetallic nanoparticles in membranes for reductive degradation of chlorinated organics. *Journal of Membrane Science*, *379*(1), 131-137.

Song, H., & Carraway, E. R. (2005). Reduction of chlorinated ethanes by nanosized zero-valent iron: kinetics, pathways, and effects of reaction conditions. *Environmental Science & Technology*, *39*(16), 6237-6245.

Sotelo, J. L., Uguina, M. A., Delgado, J. A., Celemin, L. I., 2004. Adsorption of methyl ethyl ketone and trichloroethene from aqueous solutions onto activated carbon fixed-bed adsorbers. *Separation and. Purification. Technology*,. 37, 149-160.

Stefaniuk, M., Oleszczuk, P., & Ok, Y. S. (2016). Review on nano zerovalent iron (INPs): from synthesis to environmental applications. *Chemical Engineering Journal*, *287*, 618-632.

Stone, A. T., & Morgan, J. J. (1990). Kinetics of chemical transformations in the environment. IN: Aquatic Chemical Kinetics: Reaction Rates of Processes in Natural Waters. *Environmental Science and Technology Series.* John Wiley & Sons, New York. 1-41.

Stumm, W., & Morgan, J. J. (1996). Wiley Interscience, New York.

Su, Y. F., Hsu, C. Y., & Shih, Y. H. (2012). Effects of various ions on the dechlorination kinetics of hexachlorobenzene by nanoscale zero-valent iron. *Chemosphere*, *88*(11), 1346-1352.

Sun, Y., Ding, C., Cheng, W., & Wang, X. (2014). Simultaneous adsorption and reduction of U (VI) on reduced graphene oxide-supported nanoscale zerovalent iron. *Journal of Hazardous Materials*, 280, 399-408.

Tan, I. A. W., Ahmad, A. L., & Hameed, B. H. (2009). Adsorption isotherms, kinetics, thermodynamics and adsorption studies of 2, 4, 6-trichlorophenol on oil palm empty fruit bunch-based activated carbon. *Journal of Hazardous Materials*, 164, 473-482.

Tesh, S. J., & Scott, T. B. (2014). Nano-Nanocomposites for Water Remediation: A Review. *Advanced Materials*, *26*(35), 6056-6068.

Tian, H., Li, J., Mu, Z., Li, L., & Hao, Z. (2009). Effect of pH on DDT degradation in aqueous solution using bimetallic Ni/Fe nanoparticles. *Separation and Purification Technology*, *66*(1), 84-89.

Tiraferri, A., & Sethi, R. (2009). Enhanced transport of zerovalent iron nanoparticles in saturated porous media by guar gum. *Journal of Nanoparticle Research*, *11*(3), 635.

Tiraferri, A., Chen, K. L., Sethi, R., & Elimelech, M. (2008). Reduced aggregation and sedimentation of zero-valent iron nanoparticles in the presence of guar gum. *Journal of Colloid and Interface Science*, *324*(1), 71-79.

Tomasevic, D. D., Kozma, G., Kerkez, D. V., Dalmacija, B. D., Dalmacija, M. B., Becelic-Tomin, M. R., Kukovecz, A., Konya, Z., & Roncevic, S. (2014). Toxic metal immobilization in contaminated sediment using bentonite-and kaolinite-supported nano zero-valent iron. *Journal of Nanoparticle Research*, *16*(8), 2548.

Tsubota, S., Haruta, M., Kobayashi, T., Ueda, A., & Nakahara, Y. (1991). Preparation of highly dispersed gold on titanium and magnesium oxide. *Studies in Surface Science and Catalysis*, *63*, 695-704.

Valle-Orta, M., Diaz, D., Santiago-Jacinto, P., Vázquez-Olmos, A., & Reguera, E. (2008). Instantaneous synthesis of stable zerovalent metal nanoparticles under standard reaction conditions. *The Journal of Physical Chemistry B*, *112*(46), 14427-14434.

Vodyanitskii, Y. N., Mineev, V. G., & Shoba, S. A. (2014). Role of zero-valent iron in the degradation of organochlorine substances in groundwater. *Moscow University soil science bulletin*, *69*(4), 175-183.

Vogel, T. M., Criddle, C. S., & McCarty, P. L. (1987). ES&T critical reviews: transformations of halogenated aliphatic compounds. *Environmental Science & Technology*, *21*(8), 722-736.

Wang, C. B., & Zhang, W. X. (1997). Synthesizing nanoscale iron particles for rapid and complete dechlorination of TCE and PCBs. *Environmental Science & Technology*, *31*(7), 2154-2156.

Wang, T., Jin, X., Chen, Z., Megharaj, M., & Naidu, R. (2014)A. Green synthesis of Fe nanoparticles using eucalyptus leaf extracts for treatment of eutrophic wastewater. *Science of the Total Environment*, *466*, 210-213.

Wang, T., Lin, J., Chen, Z., Megharaj, M., Naidu, R. (2014)B. Green synthesized iron nanoparticles by green tea and eucalyptus leaves extracts used for removal of nitrate in aqueous solution. *Journal of. Cleaner. Production*, 83, 413-419.

Wang, C., Luo, H., Zhang, Z., Wu, Y., Zhang, J., & Chen, S. (2014)C. Removal of As (III) and As (V) from aqueous solutions using nanoscale zero valent iron-reduced graphite oxide modified nanocomposites. *Journal of Hazardous Materials*, *268*, 124-131.

Wang, Z., Choi, F., & Acosta, E. (2017). Effect of Surfactants on Zero-Valent Iron Nanoparticles (INPS) Reactivity. *Journal of Surfactants and Detergents*, *20*(3), 577-588.

Wang, W., Zhou, M., Jin, Z., & Li, T. (2015). Reactivity characteristics of poly (methyl methacrylate) coated nanoscale iron particles for trichloroethylene remediation.*Journal of Hazardous Materials*, *173*(1), 724-730.

Wang, C. B., & Zhang, W. X. (1997). Synthesizing nanoscale iron particles for rapid and complete dechlorination of TCE and PCBs. *Environmental Science & Technology*, *31*(7), 2154-2156.

Wu, S., Sun, A., Zhai, F., Wang, J., Xu, W., Zhang, Q., & Volinsky, A. A. (2011). Fe3O4 magnetic nanoparticles synthesis from tailings by ultrasonic chemical co-precipitation. *Materials Letters*, *65*(12), 1882-1884.

Xi, Y., Sun, Z., Hreid, T., Ayoko, G. A., & Frost, R. L. (2014). Bisphenol A degradation enhanced by air bubbles via advanced oxidation using in situ generated ferrous ions from nano zero-valent iron/palygorskite nanocomposite materials. *Chemical Engineering Journal*, *247*, 66-74.

Yabe, M. J. S., & de Oliveira, E. (2003). Heavy metals removal in industrial effluents by sequential adsorbent treatment. *Advances in Environmental Research*, *7*(2), 263-272.

Zhang, W. X., Wang, C. B., & Lien, H. L. (1998). Treatment of chlorinated organic contaminants with nanoscale bimetallic particles. *Catalysis Today*, *40*(4), 387-395.

Yan, W., Lien, H. L., Koel, B. E., & Zhang, W. X. (2013). Iron nanoparticles for environmental clean-up: recent developments and future outlook. *Environmental Science: Processes & Impacts*, *15*(1), 63-77.

Yan, J., Han, L., Gao, W., Xue, S., & Chen, M. (2015). Biochar supported nanoscale zerovalent iron nanocomposite used as persulfate activator for removing trichloroethylene. *Bioresource Technology*, *175*, 269-274.

Yang, J., Wang, X., Zhu, M., Liu, H., & Ma, J. (2014). Investigation of PAA/PVDF–INPS hybrids for metronidazole removal: synthesis, characterization, and reactivity characteristics. *Journal of Hazardous Materials*, *264*, 269-277.

Zhang, Y., & Erkey, C. (2006). Preparation of supported metallic nanoparticles using supercritical fluids: a review. *The Journal of Supercritical Fluids*, *38*(2), 252-267.

Zhang, W. X. (2003). Nanoscale iron particles for environmental remediation: an overview. *Journal of Nanoparticle Research*, *5*(3), 323-332.

Zhang, X., Li, S. Q., & Ayijamali, K. (2011). Preparation, Characterization of Nanoscale Zero-Valent Iron and its Application in Coking Wastewater Treatment. *Advanced Materials Research,* 194, 511-514.

Zhang, L., Ravipati, A. S., Koyyalamudi, S. R., Jeong, S. C., Reddy, N., Smith, P. T., & Wu, M. J. (2011). Antioxidant and anti-inflammatory activities of selected medicinal plants containing phenolic and flavonoid compounds. *Journal of Agricultural and Food Chemistry*, *59*(23), 12361-12367.

Zhang, M. M., Liu, Y. G., Li, T. T., Xu, W. H., Zheng, B. H., Tan, X. F., & Wang, S. F. (2015). Chitosan modification of magnetic biochar produced from Eichhornia crassipes for enhanced sorption of Cr (vi) from aqueous solution. *RSC Advances*, *5*(58), 46955-46964.

Zhou, T., Li, Y., & Lim, T. T. (2010). Catalytic hydrodechlorination of chlorophenols by Pd/Fe nanoparticles: comparisons with other bimetallic systems, kinetics and mechanism. *Separation and Purification Technology*, *76*(2), 206-214.

Zhu, H., Jia, Y., Wu, X., & Wang, H. (2009). Removal of arsenic from water by supported nano zero-valent iron on activated carbon. *Journal of Hazardous Materials*, *172*(2), 1591-1596.

Zohre, S., Ataallah, S. G., & Mehdi, A. (2010). Experimental study of methylene blue adsorption from aqueous solutions onto carbon nano tubes. *International Journal of Water Resources and Environmental Engineering*, *2*(2), 016-028.

LIST OF PUBLICATIONS AND PAPERS PRESENTED

Batool, S., Rashid, S. A. B., Maah, M. J., & Ashraf, M. A. (2016). Geographical distribution of persistence organic pollutants in the environment: A review. (2016). *Journal of environmental biology*, *133*, 309-314.

Batool, S., Maah, M. J., Bakar, A. F., Bakar, N. K & Shah, A. A. (2016). Novel magnetic biochar for the removal of 6 OCPs from wastewater. (2016). *Postgraduate symposium for environmental engineering technology.*